INFORMATION TO USERS

This manuscript has been reproduced from the microfilm master. UMI films the text directly from the original or copy submitted. Thus, some thesis and dissertation copies are in typewriter face, while others may be from any type of computer printer.

The quality of this reproduction is dependent upon the quality of the copy submitted. Broken or indistinct print, colored or poor quality illustrations and photographs, print bleedthrough, substandard margins, and improper alignment can adversely affect reproduction.

In the unlikely event that the author did not send UMI a complete manuscript and there are missing pages, these will be noted. Also, if unauthorized copyright material had to be removed, a note will indicate the deletion.

Oversize materials (e.g., maps, drawings, charts) are reproduced by sectioning the original, beginning at the upper left-hand corner and continuing from left to right in equal sections with small overlaps.

Photographs included in the original manuscript have been reproduced xerographically in this copy. Higher quality 6" x 9" black and white photographic prints are available for any photographs or illustrations appearing in this copy for an additional charge. Contact UMI directly to order.

Bell & Howell Information and Learning
300 North Zeeb Road, Ann Arbor, MI 48106-1346 USA
800-521-0600

Gravity and the physiology of locomotion and feeding in marine bivalve larvae: results from Space Shuttle experiments

by

Daniel Lloyd Jackson

Submitted in partial fulfillment of the requirements for the degree of Doctor of Philosophy

at

Dalhousie University
Halifax, Nova Scotia, Canada
July 1999

DALHOUSIE UNIVERSITY

FACULTY OF GRADUATE STUDIES

The undersigned hereby certify that they have read and recommend to the Faculty of Graduate Studies for acceptance a thesis entitled "Gravity and the physiology of locomotion and feeding in marine bivalve larvae: results from Space Shuttle experiments"

by Daniel Lloyd Jackson

in partial fulfillment of the requirements for the degree of Doctor of Philosophy.

Dated: August 27, 1999

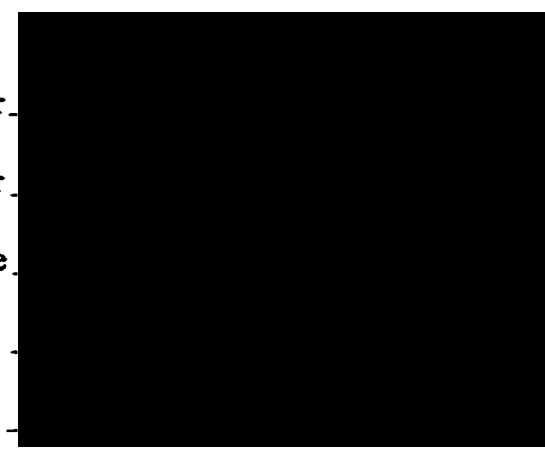

External Examiner

Research Supervisor

Examining Committee

DALHOUSIE UNIVERSITY

Date August 27, 1999

Author Daniel Lloyd Jackson

Title Gravity and the physiology of locomotion and feeding in marine bivalve larvae: results from Space Shuttle experiments

Department or School Biology

Degree: Ph.D. Convocation Fall Year 1999

Permission is herewith granted to Dalhousie University to circulate and to have copied for non-commercial purposes, at its discretion, the above title upon request of individuals or institutions.

Signature of Author

for

Cyril Howard Jackson

and

Jean Hudson Collins

TABLE OF CONTENTS

LIST OF FIGURES

LIST OF TABLES

ABSTRACT

As a force that draws zooplankters away from their food sources near the ocean surface, gravity has influenced the evolution of mechanisms and behaviours that counteract sinking. Paradoxically, it has also been suggested that gravity can be exploited by heavy zooplankters like bivalve larvae as a means of increasing feeding efficiency, notwithstanding the higher cost of locomotion. Gravity acts as a cue for orientation as veligers migrate throughout the water column, and is one of the physical forces that govern the helical swimming pattern that is typical of larval bivalve behaviour. The aim of this study was to examine how gravity affects swimming behaviour and orientation in marine bivalve larvae, and also how gravity influences their feeding, growth, and development processes.

Veliger larvae of the blue mussel *Mytilus edulis* were reared in the Canadian Space Agency's Aquatic Research Facility (ARF) on a ten day spaceflight mission aboard the NASA Space Shuttle *Endeavour*. Video recordings of larval behaviour in both microgravity and in a normal gravity control centrifuge were made twice daily, and samples of larvae were preserved on Flight Days 3, 5, and 7. One group of larvae from each gravity treatment was returned alive to Earth.

Larval growth rates were low in both gravity treatments, but there was a tendency towards greater growth and feeding rates in larvae reared in normal gravity. There was no strong evidence to suggest that mussel larvae are capable of buoyancy regulation; gravity did not influence the density of the animals nor the relative amounts of positively buoyant neutral lipid deposits. Larval development may have been affected by the absence of gravity, however. Although the larvae returned alive from space appeared normal and were capable of feeding, larvae reared in microgravity were generally in poorer condition and had thinner shells than larvae in normal gravity. Mortality rates were similar in both gravity treatments.

Most larvae in microgravity continued to swim in a helical pattern, but changed direction and helix dimensions frequently. In contrast to the vertically directed swimming behaviour of larvae in normal gravity, veligers in microgravity did not exhibit any directional orientation. Mean forward swimming speeds, pitch angles, and helix heights of larvae in microgravity were greater than their normal gravity counterparts. Larvae swimming downwards in normal gravity had greater translational and rotational swimming speeds than either upward swimmers or larvae in microgravity. The helix diameters of downward swimmers were also greater than those of larvae swimming in the absence of gravity.

A kinematic analysis of the forces produced by mussel larvae swimming in the presence and absence of gravity is presented. Larvae in microgravity required less energy to swim than larvae in normal gravity, and were able to move in higher helices and steeper pitch angles due to the lack of interactions between gravity and drag. The model decomposes total power output into power produced along the x- and y-axes, and reveals that mussel larvae can take advantage of the effect of gravity to transfer more power into the horizontal component of motion while swimming downwards. This behaviour has been implicated as an adaptation to maximise feeding success. Overall, these studies suggest that bivalve larvae have a much greater degree of control over their behaviours than has been previously considered.

LIST OF ACRONYMS & ABBREVIATIONS

AMS	ARF Main System
AMU	Algae Measurement Unit
ARF	Aquatic Research Facility
CADU	Control and Data Unit
CSA	Canadian Space Agency
KSC	Kennedy Space Center
MPB	MPB Technologies Inc.
NASA	National Aeronautics and Space Administration
OES	Orbiter Environmental Simulator
OVU	Optical Visualisation Unit
QA	Quality Assurance
SCA	Standard Container Assembly
SCU	Specimen Container Units
SSPF	Space Station Processing Facility
SSU	Sample Storage Unit
STS-77	Space Shuttle Mission # 77 (Shuttle Transport System-77)
4R0	SCA test chamber sampled on Flight Day 3
4L0	SCA test chamber sampled on Flight Day 5
3R0	SCA test chamber sampled on Flight Day 7
3L0	SCA test chamber sampled on Flight Day 10
0g	ARF MS-1 Microgravity treatment
1g	ARF MS-1 Normal gravity control treatment
"0g"	ARF MS-2 Normal gravity treatment
"1g"	ARF MS-2 Hypergravity (~1.4g) treatment

ACKNOWLEDGEMENTS

This project was an enormous undertaking, and assistance, guidance, and support were provided by many key individuals. I would like to thank my supervisor, Dr. Ron O'Dor, and the members of my supervisory committee, Dr. Roger Croll and Dr. Richard Wassersug, for their assistance and creative input during this project, and for their constructive criticism of the thesis. The technical team that helped get this project "off the ground" (Donna Krailo, Scott MacQuarrie, Darlene Manning) deserve special thanks for all the long hours they put in at Kennedy Space Center, Dryden Flight Research Lab, Cocoa Beach, and at Dalhousie University.

Many members of Dr. O'Dor's lab have been available for support, advice, and assistance over the years, including Chris Pearce, Yong Hong Guan, Dale Webber, Angel Perez, and Angelica Silva. The undergraduate research theses and other projects of Lei Chisholm, Heather Merry, Natasha Sladen, Rick Sethi, Victoria Young, Tom Wilson, and Corey Bishop provided valuable background data that was important to the success of this undertaking. Ed Officia, Charlie Thompson, Don Caswell, and Gloria Durnford were members of Dalhousie University's support staff and also deserve praise and thanks, as do Karen MacIntyre and Sonya Dudka of the Financial Services and Research Contracts offices. Barry MacDonald and Steve MacKenna provided me with larvae for my experiments over the years, and Kaija Lind kindly supplied the broodstock animals for the Space Shuttle experiment from her mussel farm in Ship Harbour, N.S. Statistical advice was provided by Dr. Bob Scheibling and Dr. Ian McLaren, and Drs. Jack McLachlan and Tom MacRae allowed me to use their microscopes in this investigation. Other assistance was provided by Dr. Alan Pinder, Ulrich Lobsiger, Yanko Andrade, Scott Gallager, Matthew O'Dor, and Cathie Kessler. Dr. John Castell deserves recognition because he fostered my interest in a scientific career in the first place, two decades ago. I also want to thank Bill Field because I forgot to mention him last time.

From the Canadian Space Agency, Alan Mortimer, Ron Wilkinson, Cathy Showalter, and Bob Hendry were ultimately responsible for making this project take flight, and Pat Sullivan provided Quality Assurance help in the pre-launch preparations. The other investigators that had experiments in the Aquatic Research Facility on this mission included Dr. Bruce Crawford and Craig Martin from the University of British Columbia, and Dr. Heide Schatten from the University of Wisconsin, all of whom contributed to the overall success of the mission.

The engineering team at MPB Technologies Inc. of Montreal (Sylvain Simard, Ming Szeto, Steve Love, Fadi Fikani, Linda Audet, John Yuen, Yvon Longpre, and Sylvie Ouellette) worked many long years to build the Aquatic Research Facility, considered and incorporated many of the suggestions and requests of biologists, and were there at Kennedy Space Center to ensure that all the spaceflight hardware worked when it had to. My travel agent Paige also deserves thanks for her help with scheduling all those trips to Florida and Montreal for the members of our lab.

The Staff at Kennedy Space Center's Life Science Support Facility (Mimi Shao, Oliver van den Ende, Ken Anderson, Rick Fiser, Howard Levine, Jacqui van Twest,

Cindy Martin, and Kelly and Susan) were of invaluable assistance in the preparations for the Space Shuttle experiment, and provided excellent support during and after the flight. The crew of Space Shuttle Endeavour's mission STS-77 (John Casper, Curtis Brown Jr., Daniel Bursch, and Andrew Thomas) deserve obvious praise, and especially Mission Specialists Mario Runco Jr. and Canada's Marc Garneau, who made sure that the Aquatic Research Facility operated properly during the flight. The Canadian Space Agency and Dalhousie University's Patrick Lett Fund provided financial support for this project, for which I am grateful.

The support and encouragement of my family over the past few years has been essential to the successful conclusion of this phase of my career, and they have my eternal thanks. And finally, I want to thank Mary McLaren for helping me through the difficult times, and showing confidence in me when I needed it the most.

CHAPTER 1

General Overview and Introduction

1.1 GENERAL OVERVIEW

1.1.1 Ecological Context

The planktonic communities of the ocean comprise an enormous ecosystem, with a complex food web consisting of a multitude of trophic level interactions ultimately dependent upon the primary production of phytoplankton. Aside from the traditionally recognised food-chain of phytoplankton being grazed upon by zooplankton which in turn are consumed by successively larger predators, there also exists the microbial food loop (Pomeroy, 1974; Azam *et al.*, 1983), consisting of a complicated community of bacteria, phototrophs, and zooplankton. In both of these coexisting food chains, zooplankton such as bivalve larvae play a dominant role in energy transfer and the recycling of nutrients. However, in spite of the importance placed upon understanding the fundamental mechanisms used by zooplankton to capture and assimilate food, there still remains a great paucity of knowledge in the field of zooplankton energetics. Clearly, a better picture of zooplankton feeding processes is necessary in order to reach a more complete assessment of the ocean's role in global climate and production.

Ocean zooplankton communities are a diverse assemblage of species representing almost every known extant phylum and a wide variety of life history strategies. The largest group of zooplankters are the holoplankton, which spend their entire life cycle within the plankton and in many environments are usually dominated, both numerically and in terms of ecological importance, by members of the Copepoda (Conover, 1968). As such, copepods have received the greatest amount of research attention, and hence it is their feeding and swimming mechanisms that are the best understood. Detailed studies

using microcinematographic techniques (Strickler, 1982, 1985; Paffenhofer, 1983; Koehl, 1983; LaBarbera, 1984) have led to new insights into the manner in which copepods behave, and have forced major revisions of the way we understand the function of "filter-feeding" or suspension feeding mechanisms.

In contrast to the holoplanktonic mode of life are the meroplankton, which spend only a portion of their life cycle in the plankton. For the most part, these animals are the larvae of benthic marine invertebrates, such as bivalves. Although they are usually outnumbered by holoplankters, they are nonetheless ecologically significant since there are times when they can numerically dominate the zooplankton in some places (Jørgensen, 1981; Gallager, 1988). Since meroplankters often are the larvae of commercially harvested species, such as mussels, scallops, or oysters, they are also of considerable economic importance. Owing in part to their small size, ephemeral nature, and the difficulties associated with studying such animals in the field, the role of benthic marine invertebrate larvae in global ocean processes remains relatively unclear. Further study of these animals is therefore essential. Marine invertebrate larvae are undeniably the dispersal phase of the life cycle of most benthic invertebrate species (Scheltema, 1986), responsible for the maintenance of a population in an existing area (Thorson, 1950), and the colonisation of new territories. With many species, mortality during the larval phase is extremely high and can have strong implications for future settlement success and recruitment to the adult population (Rumrill, 1990). With the further development of the aquaculture industry, higher priorities are also placed upon detailed knowledge of the feeding, growth, and behavioural ecology of the larvae of cultured invertebrate species.

1.1.2 Larval Bivalve Development

The common blue mussel *Mytilus edulis* is of immense ecological and commercial importance throughout the North Atlantic. In North America its range extends from the Arctic Ocean south to North Carolina, and can be found in many different habitats, attached to substrates such as rock, sand, wood, or mud, often forming very large colonies. As filter-feeding organisms, adult blue mussels play a significant role in coastal ecology and pollution removal (Widdows *et al.*, 1995). In recent years, the controlled culture of mussels has been the basis of a lucrative and rapidly expanding industry (Mallet, 1989).

The development of *Mytilus edulis* follows a pattern typical of most bivalves, and many members of the Mollusca in general (Widdows, 1991). The first external signs of activity after fertilisation are yolk-lobe and polar body formation. Cleavage of the embryo is spiral and determinate, and progresses through to formation of a ciliated epibolic gastrula at about 12-14 hours of age. Development continues with the appearance of an apical tuft of cilia, and the larvae become more active. At this stage they are known as trochophores and exhibit a directional swimming behaviour, with the apical tuft always pointing forward. This is a critical stage in development, since the internal organs and digestive tract are forming at this time, as are the rudiments of the nervous system. The shell gland begins to produce shell material, and the larva becomes capable of feeding as it reaches the straight-hinge bivalved veliger stage at approximately 48-96 hours, depending upon ambient temperature.

The veliger is characterised by the appearance of the velum, which is a ciliated structure that functions as both a locomotor and a feeding organ. The cilia are fused into cirri, which in turn are arranged in two bands along the edge of the velum, enclosing a ciliated food groove between them. The bands of cirri beat in a metachronal wave, creating currents that bring food particles toward the mouth and cause the larvae to move through the water column (Gallager, 1988). Veligers are very active, exhibiting complex swimming and feeding behaviours (Silva, 1987; Jonsson *et al.*, 1991), which may play a role in active depth regulation (Tremblay and Sinclair, 1990). As the larvae grow, they deposit aragonitic crystals of calcium carbonate in a protein-based shell matrix, apparently on a diurnal basis. As a result, their shells are demarcated by growth lines, which presumably correspond to a day's growth (Hurley *et al.*, 1987). Metamorphosis, characterised by the development of the foot as a sensory and locomotor organ, the disappearance of the velum, and the development of the gravity-sensing statocyst, marks the end of the planktonic larval stage (Cragg and Nott, 1977).

1.1.3 The Influence Of Gravity

The major chemical building blocks of living organisms, protein and carbohydrate, have a density greater than that of seawater. In addition, many plankters such as bivalve larvae possess a shell or other skeletal structure that further increases their density. As such, planktonic organisms have a tendency to sink that must be constantly compensated for, since food and nutrients are only found in the uppermost layers of the water column. Therefore, planktonic organisms must constantly counteract the downward pull of gravity by either swimming, or by attempting to achieve neutral buoyancy (Power, 1989). Although many types of zooplankters are neutrally buoyant,

most are not (Chia *et al.*, 1984), and bivalve larvae in particular are significantly heavier than seawater (> 1.3 $g \cdot cm^{-3}$; Jackson, 1992; Mann, 1986). Studies of the larvae of bivalves such as the blue mussel *Mytilus edulis* suggest that these organisms may be capable of actively regulating their buoyancy, in part by balancing the relative proportions of positively buoyant lipid reserves with negatively buoyant shell material (Gallager, 1985). Even under ideal physiological conditions, however, bivalve larvae maintain a density significantly greater than their seawater environment, and their density is maintained in spite of the fact that the cost of locomotion may exceed 50% of their total energy budget (Zeuthen, 1947; Gallager, 1992). The question then arises as to why these animals are heavier than seawater, when so much of their energy is spent just staying up in the water column. This is known as the "plankton floatation paradox" (Smayda, 1970), and leads to further questions regarding the role of gravity in the physiological ecology of this important group of marine invertebrates. The answers lie in a more thorough understanding of the physical forces acting upon small zooplankters.

1.1.3.1 Orientation and Vertical Distribution

Many zooplanktonic organisms, including bivalve larvae, adjust their vertical position in the water column on a daily basis as a function of endogenous factors such as age, physiological condition, and biological rhythms, as well as exogenous stimuli, including light, pressure, food, and gravity (Longhurst, 1976; Forward, 1988). Since net advective forces often vary in direction and velocity throughout the water column (Hill, 1991), such vertical migrations can also have an impact upon horizontal plankton distribution, and, by implication, dispersal and future recruitment success. Consequently, the mechanisms underlying vertical migration and the cues that enable a plankter to select

a position within the water column are integral components of zooplankton biology (Power, 1989). Implicit in the ability to migrate throughout the water column is the possession of a means of orientation that enables a plankter to distinguish up from down (Sulkin, 1990).

Zooplankters react to external stimuli by exhibiting either a taxis response, in which the animal moves in the direction of the stimulus, or a kinesis response, where the level of locomotor activity increases in proportion to the intensity of the stimulus (Fraenkel and Gunn, 1940). Taxis responses tend to result in the animal orienting itself in line with the stimulus and moving in a relatively direct path, whereas kinesis responses usually lead to a more circuitous route being followed (Young, 1995). In general, physical vector cues that contain directional information, such as gravity, light, and current flow, usually elicit taxis-type behaviour from plankters. Scalar stimuli, such as temperature, pressure, salinity, and light intensity, contain no such directional information at any given point, and usually result in kinetic response behaviour. The behavioural repertoire that enables a plankter to orient and move up and down within the water column often involves a combination of tactic and kinetic responses to both vector and scalar stimuli (Young, 1995).

The environmental stimuli that are most commonly used as orientation cues by zooplankton are light and gravity (Sulkin, 1990). Of these, light has traditionally been regarded as the more significant factor, since changes in the vertical position of plankters often coincide with changes in underwater illumination intensity at sunrise and sunset (Forward, 1988). A typical phototaxis response involves adjustments of the animal's body orientation to the light source in such a way that when the animal starts swimming,

movement is directed away from or toward the light (Sulkin, 1984). However, zooplankters exhibit a wide and complex variety of responses to light stimuli, and vertical migratory behaviour is not simply a taxis response to a downwardly directed light source. The intensity, wavelength, and angular distribution of light underwater varies not only with depth, but also with time, latitude, and oceanographic conditions. The highly variable nature of light in the marine environment complicates efforts to study it as a potential orientation influence (Sulkin, 1984). While many studies have examined the phototactic responses of several major groups of zooplankton, Forward (1988) criticised the experimental assumptions behind this body of literature, and its conclusion that most plankters exhibit strong phototactic responses that are the dominant factor in their ability to control their position within the water column. Most of these studies have followed the classical approach of illuminating an observation chamber at an angle orthogonal to the gravity vector, which is a situation that does not accurately simulate the natural conditions of light wavelength and angular distribution found in the field. In an extensive review of the subject, Forward (1988) presents evidence that the phototactic responses observed under these conditions are an artificial laboratory artifact, and concludes that positive phototactic responses are actually quite rare among zooplankton.

It is apparent then that phototactic responses alone are an insufficient means of orientation and navigation within a vertically stratified water column. Gravity, however, is a constant environmental parameter that provides a conservative orientation stimulus for planktonic organisms (Young, 1995). In an exhaustive review of behavioural aspects of vertical movement in crab larvae, Sulkin (1984) presented a three-part model describing the means by which a plankter can orient itself and move within the water

column. In this model, buoyancy, body orientation, and rate of locomotion interact to govern the manner in which the animal can control its position within the column, and gravity underlies all three components. Buoyancy is a direct consequence of gravitational forces, and influences the orientation response; a net positive buoyancy will cause a plankter to ascend, while a net negative buoyancy will result in sinking (Strickler, 1982). Adoption of a specific body orientation enables the animal to move in a specific direction when swimming, and can be assisted in part by buoyant forces. Rate of locomotion is often a kinetic response to external stimuli, and will determine the extent of movement in the direction set out by the animal's orientation. According to Sulkin's model, geotaxis is the predominant means by which zooplankton orient themselves in the water column, and regulation of position is a function of kinetic responses to other, more variable environmental stimuli, including light, food, and hydrostatic pressure.

The definition of geotaxis implies that the animal possesses a gravity receptor that can either actively detect gravitational force or at least provide a directional cue (Sulkin, 1990). However, examples of gravireceptors are rare among planktonic marine invertebrate larvae (Creutzberg, 1975). Bayne (1964) reported that the larvae of *Mytilus edulis* showed a strong negative geotaxis, but did not offer any possible mechanism for this behaviour. Pires and Woolacott (1983) reported that larvae of the bryozoan *Bugula stolonifera* exhibit a direct, active response to gravity, but the nature of gravity perception in these animals was unknown. Mogami *et al.* (1988) found that sea urchin larvae also have an active mechanism to control sinking, but again no gravireceptors were found. These authors suggested that echinoderm larvae may possess statocyst-like organelles similar to Müller vesicles found in loxodid ciliates, but presented no evidence for such a

mechanism. Recent experiments with *Paramecium* and *Euglena* have shown that these protozoans also exhibit gravity-dependant taxis and kinesis responses, but these graviresponses were lost in the absence of gravity on board a Space Shuttle (Häder *et al.*, 1995; Hemmersbach *et al.*, 1996). Both of these microgravity studies suggest that an active gravireceptor is involved in these behaviours, and Hemmersbach *et al.* (1996) proposed a physiological signal transduction chain mechanism that may function in the detection of gravity in protozoans. It is not known if a similar mechanism exists in the Metazoa.

Bivalve larvae develop a statocyst at the later stages of their planktonic life, when they begin to settle and explore the benthos (Cragg and Nott, 1977). The necessity of such an organ at this stage of development arises from the need for the animal to be able to orient itself as it crawls along the bottom, often upside down, searching for a suitable settlement substrate. However, in younger planktonic bivalve larvae, no gravireceptors have ever been described. This raises questions regarding the mechanism by which these animals are able to detect gravity and navigate their way through the water column. It is possible that an active gravireceptor is not necessary, owing to the morphology of the veliger and its asymmetric distribution of mass. In bivalve larvae, the heavier hinge of the shell ensures that the animal is oriented with the lower-density velum pointing upwards; this attitude is always maintained when larvae are anaesthetised or are passively sinking (Cragg, 1980). When the velar cilia beat, the direction of locomotion is always aligned along the gravity vector. The existence of a similar passive "buoy" mechanism has been proposed for protozoans, but has been discounted by Häder *et al.* (1995) and Hemmersbach *et al.* (1996) as a result of their microgravity studies. However, bivalve

larvae are significantly heavier than *Paramecium* and *Euglena*, and it has been suggested by Strickler (1982) that negative buoyancy is not only necessary for providing a means by which plankters can detect the gravity vector and orient within the water column, but also helps to enlarge the feeding currents that the animal generates while swimming.

1.1.3.2 Feeding and Locomotion

The planktonic habitat has often been described as a "nutritionally dilute environment" (Conover, 1968), in which the algae that these animals graze upon are widely dispersed throughout a huge three-dimensional space, or located in isolated patches. The mechanics of feeding in this environment are further complicated by the fact that a zooplankter's physical surroundings are dominated not by the inertial forces familiar to larger organisms, but by viscosity. In this world of low Reynolds numbers, the small size and relatively slow swimming speeds of zooplankton mean that they experience seawater as a sticky fluid that is difficult to move through or extract food from (Vogel, 1981). Under these conditions, flow past the organism is laminar and there is a thick layer of sticky water that moves with the animal and deflects food particles out of its path.

Different members of the zooplankton have evolved different life history and feeding strategies in order to survive and thrive under the unique conditions prevalent in their environment. Copepods, for instance, use their appendages to generate a feeding current from which food particles are extracted (Strickler, 1985). Bivalve larvae possess a ciliated velum that propels the animal through the water as it creates a flow field which brings algae towards the larva's mouth where they may be captured and ingested

(Gallager, 1988). Since the cilia that generate the feeding current also function in the capture of the particles, any mechanism that increases flow around the velum should also enhance feeding efficiency (Emlet and Strathmann, 1985; Emlet, 1990). Gravity appears to be one of those mechanisms, playing a significant role in regulating the size of the flow field around the velar cilia (Gallager, 1993), as well as governing many aspects of larval behaviour.

Swimming behaviour and mechanics have been described in detail for the larvae of bivalves such as *Pecten maximus* (Cragg, 1980) and *Cerastoderma edule* (Jonsson *et al.*, 1991). Larvae of the blue mussel *Mytilus edulis* exhibit a swimming behaviour that follows this same general pattern (Bayne, 1963), which is typical of most larvae within the Bivalvia. Bivalve larvae appear to be negatively geotactic, spending much of their time swimming upwards against gravity, and often accumulate at the surface. During ascent, they swim in a helical or spiral pattern, usually rotating about the central axis in a clockwise direction (when viewed from above). Alteration of the pitch angle of the spiral allows larvae to change the rate of ascent. This helical pattern is often maintained when larvae actively swim downwards, but descent in the water column is often accomplished by simple cessation of ciliary beating followed by passive sinking. While movement in the vertical plane is believed to be a searching behaviour, bivalve larvae often hover in a near-stationary position when a phytoplankton patch is encountered. Hovering behaviour is believed to increase the volume of the larva's flow field by a factor of 40 or more (Gallager, 1993), thereby maximising particle encounter and feeding efficiency (Silva and O'Dor, 1988; Gallager *et al.*, 1989; Gallager, 1993).

As a bivalve larva swims through the water column, it is influenced by a variety of physical factors, including pressure gradient, torque, drag, buoyancy, and gravity (Strickler, 1982). All of these forces act together to determine the orientation of the animal, its swimming velocity, and the properties of its flow field. Although the flow field is initially set up by the beating actions of the cilia, it has been suggested that the downward pull of gravity induces a shear stress on the surrounding layer of water, helping to enlarge the feeding current and facilitate particle capture (Strickler, 1982; Childress *et al.*, 1987). Emlet and Strathmann (1985) expanded this argument by suggesting that any force that acts as a partial tether, be it gravity or drag, will enhance the feeding current and maximise feeding efficiency in this manner.

Gravity influences the feeding mechanics of larval bivalves in complex ways. As the velar cilia beat, there is a substantial difference in velocity between the stationary base of the cilium and the tip, which is moving the fastest (Cheung and Winet, 1975; Strathmann and Leise, 1979; Gallager, 1988; Emlet, 1990). Since the movement of fluid by cilia is inherently inefficient (Blake and Sleigh, 1975), a velocity gradient is formed between the cilia and the surrounding fluid, enabling the tip of the cilia to shear through the viscous fluid and come into contact with algal food particles suspended within the fluid. The steepness of the velocity gradient, or shear field, is proportional to the magnitude of retarding forces such as gravity and drag (Emlet and Strathmann 1985), resulting in increased rates of food particle contact in heavier, denser plankters such as bivalve larvae. In this scenario, gravity acts to help a plankter enhance its feeding efficiency, at the expense of its locomotor efficiency. A trade-off between these two requirements has been made by different types of planktonic animals in their evolutionary

development. The best way to examine this relationship is by removal of the gravity component in the long-term microgravity exposure available on the Space Shuttle. Bivalve larvae are an ideal test organism for the study of gravitational adaptations in zooplankton since they are among the heaviest of all zooplankters, and their distinctive, predictable locomotor patterns make it easy to monitor any alteration of behaviour that may be due to the microgravity environment.

The Aquatic Research Facility (ARF) was developed by the Canadian Space Agency (CSA), in cooperation with NASA, as a multi-user Space Shuttle-based laboratory capable of investigating a wide variety of gravitational phenomena in aquatic organisms. The ARF provides researchers with a unique opportunity to examine the fundamental role that gravity has played in the evolution of life in the oceans. After a developmental phase that extended over five years, the ARF flew on its maiden flight (entitled "ARF-1") aboard the Space Shuttle Endeavour on Mission STS-77, May 19-29, 1996. Three investigative teams conducted experiments on the ARF during STS-77, including our group from Dalhousie University which was devoted to studying the role of gravity in the feeding and locomotor physiology of marine bivalve larvae.

1.2 RESEARCH OBJECTIVES

The overall aim of this research was to investigate the role that gravity plays in the biology of marine bivalve larvae, through the use of the microgravity environment available on a NASA Space Shuttle. Although spaceflight research offers the researcher unparalleled opportunities for manipulating gravity as an environmental variable, it also imposes a unique set of constraints upon experimental design. Among these limitations are strict CSA and NASA-imposed restrictions on the amount of working space and resources available to the experiment, and upon the time available for the astronauts to perform the experimental procedures. As a result, the design of the experiment had to be as simple as possible, while maximising the quantity and quality of data that would be retrieved at the end of the spaceflight mission. Accordingly, the research objectives were based upon a series of key questions and related hypotheses regarding the role of gravity in feeding and development of the larvae of the blue mussel *Mytilus edulis*, and the experimental design reflected the simplicity of this approach.

QUESTION A

How does gravity influence larval bivalve swimming behaviour and orientation?

Hypothesis A1

The characteristic helical swimming pattern exhibited by bivalve larvae is a consequence of the rotational and translational forces generated by the velar cilia. Gravity only indirectly affects this pattern of motion, by helping to maintain swimming attitude and by partially restraining vertical motion. Larvae will continue to swim in a helical pattern in the absence of gravity, but will do so at a faster rate of speed.

Hypothesis A2

Gravity is the primary cue for orientation amongst planktonic marine bivalve larvae. In a microgravity environment, bivalve larvae will swim in random directions.

QUESTION B

How does gravity affect feeding, growth, and development of marine bivalve larvae?

Hypothesis B1

Gravitational forces act upon zooplankters to create a retarding force that acts to increase shear between feeding appendages and the surrounding fluid, and to expand an organism's flow field. The efficiency of particle capture will be diminished in the absence of gravitational forces, resulting in lower growth.

Hypothesis B2

Larval buoyancy is regulated by a balance between accumulation of low density lipid reserves and deposition of shell material of high specific gravity. In the absence of gravity, bivalve larvae will attempt to compensate for impaired feeding efficiency by increasing their density.

Hypothesis B3

Gravity does not directly influence the early development of marine bivalve larvae. Bivalve larvae will develop normally in the absence of gravity.

These hypotheses were tested in the Aquatic Research Facility in a series of experiments that are outlined in the subsequent chapters of this thesis. Chapter 2 includes a detailed description of the ARF and its capabilities, and outlines some of the preparatory work that was required in order to ensure that the ARF functioned properly in the critical Space Shuttle mission. During the 10-day STS-77 mission, the video subsystem of the ARF was used extensively to observe and record the behaviour of mussel larvae in the microgravity environment. This experiment, designed to investigate and test Hypotheses A1 and A2, is described in Chapter 3. The ARF was also capable of preserving specimens of larvae and their algal food source at pre-determined intervals, and this capability was used in the experiments outlined in Chapter 4 that were intended to test the hypotheses related to Question B. The general conclusions of the microgravity experiments are summarised in Chapter 5, which also presents a kinematic analysis of larval bivalve locomotion and discusses the energetic costs of swimming for heavy bivalve larvae.

CHAPTER 2

The Aquatic Research Facility - Hardware Overview and Experimental Design

2.1 THE AQUATIC RESEARCH FACILITY HARDWARE OVERVIEW

The Aquatic Research Facility (ARF) was comprised of two separate hardware units that occupied adjacent lockers in the Middeck region of the Space Shuttle Endeavour; the ARF Main System (AMS) and the Sample Storage Unit (SSU). The SSU was a simple passively-cooled container that maintained the aquarium-like Specimen Container Units (SCUs) at 5°C until the experiment was started approximately 29 hours into the mission, and was also used to store accessories such as videotapes. The ARF Main System contained two thermoelectrically refrigerated (12°C) centrifuges, each of which held six SCUs. One centrifuge spun at 80 RPM, resulting in a normal (1g) gravitational acceleration during orbit, while the other centrifuge spun very slowly, and provided the microgravity (0g) treatment for the experiment. The slow rate of revolution in this centrifuge ensured that any slight variations in light levels, etc. were averaged out amongst all SCUs. The capability of running a microgravity experiment adjacent to a normal gravity control experiment in this manner made the ARF unique among Middeck flight hardware. An array of red LEDs capable of supporting photosynthesis provided the light for the specimens, and was regulated to provide a 20:4 light:dark photoperiod during each day of the mission. The Control and Data Unit (CADU) computer controlled all AMS functions, including temperature and photoperiod control, video recording, specimen fixation, and data recording.

The design of the Specimen Container Units was constrained by numerous engineering, biological, and safety considerations. Paramount among these was the

ability of the SCUs to support normal life processes. Materials used in construction were required to be transparent and non-flammable, but also had to be non-toxic to both specimens and astronauts. Gas permeability across the SCU surfaces was necessary, since the microgravity environment is not conducive to air bubbling, as is normally done with aquatic specimens on Earth. However, since seawater is considered to be a hazardous substance by NASA, spaceflight regulations required that the fluid be separated from the astronauts' living quarters by three separate, sealed levels of containment. This redundancy was necessary in order to ensure that no leakage occurred if one or even two of the levels of containment should fail. However, each level is a barrier to gas permeability, so material selection and design had to take this into consideration. The fixative required to preserve the animals throughout the experiment had to be isolated not only from the astronauts, but also from the specimens; any offgassing of volatile chemicals would have, at least, sublethal effects on the larvae. This requirement not only imposed design constraints, but also affected the choice of fixative; the preferred fixative, formalin, is a small molecule and permeates readily through many surfaces. Hence, glutaraldehyde had to be used.

At least five different renditions of the SCU were designed and tested before the final version was approved for flight (consult Fig. 2.1 and Fig. 2.2). The SCUs were composed of three major components: the Standard Container Assembly (SCA), the second level of containment Teflon bag, and the third level of containment polysulfone box. The SCA was the core unit of an SCU, being comprised of two individual test chambers, each of which could hold 35 ml of seawater and specimens. At the outside ends of the SCA test chambers were Teflon membranes that permitted oxygen and carbon

dioxide to permeate into and out of the SCA. The inner wall of the test chambers was composed of a flexible silicone-based membrane that also permitted gas exchange. The two test chambers were separated from each other by a central divider that included an air space and a stainless steel isolation plate; this plate prevented the silicone membranes of the adjacent test chambers from contacting each other when one of the chambers was injected with glutaraldehyde fixative. In the base of each SCA test chamber was the fixative block assembly, described in detail below. This assembly was mounted underneath a mirror oriented at 45° to the front surface of the SCA, which assisted in illumination of the specimens during video observation. The back surfaces of the SCA test chambers were covered with a semi-transparent silver reflective material, which functioned as a mirror as was used in the video recording process (see description of Optical Visualisation Unit below).

The components of the SCA were cast in polyurethane, a non-toxic, non-flammable material that allowed limited gas exchange across its surface. The casting process made assembly easier and more cost effective, but often resulted in diminished optical transparency and quality when compared to prototypes assembled from polyurethane sheets. Therefore, SCAs used in this experiment had to be individually selected for optimum optical quality. A gas-permeable Teflon bag was chosen as the second level of containment; it was wrapped around the SCA in the final stages of pre-flight assembly and sealed tight with a heat-sealing apparatus. This procedure introduced a risk of wrinkling the Teflon bag and impairing optical quality, but this was minimal in most cases. The wiring harness for the fixative actuator ran through the bottom of the Teflon bag, and were cemented in place and sealed with epoxy. The third level of

containment was a polysulfone box (Fig. 2.3) with a Teflon membrane on the top surface, protected by a perforated aluminium plate. Latching clips on the sides of this box allowed the entire SCU to be locked into place on the AMS centrifuge; individually distinct hardware keys on the bottom surface of the SCU ensured that the astronauts made no mistakes when arranging the SCUs on the AMS centrifuge. Electrical connectors on the bottom of the SCU plugged into the AMS centrifuge plate to enable computer control and firing of the fixative actuator.

The fixative block assembly was, by the very nature of its function, a very complicated apparatus (see Fig. 2.4). The glutaraldehyde itself (1.5 ml) was contained within a silicone containment bag; offgassing tests had shown that the fixative did not permeate through this bag. Adjacent to the bag was a small hollow piston with a spring attached. The spring and piston assembly was held in a recoiled position by a thread of spectra fibre that was tied to a set of coiling pins on the outside of the fixative block. When tied around these pins, the spectra thread was in contact with a pair of electrical resistors. When a voltage was applied to these resistors, they heated up and the spectra thread melted, allowing the spring to activate and compress the piston against the fixative containment bag. The end of the bag was pressed up against a stainless steel cutting blade, which punctured the bag and allowed the glutaraldehyde to flow through a fluid injection port and into the SCA test chamber. The fixative was thereby injected into the test chamber with great force, completely mixing with the contents in less than one second. When this occurred, the flexible silicone membrane of the SCA test chamber expanded to accommodate the extra volume, and a check valve in the fixative block prevented any fluid from retreating back into the fixative containment bag.

The Algae Measurement Unit (AMU) was included as a component of the ARF late in the development phase, when it was confirmed that there was no space during the ARF-1 mission to accommodate an SCA test chamber dedicated to include algae only as a growth control treatment for this experiment. The AMU was basically an optoelectronic circuit that functioned as an *in situ* single-beam spectrophotometer, capable of detecting changes in the amount of algal cells (*Isochrysis galbana*) within an SCA test chamber. An LED that emitted light at a peak wavelength of 700 nm, close to the absorption maximum of the algae, was aimed at an oblique angle into an SCA test chamber. Light from this LED reflected off the back surface mirror of the SCA and towards a phototransistor matched to the spectral characteristics of the LED. All substances throughout this pathlength capable of absorbing light at 700 nm, namely algal cells, would reduce the amount of light reaching the phototransistor. Once the AMU was calibrated against a blank (seawater), this circuit was designed to detect changes in the amount of algae within an SCA test chamber. Data were recorded on non-volatile media for post-flight analysis.

The Optical Visualisation Unit (OVU) was a video camera subsystem of the ARF, capable of recording the activity of the specimens in the SCUs at pre-programmed intervals. The OVU contained two Pulnix TM-7CN analogue high-resolution monochrome video cameras, fitted with Schneider Xenoplan 1.7/17mm lenses and 3mm spacer rings. A Sony Hi8 format camcorder was stripped and reassembled as the video recording device for the OVU, and both video cameras were connected to the VCR via a switching multiplexer that allowed sequential recording from each camera. The cameras were mounted close to the centre of each AMS centrifuge and aimed towards the SCUs

mounted along the periphery of the SCU carousel. The camera mounting plate was capable of rotation that was independent of the rotation of the centrifuge itself, allowing the camera to be moved around to view the SCUs in any chosen order, even as the centrifuge was spinning. Proximity sensors mounted adjacent to the SCUs ensured that the camera stopped in the correct position to observe the contents of the SCA test chambers. All video and power cabling from the cameras therefore had to be fed through a 50-line slip ring assembly to the VCR and AMS Control and Data Unit (CADU).

The small amount of space within the AMS centrifuge meant that the video cameras could not be aimed directly into the SCA test chambers, so a gold front-surface mirror assembly was constructed that enabled the cameras to be mounted where space permitted and still aim into the SCA test chambers. The entire optical path was contained within a flat-black painted housing to avoid optical degradation due to light leaks or internal reflections. Illumination of the specimens in the SCUs was provided by a bank of high-intensity infrared LEDs mounted underneath the camera's mirror assembly, and were directed at the 45° mirror at the base of each SCA test chamber. The output wavelength of these LEDs was chosen to be outside the range of spectral sensitivity of the animals, in order to avoid any response of the larvae to the video lights during recording sessions. The light striking the 45° mirror reflected straight upwards into the SCA test chamber, providing dark-field illumination of the specimens within.

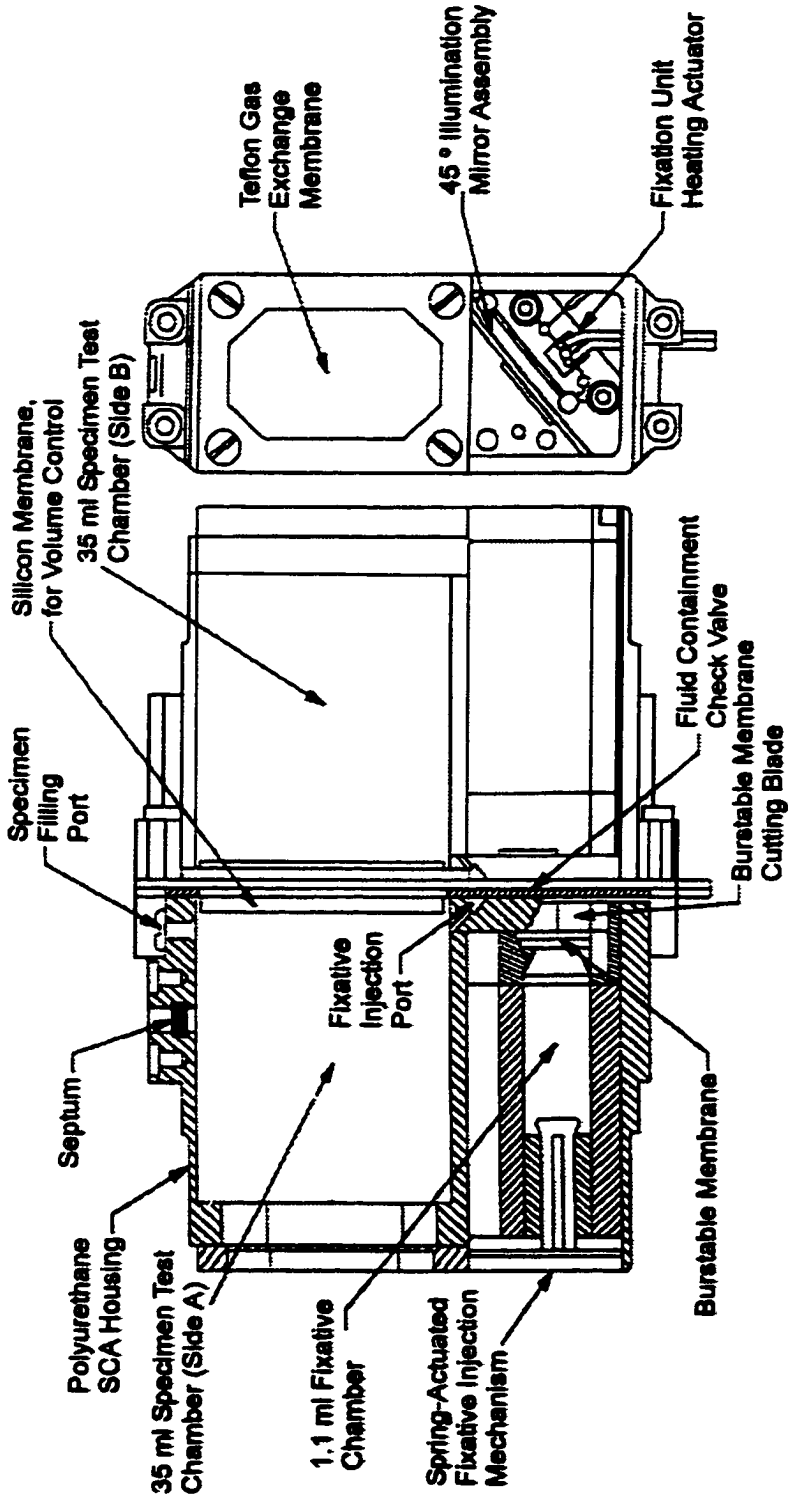

Fig. 2.1. Diagram of a Standard Container Assembly (SCA), actual size.

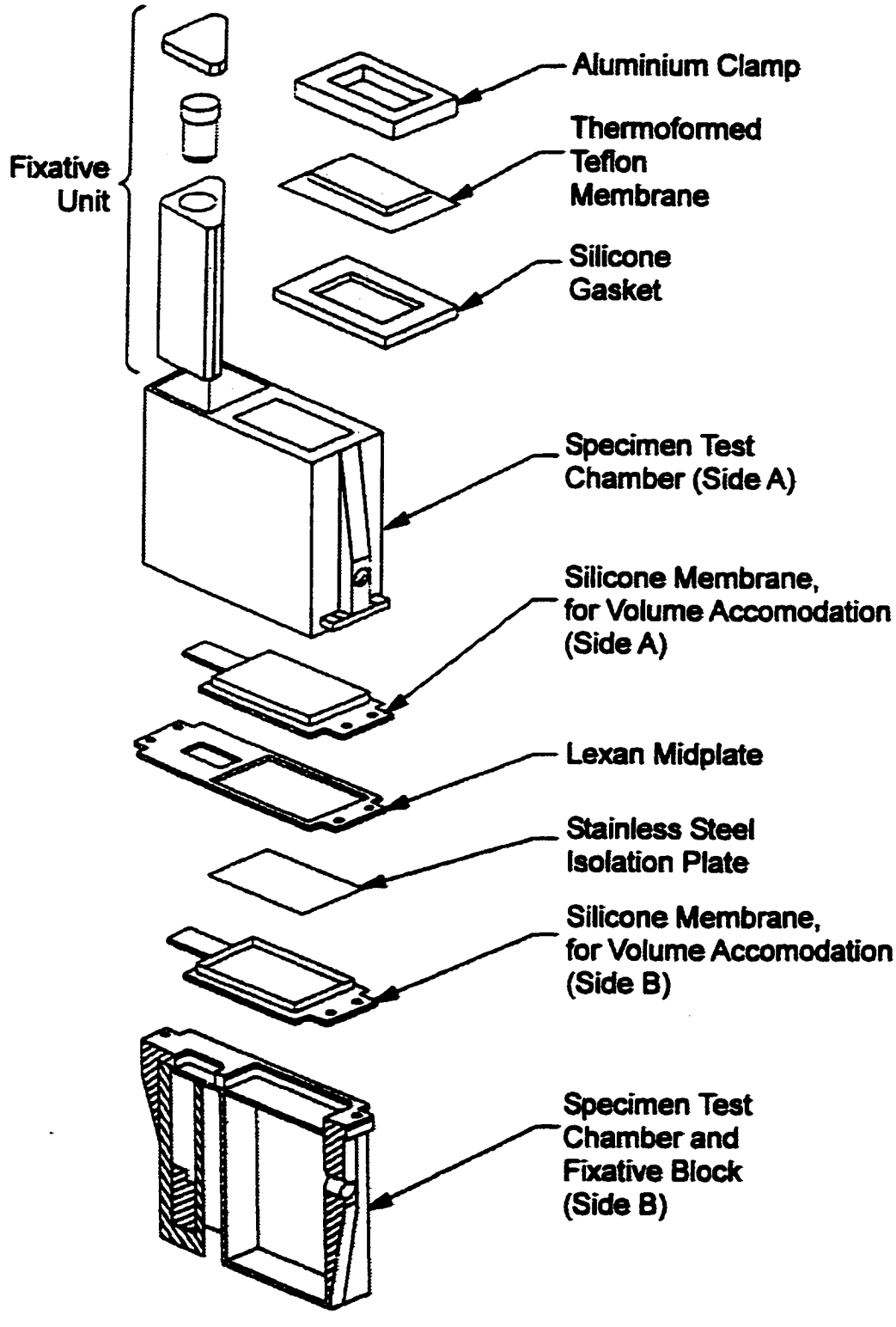

Fig. 2.2. "Exploded" view diagram of a Standard Containment Assembly (SCA) Test Chamber.

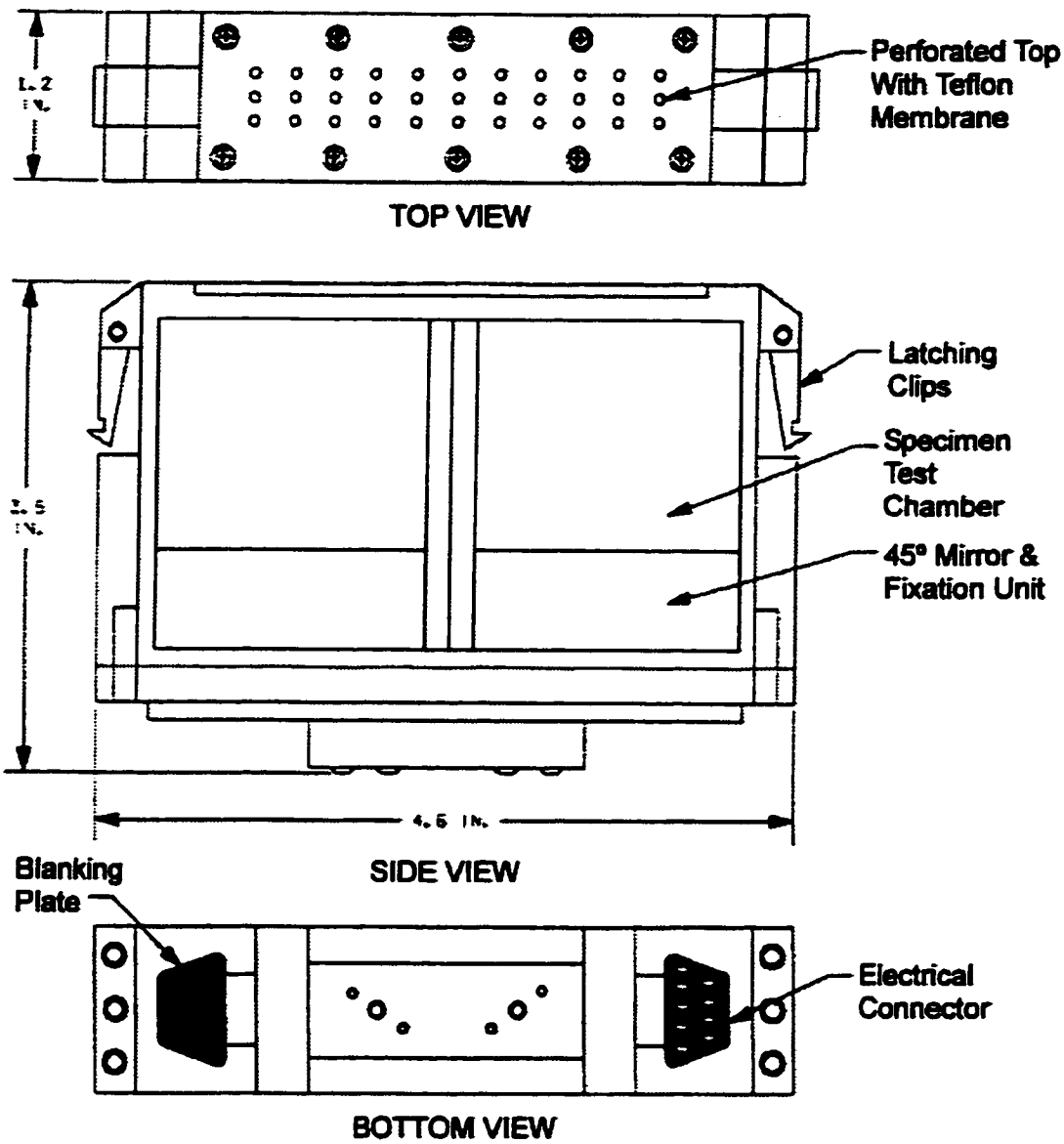

Fig. 2.3. Diagram of a fully assembled Specimen Container Unit (SCU)

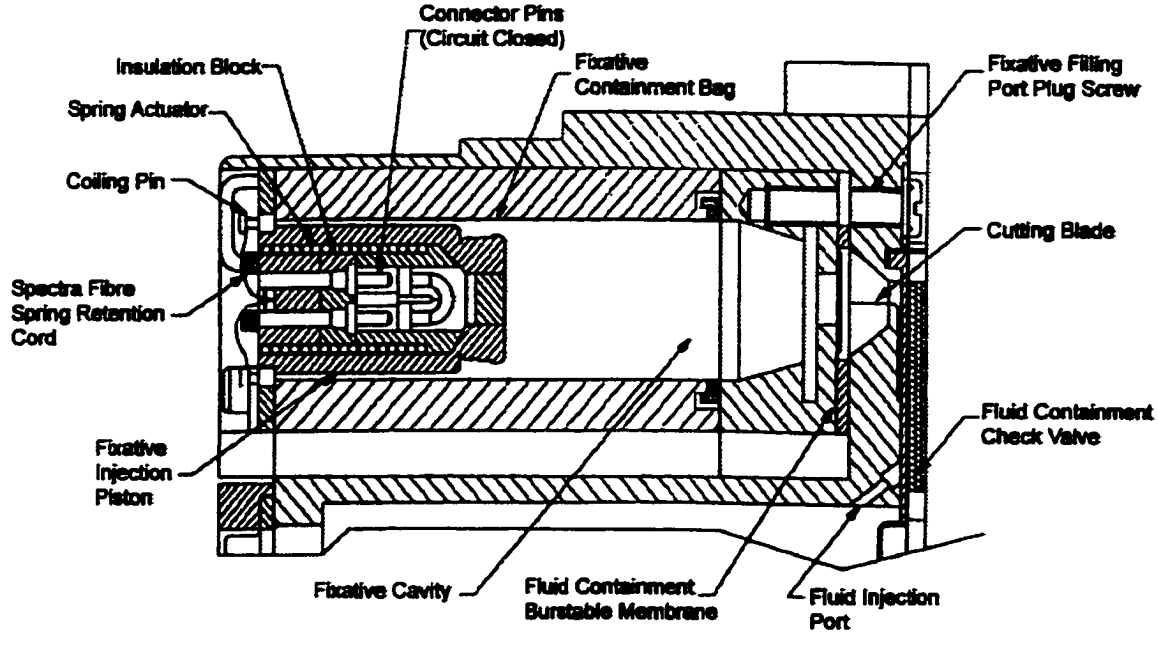

Fig. 2.4. Diagram illustrating the Fixative Block Assembly.

2.2 EXPERIMENTAL DESIGN

2.2.1 In-Flight Procedures:

Two Specimen Container Units (SCUs) on each of the two ARF Main System (AMS-1) centrifuges (microgravity and normal gravity treatments) were allocated to this experiment. Each SCU was comprised of two individual Standard Container Assembly (SCA) test chambers, for a total of 4 experimental containers per gravity treatment (SCA #3L and 3R, and SCA #4L and 4R). One day prior to launch, each SCA test chamber was loaded with 0.2 μm-filtered seawater, 100 actively swimming 6-day old mussel larvae (*Mytilus edulis*), their food source (the unicellular flagellate alga *Isochrysis galbana*), and algal growth nutrients (f/2 algal culture medium (Guillard, 1975)). Algal stocking density was approximately 23 000 cells/ml. All loading operations took place in a 5°C cold room, to minimise the possibility of condensation and gas solubility problems that could have occurred as the SCUs warmed up to the in-flight operating temperature of 12°C. After the SCUs were sealed and examined by NASA and CSA Quality Control inspectors, they were placed in the ARF's Sample Storage Unit (SSU), and transferred to the Middeck of the Shuttle Endeavour on Launch Pad 39-B. The launch of Mission STS-77 occurred on schedule at 06:30 EDT, Sunday, May 19, 1996.

For the first 29 hours of the flight, the SCUs for this experiment remained in the SSU while another experiment was conducted in the ARF Main System. Previous ground-based studies revealed that growth, feeding, and overall activity of mussel larvae are minimal when ambient temperature is 5-6°C, as it was in the SSU during this period of time (Jackson, unpub. data). Mission Specialist Mario Runco transferred the SCUs

from the SSU into the ARF Main System at 11:26 EDT on Monday, May 20, 1996; this is regarded as the official start time for the experiment. Video recording sessions were scheduled to occur for each SCA test chamber twice each flight day; one session during the 20-hour daytime, and one in the 4-hour night period. Each video recording session lasted approximately 3.5 to 4.5 minutes. In total, there were 18 video recording sessions for SCA test chambers # 3L0 & 3L1, 12 recording sessions for SCA test chambers # 3R0 & 3R1, 8 recording sessions for SCA test chambers #4L0 & 4L1, and 4 recording sessions for SCA test chambers #4R0 & 4R1. In addition to regular daytime and night-time video recordings, one SCA test chamber (#3L0) was recorded during the day-night and night-day photoperiod changes. This was done to determine if the larvae showed any signs of orientation to light in the absence of gravity, and whether orientation may have been altered during the changes in illumination. A complete detailed schedule of video recording and specimen fixation events can be found in Appendix 3.1.

The ARF was programmed to preserve samples of larvae and algae from each gravity treatment on Flight Days 3, 5, and 7 by injecting 1.1 ml of fixative (15% glutaraldehyde) into the chambers. Video recording did not continue for an SCA test chamber after its contents were fixed. One SCA test chamber from each Main System centrifuge remained unfixed, allowing detailed examination of live specimens upon return of the Shuttle to Kennedy Space Center on May 29, 1996. Table 2.1 outlines the fixation schedule for each of the SCA test chambers.

Table 2.1. Schedule of fixation for SCA test chambers in the Aquatic Research Facility, Space Shuttle Mission STS-77.

Flight Day #	Date	SCA# Fixed, 0g Chamber	SCA# Fixed, 1g Chamber
3	May 22, 1996	4R0	4R1
5	May 24, 1996	4L0	4L1
7	May 26, 1996	3R0	3R1
10 - Return to Earth	May 29, 1996	3L0	3L1

In addition to the ARF hardware that flew aboard Endeavour, a complete back-up ARF system (AMS-2) was used as a Ground Control unit in a replicated experiment. This experiment was conducted in KSC's Orbiter Environmental Simulator (OES), which was capable of simulating environmental parameters prevalent on the Shuttle. Data on Middeck temperature, humidity, and carbon dioxide levels were telemetered down to the OES, which replicated those conditions on a 24-hour delay basis. All procedures that were performed on the Flight Unit ARF were also performed on the Ground Control unit, 24 hours later, thereby providing a strong pseudo-replicated experiment of the 1g conditions prevalent in the Flight Unit ARF. Under the normal gravity conditions present in the OES, however, the "0g" centrifuge provided the 1g conditions for this MS-2 experiment, while the "1g" centrifuge, spinning at 80 rpm, produced a gravitational acceleration that was approximately 1.4g. The video recording schedule for the MS-2 Ground Control was identical to that previously described (see Appendix 3.1) for the MS-1 Flight Unit, except that all operations occurred 24 hours later.

Further control experiments were set up in a lab at Kennedy Space Center's Space Station Processing Facility (SSPF) and at Dalhousie University as well. In the lab control experiments at SSPF, mussel larvae and algae from the same batches used in the ARF Main System 1 and ARF Main System 2 were placed in small uncovered beakers and

tissue culture flasks that simulated the size and volume of the ARF SCA test chambers. The amount of larvae and the concentration of algae was the same as that used in the AMS-1 and AMS-2 experiments. All SSPF lab control containers were held in a Percival temperature-controlled incubator at 12°C, and the photoperiod was the same as that used in both ARF experiments. The control experiment conducted in a lab at Dalhousie University was the so-called "ideal condition control", in that the larvae were grown in a large 1000-litre tank, fed 25 000 cells/ml *Isochrysis galbana* (clone ISO), and the water was changed every 2 days. These conditions have been found to promote optimal growth in *Mytilus edulis* larvae (Jackson, unpub. data). All larvae used in all experiments were spawned on May 13, 1996, the product of six females and 4 males. Broodstock were obtained from Aqua Prime mussel farms, of Ship Harbour, Nova Scotia.

2.2.2 Post-Flight Procedures:

The Space Shuttle Endeavour landed at Kennedy Space Center on schedule at 07:09 EDT on Wednesday May 29, 1996 after a successful 10-day mission. The ARF was delivered to the Space Station Processing Facility (SSPF) at approximately 10:20 EDT, where it was inspected immediately by CSA/NASA officials and engineers from MPB Technologies Inc., the engineering firm that designed and built the ARF. In order to capture video recordings of the larvae as soon as possible after they were re-introduced to a normal gravity environment, the ARF MS-1 Optical Visualisation Unit (OVU) was used to record the behaviour of the larvae in SCA# 3L0 and SCA# 3L1. All SCUs were then removed from the centrifuges and photographed by NASA, and handed over to the science teams for examination.

The MS-1 SCUs were carefully inspected upon delivery to the lab at SSPF. Before the SCUs were opened, the live larvae in SCA test chamber # 3L0 and SCA test chamber # 3L1 were observed under a dissecting microscope and an inverted microscope at several magnifications, and video recordings were made on Hi8 format videotape. These SCA test chambers were then opened and emptied according to the detailed procedures outlined in Appendix 3.4, and the larvae were placed in Petri dishes and counted. The pH of the seawater and algae fractions retrieved from the SCA test chambers was measured, and these samples were preserved in glutaraldehyde and stored at 4°C until the algae cells could be counted at a later date. The larvae were examined in more detail on an inverted microscope at higher magnification, and their images were recorded on videotape for later analysis of their condition and behaviour. Approximately twenty of the larvae were stained with the lipid-specific fluorescent stain Nile Red, as a method of assessing the overall physiological condition of the animals (Jackson, 1993). The specific density of another subsample of larvae was measured by suspending the animals in a calibrated density gradient of sodium metatungstate. In order to observe any changes in behaviour as the animals re-adapted to a normal gravity environment, several larvae were transferred to a clean glass 10ml vial, and were provided with fresh filtered seawater and algae. These larvae were kept alive for several days after their return from orbit, and were regularly monitored and recorded on videotape. The rest of the larvae were fixed in formalin and stored at 4°C for subsequent measurement and analysis.

Larvae in the remaining MS-1 SCA test chambers, which had been preserved in glutaraldehyde during the flight, were carefully removed from the test chambers in accordance with the Appendix 3.4 procedures. Samples of preserved algae and larvae

were collected and stored in labelled vials at 4°C for subsequent counting and analysis. The lab control experiments were terminated, and larval and algal specimens taken and preserved. On May 30, 1996, the MS-2 Ground Control experiment and associated lab controls were terminated, and samples were processed as described above for the MS-1 Flight experiment.

2.2.3 Detailed Pre-Flight and Post-Flight Procedures:

As part of Quality Assurance (QA) protocols required by CSA and NASA, detailed descriptions of the procedures involved in pre-launch lab preparations, including SCU cleaning, fixative block loading, and specimen loading were prepared and are included in Appendix 3.2. These procedures were designed to minimise error and optimise efficiency during these critical operations and were worked out months in advance of the Shuttle Mission, based upon extensive practice and systematic analysis of the optimal process flow. All QA procedures required detailed inspection of each individual step by a CSA or NASA QA inspector. Appendix 3.3 contains details of the pre-launch lab procedures that did not require Quality Assurance inspection by CSA/NASA officials. The detailed procedures followed in the post-flight operations at KSC are included as Appendix 3.4.

CHAPTER 3

Effects of Gravity on Swimming Behaviour and Orientation of Marine Bivalve Larvae

3.1 INTRODUCTION

3.1.1 Overview and Objectives:

Section 1.1 introduced the ecological, physical, and physiological contexts within which gravity is believed to affect marine bivalve larvae and other zooplankters. As a force that draws plankters away from their food sources near the ocean surface, gravity has influenced the evolution of mechanisms and behaviours designed to resist sinking. Paradoxically, it has also been suggested that gravity can be exploited by heavy zooplankters as a means of increasing feeding efficiency. As a conservative physical parameter, gravity can also function as an orientation cue for planktonic organisms as they swim throughout the water column. This portion of the Aquatic Research Facility study was designed to investigate the question of how gravity affects swimming behaviour and orientation mechanisms of marine bivalve larvae.

3.1.2 Tests of the Hypotheses:

The video observation and recording capabilities of the Aquatic Research Facility were employed in experiments designed to test the hypotheses outlined in Section 1.2. Larvae of the blue mussel *Mytilus edulis* were used as a model species for this investigation because their predictable behavioural patterns enable easy assessment of alterations in behaviour that may result from removal of gravitational forces. In addition, *Mytilus edulis* larvae are known to be very hardy under adverse rearing conditions, making them an excellent candidate for use as a "lab rat" in this pioneering experiment. The manner in which these two hypotheses were tested is outlined below.

Helical locomotion is common amongst microscopic aquatic animals, and is nearly universal for organisms smaller than 0.5 mm (Crenshaw, 1993). The larvae of marine bivalves are no exception to this general observation; helical motion is the normal pattern of locomotion for the majority of these plankters (Chia *et al.*, 1984; Young, 1995). As described in detail for representative bivalves such as *Pecten maximus* (Cragg, 1980) and *Cerastoderma edule* (Jonsson *et al.*, 1991), veliger behaviour consists of upward helical swimming interspersed with periods of hovering and bouts of downward swimming or sinking. While swimming, the larva of *Mytilus edulis* rotates about the central axis of the helix in a clockwise direction, producing a left-handed helix in which one side of the larva always faces inwards (see Fig. 3.2.1). The swimming attitude of the larva is such that the heavier hinge area hangs lowermost, with the more buoyant velum pointing upwards. Since the velar cilia beat in a direction perpendicular to the edge of the velum (Chia *et al.*, 1984), the net resultant force of locomotive propulsion will always be upwardly directed. Hypothesis A1 proposes that gravity only has an indirect influence on this mode of locomotion by retarding vertical motion; the rotational and forward propulsive forces that generate the helical swimming pattern function independently of gravity.

Larval bivalve ascent is controlled by altering the height and diameter of the helix via the actions of the velar retractor muscles, and by adjusting translational swimming speed and the rate of rotation (Cragg, 1980). The larva is constantly subjected to the pull of gravity, which restricts its motion so that it is oriented along the vertical dimension. As a result, descent is achieved simply by cessation of ciliary beating, or via controlled downward swimming. Adjustment of the proportion of time spent in upward and

downward locomotion thereby enables the larva to regulate its vertical position within the water column, with inherent implications for feeding, dispersal, and settlement. The flexibility of the veliger behavioural repertoire therefore enables it to contend with the gravity-derived problems that are intrinsic to a planktonic existence.

The direct influences of gravity on larval bivalve locomotion are thus twofold; it is a force that draws larvae away from the surface ocean layers where food may be more abundant, and it acts as a cue for orientation in a complex three-dimensional environment. Based upon what is known about veliger locomotion, some predictions can be made regarding how larval bivalves would behave when gravity is removed from their environment. The helical pattern of swimming would be retained in microgravity, as helical motion is a function of morphology and of propulsive forces that are not directly influenced by gravity (Cragg, 1980). Support for this argument comes from reports of helical motion exhibited by neutrally buoyant plankters (Crenshaw, 1996), and from observations of larval scallop (*Placopecten magellanicus*) behaviour in short-term microgravity exposures on a parabolic aircraft (Jackson, unpub. data). However, as the heavy shell of a bivalve larva is presumed to be an energetically costly impediment to locomotion (Gallager, 1992), larvae that are not restrained by gravity would be expected to be able to swim faster, and have higher helices (Hypothesis A1). Since bivalve larvae are significantly denser than seawater, the pull of gravity tends to overcome any tendency for larvae to move horizontally, thereby limiting their motion to the vertical dimension. Without gravity as a cue for orientation, larvae would be expected to swim in any direction (Hypothesis A2).

The Aquatic Research Facility experiments were designed to test Hypothesis A1 by examining the swimming patterns of mussel larvae swimming in the presence and absence of gravity. The ARF's video subsystem was programmed to automatically record on videotape the behaviour of bivalve larvae at regular intervals throughout the duration of the Space Shuttle mission. Image/motion analysis techniques were used to measure and digitally reconstruct the larval swimming paths, enabling direct comparisons of swimming geometry and behaviour between gravity treatments and over time.

Hypothesis A2 was tested in the ARF experiments by examination of the paths travelled by mussel larvae in both the microgravity and normal gravity environments. The larval swimming trajectories were reconstructed using digital imaging methodologies, and the directions in which larvae travelled were measured and compared between gravity treatments. Circular statistics tests were used to determine if mussel larvae exhibited any preferred direction of motion in the absence of gravity. The results of these analyses were expected to provide insight into the orientational cues used by swimming zooplankton.

3.2 MATERIALS AND METHODS

3.2.1 Post-Flight Procedures:

After the flight, the original Hi8 videotapes recorded by the ARF MS-1 OVU during the STS-77 spaceflight mission were copied onto broadcast-quality high-resolution Betacam SP videotape, to ensure that no video quality would be lost when making subsequent copies. Since the video/image analysis equipment (see Section 3.2.2) utilises a Hi8 format VCR, a copy of each MS-1 Flight Unit tape was made onto Hi8 videotape from the Betacam SP "masters". These tapes were then reviewed and a detailed index was made of all events related to this experiment throughout the mission, that was cross-referenced to the Hi8 videotape time code and the Mission Elapsed Time (MET). The sections of tape relevant to this experiment were then subjected to motion analysis procedures in an attempt to gain insight into the response of the mussel larvae to the absence of gravity.

Review of the ARF videotapes revealed that in all of the video recording sessions for the SCA test chambers in the MS-1 1g centrifuge, and in both MS-2 centrifuges, video quality was poor. It is believed that this was the result of electrical noise generated by malfunctioning slip ring assemblies that carried the video signal on those units. As a result, no meaningful data could be extracted from those portions of the videotapes that included recordings of the larvae swimming in a unit gravity environment, and data on larval swimming mechanics in normal gravity had to be obtained from recordings of a previous ground-based study involving mussel larvae of a size, density, and age similar to those used in the ARF. In that experiment a Pulnix TM-7EX monochrome camera was

fitted with a 75 mm lens and 45 mm extension tubes, and was mounted 15 cm in front of a 250 ml tissue culture flask that functioned as an observation chamber. A 25 watt halogen lamp covered with a red 650nm filter was placed 100 cm directly behind the observation chamber, and a frosted glass diffuser located 48 cm from the chamber assisted in providing even illumination. A Hi8 videotape recorder (Sony EVO-9650) was used to record larval swimming behaviour, and motion analyses were performed in a manner similar to those used for the videotapes from the ARF experiment (see section 3.2.2).

3.2.2 Motion Analysis:

To facilitate interpretation of the ARF Mission videotapes, a PC-based motion analysis system was built using off-the-shelf components and Optimas® version 5.2 image analysis software. The original system was based upon a Pentium 90 computer running Microsoft Windows 3.11 with 48 MB RAM and a 17" Sony Trinitron monitor, but this was later upgraded to a Windows NT workstation with a Pentium Pro 200 CPU, 128 MB RAM, and Optimas version 6.1. An Imaging Technology (Bedford, MA, USA) IC-PCI frame grabber with AM-CLR colour acquisition module and 4 MB VRAM was used to digitise the video signals in real-time (30 frames/second) at a 640 x 480 resolution, and a Number Nine 9FX Motion 771 4MB VRAM VGA board was used for video display. A Sony EVO-9650 Hi8 VCR with on-board digital frame memory, time code generator, and RS-232 serial port was interfaced directly to the computer workstation. In this configuration, the VCR was under the control of the computer, and Optimas ALI macro code was written to automate motion analysis tasks.

The Optimas macro started the VCR in playback mode at the start of each video session, adjusted image quality, and stored images at a rate of 3 frames per second into RAM. Successive frames were arithmetically added to the preceding ones, so that a multiple-exposure type image was created that illustrated the motion patterns of all moving targets over a 30 second section of videotape. These images were then stored to disk in TIFF format, along with information regarding the start and stop time codes, videotape and video session number, sampling frequency, etc. Using this procedure, each 3-4 minute recording session was covered by approximately 6-10 individual summary images. All of these images could then be added together successively in order to reconstruct the entire video session; as each summary image was added to the previous one, an indication of the direction of each individual track was revealed. Track direction was confirmed by reviewing the videotape. The actual start and stop times of each individual larval track as they entered or moved out of the camera's field of view was also determined by videotape review. An example of an aggregate summary image representing an entire video session is shown in Fig. 3.2.2.

After compilation of the summary and aggregate images, the tracks of larvae swimming approximately parallel to the camera's plane of focus were traced using Optimas image analysis software (see Fig. 3.2.3 for an example). The total 2-dimensional length of these tracks was measured as the gross displacement, and net displacement was defined as the distance between the starting and ending points of each track. The general direction of larval locomotion was measured using the horizontal X-axis as the 0° reference line. The height, diameter, and pitch angle of a single helix that was considered to be representative of each track were also measured (See Fig. 3.2.1).

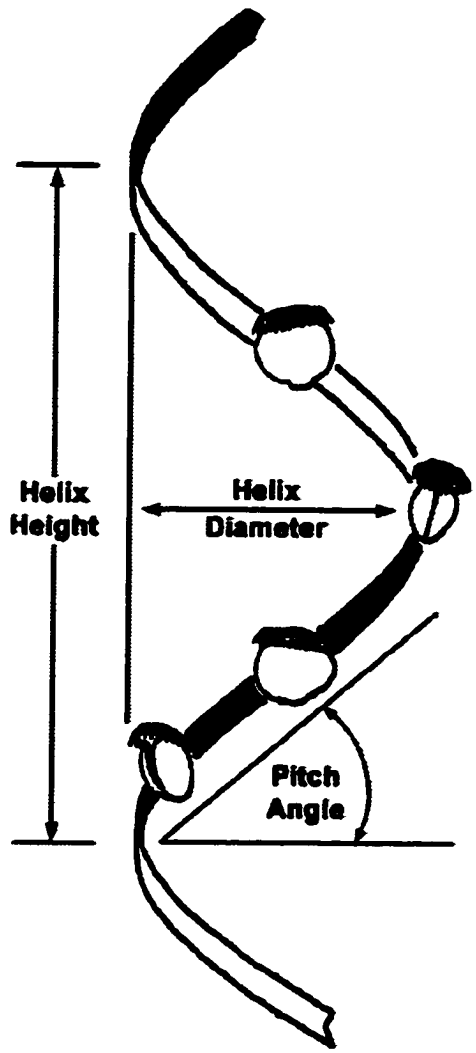

Fig. 3.2.1. Diagram illustrating the helix parameters that were measured for each larval track (Adapted from Cragg, 1980).

Forward swimming velocity was calculated as a means of comparing the swimming velocities of mussel larvae in microgravity with data on vertical swimming velocities of bivalve larvae under normal, earthbound conditions. Since the larvae in microgravity swam in different directions and often changed direction as they swam, forward swimming velocity was measured using the distance travelled along the axis of the helical trajectory.

The true swimming velocity of the larvae as they travelled along the 3-D helical trajectory was calculated according to Cragg (1980) as:

$$V = \frac{k\sqrt{(H^2 + (\pi D)^2)}}{HT} \qquad \text{(eq. 3.2.1)}$$

where V is defined by Blake and Sleigh (1974) as "instantaneous linear velocity", k is the vertical or forward distance travelled during time T, H is the height of one helical spiral, and D is helix diameter.

The net-to-gross-displacement ratios (NGDR) were also calculated from these data. NGDR values were used as an index of track complexity; values close to 1 indicate a relatively straight path, while smaller values represent tracks that are more circuitous (Buskey and Stoecker, 1988; Villanueva *et al.*, 1996). When applied to the helical motion of larval bivalves, NGDR values closer to zero indicate that horizontal motion predominates over vertical movement (Gallager, 1992). For final data presentation, the X,Y coordinates of each larval track were plotted in a Microsoft Excel spreadsheet chart, and the track directions were indicated (see Fig. 3.2.4. for an example).

Fig. 3.2.2. Processed aggregate image summarising the tracks of 16 mussel larvae (*Mytilus edulis*) swimming in microgravity during the Day 1 Day video session in SCA #3L0. In this example, eight individual summary images are combined to illustrate the motion of all moving larvae within the entire 236.6 second video recording session. This image includes 852 individual frames of video.

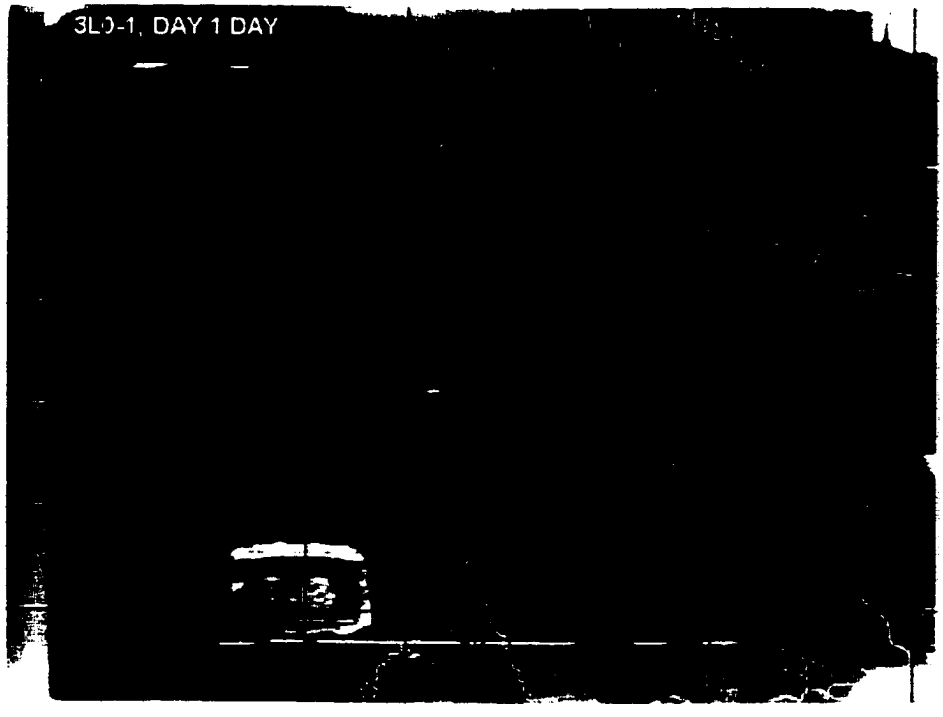

Fig. 3.2.3. The same aggregate image as that shown in Fig. 3.2.1, with grid overlays, and larval paths traced using Optimas image analysis software. Larval track parameters measured included gross and net displacement, general swimming direction, and helix pitch angle, height, and diameter.

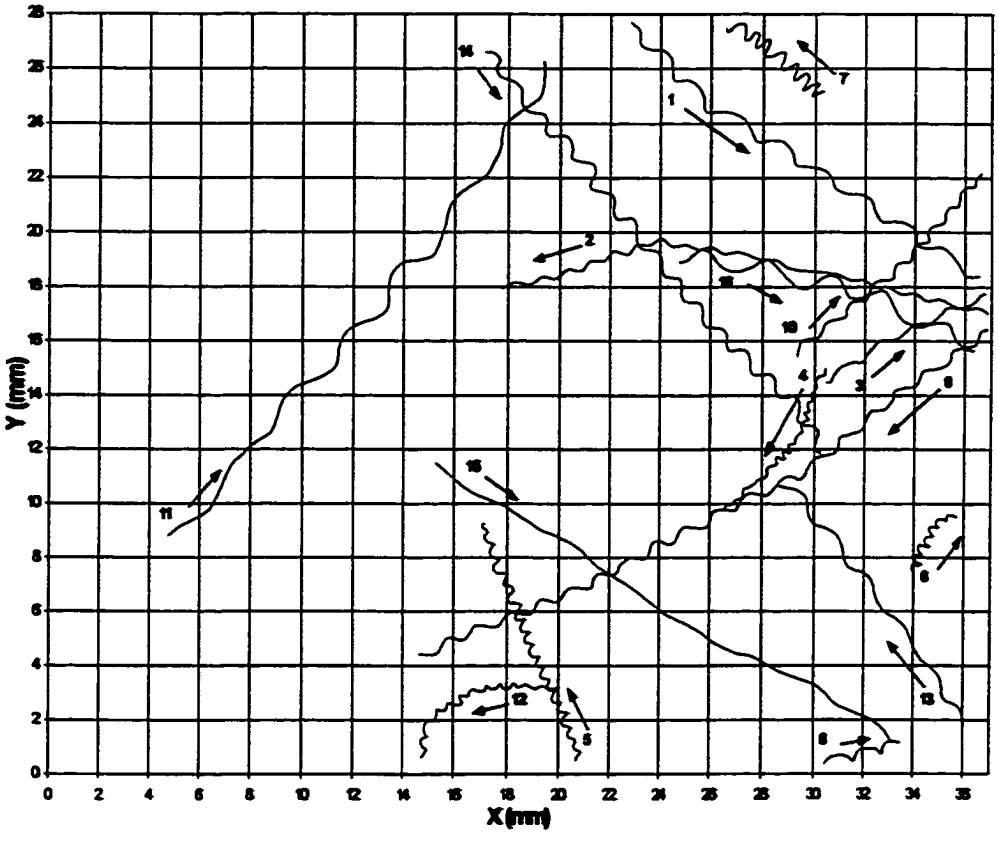

Fig. 3.2.4. An example of the data collected from the sample image shown in Fig 3.2.1 in its final form for data presentation. X, Y coordinates from the Optimas line object tracings were exported to a spreadsheet package, plotted, and track directions indicated.

3.2.3 Data Analysis:

Interpretation of the larval swimming behaviour in the microgravity experiment included creation of circular scatterplots of the directional data, in which the general direction of each larval track was displayed as a point on the circumference of a unit circle. SYSTAT version 8.0 was employed to create these plots. This type of diagram provides a good visual representation of the distribution of the various swimming directions of the larvae, and is acknowledged as the preferred manner in which circular data should be presented (Zar, 1984). For each set of circular directional data, a quantity known as the mean vector length (r), an indicator of the degree of angular dispersion, was calculated as:

$$r = \sqrt{X^2 + Y^2} \qquad \text{(eq. 3.2.2)}$$

where X and Y are the rectangular coordinates of the mean angle (Batschelet, 1981; Zar, 1984):

$$X = \frac{\sum_{i=1}^{n} \cos a_i}{n} \qquad \text{(eq. 3.2.3)}$$

$$Y = \frac{\sum_{i=1}^{n} \sin a_i}{n} \qquad \text{(eq. 3.2.4)}$$

The value of r ranges between 0, in which the dispersion of angular data is so great that a mean angle cannot be described, and 1, indicating that all data are concentrated in the

same direction. The value of the sample mean angle, $\bar{a}$, was determined as the angle having the following sine, cosine, and tangent:

$$\cos \bar{a} = \frac{X}{r} \qquad \text{(eq. 3.2.5)}$$

$$\sin \bar{a} = \frac{Y}{r} \qquad \text{(eq. 3.2.6)}$$

$$\tan \bar{a} = \frac{Y}{X} \qquad \text{(eq. 3.2.7)}$$

The significance of the value of $\bar{a}$ was tested using the Rayleigh Test, as described below by equation 3.2.9. The values of r and $\bar{a}$ were then plotted on the circular scatterplots, providing a visual indication of the degree of angular dispersion. Longer mean vector lengths (r) indicate a greater tendency towards a preferred swimming direction by those larvae in the sample. The mean angular deviation (analogous to the standard deviation of linear scale data) for larval track directions from each video session was calculated as:

$$s = \frac{180°}{\pi}\sqrt{2(1-r)} \qquad \text{(eq. 3.2.8)}$$

Finally, the Rayleigh Test was used to determine if the distribution of the general track directions of the larvae was uniform, or if they followed a preferred mean direction. This test determines the minimum size that a sample r must be in order to confidently indicate a nonuniform population distribution of angular data. Rayleigh's z statistic was calculated as:

$$z = nr^2 \qquad \text{(eq. 3.2.9)}$$

Critical values of $z_{\alpha,n}$ can be found in tables in Batschelet (1981) or Zar (1984). If the null hypothesis of no mean direction was rejected by Rayleigh's Test, then it could be concluded that the larvae swam in a preferred direction, and that direction was described by the value of $\bar{a}$.

The general track direction data from each video session for each SCA test chamber in the microgravity treatments were subjected to these analyses. In addition, data from all SCAs for each recording session were pooled together, circular scatterplots created, and descriptive statistics calculated in the same manner. Data from all SCAs over all video sessions were also pooled together, binned in groups of 15°, and a circular histogram plotted using SYSTAT version 8.0.

3.3 RESULTS

3.3.1 Larval Bivalve Locomotion in Microgravity

Soon after the landing of the Shuttle on May 29, 1996, detailed observations were made of the swimming behaviour of mussel larvae in the SCA test chambers before the containers were opened and emptied. In general, most larvae that had spent the previous ten days in microgravity exhibited normal behaviour, in that they were observed to swim in helices in both upwards and downwards directions. Two larvae were seen to interrupt normal swimming with bouts of a peculiar tumbling behaviour when they were sitting on the bottom, but these episodes were brief and infrequent.

General examination of the videotape records of larval behaviour in the ARF MS-1 flight experiment revealed that most mussel larvae were active during their exposure to a microgravity environment, with the exception of larvae in SCA test chamber #4R0. In this chamber, only three larvae were swimming in the first video recording session (Day 1 Day) and no larvae were observed to be swimming in subsequent recording sessions. Post-flight examination of the larvae that were fixed in this chamber on Flight Day 3 revealed that many of these larvae were either dead (20%) or were considered to be in poor condition (29%); only 51% of the larvae were in good condition at the time of fixation. These results raise the possibility that the larvae in SCA test chamber #4R0 had been adversely affected by a noxious substance to the extent that their mobility was impaired, and mortality and injurious sublethal impacts were increased (Section 4.4.3.5).

The reconstructed tracks of microgravity-reared mussel larvae swimming during all eighteen video recording sessions are illustrated in Appendix 1 Figs. A1.1 to A1.38,

and trajectory measurement data pertaining to these tracks are recorded in Appendix 1 Tables A1.1 to A1.38. The figures represent the tracks of the larvae as they swam across the video camera's field of view, which measured 37 mm wide by 28 mm high. The ARF Main System illumination LEDs were located at the top of each SCA test chamber, providing a downwardly directed light source. These figures and tables are organized chronologically according to the Flight Day (and time of day) on which the video observations took place; SCA test chambers that were observed on Flight Day One are listed first, followed by Flight Day Two, etc. Table 3.3.1 summarizes the mean track measurement data compiled for mussel larvae swimming in the SCA test chambers during all video recording sessions.

In general, mussel larvae in microgravity continued to swim in a helical pattern, albeit with some variations. While the majority of larvae swam along a straight line, many larvae often changed direction by a few degrees, and others changed their swimming direction dramatically. These alterations in swimming direction were not observed when larvae were swimming in a normal gravity environment, where larvae typically swim straight upwards in a helix and accomplish downwards movement by either passive sinking or helical swimming (see Section 3.3.2). A summary of the percentage of mussel larvae that changed direction during video recording sessions in microgravity is provided in Table 3.3.4. While no general pattern could be observed over the course of the experiment, the percentage of larvae changing swimming direction exceeded 40% in most samples.

Table 3.3.1. Summary of mean trajectory measurement data for *Mytilus edulis* larvae swimming in microgravity, from all video recording sessions.

SCA #	VIDEO SESSION NUMBER	VIDEO SESSION TITLE	HELIX HEIGHT (mm)	HELIX DIAMETER (mm)	HELIX PITCH ANGLE	TIME (s)	ANGULAR VELOCITY (rad/s)	LINEAR VELOCITY (mm/s)	FORWARD VELOCITY (mm/s)	NGDR
3L0-1	1	Day 1 - DAY	1.39	0.42	45	65.9	1.12	0.32	0.22	0.75
3R0-1	1	Day 1 - DAY	1.98	0.57	52	55.3	1.13	0.41	0.32	0.82
4L0-1	1	Day 1 - DAY	2.02	0.45	55	60.8	1.39	0.47	0.38	0.80
3L0-2	2	Day 2 - NIGHT	1.46	0.41	48	86.1	0.86	0.28	0.17	0.81
3R0-2	2	Day 2 - NIGHT	2.25	0.59	50	64.0	1.09	0.45	0.35	0.80
4L0-2	2	Day 2 - NIGHT	2.07	0.50	54	48.9	1.37	0.47	0.39	0.85
3L0-3	3	Day 2 - DAY	1.21	0.41	48	111.7	1.02	0.29	0.18	0.67
3R0-3	3	Day 2 - DAY	2.70	0.60	60	46.9	1.04	0.46	0.38	0.82
4L0-3	3	Day 2 - DAY	1.61	0.48	50	50.7	1.45	0.48	0.37	0.79
3L0-4	4	Day 3 - NIGHT	1.79	0.53	58	91.2	0.88	0.29	0.21	0.70
3R0-4	4	Day 3 - NIGHT	2.39	0.56	47	57.0	1.01	0.45	0.35	0.78
4L0-4	4	Day 3 - NIGHT	2.12	0.52	56	41.4	1.35	0.51	0.40	0.82
3L0-5	5	Day 3 - DAY	2.00	0.57	55	164.4	1.12	0.48	0.36	0.84
3R0-5	5	Day 3 - DAY	1.93	0.46	61	40.9	1.35	0.48	0.38	0.86
4L0-5	5	Day 3 - DAY	2.15	0.63	52	57.2	1.21	0.51	0.37	0.71
3L0-6	6	Day 4 - NIGHT	1.05	0.47	32	106.1	1.45	0.30	0.16	0.53
3R0-6	6	Day 4 - NIGHT	2.35	0.67	52	55.4	1.15	0.55	0.39	0.77
4L0-6	6	Day 4 - NIGHT	2.34	0.62	52	79.0	1.02	0.43	0.29	0.80
3L0-7	7	Day 4 - DAY	1.74	0.53	44	129.7	0.98	0.34	0.21	0.70
3R0-7	7	Day 4 - DAY	2.17	0.72	46	35.4	1.03	0.47	0.33	0.76
4L0-7	7	Day 4 - DAY	2.45	0.85	48	53.0	1.00	0.50	0.35	0.79
3L0-8	8	Day 5 - NIGHT	1.33	0.46	42	82.0	1.18	0.30	0.20	0.67
3R0-8	8	Day 5 - NIGHT	2.29	0.52	57	58.5	0.90	0.36	0.29	0.80
4L0-8	8	Day 5 - NIGHT	2.39	0.64	47	80.0	1.78	0.60	0.31	0.76
3L0-9	9	Day 5 - DAY	2.36	0.60	56	61.3	0.72	0.36	0.27	0.77
3R0-9	9	Day 5 - DAY	2.86	0.78	49	59.7	0.9	0.46	0.34	0.81
3L0-10	10	Day 6 - NIGHT	1.56	0.48	47	77.9	1.15	0.36	0.25	0.77
3R0-10	10	Day 6 - NIGHT	2.75	0.66	54	57.4	0.87	0.44	0.35	0.80
3L0-11	11	Day 6 - DAY	1.86	0.54	50	83.8	1.02	0.37	0.26	0.72
3R0-11	11	Day 6 - DAY	2.33	0.73	50	57.3	0.87	0.44	0.32	0.75
3L0-12	12	Day 7 - NIGHT	2.16	0.49	61	76.7	0.95	0.38	0.29	0.78
3R0-12	12	Day 7 - NIGHT	3.39	0.89	56	59.1	0.74	0.43	0.34	0.81
3L0-13	13	Day 7 - DAY	2.38	0.66	54	74.6	0.85	0.38	0.28	0.82
3L0-14	14	Day 8 - NIGHT	1.97	0.54	51	66.3	0.85	0.33	0.23	0.82
3L0-15	15	Day 8 - DAY	1.52	0.58	50	64.4	0.89	0.30	0.20	0.69
3L0-16	16	Day 9 - NIGHT	1.66	0.56	51	75.7	0.86	0.33	0.22	0.76
3L0-17	17	Day 9 - DAY	1.52	0.56	46	71.3	0.90	0.35	0.19	0.66
3L0-18	18	Day 10 - NIGHT	2.09	0.55	51	56.7	0.72	0.33	0.23	0.82

Table 3.3.2. Summary of mean trajectory measurement data for *Mytilus edulis* larvae swimming in microgravity. Data from all video recording sessions are pooled together separately for each SCA test chamber, and also for the total dataset including measurements from all chambers.

SCA #		HELIX HEIGHT (mm)	HELIX DIAMETER (mm)	HELIX PITCH ANGLE (°)	NGDR	FORWARD VELOCITY (mm/s)	ANGULAR VELOCITY (rad/s)	LINEAR VELOCITY (mm/s)
3L0	Mean	1.75	0.52	49.84	0.74	0.23	0.96	0.34
	s.d.	0.89	0.22	16.57	0.20	0.12	0.40	0.11
	N	190	197	189	202	208	151	159
3R0	Mean	2.46	0.64	54.14	0.80	0.35	1.01	0.45
	s.d.	1.28	0.37	23.34	0.18	0.13	0.42	0.13
	N	252	253	251	270	268	223	229
4L0	Mean	2.05	0.54	54.65	0.80	0.37	1.35	0.49
	s.d.	0.97	0.33	27.13	0.18	0.14	0.61	0.14
	N	171	172	170	196	195	149	164
ALL SCAs	Mean	2.13	0.57	51.92	0.78	0.32	1.09	0.43
	s.d.	1.13	0.32	16.38	0.78	0.14	0.50	0.14
	N	613	622	610	668	671	523	552

Table 3.3.3. The influence of light on swimming mechanics of *Mytilus edulis* larvae swimming in microgravity. Data from all Daytime and Night-time video recording sessions are reported separately for each SCA test chamber, and for all SCAs pooled together.

SCA #	TIME OF DAY		HELIX HEIGHT (mm)	HELIX DIAMETER (mm)	HELIX PITCH ANGLE (°)	NGDR	FORWARD VELOCITY (mm/s)	ANGULAR VELOCITY (rad/s)	LINEAR VELOCITY (mm/s)
3L0	DAY	Mean	1.79	0.54	49.16	0.73	0.23	0.96	0.35
		s.d.	0.90	0.23	13.15	0.20	0.12	0.42	0.11
		N	88	90	88	93	94	69	73
	NIGHT	Mean	1.72	0.50	49.54	0.75	0.22	0.96	0.33
		s.d.	0.88	0.20	15.86	0.20	0.12	0.39	0.11
		N	102	107	101	109	114	82	86
3R0	DAY	Mean	2.36	0.64	53.39	0.81	0.35	1.06	0.46
		s.d.	1.27	0.39	17.02	0.18	0.13	0.47	0.12
		N	128	129	127	137	135	117	120
	NIGHT	Mean	2.56	0.64	52.73	0.80	0.35	0.96	0.44
		s.d.	1.29	0.34	18.05	0.19	0.13	0.36	0.14
		N	124	124	124	133	133	106	109
4L0	DAY	Mean	1.93	0.54	51.59	0.77	0.37	1.35	0.49
		s.d.	0.92	0.34	17.35	0.21	0.13	0.56	0.13
		N	86	86	85	99	99	77	86
	NIGHT	Mean	2.17	0.54	54.54	0.81	0.37	1.36	0.49
		s.d.	1.02	0.33	15.13	0.14	0.14	0.66	0.16
		N	85	86	85	97	96	72	78
ALL SCAs	DAY	Mean	2.06	0.58	51.64	0.78	0.32	1.12	0.44
		s.d.	1.10	0.34	16.13	0.19	0.14	0.51	0.13
		N	302	305	300	329	328	263	279
	NIGHT	Mean	2.18	0.57	52.18	0.79	0.31	1.07	0.42
		s.d.	1.15	0.30	16.65	0.18	0.15	0.50	0.15
		N	311	317	310	339	343	280	273

Table 3.3.4. Percentage of mussel larvae (*Mytilus edulis*) changing swimming direction, in microgravity environment (Flight Unit MS-1) during each video recording session, ARF-1 Mission, May 1996.

SCA #	VIDEO SESSION #	% LARVAE CHANGING DIRECTION
3L0-1	Day 1 - DAY	19
3R0-1	Day 1 - DAY	47
4L0-1	Day 1 - DAY	54
3L0-2	Day 2 - NIGHT	38
3R0-2	Day 2 - NIGHT	52
4L0-2	Day 2 - NIGHT	43
3L0-3	Day 2 - DAY	50
3R0-3	Day 2 - DAY	43
4L0-3	Day 2 - DAY	48
3L0-4	Day 3 - NIGHT	63
3R0-4	Day 3 - NIGHT	64
4L0-4	Day 3 - NIGHT	43
3L0-5	Day 3 - DAY	0
3R0-5	Day 3 - DAY	33
4L0-5	Day 3 - DAY	70
3L0-6	Day 4 - NIGHT	50
3R0-6	Day 4 - NIGHT	55
4L0-6	Day 4 - NIGHT	60
3L0-7	Day 4 - DAY	50
3R0-7	Day 4 - DAY	29
4L0-7	Day 4 - DAY	38
3L0-8	Day 5 - NIGHT	33
3R0-8	Day 5 - NIGHT	45
4L0-8	Day 5 - NIGHT	50
3L0-9	Day 5 - DAY	25
3R0-9	Day 5 - DAY	57
3L0-10	Day 6 - NIGHT	37
3R0-10	Day 6 - NIGHT	70
3L0-11	Day 6 - DAY	63
3R0-11	Day 6 - DAY	56
3L0-12	Day 7 - NIGHT	40
3R0-12	Day 7 - NIGHT	42
3L0-13	Day 7 - DAY	46
3L0-14	Day 8 - NIGHT	33
3L0-15	Day 8 - DAY	33
3L0-16	Day 9 - NIGHT	50
3L0-17	Day 9 - DAY	50
3L0-18	Day 10 - NIGHT	9

3.3.1.1 Summary of NGDR Data

The ratio of net displacement to gross displacement was calculated as an index of the complexity of the paths travelled by the mussel larvae swimming in microgravity. The mean net-to-gross displacement ratios (NGDRs) for the larval tracks from each microgravity SCA test chamber are plotted against sample time in Fig. 3.3.1. A scatterplot of individual NGDR values for all 668 larval tracks is shown in Fig. 3.3.2, while Figs. 3.3.3 - 3.3.5 show scatterplots of the NGDR measurements from larval tracks in each of the three SCA test chambers. Linear regression lines and equations are indicated for all four scatterplots. Analysis of variance testing of these regression equations revealed that the slopes were not significantly different from zero for all datasets, indicating that there were no changes in net-to-gross displacement ratio of the larval tracks throughout the microgravity experiment. Larval age and duration of space exposure did not affect the general shape of the larval tracks.

After pooling the data from all video sessions for each SCA test chamber together (see Table 3.3.2), an ANOVA model was used to compare the mean NGDR values amongst the three SCAs. No significant differences in mean NGDR were found between larvae from SCA# 3R0 (0.80) and SCA# 4L0 (0.80); however, the mean NGDR for larvae from SCA#3L0 (0.74) was significantly lower than that measured for larval tracks from the other two SCAs ($P < 0.05$). The mean NGDR for all 668 tracks measured in this study was 0.78 (standard error = 0.03).

To assess the effect of light upon NGDR amongst larvae reared in microgravity, NGDR values were compared between the Daytime and Night-time video recording

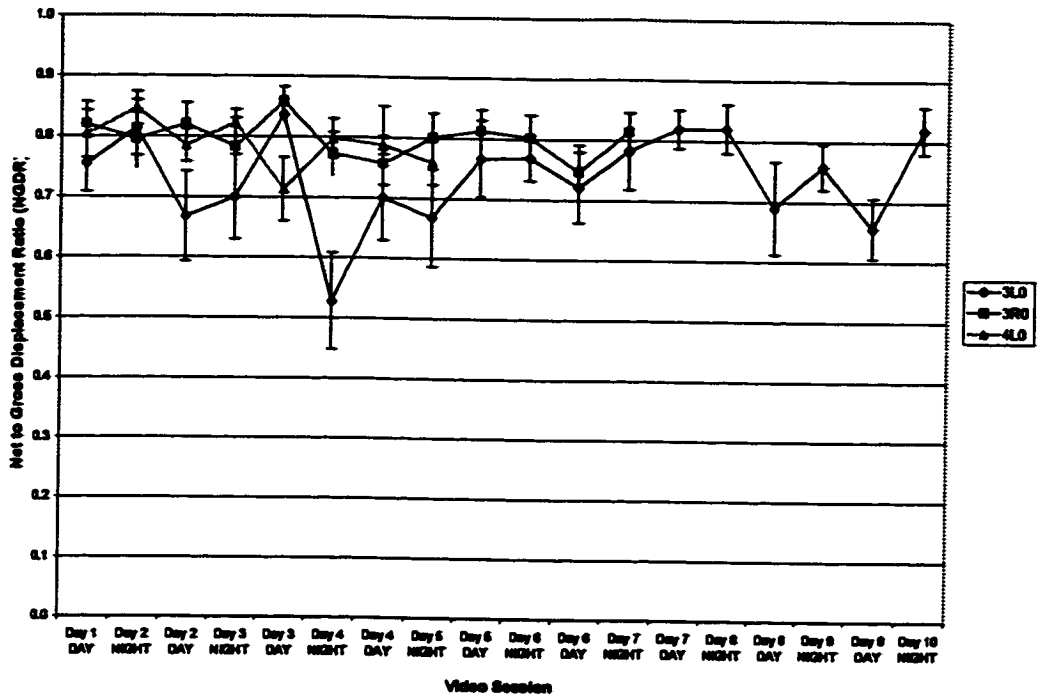

Fig. 3.3.1. Summary of Net-to-Gross Displacement Ratio (NGDR) data for tracks of microgravity-reared larvae from all video recording sessions for each SCA test chamber in the ARF MS-1, May 19-29, 1996. Values are plotted as mean NGDR ± standard error.

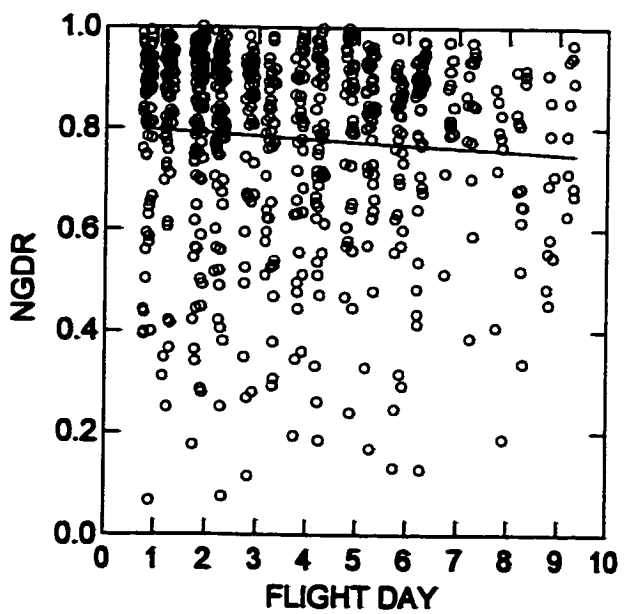

Fig. 3.3.2. Scatterplot of Net-to-Gross Displacement Ratio (NGDR) data for tracks of microgravity-reared larvae from all video recording sessions for all SCA test chambers pooled together. NGDR = 0.803 - 0.006 x Flight Day. N=668, $r^2 = 0.005$. Slope = 0 ($P > 0.05$).

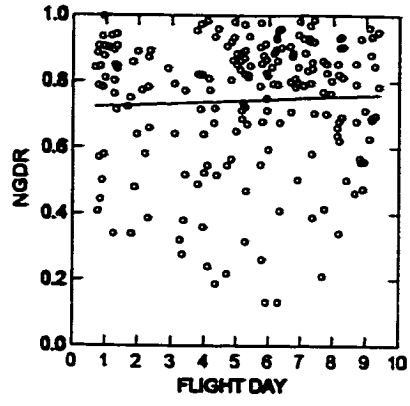

Fig. 3.3.3. Scatterplot of NGDR measurements from larval tracks in SCA test chamber 3L0. NGDR = 0.722 + 0.004 x Flight Day. N=202, r^2 = 0.003. Slope = 0 ($P > 0.05$).

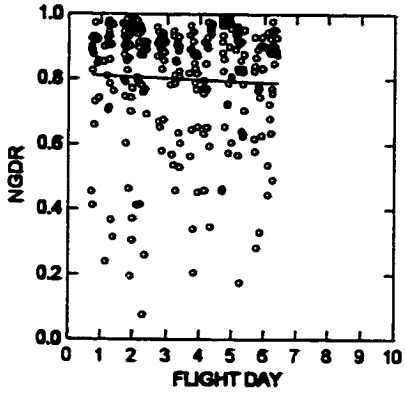

Fig. 3.3.4. Scatterplot of NGDR measurements from larval tracks in SCA test chamber 3R0. NGDR = 0.814 - 0.004 x Flight Day. N=270, r^2 = 0.001. Slope = 0 ($P > 0.05$).

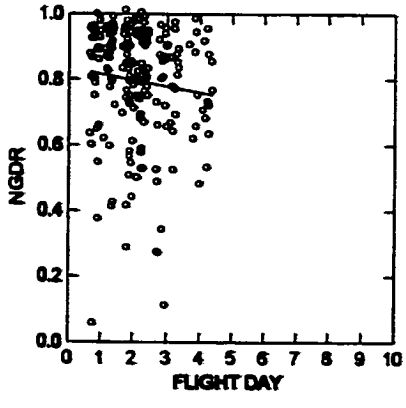

Fig. 3.3.5. Scatterplot of NGDR measurements from larval tracks in SCA test chamber 4L0. NGDR = 0.839 - 0.020 x Flight Day. N=196, r^2 = 0.012. Slope = 0 ($P > 0.05$).

sessions. Table 3.3.3 shows that the mean NGDR values for the larval tracks observed at night were very similar to those recorded during the daytime video sessions; two-sample t-tests confirmed that there were no significant differences between the two datasets ($P > 0.05$). Using data pooled together from all three SCAs (see Table 3.3.3), two-sample t-tests revealed that the time of day in which the larvae were observed did not significantly affect the NGDR ($P > 0.05$). The shape of the larval tracks exhibited a similar degree of complexity regardless of the presence of a light source.

3.3.1.2 Summary of Helix Diameter Data

Fig. 3.3.6 illustrates the changes in mean helix diameter throughout the 10-day duration of the microgravity experiment for larvae from all three SCA test chambers. Scatterplots and regression lines for the helix diameter measurements from each individual SCA are shown in Figs. 3.3.8 to 3.3.10. ANOVA testing of these regressions revealed that the slopes of all three regression lines were significantly greater than zero ($P < 0.05$). Among the larvae in SCA# 3L0, helix diameter increased at an average rate of 0.021 mm·day^{-1}, while the diameter of larval track helices in SCA# 3R0 and SCA# 4L0 increased at rates of 0.045 mm·day^{-1} and 0.078 mm·day^{-1} respectively. Pooling together the helix diameter measurements from all SCA test chambers produced the scatterplot shown in Fig. 3.3.7, which shows an average increase in helix diameter of 0.02 mm·day^{-1}. The slope of this regression equation is significantly greater than zero ($P < 0.05$), indicating that the larvae reared in microgravity altered their behaviour over the course of the experiment by increasing the diameter of the helices as they swam.

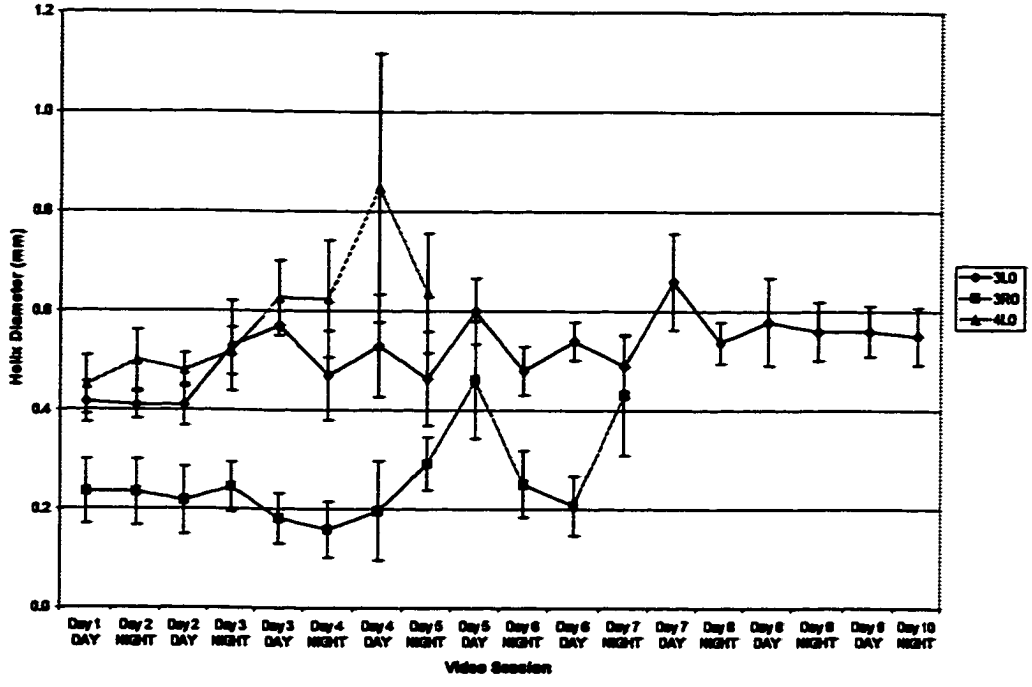

Fig. 3.3.6. Summary of Helix Diameter data for tracks of microgravity-reared larvae from all video recording sessions for each SCA test chamber in the ARF MS-1, May 19-29, 1996. Values are plotted as mean helix diameter ± standard error.

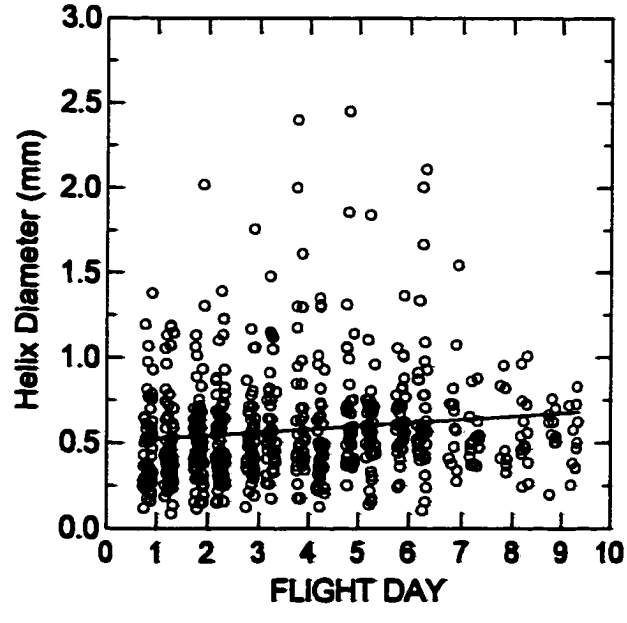

Fig. 3.3.7. Scatterplot of Helix Diameter data for tracks of microgravity-reared larvae from all video recording sessions for all SCA test chambers pooled together. Helix Diameter = 0.503 + 0.019 x Flight Day. N=622, $r^2 = 0.016$. Slope > 0 ($P < 0.05$).

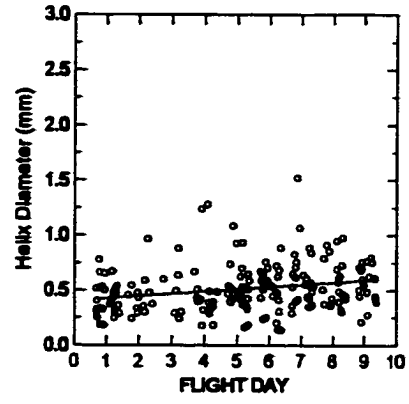

Fig. 3.3.8. Scatterplot of Helix Diameter measurements from larval tracks in SCA test chamber 3L0. Helix Diameter = 0.407 + 0.021 x Flight Day. N=197, $r^2 = 0.060$. Slope > 0 ($P < 0.05$).

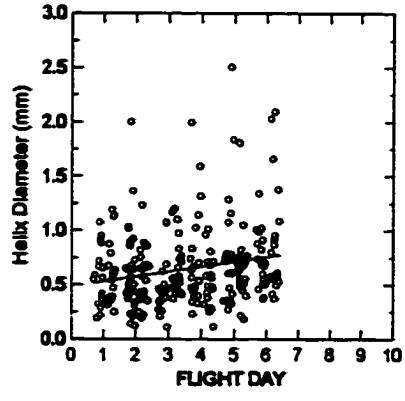

Fig. 3.3.9. Scatterplot of Helix Diameter measurements from larval tracks in SCA test chamber 3R0. Helix Diameter = 0.484 + 0.045 x Flight Day. N=253, $r^2 = 0.043$. Slope > 0 ($P < 0.05$).

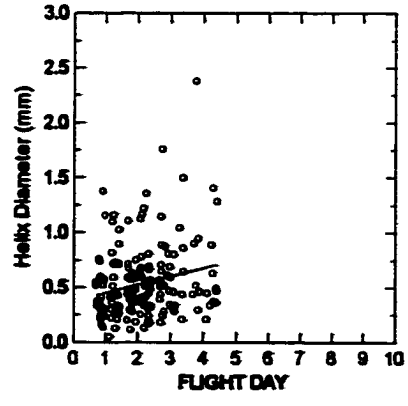

Fig. 3.3.10. Scatterplot of Helix Diameter measurements from larval tracks in SCA test chamber 4L0. Helix Diameter = 0.373 + 0.078 x Flight Day. N=172, $r^2 = 0.052$. Slope > 0 ($P < 0.05$).

Table 3.3.2 includes the mean helix diameter data for each of the three SCA test chambers that resulted from pooling together the measurements from all video recording sessions. No significant differences were detected by ANOVA between mean helix diameter measurements from SCA# 3L0 (0.52 mm) and SCA# 4L0 (0.54 mm), but larvae from SCA #3R0 had a significantly larger mean helix diameter (0.64 mm) than those from the other two SCA test chambers. After pooling together the helix diameter data from all 622 larval tracks measured in the microgravity experiment, a mean value of 0.57 mm was obtained.

Mean helix diameter of larval tracks observed during the Daytime and Night-time video recording sessions were compared as a method of determining if the presence of light affected larval swimming behaviour. Table 3.3.3 summarises data from each individual SCA, as well as a pooled total dataset comprising measurements from all daytime and night-time video recording sessions. The mean helix diameters from both daytime and night-time sessions were very similar, and a series of two-sample t-tests confirmed that there were no significant differences in helix diameter that could be attributed to the presence of light in the test chambers.

3.3.1.3 Summary of Helix Height Data

Changes in mean helix height measured in each of the three SCA test chambers throughout the microgravity experiment are illustrated in Fig. 3.3.11. For each individual SCA, Figs. 3.3.13 to -3.3.15 illustrate scatterplots and linear regressions for helix height measurements of the larval tracks from all video recording sessions. Among the larvae in SCA# 3L0, helix height increased at a rate of 0.065 mm·day^{-1}, and the height of larval

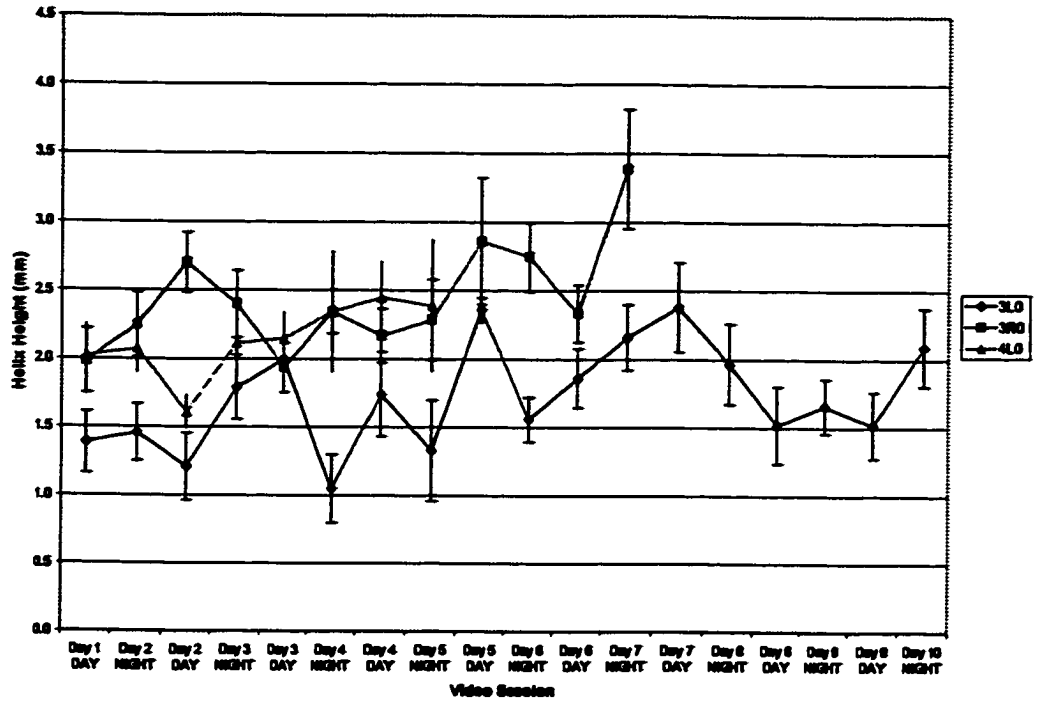

Fig. 3.3.11. Summary of Helix Height data for tracks of microgravity-reared larvae from all video recording sessions for each SCA test chamber in the ARF MS-1, May 19-29, 1996. Values are plotted as mean helix height ± standard error.

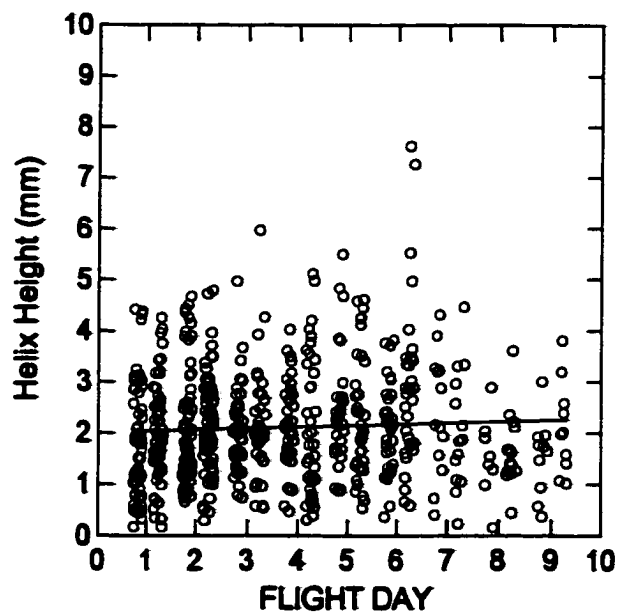

Fig. 3.3.12. Scatterplot of Helix Height data for tracks of microgravity-reared larvae from all video recording sessions for all SCA test chambers pooled together. Helix Diameter = 0.503 + 0.019 x Flight Day. N=613, $r^2 = 0.003$. Slope = 0 ($P > 0.05$).

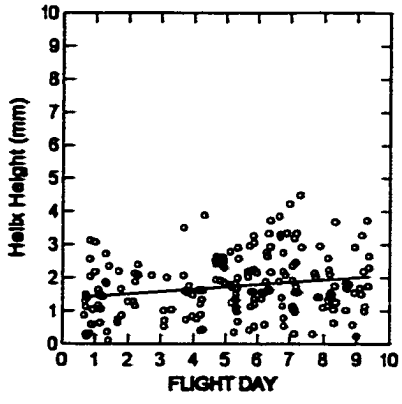

Fig. 3.3.13. Scatterplot of Helix Height measurements from larval tracks in SCA test chamber 3L0. Helix Height = 1.408 + 0.065 x Flight Day. N=190, r^2 = 0.036. Slope > 0 ($P < 0.05$).

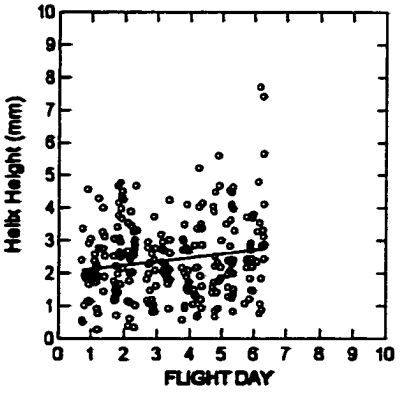

Fig. 3.3.14. Scatterplot of Helix Height measurements from larval tracks in SCA test chamber 3R0. Helix Height = 2.018 + 0.128 x Flight Day. N=252, r^2 = 0.028. Slope > 0 ($P < 0.05$).

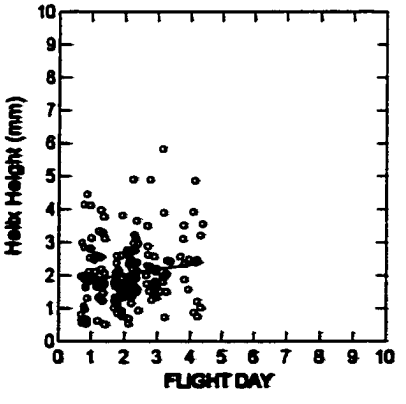

Fig. 3.3.15. Scatterplot of Helix Height measurements from larval tracks in SCA test chamber 4L0. Helix Height = 1.751 + 0.140 x Flight Day. N=171, r^2 = 0.019. Slope = 0 ($P > 0.05$).

track helices in SCA# 3R0 increased at an average rate of 0.128 mm·day^{-1}. ANOVA testing of the regression line equations for these two datasets confirmed that the slopes were significantly greater than zero ($P < 0.05$); however, the slope of the regression equation for the SCA# 4L0 dataset was not significantly different from zero. The pooled dataset including all 613 helix height measurements from the three SCA test chambers (see Fig. 3.3.12) produced a linear regression equation that indicated that helix height did not appreciably increase throughout the experiment, as confirmed by ANOVA testing of the regression ($P > 0.05$).

Mean helix height data for individual SCA test chambers and for the total pooled dataset are presented in Table 3.3.2. Values ranged between 1.75 mm in SCA# 3L0 and 2.46 mm in SCA# 3R0. An analysis of variance model and post-hoc pairwise comparisons found significant differences in mean helix height between all three SCAs. The mean helix height for all 613 tracks measured in this study was 2.13 mm.

Light did not appear to have any influence on the height of the helical paths tracked by larvae swimming in microgravity. Table 3.3.3 shows that mean helix height measurements were very similar during both daytime and night-time video recording sessions. This conclusion was confirmed by two-sample t-tests that compared helix height measurements between daylight and night-time samples from all three SCA test chambers separately, as well as on the entire pooled dataset ($P > 0.05$).

3.3.1.4 Summary of Helix Pitch Angle Data

Fig 3.3.16 summarises the helix pitch angle data from the ARF-1 microgravity experiment. Scatterplots of the individual measurements made on larval tracks from each

SCA test chamber are included as Figs. 3.3.18 to 3.3.20. In all samples, ANOVA testing of the linear regression equations confirmed that there was no significant change in helix pitch angle throughout the experiment. The same result was obtained when all 610 helix pitch angle measurements were pooled together (see Fig. 3.3.17) and the associated regression equation was tested by ANOVA.

Table 3.3.2 lists the mean helix pitch angle measurements for each individual SCA test chamber, and for the entire pooled dataset. The mean pitch angle for larvae from SCA# 3L0 was 49.8°, and larvae in SCA# 3R0 and 4L0 had average helix angles of 54.1° and 54.7° respectively. No significant differences in helix angle between the three SCAs were detected by ANOVA and post-hoc pairwise comparisons. Overall, the mean helix pitch angle for all 610 larval tracks measured in this study was 51.9°.

Helix pitch angle was not affected by the time of day in which observations and measurements were made. Table 3.3.3 categorises helix angle measurements for each SCA test chamber according to observation time. In all SCA test chambers, and for the entire pooled dataset of 610 measurement, mean helix angle for both daytime and night-time observations were very similar. This conclusion was supported by the results of two-sample t-tests which failed to detect any differences in mean helix pitch angle according to the presence of light.

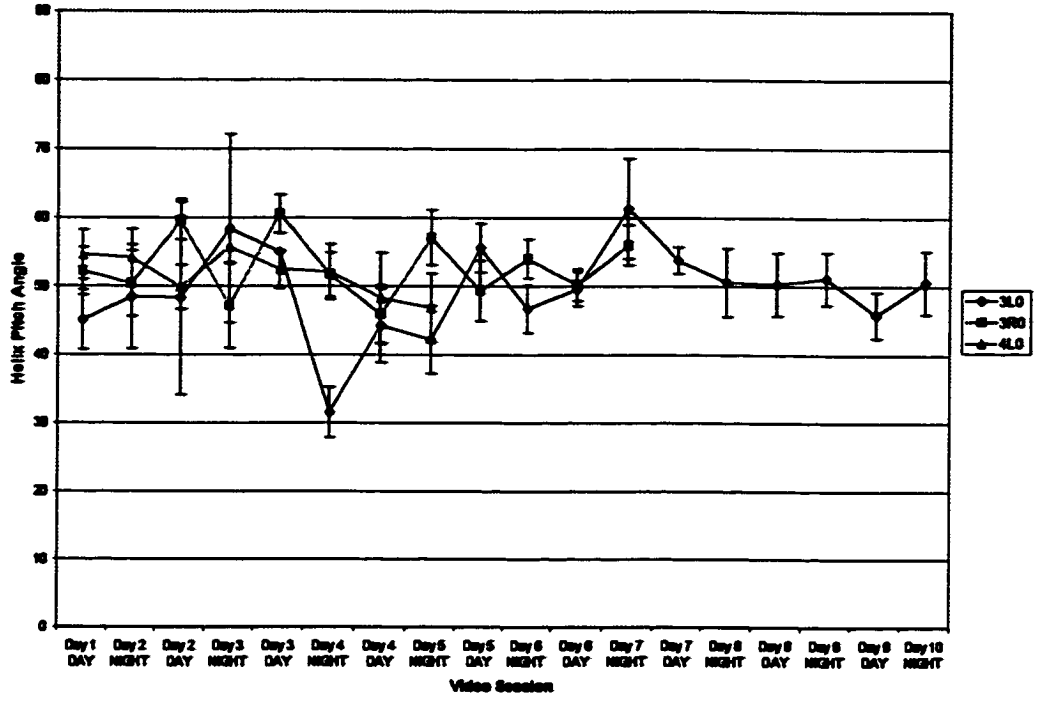

Fig. 3.3.16. Summary of Helix Pitch Angle data for tracks of microgravity-reared larvae from all video recording sessions for each SCA test chamber in the ARF MS-1, May 19-29, 1996. Values are plotted as mean helix height ± standard error.

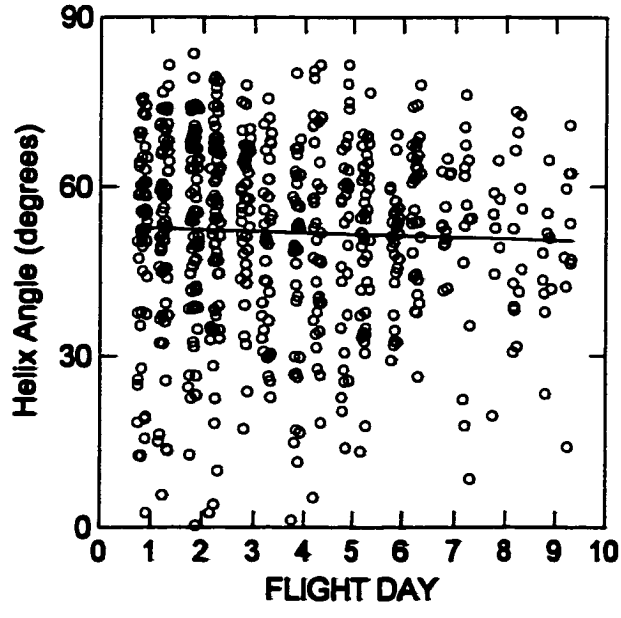

Fig. 3.3.17. Scatterplot of Helix Pitch Angle data for tracks of microgravity-reared larvae from all video recording sessions for all SCA test chambers pooled together. Helix Pitch Angle = 52.992 - 0.293 x Flight Day. N=610, $r^2 = 0.002$. Slope = 0 ($P > 0.05$).

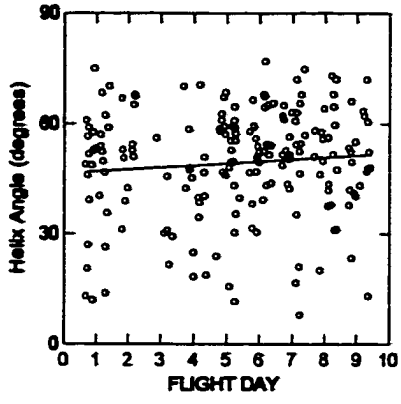

Fig. 3.3.18. Scatterplot of Helix Angle measurements from larval tracks in SCA test chamber 3L0. Helix Angle = 46.538 + 0.530 x Flight Day. N=189, r^2 = 0.009. Slope = 0 ($P > 0.05$).

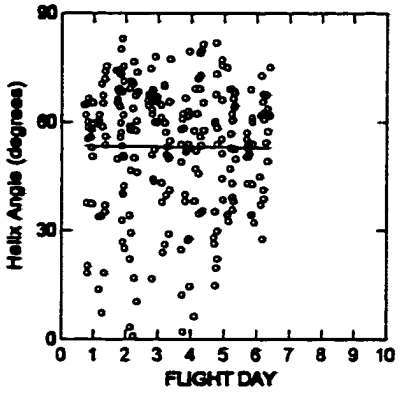

Fig. 3.3.19. Scatterplot of Helix Angle measurements from larval tracks in SCA test chamber 3R0. Helix Angle = 53.710 - 0.185 x Flight Day. N=251, r^2 = 0.000. Slope = 0 ($P > 0.05$).

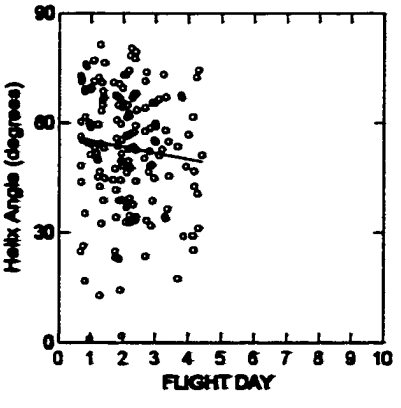

Fig. 3.3.20. Scatterplot of Helix Angle measurements from larval tracks in SCA test chamber 4L0. Helix Angle = 56.994 - 1.850 x Flight Day. N=170, r^2 = 0.012. Slope = 0 ($P > 0.05$).

3.3.1.5 Summary of Forward Swimming Velocity Data

Mean forward swimming velocity data from each of the three microgravity SCA test chambers are summarised in Fig. 3.3.21, and scatterplots for individual measurements from each SCA are shown in Figs. 3.3.23 to 3.3.25. ANOVA testing of the linear regression equations for SCA# 3L0 and SCA# 3R0 revealed that the slopes were not significantly different from zero, indicating that forward larval swimming speed did not change over the course of the experiment in those containers. However, the forward swimming speed of larvae in SCA# 4L0 decreased at a mean rate of 0.022 $mm \cdot s^{-1} \cdot day^{-1}$; this decrease was found to be significant by ANOVA testing ($P < 0.05$). A scatterplot of 671 individual measurements pooled together from all SCA test chambers is illustrated in Fig. 3.3.22. The linear regression for this pooled dataset indicated a significant ($P < 0.05$) decrease in forward larval swimming speed of 0.014 $mm \cdot s^{-1} \cdot day^{-1}$.

A summary of the mean forward swimming velocity data for pooled measurements from each SCA test chamber is presented in Table 3.3.2. An ANOVA model detected significant differences in mean swimming velocity between larvae from SCA# 3L0 (0.23$mm \cdot s^{-1}$) and the other two test chambers, but mean swimming velocities of larvae from SCA# 3R0 (0.35 $mm \cdot s^{-1}$) and 4L0 (0.37 $mm \cdot s^{-1}$) were not significantly different from each other. Overall, a mean forward swimming velocity of 0.32 $mm \cdot s^{-1}$ was obtained after pooling together all 671 velocity measurements.

The presence of light did not have any impact upon forward swimming velocity of mussel larvae reared in microgravity, as can be seen by examination of the data presented in Table 3.3.3. Mean forward swimming velocities recorded during both

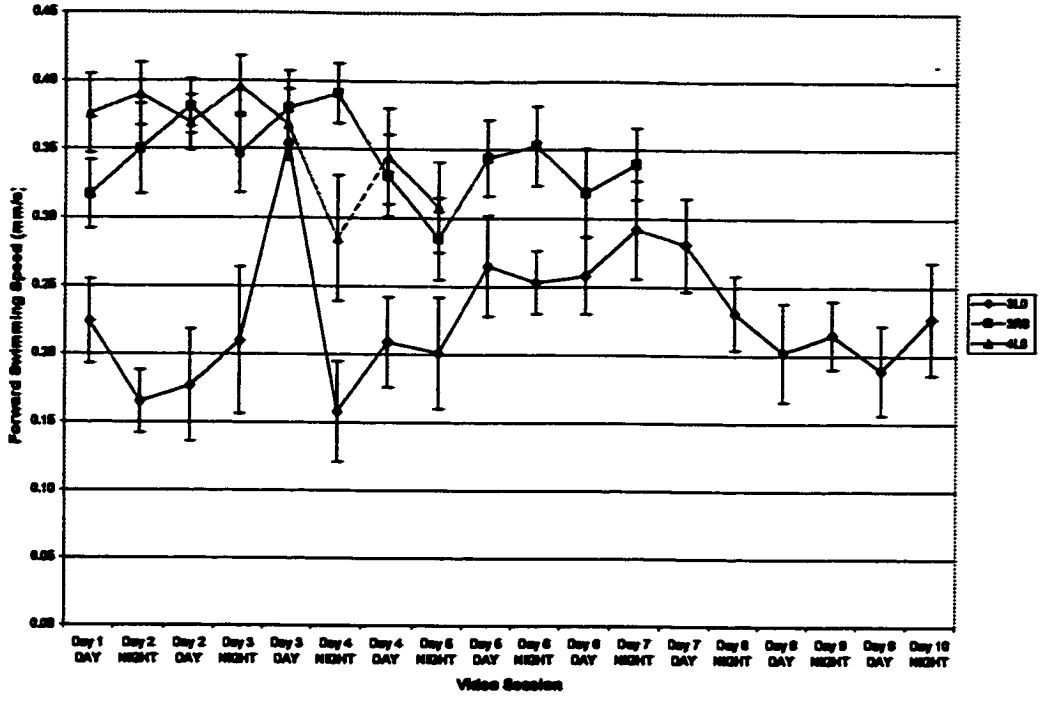

Fig. 3.3.21. Summary of Forward Swimming Velocity data for tracks of microgravity-reared larvae from all video recording sessions for each SCA test chamber in the ARF MS-1, May 19-29, 1996. Values are plotted as mean swimming velocity ± standard error.

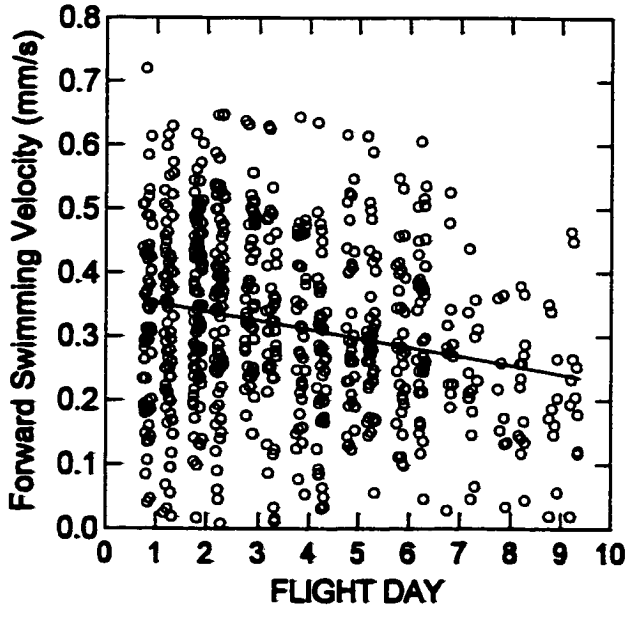

Fig. 3.3.22. Scatterplot of Forward Swimming Velocity data for tracks of microgravity-reared larvae from all video recording sessions for all SCA test chambers pooled together. Forward Swimming Velocity = 0.367 - 0.014 x Flight Day. N=671, $r^2 = 0.049$. Slope < 0 ($P < 0.05$).

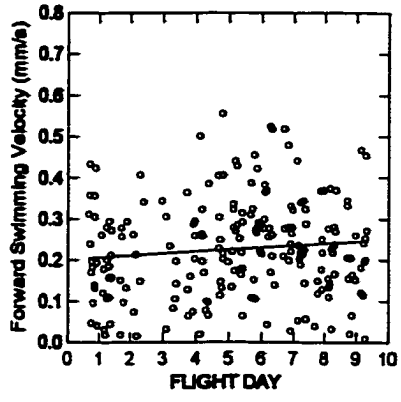

Fig. 3.3.23. Scatterplot of Forward Swimming Velocity measurements from larval tracks in SCA test chamber 3L0. Swimming Velocity = 0.291 + 0.006 x Flight Day. N=208, r^2 = 0.012. Slope = 0 ($P > 0.05$).

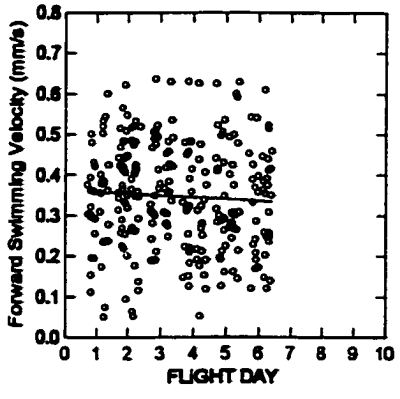

Fig. 3.3.24. Scatterplot of Forward Swimming Velocity measurements from larval tracks in SCA test chamber 3R0. Swimming Velocity = 0.364 - 0.006 x Flight Day. N=268, r^2 = 0.004. Slope = 0 ($P > 0.05$).

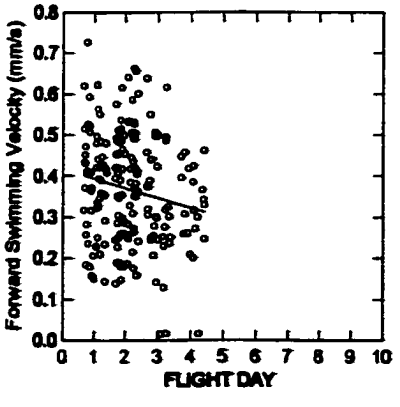

Fig. 3.3.25. Scatterplot of Forward Swimming Velocity measurements from larval tracks in SCA test chamber 4L0. Swimming Velocity = 0.414 - 0.022 x Flight Day. N=196, r^2 = 0.023. Slope < 0 ($P < 0.05$).

daytime and night-time video sessions were very similar in each of the three microgravity SCA test chambers. A series of two-sample t-tests confirmed that there were no significant differences in mean forward swimming velocity due to photoperiod in each of the SCA test chambers, nor in the pooled dataset of 671 observations ($P > 0.05$).

3.3.1.6 Summary of Instantaneous Linear Swimming Velocity Data

The instantaneous linear swimming velocity as calculated according to Cragg (1980) describes the actual speed at which the mussel larvae were swimming as they travelled along a path. Since Cragg's equation assumes that the dimensions of all helices within a larval track are similar, the tracks of larvae that changed helical parameters or were of irregular shape could not be included in these calculations and analyses. The speed of larvae that swam in straight lines was calculated directly using the gross displacement of the track trajectory. Fig. 3.3.26 summarises the changes in mean linear swimming velocity amongst larvae in all three SCA test chambers throughout the experiment, and the measurements of linear velocity for each individual larval track from each SCA are illustrated in the scatterplots shown in Figs. 3.3.28 to 3.3.30. ANOVA testing of the linear regressions for the datasets from each of the three SCA test chambers revealed that no significant changes in instantaneous linear swimming velocity occurred over the duration of the microgravity experiment. However, when the results of the entire dataset of 552 individual linear velocity measurements were pooled together (see Fig. 3.3.27), ANOVA testing of the linear regression indicated a significant ($P < 0.05$) decrease in linear swimming velocity of 0.012 $mm \cdot s^{-1} \cdot day^{-1}$.

Table 3.3.2 summarises the mean instantaneous linear swimming velocity data for pooled measurements from each of the three SCA test chambers. Using an analysis of variance model, significant differences in linear swimming velocity were detected between larvae from all three containers. Larvae from SCA# 4L0 had the greatest mean linear swimming speeds (0.49 $mm \cdot s^{-1}$), followed by larvae from SCA# 3R0, which had a mean linear swimming velocity of 0.45 $mm \cdot s^{-1}$. The slowest mean swimming speed was recorded for larvae from SCA# 3L0, which swam at a mean velocity of 0.34 $mm \cdot s^{-1}$. Pooling together all 552 individual measurements, a mean instantaneous linear swimming velocity of 0.43 $mm \cdot s^{-1}$ was obtained.

Table 3.3.3 outlines the mean instantaneous linear swimming velocity data for larvae observed in the daytime and night-time video recording sessions from each SCA test chamber. Examination of these data reveal that the presence of light did not affect the linear swimming speeds of larvae in this experiment; mean swimming speeds were similar in both the day and night video recording sessions. A series of two-sample t-tests confirmed that there were no significant differences ($P > 0.05$) in linear swimming velocity due to the presence of light in each of the three SCA test chambers, nor in the pooled dataset of 552 measurements.

3.3.1.7 Summary of Angular Swimming Velocity Data

Data summarising changes in mean larval angular swimming velocity, also known as rotational velocity (Crenshaw, 1996), are represented in Fig. 3.3.31, and scatterplots of individual angular velocity measurements from each of the three SCA test chambers are depicted in Figs. 3.3.33 - 3.3.35. In SCA# 3L0 and SCA# 3R0, there was a

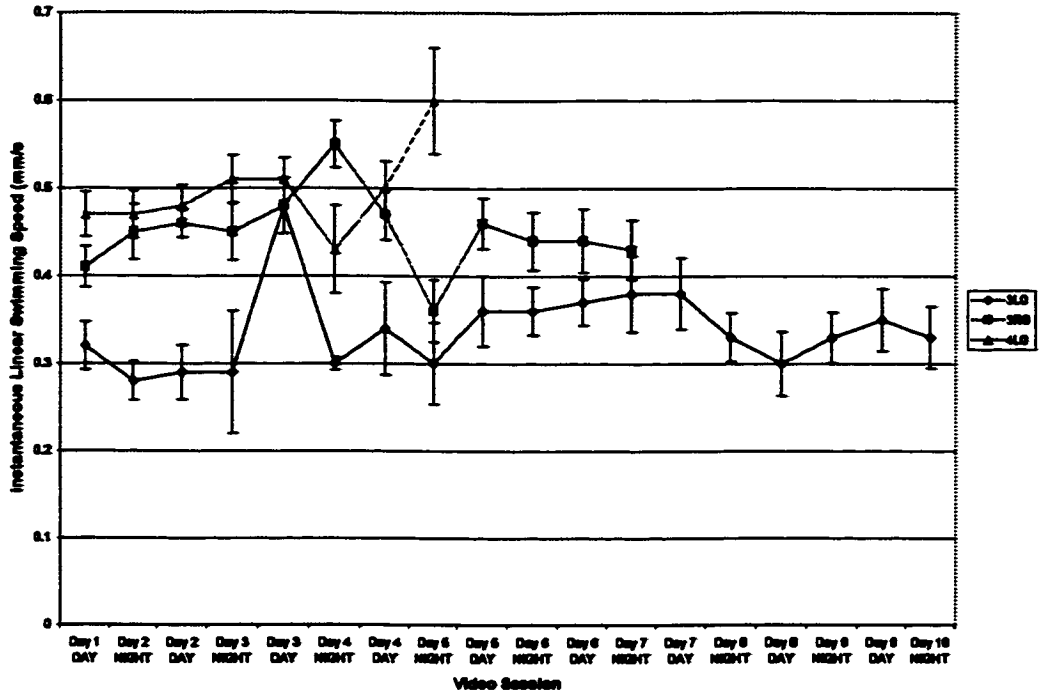

Fig. 3.3.26. Summary of Instantaneous Linear Swimming Velocity data for tracks of microgravity-reared larvae from all video recording sessions for each SCA test chamber in the ARF MS-1, May 19-29, 1996. Values are plotted as mean instantaneous linear swimming velocity ± standard error.

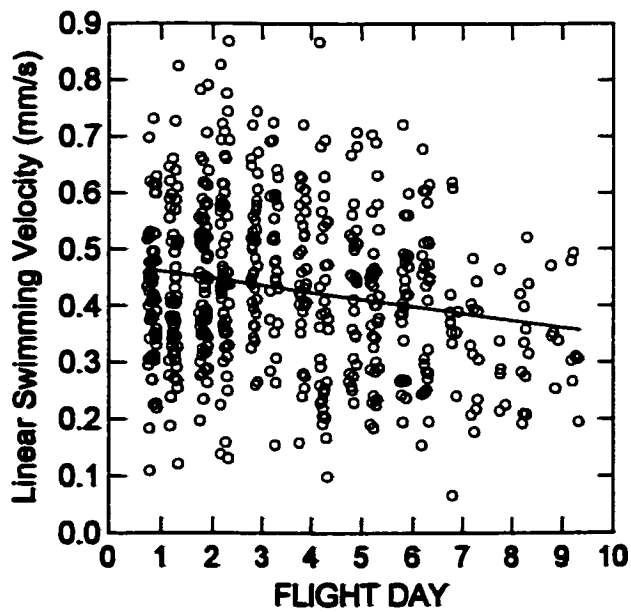

Fig. 3.3.27. Scatterplot of Instantaneous Linear Swimming Velocity data for tracks of microgravity-reared larvae from all video recording sessions for all SCA test chambers pooled together. Forward Swimming Velocity = 0.474 - 0.012 x Flight Day. N=662, r^2 = 0.037. Slope < 0 ($P < 0.05$).

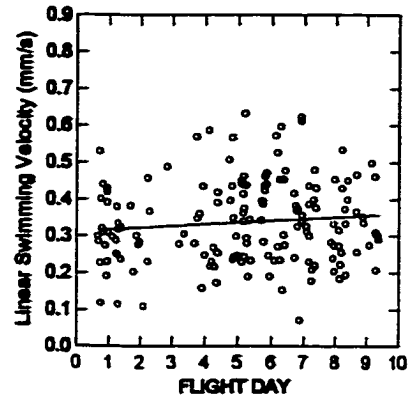

Fig. 3.3.28. Scatterplot of instantaneous Linear Swimming Velocity measurements from larval tracks in SCA test chamber 3L0. Swimming Velocity = 0.368 + 0.006 x Flight Day. N=169, r^2 = 0.017. Slope = 0 ($P > 0.05$).

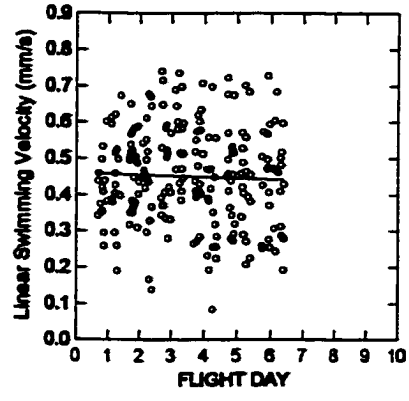

Fig. 3.3.29. Scatterplot of instantaneous Linear Swimming Velocity measurements from larval tracks in SCA test chamber 3R0. Swimming Velocity = 0.469 - 0.003 x Flight Day. N=229, r^2 = 0.001. Slope = 0 ($P > 0.05$).

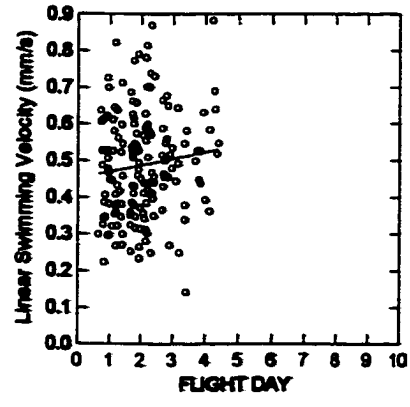

Fig. 3.3.30. Scatterplot of instantaneous Linear Swimming Velocity measurements from larval tracks in SCA test chamber 4L0. Swimming Velocity = 0.461 + 0.019 x Flight Day. N=164, r^2 = 0.015. Slope = 0 ($P > 0.05$).

significant decrease in angular velocity throughout the experiment, as detected by ANOVA testing of the linear regression, but there was no significant change in angular velocity with time in SCA# 4L0. Combining all 523 individual measurements of angular velocity together into a single dataset produced the scatterplot shown in Fig. 3.3.32. ANOVA testing of the linear regression for this pooled dataset revealed an overall average decrease in angular velocity of 0.07 $rad \cdot s^{-1} \cdot day^{-1}$ over the duration of the experiment.

The mean angular velocities for pooled measurements from each of the three SCA test chambers are summarised in Table 3.3.2. An ANOVA model detected significant differences in mean angular velocity between larvae from SCA# 4L0 and the other two test chambers, but mean angular velocity in SCA# 3L0 and SCA# 3R0 were not significantly different from each other. A mean angular velocity of 1.09 $rad \cdot s^{-1}$ was obtained by pooling together all 523 individual measurements.

Mean angular velocity data for each SCA test chamber are summarised in Table 3.3.3 according to the time of day in which video observations were made. The presence of light did not have an effect upon the angular swimming velocity of larvae in this experiment, since mean rotational velocities among larvae in each SCA test chamber were similar regardless of the time of day in which measurements were made. A series of two-sample t-tests supported this conclusion in that they failed to detect any significant differences in angular swimming velocity due to the presence of light in any of the SCA test chambers, nor were the daytime and night-time observations of angular velocity significantly different from each other in the pooled dataset of 523 observations.

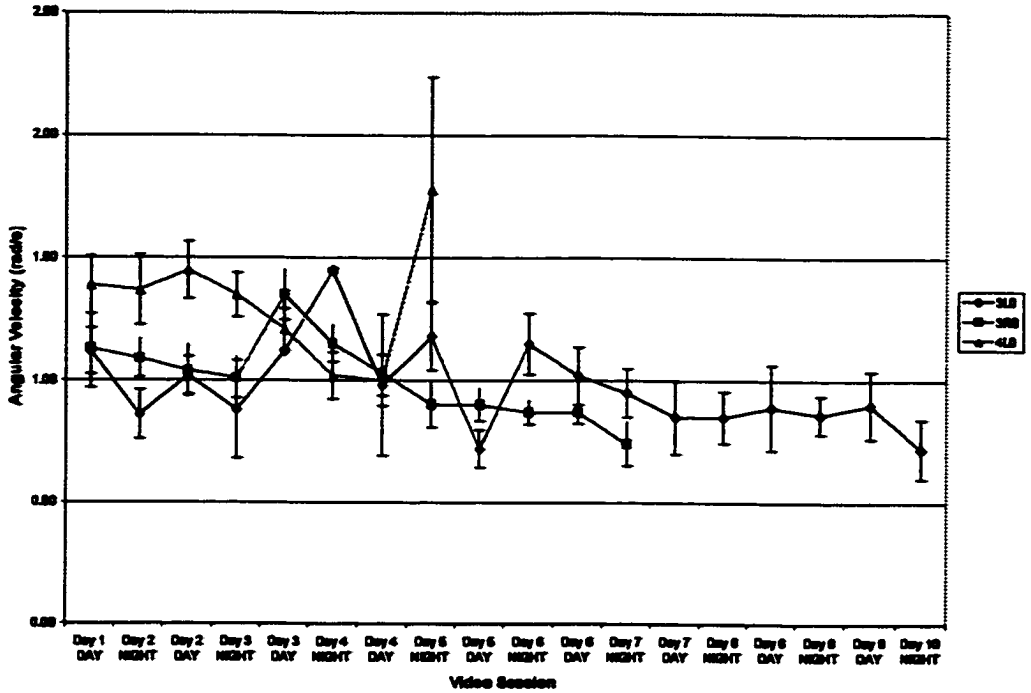

Fig. 3.3.31. Summary of Angular Velocity data for tracks of microgravity-reared larvae from all video recording sessions for each SCA test chamber in the ARF MS-1, May 19-29, 1996. Values are plotted as mean angular velocity ± standard error.

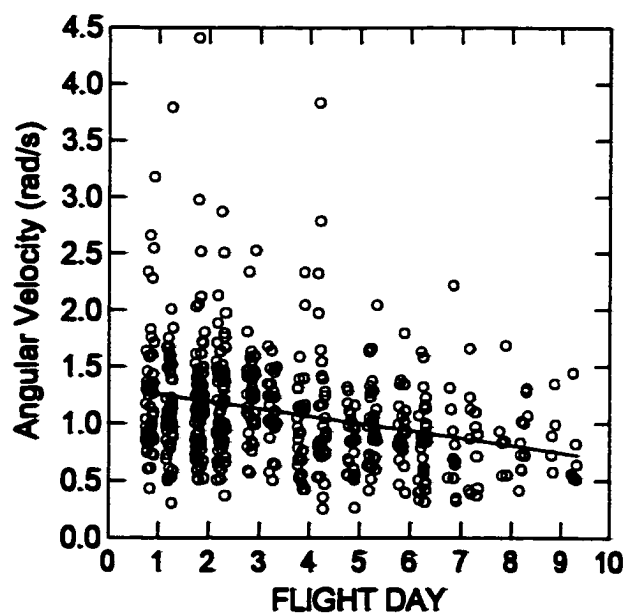

Fig. 3.3.32. Scatterplot of Angular Velocity data for tracks of microgravity-reared larvae from all video recording sessions for all SCA test chambers pooled together. Angular Velocity = 1.324 - 0.086 x Flight Day. N=623, r^2 = 0.000. Slope < 0 (P < 0.05).

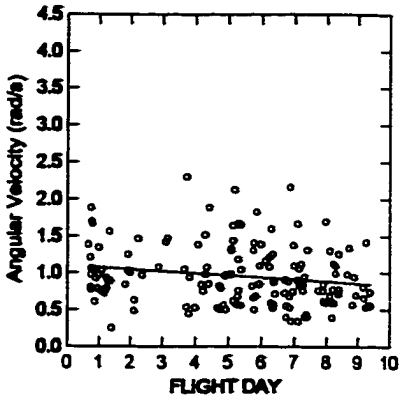

Fig. 3.3.33. Scatterplot of Angular Velocity measurements from larval tracks in SCA test chamber 3L0. Angular Velocity = 1.101 - 0.027 x Flight Day. N=151, r^2 = 0.031. Slope < 0 (P < 0.05).

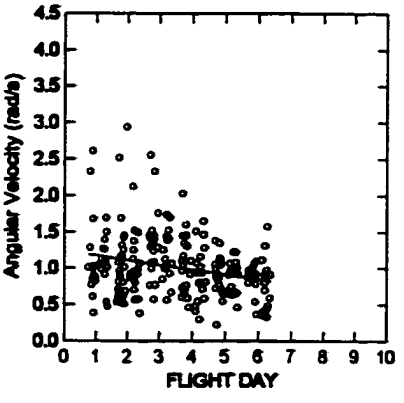

Fig. 3.3.34. Scatterplot of Angular Velocity measurements from larval tracks in SCA test chamber 3R0. Angular Velocity = 1.236 - 0.065 x Flight Day. N=223, r^2 = 0.066. Slope < 0 (P < 0.05).

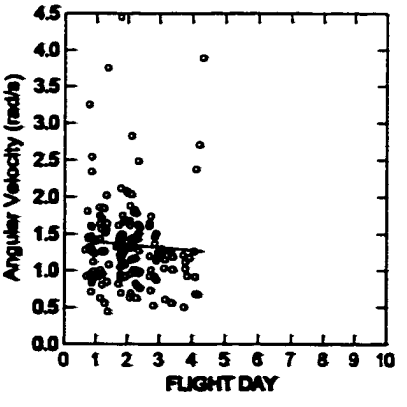

Fig. 3.3.35. Scatterplot of Angular Velocity measurements from larval tracks in SCA test chamber 4L0. Angular Velocity = 1.439 - 0.038 x Flight Day. N=149, r^2 = 0.003. Slope = 0 (P > 0.05).

3.3.2 Larval Bivalve Locomotion in Normal Gravity

The poor quality of the video recordings from the ARF 1g centrifuge meant that larval tracks from the unit gravity SCA test chambers could not be accurately traced and measured. Consequently, video recordings from a previous ground-based experiment were analysed in order to quantify the behaviour of mussel larvae swimming in a normal gravity environment. Using larvae of the same size as those used in the ARF experiment, the ground-based study compiled trajectory measurement data for the tracks of 59 swimming larvae. The paths travelled by these larvae are illustrated in Figs. 3.3.36 through 3.3.41, and measurement data pertaining to these tracks are recorded in Tables 3.3.6 to 3.3.11.

In contrast to the larvae reared in microgravity, mussel larvae in normal gravity swam in only two main directions. In this experiment, twenty larvae were observed to be swimming in an upward direction, while 38 larvae were found to be swimming downwards. All larvae exhibited the helical swimming pattern typical of bivalve larvae, and in spite of a slight current in the observation chamber that caused some drifting towards the left side, the larvae aligned themselves along the vertical gravity vector (see Section 3.3.3). One larva (track # 41) was observed to climb upwards, then hover somewhat and slowly swim downwards, and finally swim back towards the top of the chamber.

Table 3.3.5 summarises the helix measurement data for the larvae swimming in normal gravity, grouped according to general swimming direction. As determined by a two-sample t-test, the average vertical swimming speed for larvae travelling downwards

(0.22 mm/s) was not significantly different ($P > 0.05$) from the speed of larvae swimming upwards (0.19 mm/s). However, the instantaneous linear velocities and angular velocities for downward swimmers were significantly greater than those observed in upward swimming larvae. The mean helix diameter of downward swimming larvae (0.80 mm) was also significantly greater than that observed in the tracks of the larvae swimming upwards (0.63 mm). The mean net-to-gross displacement ration (NGDR) for the upwardly-directed swimmers (0.57) was significantly greater than the mean NGDR calculated for the downward swimming larvae (0.45). There were no significant differences detected by Student's t-tests between both groups of larvae in terms of helix pitch angle or helix height.

Table 3.3.5. Summary of trajectory measurement data from tracks of mussel larvae (*Mytilus edulis*) swimming in upward and downward directions in the ground-based normal gravity experiment.

	Upward Swimmers			Downward Swimmers		
	MEAN	s.d.	N	MEAN	s.d.	N
HELIX HEIGHT (mm)	1.05	0.56	19	1.04	0.77	39
HELIX DIAMETER (mm)	0.63	0.31	20	0.80	0.27	38
HELIX PITCH ANGLE	33.21	16.67	19	30.42	10.72	38
VERTICAL VELOCITY (mm/s)	0.19	0.09	20	0.22	0.07	38
LINEAR VELOCITY (mm/s)	0.40	0.11	19	0.62	0.10	37
ANGULAR VELOCITY (rad/s)	1.25	0.49	19	1.61	0.58	37
NGDR	0.57	0.23	20	0.45	0.12	39
TRACK DIRECTION (degrees)	102	10.1	20	258	5.8	38

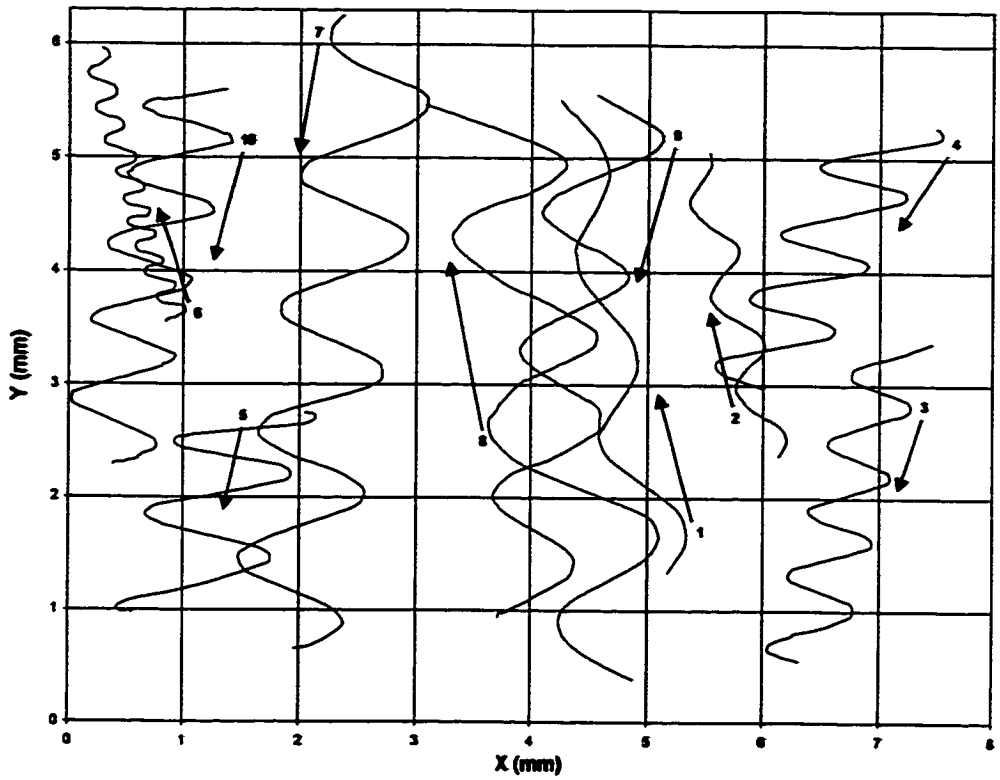

Fig. 3.3.36. Reconstructed tracks of mussel larvae (*Mytilus edulis*) swimming in normal gravity. Track direction indicated by arrows. Larval tracks #1-10.

Table 3.3.6. Trajectory measurement data from tracks of mussel larvae (*Mytilus edulis*) swimming in normal gravity in the ground-based experiment. Larval tracks #1-10.

LARVAL TRACK #	HELIX HEIGHT (mm)	HELIX DIAMETER (mm)	HELIX PITCH ANGLE	TIME (s)	ANGULAR VELOCITY (rad/s)	LINEAR VELOCITY (mm/s)	VERTICAL VELOCITY (mm/s)	NGDR	TRACK DIRECTION (degrees) *
1	1.64	0.40	52	15.8	1.04	0.34	0.27	0.86	100
2	0.85	0.32	43	10.5	1.93	0.41	0.26	0.78	104
3	0.62	0.60	33	15.8	1.97	0.62	0.19	0.44	254
4	0.67	0.79	37	21.1	1.22	0.50	0.13	0.37	241
5	0.79	1.14	25	15.8	1.17	0.68	0.15	0.35	252
6	0.31	0.20	21	21.1	2.36	0.26	0.12	0.48	107
7	1.21	0.97	30	21.2	1.38	0.71	0.26	0.50	281
8	1.90	1.06	13	31.8	0.56	0.34	0.17	0.58	104
9	1.32	0.81	20	15.9	1.41	0.64	0.30	0.58	259
10	0.69	0.77	7	21.2	1.50	0.60	0.16	0.37	257

* Reference line, 0°, is the horizontal axis.

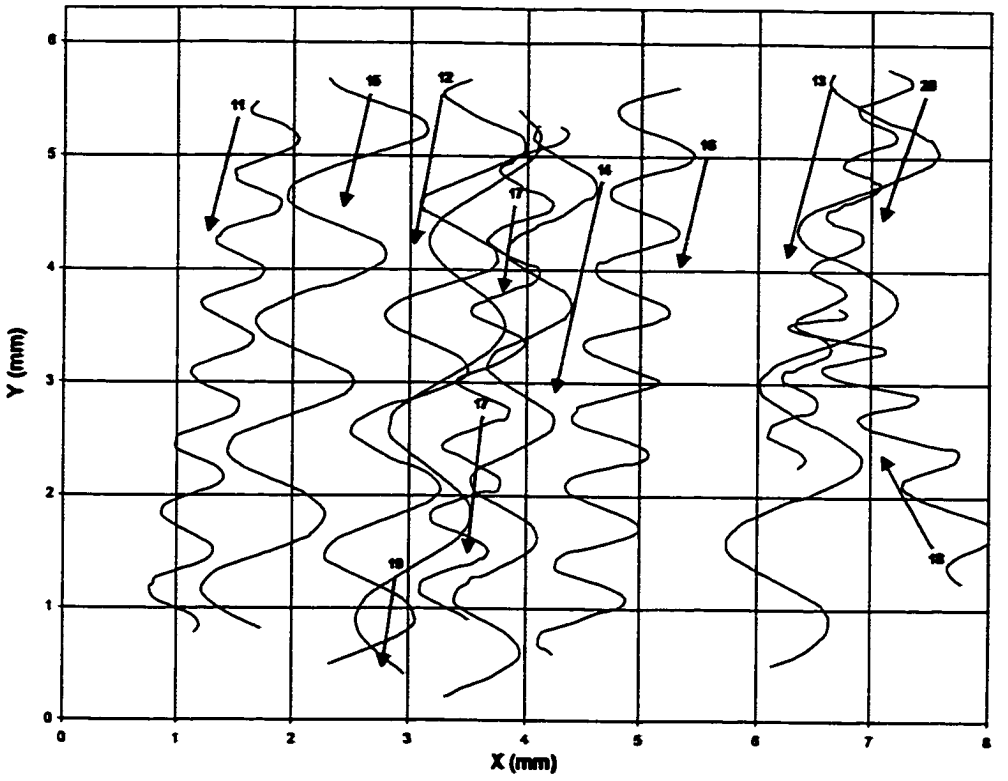

Fig. 3.3.37. Reconstructed tracks of mussel larvae (*Mytilus edulis*) swimming in normal gravity. Track direction indicated by arrows. Larval tracks #11-20.

Table 3.3.7. Trajectory measurement data from tracks of mussel larvae (*Mytilus edulis*) swimming in normal gravity in the ground-based experiment. Larval tracks #11-20.

LARVAL TRACK #	HELIX HEIGHT (mm)	HELIX DIAMETER (mm)	HELIX PITCH ANGLE	TIME (s)	ANGULAR VELOCITY (rad/s)	LINEAR VELOCITY (mm/s)	VERTICAL VELOCITY (mm/s)	NGDR	TRACK DIRECTION (degrees) *
11	0.64	0.45	20	21.2	2.20	0.54	0.22	0.52	259
12	1.09	0.79	15	26.5	1.15	0.50	0.20	0.52	257
13	1.46	1.02	34	26.5	0.86	0.48	0.20	0.54	258
14	1.07	0.67	40	15.9	1.88	0.70	0.32	0.59	261
15	1.24	0.95	35	21.2	1.17	0.60	0.23	0.49	256
16	0.71	0.66	75	21.2	2.13	0.75	0.24	0.43	262
17	0.70	0.51	28	15.9	2.50	0.69	0.28	0.49	259
18	0.82	0.48	44	26.5	0.77	0.21	0.10	0.40	122
19	1.77	0.81	42	15.9	1.14	0.56	0.32	0.71	260
20	0.51	0.37	40	15.9	2.62	0.57	0.23	0.51	254

* Reference line, 0°, is the horizontal axis.

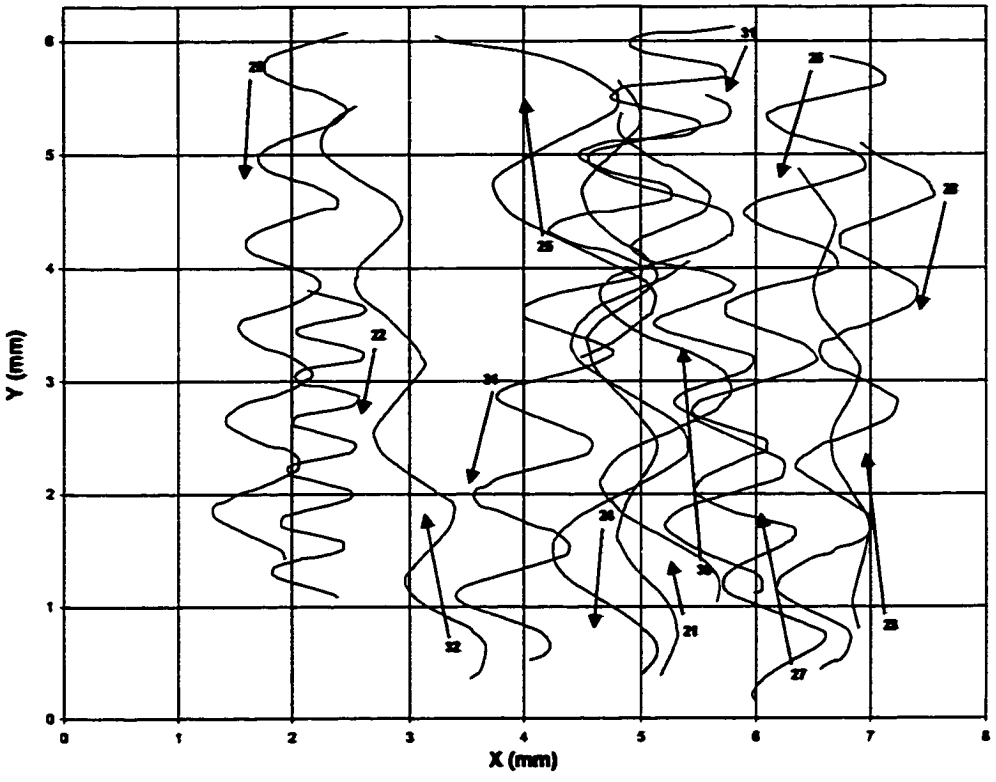

Fig. 3.3.38. Reconstructed tracks of mussel larvae (*Mytilus edulis*) swimming in normal gravity. Track direction indicated by arrows. Larval tracks #21-32.

Table 3.3.8. Trajectory measurement data from tracks of mussel larvae (*Mytilus edulis*) swimming in normal gravity in the ground-based experiment. Larval tracks #21-32.

LARVAL TRACK #	HELIX HEIGHT (mm)	HELIX DIAMETER (mm)	HELIX PITCH ANGLE	TIME (s)	ANGULAR VELOCITY (rad/s)	LINEAR VELOCITY (mm/s)	VERTICAL VELOCITY (mm/s)	NGDR	TRACK DIRECTION (degrees) *
21	1.76	0.45	57	16.0	1.18	0.42	0.33	0.81	94
22	0.45	0.56	19	16.0	2.40	0.70	0.17	0.34	265
23	1.46	0.32	57	10.7	1.65	0.47	0.39	0.92	97
24	1.91	1.01	38	0.0	N/A	N/A	0.35	0.64	264
25	1.85	1.17	39	21.3	0.49	0.32	0.15	0.55	101
26	0.87	0.89	30	31.9	1.08	0.51	0.15	0.42	256
27	0.76	0.78	18	31.9	1.39	0.57	0.17	0.49	104
28	1.10	0.79	33	15.9	1.68	0.72	0.29	0.53	259
29	0.76	0.69	29	15.9	2.44	0.89	0.30	0.48	264
30	1.71	1.12	29	15.9	1.04	0.65	0.28	0.50	91
31	0.86	0.86	29	37.1	1.16	0.52	0.16	0.36	254
32	1.38	0.57	38	21.3	1.11	0.40	0.24	0.74	101

* Reference line, 0°, is the horizontal axis.

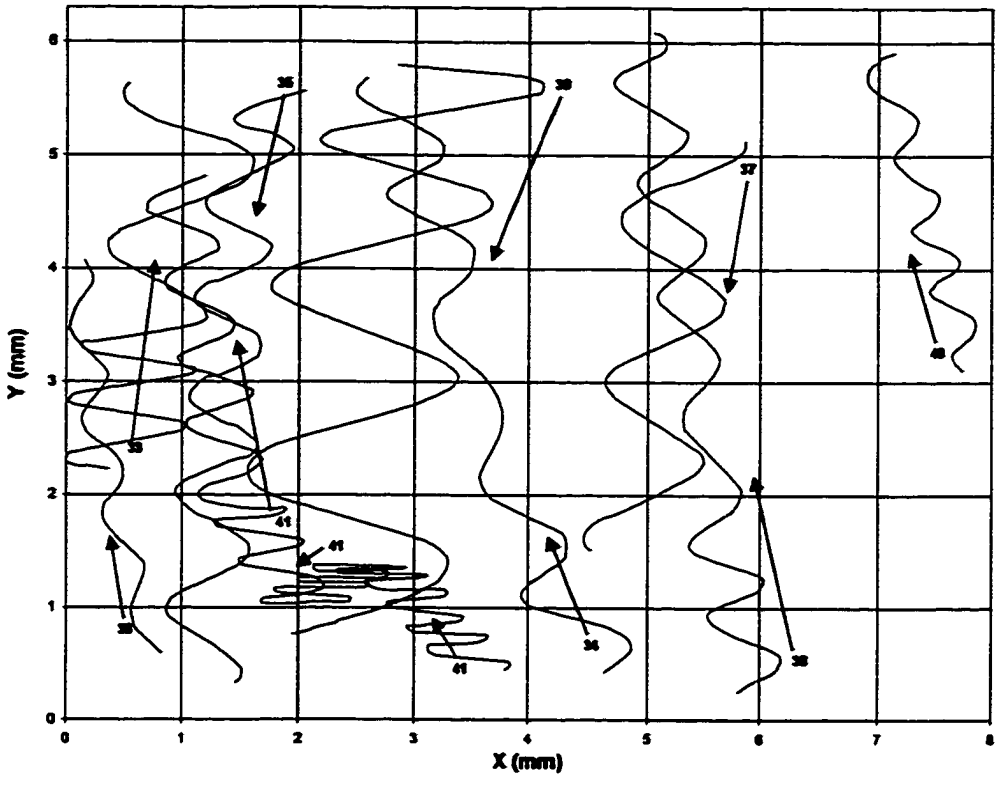

Fig. 3.3.39. Reconstructed tracks of mussel larvae (*Mytilus edulis*) swimming in normal gravity. Track direction indicated by arrows. Larval tracks #33-41.

Table 3.3.9. Trajectory measurement data from tracks of mussel larvae (*Mytilus edulis*) swimming in normal gravity in the ground-based experiment. Larval tracks #33-41.

LARVAL TRACK #	HELIX HEIGHT (mm)	HELIX DIAMETER (mm)	HELIX PITCH ANGLE	TIME (s)	ANGULAR VELOCITY (rad/s)	LINEAR VELOCITY (mm/s)	VERTICAL VELOCITY (mm/s)	NGDR	TRACK DIRECTION (degrees) *
33	N/A	0.97	N/A	21.2	N/A	N/A	0.16	0.34	75
34	1.10	0.51	24	37.1	0.87	0.27	0.15	0.69	110
35	0.93	0.62	28	21.3	1.67	0.57	0.25	0.55	265
36	0.97	0.22	60	15.9	1.45	0.28	0.22	0.85	100
37	1.46	0.93	33	10.6	1.57	0.82	0.36	0.60	262
38	0.75	0.54	37	26.7	1.85	0.55	0.22	0.63	100
39	1.57	1.73	26	37.3	0.55	0.49	0.14	0.35	264
40	0.66	0.30	25	16.0	1.70	0.31	0.18	0.68	108
41	5.09	N/A	N/A	N/A	N/A	N/A	0.08	0.23	138,180,213,102

* Reference line, 0°, is the horizontal axis.

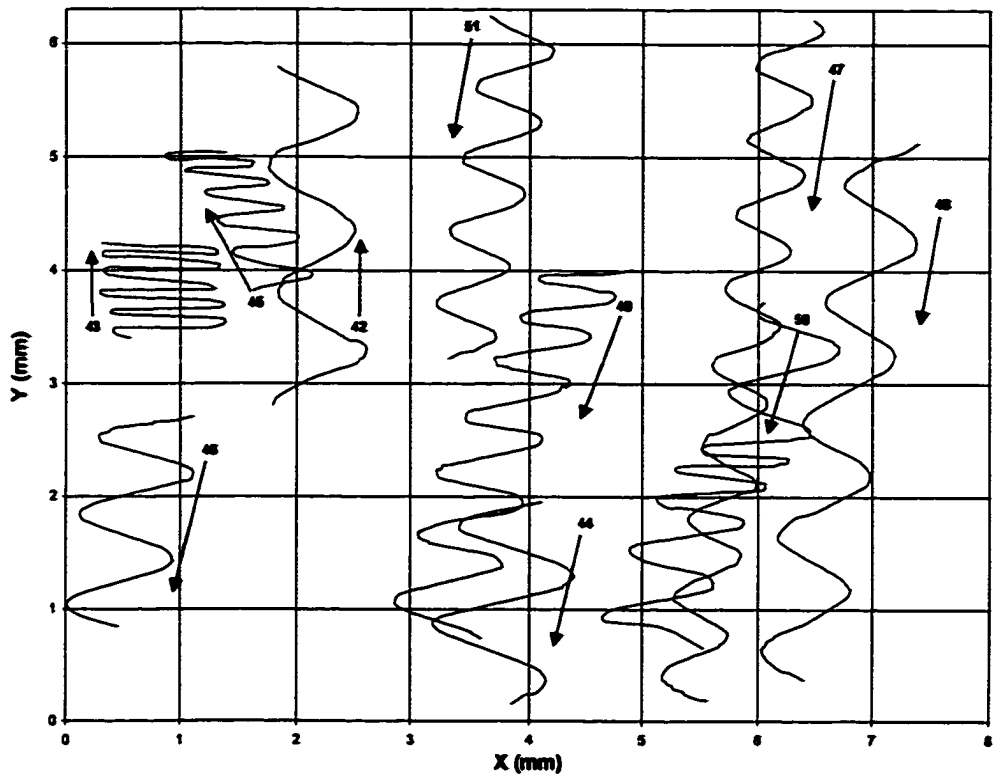

Fig. 3.3.40. Reconstructed tracks of mussel larvae (*Mytilus edulis*) swimming in normal gravity. Track direction indicated by arrows. Larval tracks #42-51.

Table 3.3.10. Trajectory measurement data from tracks of mussel larvae (*Mytilus edulis*) swimming in normal gravity in the ground-based experiment. Larval tracks #42-51.

LARVAL TRACK #	HELIX HEIGHT (mm)	HELIX DIAMETER (mm)	HELIX PITCH ANGLE	TIME (s)	ANGULAR VELOCITY (rad/s)	LINEAR VELOCITY (mm/s)	VERTICAL VELOCITY (mm/s)	NGDR	TRACK DIRECTION (degrees) *
42	1.17	0.73	27	15.7	1.03	0.42	0.19	0.53	92
43	0.20	1.00	2	36.6	0.76	0.38	0.02	0.09	94
44	1.00	1.08	29	10.4	1.09	0.61	0.17	0.39	256
45	0.29	0.62	10	20.9	1.31	0.41	0.06	0.18	117
46	0.83	0.87	26	10.4	1.43	0.65	0.19	0.37	258
47	0.69	0.51	31	20.9	2.65	0.74	0.29	0.52	261
48	1.11	0.66	36	15.7	1.76	0.65	0.31	0.58	260
49	0.61	0.78	31	31.4	1.17	0.47	0.11	0.30	249
50	0.40	0.74	34	26.1	1.89	0.71	0.12	0.26	237
51	0.71	0.56	31	15.7	1.72	0.52	0.19	0.47	259

* Reference line, 0°, is the horizontal axis.

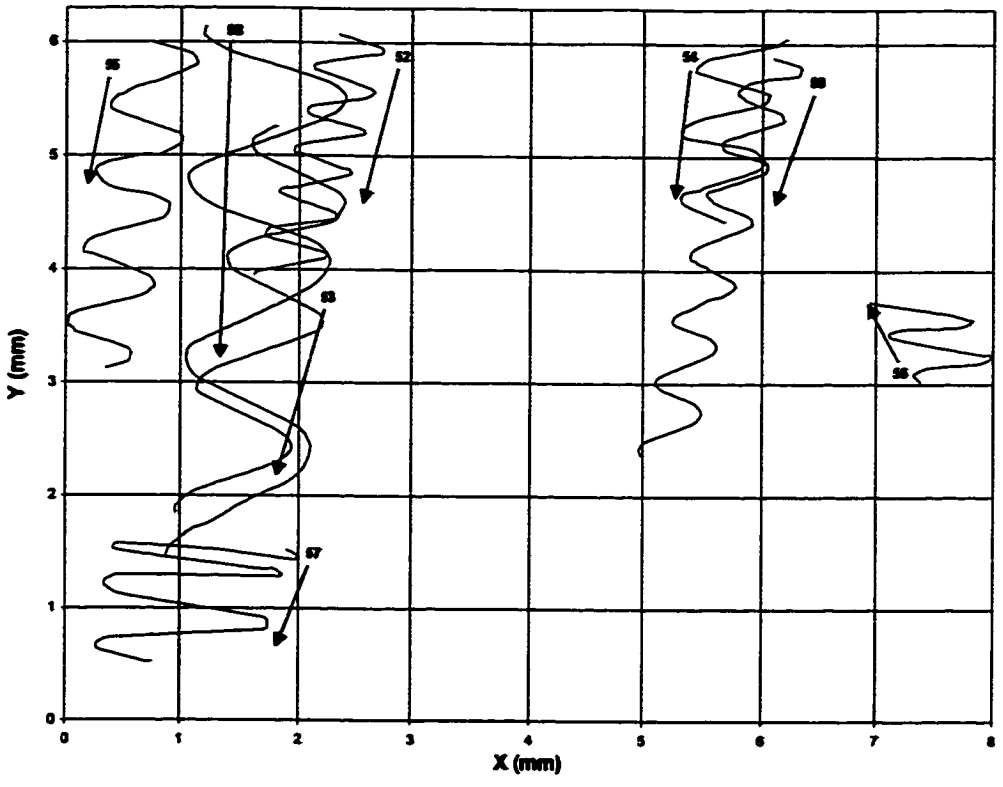

Fig. 3.3.41. Reconstructed tracks of mussel larvae (*Mytilus edulis*) swimming in normal gravity. Track direction indicated by arrows. Larval tracks #52-59.

Table 3.3.11. Trajectory measurement data from tracks of mussel larvae (*Mytilus edulis*) swimming in normal gravity in the ground-based experiment. Larval tracks #52-59.

LARVAL TRACK #	HELIX HEIGHT (mm)	HELIX DIAMETER (mm)	HELIX PITCH ANGLE	TIME (s)	ANGULAR VELOCITY (rad/s)	LINEAR VELOCITY (mm/s)	VERTICAL VELOCITY (mm/s)	NGDR	TRACK DIRECTION (degrees) *
52	0.40	0.54	28	15.7	2.24	0.62	0.14	0.31	253
53	1.19	0.88	36	15.7	1.18	0.56	0.22	0.51	258
54	0.58	0.71	22	10.4	1.76	0.64	0.16	0.39	263
55	0.76	0.64	28	15.7	1.53	0.53	0.19	0.41	258
56	0.38	0.74	35	10.4	1.34	0.50	0.08	0.25	116
57	0.52	1.45	12	20.9	0.87	0.63	0.07	0.18	260
58	1.70	1.11	33	20.9	0.83	0.51	0.23	0.52	264
59	0.59	0.41	37	15.7	2.51	0.57	0.24	0.49	255

* Reference line, 0°, is the horizontal axis.

3.3.3 Comparison of Locomotion in Normal Gravity and Microgravity

Measurements describing the swimming mechanics of larvae in the presence and absence of gravity are summarised in Table 3.3.12. As confirmed by analysis of variance testing, the vertical velocity of larvae swimming in both directions in normal gravity was significantly slower ($P<0.05$) than that measured for larvae that were swimming in a forward direction in microgravity (Fig. 3.3.42). However, the instantaneous linear velocity and angular velocity of downward swimming larvae were greater than those of upward swimmers and larvae in microgravity (Fig. 3.3.43 and 3.3.44). Fig. 3.3.45 shows that the mean helix diameter of larvae swimming in the absence of gravity (0.57 mm) was smaller than that recorded for downward swimmers (0.80 mm), but not significantly different from upward swimming larvae (0.63 mm). Conversely, larvae swimming in microgravity had significantly greater helix heights and steeper helix pitch angles than larvae in normal gravity (Fig. 3.3.46 and 3.3.47). As an index of the complexity of the helical trajectories, the net-to-gross displacement ratio (NGDR) data revealed that larvae in microgravity swam in helices in which the vertical component of motion predominated over horizontal movement, unlike larvae swimming in either an upward or downward direction in normal gravity (Fig 3.3.48).

Table 3.3.12. Comparison of trajectory measurement data from tracks of mussel larvae (*Mytilus edulis*) swimming in normal gravity and microgravity.

	1g Upward Swimmers			1g Downward Swimmers			Microgravity Swimmers		
	MEAN	s.d.	N	MEAN	s.d.	N	MEAN	s.d.	N
VERTICAL VELOCITY (mm/s)	0.19	0.09	20	0.22	0.07	38	0.32	0.14	671
LINEAR VELOCITY (mm/s)	0.40	0.11	19	0.62	0.10	37	0.43	0.14	552
ANGULAR VELOCITY (rad/s)	1.25	0.49	19	1.61	0.58	37	1.09	0.50	523
HELIX DIAMETER (mm)	0.63	0.31	20	0.89	0.27	38	0.67	0.32	622
HELIX HEIGHT (mm)	1.96	0.56	19	1.84	0.77	39	2.13	1.13	613
HELIX PITCH ANGLE	33.21	16.67	19	30.42	10.72	38	51.9	16.38	610
NGDR	0.57	0.23	20	0.45	0.12	39	0.78	0.19	668

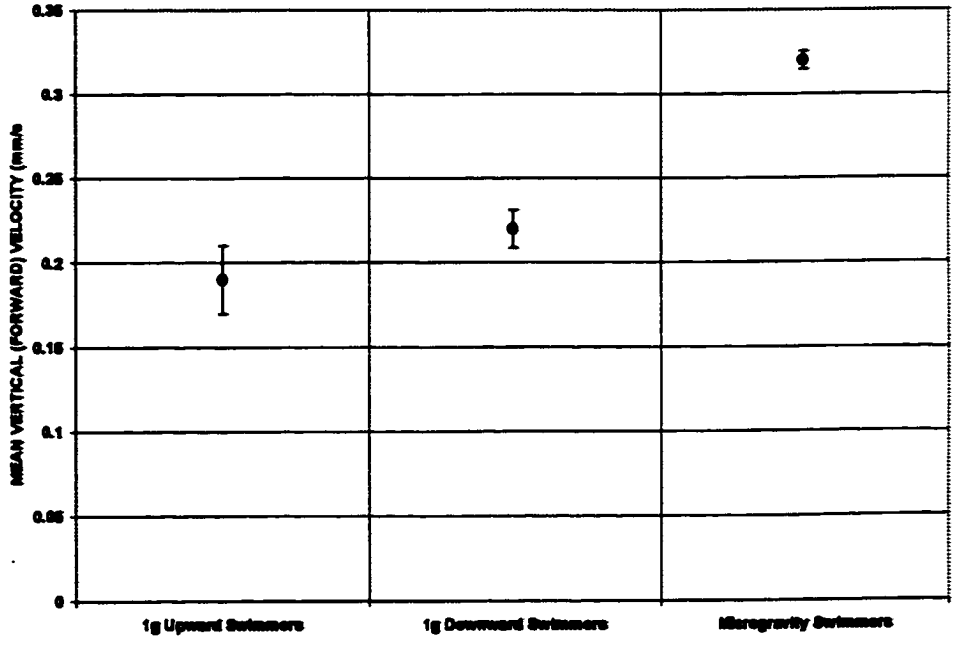

Fig 3.3.42. Comparison of mean vertical (or forward) swimming velocities (±S.E.) amongst mussel larvae (*Mytilus edulis*) in normal gravity and microgravity. Data are from Table 3.3.12.

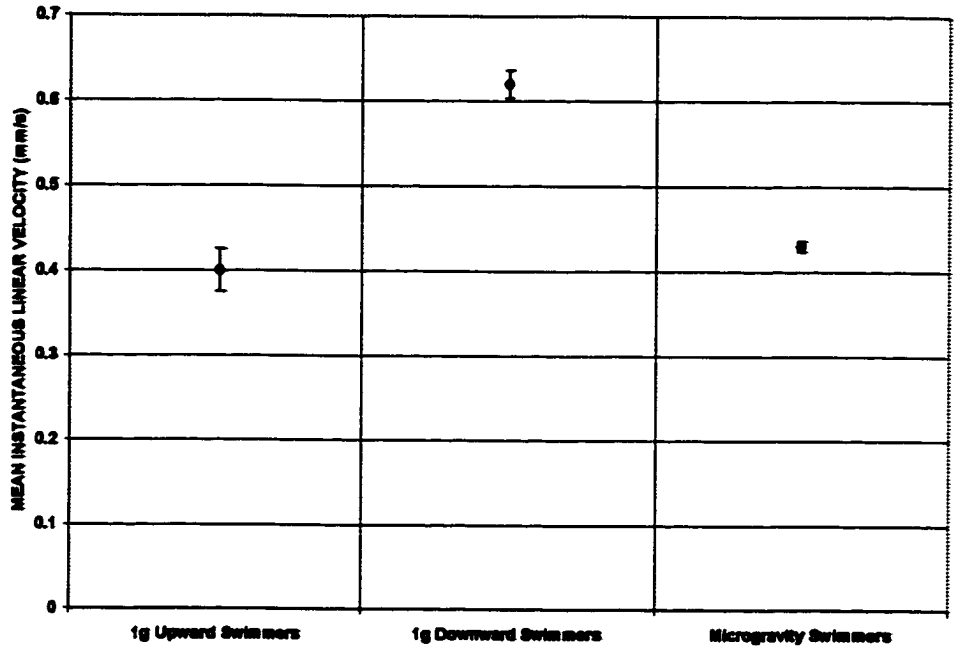

Fig 3.3.43. Comparison of mean instantaneous linear swimming velocities (±S.E.) amongst mussel larvae (*Mytilus edulis*) in normal gravity and microgravity. Data are from Table 3.3.12.

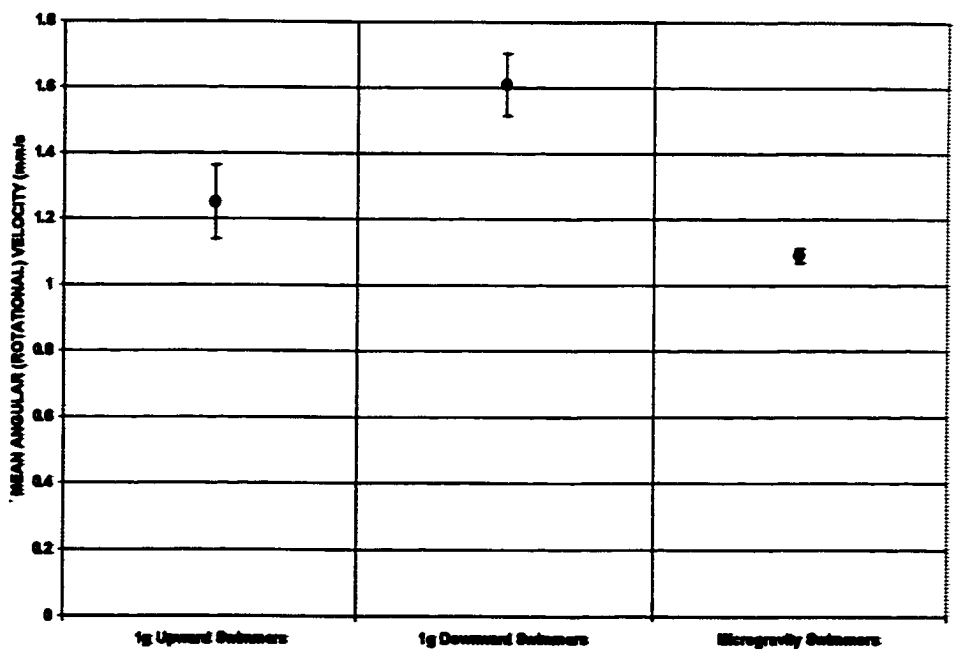

Fig 3.3.44. Comparison of mean angular swimming velocities (±S.E.) amongst mussel larvae (*Mytilus edulis*) in normal gravity and microgravity. Data are from Table 3.3.12.

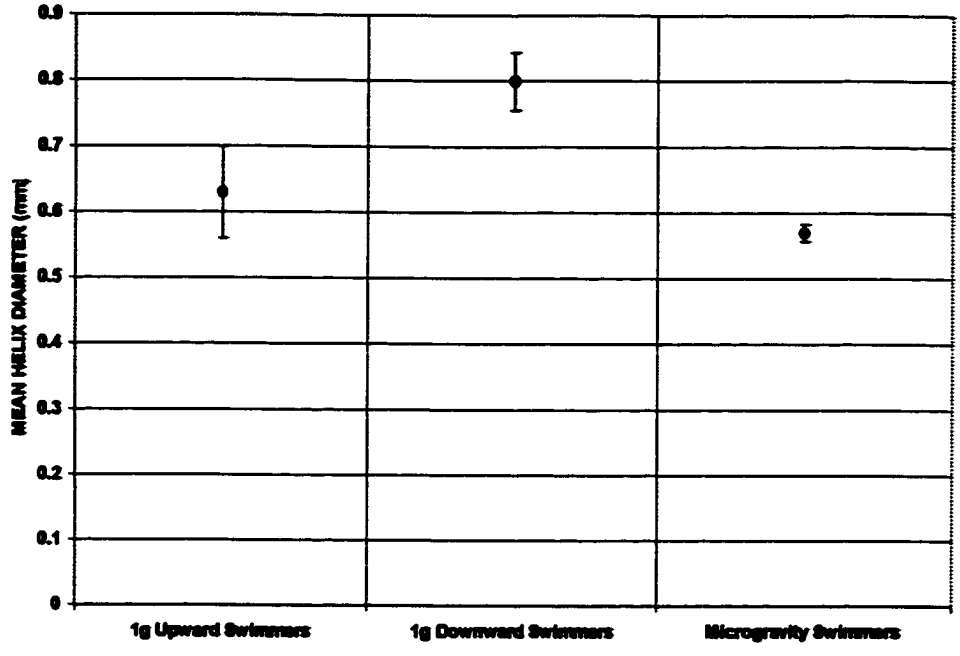

Fig 3.3.45. Comparison of mean helix diameters (±S.E.) amongst mussel larvae (*Mytilus edulis*) swimming in normal gravity and microgravity. Data are from Table 3.3.12.

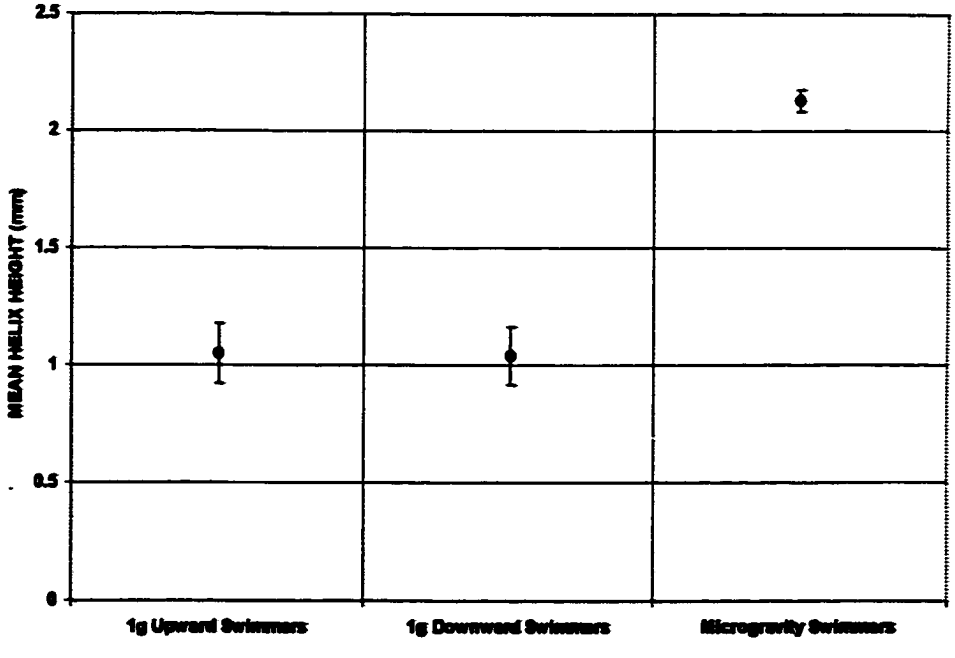

Fig 3.3.46. Comparison of mean helix heights (±S.E.) amongst mussel larvae (*Mytilus edulis*) swimming in normal gravity and microgravity. Data are from Table 3.3.12.

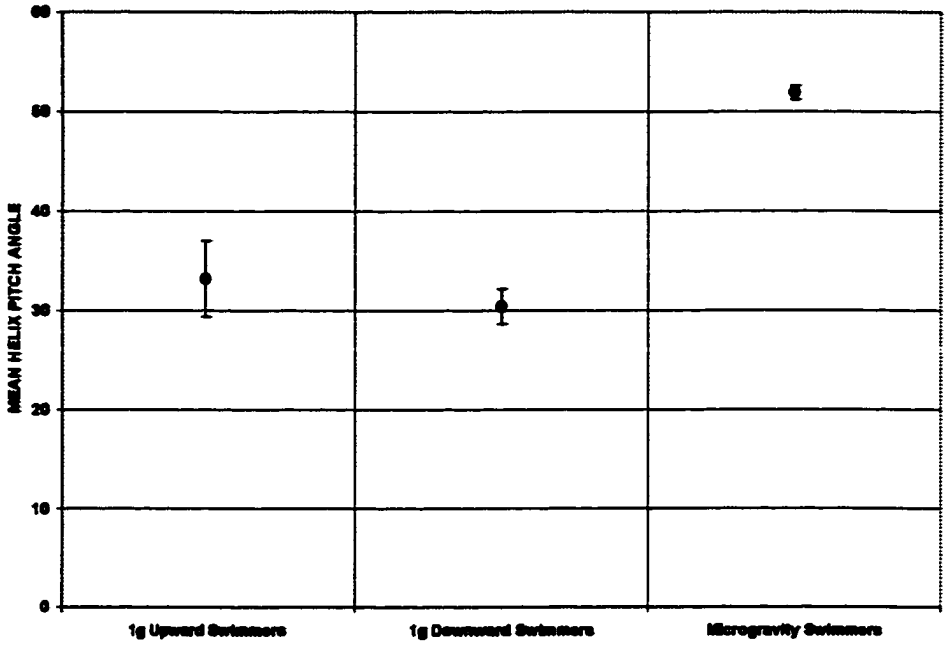

Fig 3.3.47. Comparison of mean helix pitch angles (±S.E.) amongst mussel larvae (*Mytilus edulis*) swimming in normal gravity and microgravity. Data are from Table 3.3.12.

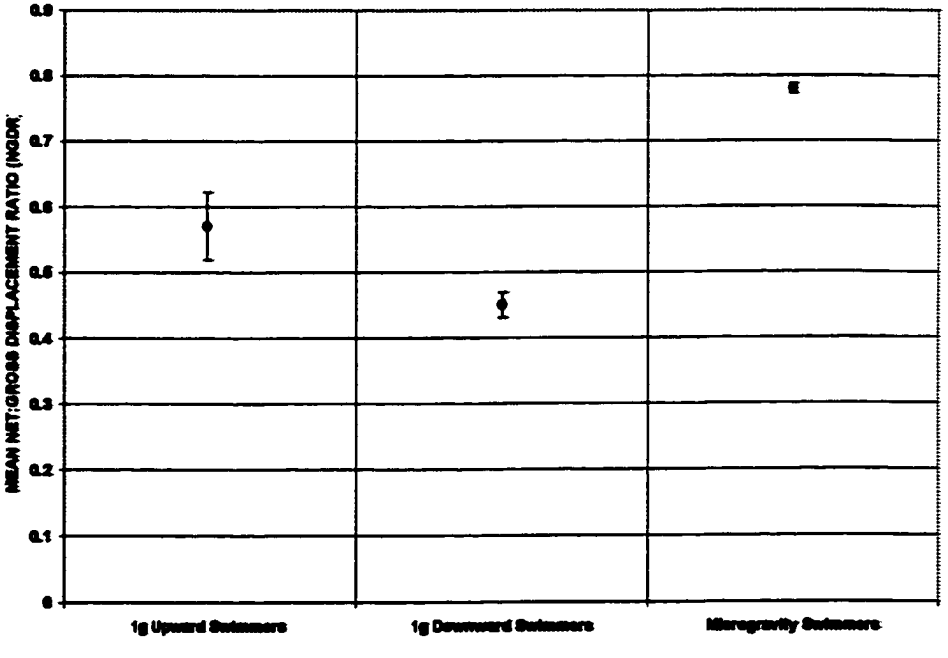

Fig 3.3.48. Comparison of mean net:gross displacement ratios (NGDR) (±S.E.) amongst mussel larvae (*Mytilus edulis*) swimming in normal gravity and microgravity. Data are from Table 3.3.12.

3.3.4 Gravity and Larval Bivalve Orientation

There appeared to be no common direction in which the mussel larvae traveled during their exposure in a microgravity environment. This is clearly apparent in the circular scatter diagrams shown in Appendix 2, Figs. A2.1 to A2.18, which include data pooled from all SCA test chambers observed during each of the eighteen video recording sessions. In these plots, the net direction traveled by each individual larva is plotted on the circumference of a unit circle, and the sample mean vector (r) is calculated and depicted as described in Section 3.2.6. The length of the mean vector is an indicator of the degree of angular dispersion; longer arrows on the scatter diagrams indicate a greater tendency towards a preferred swimming direction. The data that are tabulated with each scatter diagram include the length of the mean vector and the results of the Rayleigh Test, which was used to determine if the distribution of the larval track directions was uniform, or if a preferred mean direction was followed.

In sixteen of the eighteen video recording sessions, the Rayleigh Test revealed that the larvae swimming in microgravity exhibited no preferred direction; the orientation of the tracks was indeed random (using a significance level of α=0.05). The only exceptions to this observation occurred during the Day 3 Day recording session (Appendix 2, Fig. A2.5), and in the Day 10 Night session (Appendix 2, Fig. A2.18). In the Day 3 Day session, there was a slight tendency for the larvae to swim in a mean direction of 52°; the Rayleigh test rejected the hypothesis of uniform distribution at the α=0.05 level of significance, but not at the α=0.10 level. In the case of the Day 10 Night session, the results are from a sample size of only 10 larvae and represent only one SCA test chamber, as the other two chambers were fixed on an earlier date. Again, the

hypothesis of uniform distribution was rejected at the α=0.05 level of significance, but not at the α=0.10 level. Since the general trend of randomly-directed motion was observed in both Day and Night video recording sessions, it is evident that mussel larvae are not using light as an orientation cue in the absence of gravity.

A total of 679 individual tracks of larvae swimming in microgravity were measured in all eighteen video recording sessions. The net directional data from all of these tracks were pooled together, grouped in twenty-four bins of 15°, and plotted on a circular histogram (Fig. 3.3.49). This histogram shows that the track directions appear to be randomly distributed, and the Rayleigh test confirms this observation by accepting the hypothesis of uniform distribution at the α=0.05 level. It is evident that mussel larvae swimming in the absence of gravity exhibited no directional orientation, and moved in random directions. These data suggest that mussel larvae use gravitaxis as their primary means of orientation within the water column.

Fig. 3.3.50 illustrates the track directions of 58 larvae swimming in a normal gravity environment. In this experiment, it was apparent that larvae were swimming in two preferred directions, as evidenced by the two clusters of points in the upper and lower portions of the scatter diagram. While these clusters were not centred exactly around 90° and 270°, presumably due to a slight right-to-left current in the observation chamber, it is clear that the track directions of the larvae were aligned with the vertical gravity vector. Of the twenty larvae swimming upwards the mean angular direction was 102°, while the track directions of the 38 downward-swimming larvae had a mean of 258°. The track directions of both groups of larvae were tightly clustered together, as

revealed by the low angular deviations and long mean vector lengths. The results of the Rayleigh test confirmed that the distribution of larval track directions was not uniform; the larvae were swimming in preferred directions, and these directions were oriented along the gravity vector.

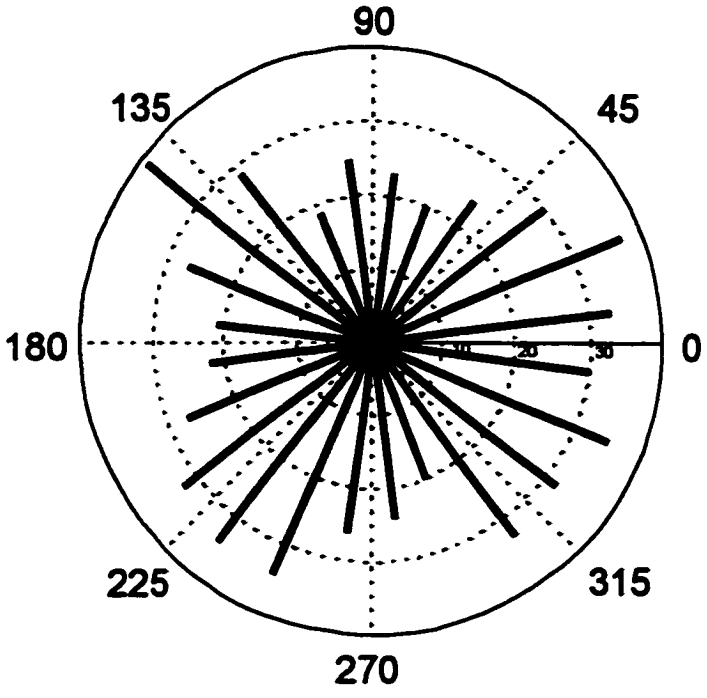

Sample size, *n*	679
Sample mean angle, $\bar{a}$	313.5°
Length of mean vector, *r*	0.04
Angular deviation, *s*	79.4
Rayleigh's z statistic (nr^2)	1.058
Uniform Distribution? (α= 0.05)	Yes

Fig. 3.3.49. Circular histogram illustrating track orientations of mussel larvae (*Mytilus edulis*) swimming in a microgravity environment. Data are pooled from all SCAs over the duration of the microgravity experiment, May 20 - 29, 1996. Concentric circles represent frequency increments of 10 observations. Directional data from the tracks of 679 larvae are grouped into bins of 15°.

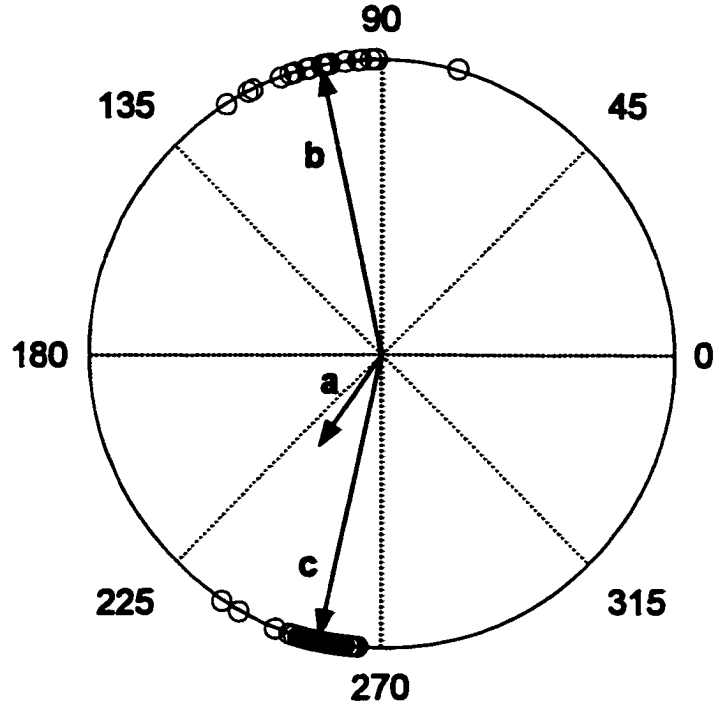

	a - All Swimming Larvae	b - Upward Swimming Larvae	c - Downward Swimming Larvae
Sample size, *n*	58	20	38
Sample mean angle, $\bar{a}$	236°	102°	258°
Length of mean vector, *r*	0.37	0.98	0.99
Angular deviation, *s*	64.4	10.1	5.8
Rayleigh's z statistic (nr^2)	7.900	19.379	37.612
Uniform Distribution? (α= 0.05)	No	No	No

Fig. 3.3.50. Scatter diagram illustrating track orientations of mussel larvae (*Mytilus edulis*) swimming in a normal gravity environment. The arrows indicate the sample mean vectors *m*, and descriptive statistics are tabulated separately for larvae travelling in both upwards and downwards directions. Rayleigh's z statistic tests the null hypothesis that larvae exhibit no preferred direction.

3.4 DISCUSSION

3.4.1 The Role of Gravity in the Swimming Behaviour of Marine Bivalve Larvae

In his descriptions of the swimming behaviours exhibited by larvae of the scallop *Pecten maximus*, Cragg (1980) offered an explanation for why bivalve larvae rotate as they travel upwards, producing a helical pattern. According to this mechanism, the power stroke of beating velar cilia is not exactly perpendicular to the velar edge (see Fig. 3.4.1 B, line *z-z*), but is rather at a slight angle to it (line *y-y* in Fig. 3.4.1 B). Resolution of this force into two vectors produces a vector *p* perpendicular to the velum, and a vector *t* tangential to it. The sum of the *p* force vectors produces the overall downwards propulsive force *P*, shown in Fig. 3.4.1 A, while the *t* force vectors are responsible for rotation of the larva's body (Fig. 3.4.1 C). Since the cilia beat in a coordinated pattern of diaplectic metachrony (Chia *et al.*, 1984), the wave of ciliary beating propagates along the velar edge in a counterclockwise direction, causing the larva to rotate. As the hinge region of the larva is heavier than the velum and therefore hangs lowermost in the larva's normal gravity swimming attitude (Fig. 3.4.1 A), the larva moves upwards in a helix when the velar cilia beat. The pitch angle of the helix is controlled by the action of the velar retractor muscles.

It is apparent that the mechanics of larval swimming in *Mytilus edulis* are similar to those described by Cragg (1980) for *Pecten maximus*. Mussel larvae swimming in normal gravity exhibited the same helical swimming behaviour and degree of control over their locomotion that Cragg observed with scallop larvae (see Section 3.3.2). According to Cragg's model, gravity has only indirect influences upon the formation of a

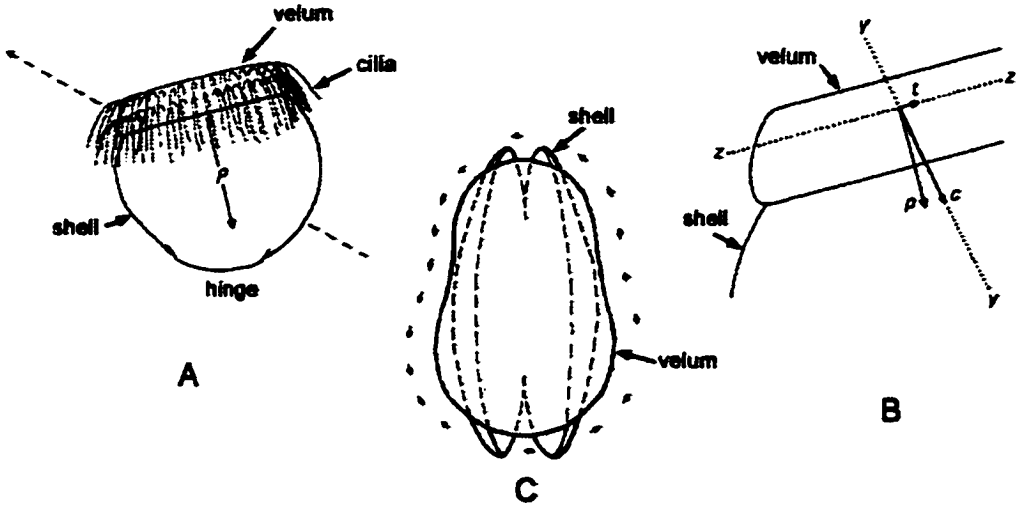

Fig. 3.4.1. Swimming dynamics of larval *Pecten maximus*. (A) Normal veliger swimming attitude, with direction of movement indicated by dashed arrow. (B) Magnified view of the velar edge, with cilia hidden. Beat plane of cilia indicated by line *y*-*y*, resultant force vectors *p* and *t* shown. (C) View of velum from above, showing the direction of tangential force vectors *t* and of metachronal wave propagation. (Adapted from Cragg, 1980).

helix as a larva swims; it may help to maintain larval attitude, and it partially counteracts the propulsive force of the velum so that the net forward motion of the animal is displaced towards the horizontal (see Fig. 3.4.1 A). The results from the ARF experiment support this contention that gravity is not directly involved in the generation of the helical swimming pattern of larval bivalves, as defined by Hypothesis A1. Microgravity-reared larvae continued to swim in a helical pattern, although the overall behavioural patterns of larvae swimming in microgravity were often markedly different from those exhibited by larvae in normal gravity. Many of these differences can be explained, however, by the influence of gravity acting in more indirect ways.

The geometry of the tracks of larvae swimming in microgravity clearly differed from those made by larvae under conditions of normal gravity. Both the helix height and the helix pitch angles of larvae swimming in microgravity were significantly greater than those tracked by larvae in the presence of gravity, supporting the prediction of Hypothesis A1 that gravity acts as a restraining force on bivalve larvae. With gravity not present to counter the larva's propulsive efforts, forward motion was unimpaired and larvae moved in alignment with the direction of force produced by the velar cilia. This meant that the larvae were not only able to advance at a steeper angle and produce a higher helix, but also resulted in the faster forward swimming speeds observed for the microgravity reared larvae. Lending further support to Hypothesis A1 was the observation that the net-to-gross displacement ratios (NGDRs) of larval tracks from the microgravity treatment were significantly higher than those calculated for either of the two normal gravity groups. This indicates that the vertical (or forward) component of helical travel predominated over horizontal motion for larvae swimming in microgravity

(Gallager, 1992). The interaction of gravity with other physical forces acting upon swimming bivalve larvae is investigated in more detail in the kinematic analysis model outlined in Chapter 5.

Other differences in the motion patterns of larvae were noted that appeared to be gravity related. The diameter of helices tracked by microgravity reared larvae and upward swimming larvae were significantly smaller than those of larvae that were swimming downwards. A similar trend was observed with measurements of the rotational and translational linear velocities; both measures of speed were significantly greater for larvae swimming downward in normal gravity than those recorded for the microgravity and upward swimming larvae. Taken together, these observations mean that the downward swimming larvae were swimming in wider helices, at a greater rate of speed, and at a less acute pitch angle than either upward moving larvae, or larvae swimming in microgravity. Downward swimming may be an adaptation for optimising larval feeding success. Gallager (1993) reported that bivalve larvae can hover in the horizontal plane and create larger flow fields than are possible when the animals are moving upwards or sinking. This behaviour is of great advantage when larvae are in a patch of food, where the larger flow fields enable them to maximise feeding rates. Although reports and descriptions of downward swimming behaviour are rare in the literature, it is likely that the larvae swimming downward in this study were also exercising a variation of the hovering activity reported by Gallager (1993).

The analyses of helical motion suggest that the mussel larvae altered their behaviour somewhat over the 10-day duration of the microgravity experiment. There was a trend towards larger helix height and diameter dimensions as the experiment

progressed, while no changes were observed in the NGDR, forward velocity, or instantaneous linear velocity datasets. Although the pitch angle of the helices may have been expected to become steeper to account for the higher helices, this was not the case; pitch angle also remained constant throughout the experiment. However, the increased height and diameters of the helices can be explained with the observation that the angular (or rotational) velocity decreased as helix height and diameter increased. A slower rate of rotation resulted in the larvae moving forward in a higher and wider arc before turning around through 360° to complete a helix. This behaviour may be related to an increased propulsive capacity as the larvae got older and the velum expanded in size (Cragg, 1980), but this is improbable since larvae in the microgravity experiment did not grow much during the experiment (see Section 4.4.1.1). It is possible that the larvae were exhibiting a food searching behaviour. If gravity is actually required to enable bivalve larvae to create sufficient shear to extract algae from their surroundings (see Hypothesis B1, Chapter 4), then larvae in the absence of gravity may have been food-limited. Swimming in higher, wider helices as the experiment progressed may have been an attempt to scan more territory in order to locate food patches in response to nutritional stress.

A distinctive feature of the patterns of larvae swimming in microgravity is that many of them changed direction and helix shape as they moved forward (see Appendix 1). The result is often very bizarre looking tracks, with helices of different heights, pitch angles, and diameters, and frequent changes of direction. This behaviour may have been an attempt on the part of the larvae to orient themselves, or it may reflect alterations of individual components of locomotion and feeding behaviours that are otherwise masked by the influence of gravity. In some cases, larvae were observed to stop swimming

altogether for a period of time, then move away in another direction. This particular behaviour was undoubtedly the result of a cessation of ciliary beating, which would have corresponded to sinking behaviour under conditions of normal gravity. Although larvae swimming in normal gravity can alter the height and diameter of their helices, directional changes are a behaviour that is not observed when gravity is present. In some cases in the microgravity experiment, it is possible that larvae changed swimming direction when they came into contact with another larva, or with the flow field generated by another larva. However, this is unlikely for the majority of the tracks where directional changes were observed, since the low stocking density of larvae in the SCA test chambers (~3 larvae/ml) ensured that interactions between larvae was minimal.

Another explanation for the unique behaviours seen in microgravity can be found with a more detailed examination of the kinematics of helical locomotion. Crenshaw (1990, 1993, 1996) described the mechanics of helical swimming for small aquatic organisms in great mathematical detail. The models presented in this series of papers describe how an organism's translational and rotational velocities interact to define helical motion, and how control of these two velocity parameters can account for the entire range of motions available to these organisms. By manipulation of these two components of velocity, organisms can change their swimming direction and thereby orient themselves to external stimuli. Crenshaw (1996) reported that a neutrally buoyant organism (sea urchin spermatozoa) can change its direction and helical height by altering its rotational velocity while keeping its translational velocity constant. It is likely that a similar mechanism can account for the directional changes exhibited by mussel larvae in the ARF microgravity experiment. When mussel larvae in microgravity changed the

direction in which they were swimming, Crenshaw's model suggests that they were changing their rotational velocity at the same time. Further analyses of the videotapes from the ARF experiment would have to be performed to confirm this. Alteration of rotational velocity may also have resulted in changes in helical dimensions, but it is possible that changes in the size of the helix was a result of manipulation of the velar retractor musculature (Cragg, 1980). In any case, the ability to change rotational velocity is a mechanism of behavioural modification that has hitherto not been described for bivalve larvae.

Since changes in direction are not observed when bivalve larvae swim under normal environmental conditions, it is apparent that gravity overrides the effect of behaviours that result in directional changes in microgravity. The force of gravity is therefore greater than any force that bivalve larvae can generate in the horizontal plane; the larvae are, in effect, tethered in the vertical direction by the pull of gravity. All actions of the larva are thus oriented in line with the gravity vector, resulting in a form of passive gravitaxis.

Bivalve larvae have a variety of mechanisms at their disposal for movement within their environment, the sum of which comprise a flexible repertoire that enables these animals to successfully function within the plankton. These include, firstly, modulation of ciliary beat frequency; propulsive power and vertical velocity are proportional to the frequency at which the velar cilia beat, up to a certain maximum where propulsive efficiency diminishes (Gallager, 1993). Secondly, the velum of the bivalve veliger has a complex system of paired retractor muscles, which function to orient the velum with respect to the rest of the body in a variety of positions (Cragg,

1985). This musculature is presumed to be responsible for enabling the larva to alter the helical pitch angle, and thereby the height and diameter of the helix as well. In addition, complete retraction of the velum within the shell is an effective means of achieving rapid downward locomotion. Finally, the ability to modify rotational velocity may be another means by which larvae can change the shape of either their swimming helix, or the feeding flow fields that their swimming actions create. Recent descriptions of a complex nervous system within larval *Mytilus edulis* (Croll *et al.*, 1997) suggest that bivalve larvae possess a sophisticated degree of control and integration of these locomotor and feeding activities, that enables them to feed and migrate within a vertically structured environment.

3.4.2 The Role of Gravity as an Orientation Cue in Marine Bivalve Larvae

In accordance with the prediction of Hypothesis A2, the results from the ARF experiment clearly indicate that the larvae of *Mytilus edulis* use gravitaxis as their primary method of orientation within the water column. In the absence of gravity, larvae swam in random directions throughout the ten day experiment, as shown by the results from the Rayleigh test of the distribution of track directions (see Section 3.3.4). While the ARF study was not designed to determine if mussel larvae can orient themselves to other environmental stimuli such as light, the configuration of the ARF provided a directed light source at the top and a heat-producing bank of infrared video illumination LEDs at the bottom of each Specimen Container Unit (see Chapter 2). Since the larvae exhibited no preferred direction of swimming whatsoever, this also provides some evidence that these animals may not be capable of orienting to light or temperature as directional cues.

To date, few other studies have attempted to elucidate the mechanisms underlying gravitactic behaviour in planktonic organisms by manipulation of the gravity vector. In July 1994, the Spacelab IML-2 (International Microgravity Laboratory) mission included the German-built NIZEMI slow-rotating centrifuge microscope aboard the space shuttle Columbia. This payload was capable of observing and recording the swimming paths of microorganisms subjected to gravitational accelerations ranging from 10^{-3}g (the ambient gravitational force aboard the shuttle) to a maximum of 1.5g (Hemmersbach *et al.*, 1996). The investigators using this facility were testing the hypothesis that aquatic microorganisms orient to gravity by using an active gravireceptor, and not by means of a passive "buoy" mechanism. The protozoans *Paramecium biaurelia* and *Euglena gracilis* were subjected to periods of stepwise increases and decreases in gravitational acceleration, and their direction of movement and swimming velocities were measured post-flight using image analysis routines. Both *Paramecium* and *Euglena* exhibited a loss of directed orientation in the absence of gravity, and increased swimming speeds. It was also apparent that a minimum threshold value for graviresponses existed between 0.08g and 0.16g for *Euglena* (Häder *et al.*, 1996), and between 0.16g and 0.3g for *Paramecium* (Hemmersbach *et al.*, 1996). As gravitational force was increased through these thresholds, the organisms began to align themselves with the gravity vector. The dose-response curve of gravitational force versus precision of vertical orientation followed a sigmoidal pattern typical of physiological responses (Häder *et al.*, 1996).

These results supported the authors' contention that an active physiological signal transduction chain is the mechanism behind gravitactic orientation (Hemmersbach *et al.*, 1996; Häder, 1997). In this model, the cytoplasm is heavier than the surrounding

medium, and exerts a pressure on the lower cell membrane. As the organism moves, or alters its swimming attitude, the pressure on different regions of the cell membrane changes. The resulting deformations in the cell membrane activate stretch-sensitive ion channels, altering membrane potential and thereby stimulating locomotor activity. The model assumes that these ion channels are unevenly distributed across the cell, and that during vertical swimming activity the degree of ion channel stimulation would be minimal. In this system, the entire organism functions as a statolith (Hemmersbach *et al.*, 1996). It has been suggested that this hypothesis may also be applicable to other Protozoa that exhibit gravitactic orientation responses (Lebert and Häder, 1996).

The ARF experiment was not intended to test hypotheses regarding the actual mechanisms of gravireception and gravitaxis. However, the evidence from this experiment suggests that bivalve larvae orient themselves to gravity by means of a simple, passive "buoy" mechanism, as suggested by Cragg (1980). Since they are significantly heavier than seawater, they have a tendency to sink when locomotion ceases; in this way, downward motion is oriented directly along the gravity vector. The hinge area of the larva's shell is much heavier than the velum region (see Fig. 3.4.1), and as such the velum always remains pointed upwards as the normal attitude of the animal. The velar cilia are arranged so that the power stroke is effective in the downward direction, meaning that whenever the larva applies propulsive force the resulting motion is always directed in an upwards direction. This simple mechanism allows the animal to navigate throughout the three-dimensional water column without the need for specialised receptor organs.

3.4.3 Overall Summary

This study was designed to use the microgravity environment of a Space Shuttle laboratory as a means of investigating the role that gravity plays in the swimming behaviour and orientation mechanisms of marine bivalve larvae. To address this fundamental question, two hypotheses were tested and some overall conclusions can be drawn from the results of these experiments. Gravity helps to maintain the swimming attitude of bivalve larvae, thereby holding them to an orientation that results in vertically-directed movement. By acting as a restraint on upward movement gravity causes larval swimming paths to be displaced towards the horizontal axis, a consequence that may be exploited by larvae to maximise feeding efficiency. Bivalve larvae may also have the ability to change their locomotor patterns by adjusting their rotational velocity, a behavioural mechanism that has not previously been considered for these animals. And finally, it has been demonstrated that the larvae of *Mytilus edulis* definitely use gravitaxis as their primary means of orientation and navigation within the water column. The results from these experiments will be further discussed in context with the results of the feeding and growth studies from Chapter 4 in the final section of this thesis.

CHAPTER 4

Effects of Gravity on Feeding and Development of Marine Bivalve Larvae

4.1 INTRODUCTION

4.1.1 Overview and Objectives:

The pathways by which gravity plays a role in the biology of marine bivalve larvae and other zooplankters have been outlined in Section 1.1. Gravity acts as an orientation cue for planktonic organisms as they migrate throughout the water column, and is one of the physical forces governing the helical swimming pattern that is typical of larval bivalve behaviour. In addition, gravity is a force that can draw zooplankters away from their food source near the ocean surface, but it has also been implicated as a means by which bivalve larvae can optimise their feeding efficiency. The aim of this portion of the Aquatic Research Facility investigation was to address the basic question of how gravity affects feeding, growth, and development of marine bivalve larvae.

4.1.2 Tests of the Hypotheses:

The hypotheses outlined in Section 1.2 were tested by experiments designed to take advantage of the capabilities of the Aquatic Research Facility. The larvae of the blue mussel *Mytilus edulis* was chosen as the model species for this investigation, in part because it has a density greater than most zooplankters, and also because there is a wealth of data in the literature regarding its feeding and growth physiology in a normal gravity environment (see Bayne, 1965; Beaumont and Budd, 1982; Jespersen and Olsen, 1982; Sprung, 1984 a,b,c,d; Pechenik *et al.*, 1990; Widdows, 1991). The experimental design was such that data collected in the testing procedure of one hypothesis could also be used when another was tested. The basic approach used to test these hypotheses is outlined below.

4.1.2.1 Test of Hypothesis B1:

The influence of gravity in zooplankton feeding mechanisms was discussed by Strickler (1982), where he addressed the paradoxical situation in which zooplankters do not attain neutral buoyancy in spite of the high energetic cost of swimming against the force of gravity. In this scenario, small plankters are faced with the problem of extracting food from a viscous fluid environment in which food particles are widely dispersed or located in isolated patches. The creation of flow fields by the animal alleviates this problem by enabling large volumes of water to be moved past its feeding appendages, thereby concentrating food particles from its nutritionally dilute surroundings. For plankters that are heavier than seawater, the interaction between the movement of feeding appendages and the pull of gravity expands the size of the feeding current. This model was elaborated upon by Emlet and Strathmann (1985), who proposed that the feeding process of plankters is enhanced by any retarding force, including drag as well as gravity. Their argument suggests that the movement of feeding appendages against a tethering force steepens the velocity gradient around the appendages, thereby shearing through the thick viscous fluid and increasing contact with food particles. Feeding is further enhanced if the magnitude of these forces are increased, either by increasing drag via the motion of complex appendages, or by increasing the density of the organism relative to seawater. However, the locomotor cost of moving against gravitational and/or drag forces can be high, and zooplankters may face a trade-off between optimising locomotor and feeding efficiencies.

The model as outlined here can be investigated by modification of one of the restraining forces acting upon swimming zooplankton. The microgravity environment

available in a Space Shuttle laboratory provides an ideal opportunity to eliminate the gravity component, thereby enabling certain predictions regarding this model to be made. For a relatively heavy zooplankter like the veliger larva of the blue mussel *Mytilus edulis*, the model predicts that the absence of gravity will disable the means by which the animal can maintain and increase the size of its flow field. With gravity not present to act as a tethering force, the cilia used by the larva as feeding appendages will not be able to create sufficient shear to overcome viscous forces and maximise food particle encounter. Overall food intake will be reduced, as will the growth of the animal. As feeding efficiency is inhibited, however, the model also predicts that the removal of gravity will enhance the locomotor capabilities of the animal (see Chapter 3).

The experiments conducted in the Aquatic Research Facility were designed to test Hypothesis B1 by examining feeding and growth of larvae reared under microgravity and normal gravity conditions over the ten day duration of the Space Shuttle mission STS-77. Samples of larvae were scheduled to be preserved at regular intervals during the flight, and post-landing measurements of shell length, height, and square area were to be made in order to assess larval growth rate as a function of gravity. As a means of assessing the impact of gravity on larval feeding, algal cell concentration was to be determined precisely on a pre- and post-flight basis. Changes in the concentration of the flagellate alga *Isochrysis galbana* were expected to reflect variations in the net balance between algal growth and larval grazing. In addition, the ARF's Algae Measurement Unit (AMU) was programmed to monitor algal concentration in the SCA test chambers several times a day throughout the experiment.

4.1.2.2 Test of Hypothesis B2:

Most marine invertebrate larvae are denser than their seawater environment (Chia *et al.*, 1984). In order to remain suspended within the upper reaches of the water column where food is concentrated, zooplankters must counter their tendency to sink by either swimming, increasing their buoyancy, or a combination of both (Power, 1989; Alexander, 1990). A variety of mechanisms facilitating buoyancy regulation exist amongst the different groups of plankton. These adaptations include gas-filled vacuoles or chambers and the maintenance of low-density body fluids through the use of active ion pumping, but the majority of zooplankton achieve increased buoyancy through the accumulation of lipids such as triglycerides or wax esters (Marszalek, 1982; Alexander, 1990). Since lipids are also the principal energy reserve of marine invertebrate larvae that are catabolised in times of stress (Holland, 1978), their dual-purpose role in larval bivalve physiology can present these animals with unique problems.

Gallager (1992) presented a model describing a possible mechanism by which bivalve larvae can actively regulate their buoyancy. The overall specific gravity of the larva is the result of a balance between the positive buoyancy provided by the lipid reserves and the negative buoyancy imparted by the heavy calcified shell. As the larva feeds at a satiating level, new shell material is added and the animal grows in size, and surplus energy is stored in the form of low density triglyceride globules in the digestive gland. The density of the larva remains relatively constant, presumably at a level that enables the animal to optimize feeding efficiency (see Hypothesis B1). If the animal is starved, however, the lipid reserves are catabolised to provide for the larva's energy requirements, and the density of the larva increases. This means that more energy must

be allocated to locomotion in order to stay up in the water column where food is most likely to be found. Since the cost of locomotion can account for up to 50% of the total larval energy budget (Zeuthen, 1947), this increased energy expenditure would deplete the lipid reserves even more rapidly. The positive feedback loop thus described can cause the rapid exhaustion of both the larva's energy reserves and its ability to maintain buoyancy, leading to an increased probability of death. On the other hand, if food is encountered, the lipid reserves will be replenished and optimal buoyancy would be restored.

Gallager's model indicates that buoyancy must be tightly regulated by bivalve larvae, not only in order to optimize feeding efficiency, but also as a means of maintaining position within the water column, and hence survival. If buoyancy is indeed regulated by balancing the accumulation of low density lipid deposits and high density aragonitic shell material, then certain predictions can be made regarding buoyancy control when gravity is removed. According to the model, microgravity will not only deprive the larva of a directional cue, but the tethering action hitherto provided by gravity will also be lost. The larva will encounter difficulties in feeding because of the inability to create enough shear to allow the velar cilia to contact and capture a sufficient amount of food particles. If the larva is capable of active buoyancy regulation, more negatively buoyant shell material should be added and fewer positively buoyant lipid reserves will be stored. The result would be a larva that has increased its overall specific gravity in an attempt to compensate for the microgravity environment by increasing shear around the feeding appendages.

The Aquatic Research Facility experiment was designed to test Hypothesis B2 by comparing the density, lipid content, and degree of shell mineralization in groups of larvae reared in both a microgravity and a control normal gravity environment. Differences between microgravity and normal gravity treatments in terms of the balance of specific gravity, lipid reserves, and shell calcification were expected to provide insight into the interactions between buoyancy regulation, feeding efficiency, and energy utilisation in marine bivalve larvae.

4.1.2.3 Test of Hypothesis B3:

The study of early developmental processes in a variety of organisms has long been a priority of the life science programs of both NASA and CSA. Of particular interest has been the attempt to determine if critical early stages of development can proceed normally in the absence of gravity. Some attention has focused on using the microgravity environment of space to study the development of aquatic invertebrates, including sea urchins (Marthy *et al.*, 1996; Marthy *et al.*, 1998), jellyfish (Spangenberg *et al.*, 1995), sea stars (Crawford and Martin, 1998), and the brine shrimp *Artemia* (Spooner *et al.*, 1994). To date, however, no long-term microgravity studies have examined the role of gravity in the early development of any representative of the Bivalvia. This investigation of larval development in the blue mussel *Mytilus edulis* is therefore a pioneering study in the field of gravitational biology. Results from this study were also expected to aid in the assessment of *Mytilus edulis* as a candidate species for further space-based study.

Hypothesis B3 was tested in the Aquatic Research Facility experiment by examination and measurement of several indicators of larval bivalve development. Although the progress of molluscan development can be difficult to assess due to the lack of distinctive staging criteria (Pechenik *et al.*, 1990), certain observations could be made that allow for comparisons between the gravity treatments. The distribution and relative amount of neutral lipid deposits was examined in live larvae from both gravity treatments as a means of detecting any gross differences in lipid metabolism. To determine if gravity is required in order for normal shell mineralisation to occur, the degree of shell calcification was compared amongst larvae sampled at various intervals throughout the experiment. Larval survival and the overall appearance and general condition of larvae were also used as criteria to determine the influence of gravity in larval mussel development.

4.2 MATERIALS AND METHODS

4.2.1 Post-Flight Procedures:

Detailed analyses of all samples commenced immediately after returning to Dalhousie University from Kennedy Space Center on June 4, 1996. The larvae from MS-1 SCA test chamber #3L0 and MS-1 SCA test chamber #3L1 that were kept alive after return from orbit were individually transferred to wells of a sterile tissue culture plate, and were supplied with fresh 0.2-μm filtered seawater and *Isochrysis galbana* (clone ISO). They were maintained in a 12°C refrigerated chamber, and their condition was monitored on a Nikon inverted microscope equipped with a high-resolution monochrome video camera (Pulnix TM-7EX). Larval behaviour was recorded daily on Hi8 format videotape, and digital images of each larva were grabbed and saved to disk to allow for quantification of changes in shell size.

Larvae preserved during the MS-1 Flight Experiment, the MS-2 Ground Control Experiment, and the lab control experiments were carefully removed from their storage vials and counted under a dissecting microscope, to provide an indication of survival rates during the shuttle mission. All larvae were examined on a compound microscope (Nikon Microphot-FXA), and a high-resolution digital image of each larva was obtained and saved to disk, using a Pulnix TMC-7 analogue video camera coupled with an Imaging Technology (Bedford, MA, USA) IC-PCI digital frame grabber. Image analysis software (Optimas version 5.2) was used to measure the shell length, height, and square area of each larva (see Fig. 4.2.1 for illustration of these parameters).

As a method of measuring the degree of shell calcification, the birefringence of each larva was observed under polarised bright field illumination. In this procedure, the microscope's polariser and analyser are oriented at 90 degrees to each other, producing 100% extinction of all light transmitted by the soft tissues of the larval specimen. The aragonitic calcium carbonate crystals of the shell, however, reorient the polarised light in a distinctive pattern known as birefringence; the intensity of this pattern is proportional to shell thickness. A digital image of the birefringence pattern of each larva was also saved to disk (see example in Fig. 4.2.1). The intensity of shell birefringence for each larva was measured by multiplying the mean digital grey value (ie., luminance) of the shell's birefringence image by the shell area for each larva, using image analysis software (Optimas version 5.2). The condition of each larva was subsequently assessed and assigned to one of three categories; good, poor, or dead. Larvae in poor condition were distinguished by deteriorated internal tissues, or shells that were decalcified or otherwise deformed.

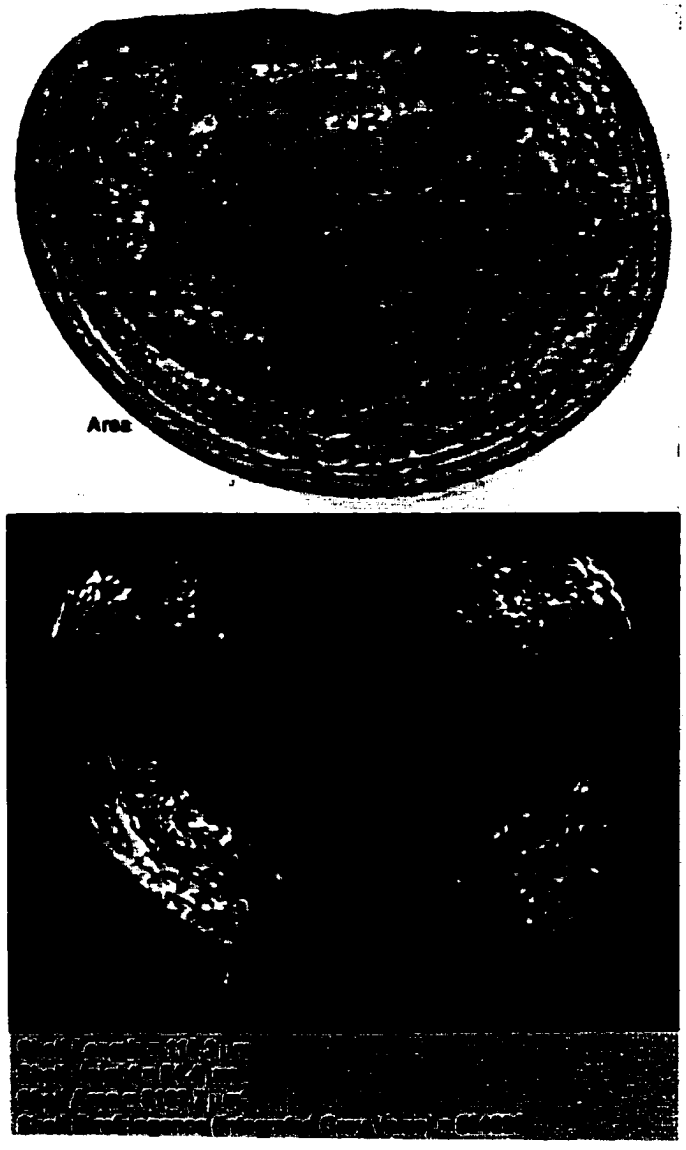

Fig 4.2.1. Illustration of the morphometric parameters that were measured with image analysis software for each mussel larva used in the Aquatic Research Facility experiment on Space Shuttle Mission STS-77, May 19-29, 1996. In these sample images of one individual, shell length, height, and square area are indicated in the top image, and the pattern of shell birefringence observed through cross-polarised filters is shown below.

The algae samples (*Isochrysis galbana*) were counted using an epifluorescence microscopy technique described by Waterbury *et al.* (1986). In this approach, a known volume of sample was filtered onto black 0.8 μm Millipore filter paper, which was then mounted on a glass slide in fluorescence-free immersion oil and examined on an epifluorescence microscope (Nikon Microphot-FXA) outfitted with a blue excitation filter block (420-490nm band pass excitation filter, 510nm dichroic mirror, and 520nm barrier filter). The chlorophyll in the algal cells fluoresce bright red, allowing them to be easily identified and enumerated. Using a 100x oil immersion objective, all algal cells within each of thirty randomly selected 0.014mm^2 fields were counted. By comparing the total number of cells within these thirty fields with the total area of the filter paper and the volume of the water sample, the concentration of algal cells within the SCA test chambers was calculated. A minimum of two replicate subsamples from each algae sample were counted using this procedure, and the data were compiled to provide an indication of the larval feeding rate.

4.2.2 Data Analysis:

Data were processed and manipulated using Microsoft Excel 97, and all statistical analyses were performed using SYSTAT version 8.0.2. Both of these software packages were used for the creation of graphs and figures.

The larval survival and condition data were analysed using a series of two-way contingency tables. The variable used in the table rows was the sample time, as represented by the four SCA test chambers (Days 3, 5, 7, and 10). The column variable for the condition data was the three categories of larval condition, assessed according to

the criteria outlined in Section 4.2.1, while "Dead" or "Alive" were used as the two levels of the column variable for the survival data.

Larval survival data were examined by grouping the "Good" and "Poor" categories together as a single "Alive" category, and a series of 2 x 2 pairwise tables tested the independence of survival from gravity treatment on each sampling day. A series of 4 x 3 contingency tables tested the null hypothesis of independence between larval condition and the four SCA test chambers (ie., sample time), for each gravity treatment. Pairwise 2 x 4 tables tested the independence of larval condition from gravity treatment on each sampling day. In all analyses, the log-likelihood ratio G-test was used for hypothesis testing, with a significance level of $\alpha = 0.05$ chosen as the criterion for rejection of the null hypotheses. The G-test is commonly preferred by biostatisticians over the chi-square test for two-way contingency table analysis (Sokal and Roelf, 1981).

Larval growth data were analysed using SYSTAT's linear regression and analysis of variance (ANOVA) modelling techniques. Morphometric data for each sample date were fitted with linear regression lines and analyses of variance were used to test if the slopes of these lines were significantly different from a zero slope, thereby indicating positive growth rates (Zar, 1984). Two-way ANOVA models were used to test for the dependence of the morphometric parameter in question (shell length, height, square area, and shell birefringence) upon gravity treatment, sample date, and the interaction term of these two factors. When significant differences due to one or more factors were detected by ANOVA, post-hoc Tukey's multiple comparisons were used to determine which samples were responsible for the differences.

4.3 RESULTS

4.3.1 Qualitative Observations of Live Larvae Returned From Space

On Landing Day, May 29 1996, examination of the larvae from the two ARF MS-1 Specimen Container Units (SCUs) that were not injected with glutaraldehyde in orbit (SCA test chamber #3L0 and SCA test chamber #3L1) revealed that many of these larvae were still alive after 10 days in space, and several were in good condition. Surviving larvae from SCA test chamber #3L0, which had undergone the majority of their development in a microgravity environment, appeared to have developed normally. Their general physiological and anatomical condition was similar to larvae from SCA test chamber #3L1, which were raised in a control normal gravity environment. Internal organs, as well as the vela and velar cilia, appeared to be normal and functional. The thickness of the larval shells, as indicated by the intensity of shell birefringence under polarised light, also appeared normal in the larvae raised in microgravity. The pattern of lipid distribution within a sample of these larvae (as observed using the Nile Red lipid staining technique) was also found to be similar to that seen in the larvae from SCA test chamber #3L1. The specific gravity of a subsample of six larvae was found to be approximately 1.35 $g \cdot cm^{-3}$, the same as the density of larvae grown in normal gravity. The pH of the seawater from SCA test chamber #3L1 was 7.2, but unfortunately the sample from SCA test chamber #3L0 was accidentally contaminated and could not be measured. Many of the microgravity-reared larvae were actively swimming, and their behaviour was generally considered to be normal and similar to that exhibited by animals raised under normal gravity conditions. The condition of the six larvae from SCA test chamber #3L0 that were kept alive and returned to Halifax deteriorated in the days

following their return from space, and all had died within three weeks. The growth of these larvae during this time was negligible.

4.3.2 Larval Survival and Condition

Recovery data and condition assessment of all larvae retrieved from the eight SCA test chambers used in the ARF MS-1 Flight Unit are summarised in Table 4.3.1 and Fig. 4.3.1. There was a common trend in both the 0g and 1g treatments towards lower recovery in SCA test chambers that were fixed later in the experiment. These "missing" larvae may be the result of increased mortality, or loss due to handling operations. Since every precaution was taken during unloading procedures to ensure that the maximum number of larvae was retrieved, the possibility that some larvae were lost during retrieval operations is remote. It is more likely that the larvae missing from the samples represent mortalities. Although some dead, empty-shelled larvae were found in all samples, it is probable that larvae that died early in the experiment decomposed to the point where their shells decalcified and could no longer be identified in the retrieved samples. For the purposes of this investigation, the "missing" larvae were grouped together with the dead larvae that were found in the retrieved samples.

Survival data from the ARF MS-1 Flight Unit are recorded in Table 4.3.1, and can be visualised in Fig. 4.3.1 as the sum of larvae in the good and poor condition categories. In both the microgravity and the normal gravity treatments, the proportion of live larvae decreased throughout the experiment at similar rates. In the Day 3 samples, 80 larvae were still alive in the microgravity SCA test chamber, and 79 larvae were alive in the normal gravity chamber. By Day 10, only 31 live larvae were found in the microgravity

Table 4.3.1. Summary of larval mussel recovery, survival, and condition data from ARF Main System #1 SCA test chambers during microgravity (0g) and normal gravity (1g) exposures on board Space Shuttle Mission STS-77, May 19-29, 1996. One hundred larvae were initially loaded into each SCA test chamber before launch. In SCA test chambers that were fixed in orbit, "Larvae Alive" refers to those larvae that appeared to have been alive at time of fixation.

				CONDITION				
SAMPLE #	SCA #	# LARVAE RECOVERED	# LARVAE ALIVE	GOOD	POOR	DEAD	MISSING	DEAD + MISSING
0g Day 3	4R0	96	80	51	29	16	4	20
0g Day 5	4L0	77	76	59	17	1	23	24
0g Day 7	3R0	66	52	36	16	14	34	48
0g Day 10	3L0	47*	31	23	8	16	53	69
1g Day 3	4R1	82	79	65	14	3	18	21
1g Day 5	4L1	90	84	80	4	6	10	16
1g Day 7	3R1	60	53	42	11	7	40	47
1g Day 10	3L1	43	37	30	7	6	57	63

* Includes 6 live larvae that were used in density measurements, and 6 larvae that were kept alive after landing.

Table 4.3.2. Summary of larval mussel recovery, survival, and condition data from ARF Main System #2 SCA test chambers during hypergravity ("1g") and normal gravity ("0g") exposures in Orbiter Environmental Simulator (OES) during Space Shuttle Mission STS-77, May 20-30, 1996. One hundred larvae were initially loaded into each SCA test chamber before launch. In SCA test chambers that were fixed in orbit, "Larvae Alive" refers to those larvae that appeared to have been alive at time of fixation.

				CONDITION				
SAMPLE #	SCA #	# LARVAE RECOVERED	# LARVAE ALIVE	GOOD	POOR	DEAD	MISSING	DEAD + MISSING
"0g" Day 3	4R0	88	81	72	9	7	12	19
"0g" Day 5	4L0	82	76	76	0	6	18	24
"0g" Day 7	3R0	68	45	40	5	23	32	55
"0g" Day 10	3L0	43	34	27	7	9	57	66
"1g" Day 3	4R1	87	80	77	3	7	13	20
"1g" Day 5	4L1	77	72	71	1	5	23	28
"1g" Day 7	3R1	29	11	10	1	18	71	89
"1g" Day 10	3L1	79	73	62	11	6	21	27

sample, and 37 larvae were still alive in the 1g chamber. These slight differences in survival between the two gravity treatments are not significant on any of the four sample dates ($P > 0.05$), as can be seen by examination of the series of pairwise two-way contingency tables shown in Table 4.3.3. In all cases, the tests concluded that larval survival is independent of gravity treatment.

The numbers of larvae from the ARF MS-1 SCA test chambers that were dead, in good condition, or in poor condition are represented in Fig. 4.3.1. The percentage of larvae that were in good condition decreased throughout the flight experiment in the 0g treatment SCAs, from a high of 59% in the Day 5 sample to a low of 23% among the larvae that returned from orbit on Day 10. The proportion of dead larvae increased during this time from 20% on Day 3 to 69% on Day 10, while the percentage of larvae in poor condition declined from 29% to 8% in the same period. A two-way contingency table analysis (see Table 4.3.4) compared the numbers of larvae within each of the condition categories across the four different sample dates. The results of this test confirmed that the condition of larvae raised in microgravity was dependent upon the day on which they were sampled ($P < 0.05$); in other words, the relative amount of larvae in each of the condition categories was significantly different on each of the four sample dates.

The 0g Day 3 (SCA# 4R0) sample was noteworthy in that many of the larvae were either dead (20%) or in poor condition (29%); only 51% of the larvae were regarded as being in good condition at the time of fixation. The rather poor condition of larvae in this SCA test chamber is particularly relevant in light of the observations of larval behaviour noted in this chamber after review of the videotape recordings made

Table 4.3.3. Two-way contingency tables used in analyses of larval mussel survival data from the microgravity (0g) and normal gravity (1g) SCA test chambers in ARF Main System #1 during Space Shuttle Mission STS-77, May 19-29, 1996. One hundred larvae were initially loaded into each SCA test chamber before launch.

H_0: Larval survival is independent of gravity on sample date indicated
H_A: Larval survival is not independent of gravity on sample date indicated

SAMPLE #	ALIVE	DEAD	TOTALS
0g Day 3	80	20	100
expected	*79.5*	*20.5*	
1g Day 3	79	21	100
expected	*79.5*	*20.5*	
TOTALS	159	41	200

Test statistic	Value	df	Prob
Log-Likelihood Ratio (G)	0.031	1	0.861

∴Accept H_0, and conclude that larval survival is independent of gravity on Day 3.

SAMPLE #	ALIVE	DEAD	TOTALS
0g Day 5	76	24	100
expected	*80*	*20*	
1g Day 5	84	16	100
expected	*80*	*20*	
TOTALS	160	40	200

Test statistic	Value	df	Prob
Log-Likelihood Ratio (G)	2.011	1	0.156

∴Accept H_0, and conclude that larval survival is independent of gravity on Day 5.

SAMPLE #	ALIVE	DEAD	TOTALS
0g Day 7	52	48	100
expected	*52.5*	*47.5*	
1g Day 7	53	47	100
expected	*52.5*	*47.5*	
TOTALS	105	95	200

Test statistic	Value	df	Prob
Log-Likelihood Ratio (G)	0.020	1	0.887

∴Accept H_0, and conclude that larval survival is independent of gravity on Day 7.

SAMPLE #	ALIVE	DEAD	TOTALS
0g Day 10	31	69	100
expected	*34*	*66*	
1g Day 10	37	63	100
expected	*34*	*66*	
TOTALS	68	132	200

Test statistic	Value	df	Prob
Log-Likelihood Ratio (G)	0.983	1	0.370

∴Accept H_0, and conclude that larval survival is independent of gravity on Day 10.

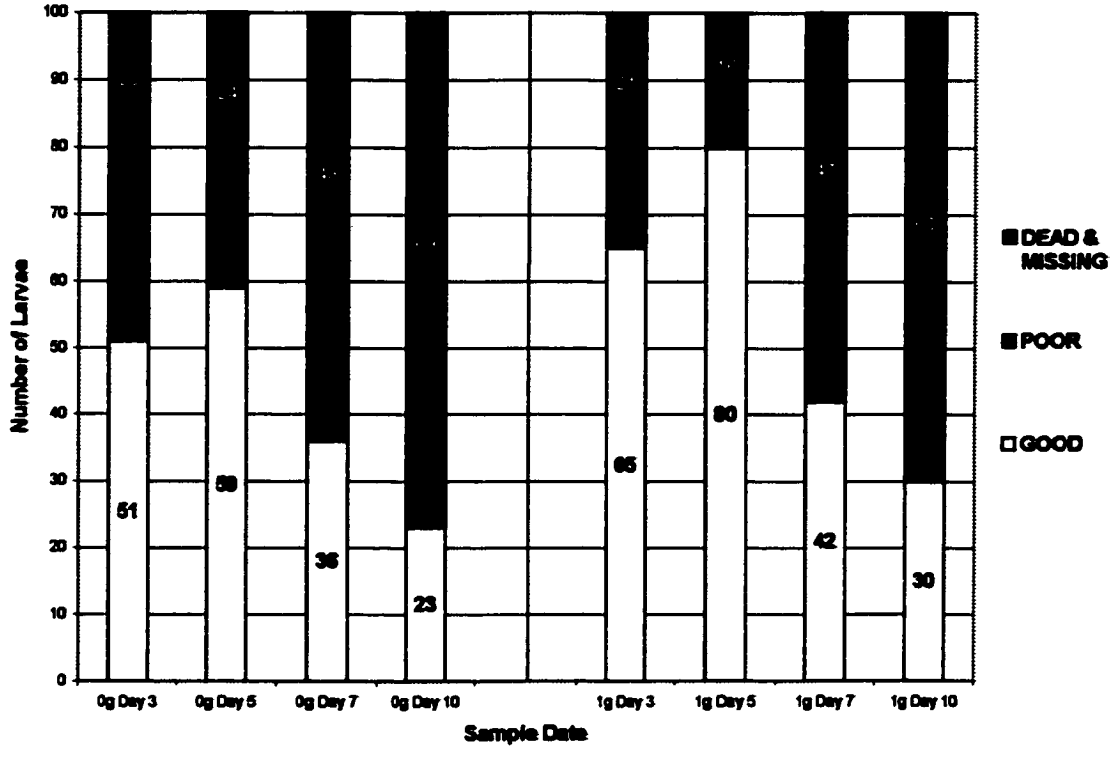

Fig. 4.3.1. Stacked bar graph summarising condition of mussel larvae from ARF Main System #1 SCA test chambers during microgravity (0g) and normal gravity (1g) exposures on board Space Shuttle Mission STS-77, May 19-29, 1996. The numbers of larvae in each condition category are superimposed on each bar segment. One hundred larvae were initially loaded into each SCA test chamber before launch. Data are from Table 4.3.1.

Table 4.3.4. Two-way contingency table used in analyses of larval mussel condition data from the microgravity (0g) treatment SCA test chambers in ARF Main System #1 during Space Shuttle Mission STS-77, May 19-29, 1996. One hundred larvae were initially loaded into each SCA test chamber before launch.

H_0: Larval condition is independent of sample date
H_A: Larval condition is not independent of sample date

	CONDITION			
SAMPLE #	GOOD	POOR	DEAD	TOTALS
0g Day 3	51	29	20	100
expected	*42.25*	*17.50*	*40.25*	
0g Day 5	59	17	24	100
expected	*42.25*	*17.50*	*40.25*	
0g Day 7	36	16	48	100
expected	*42.25*	*17.50*	*40.25*	
0g Day 10	23	8	69	100
expected	*42.25*	*17.50*	*40.25*	
TOTALS	169	70	161	400

Test statistic	Value	df	Prob
Log-Likelihood Ratio (G)	70.514	6	0.000

$\therefore$Reject H_0, and conclude that larval condition is dependent upon sample date.

Table 4.3.5. Two-way contingency table used in analyses of larval mussel condition data from the normal gravity (1g) control SCA test chambers in ARF Main System #1 during Space Shuttle Mission STS-77, May 19-29, 1996. One hundred larvae were initially loaded into each SCA test chamber before launch.

H_0: Larval condition is independent of sample date
H_A: Larval condition is not independent of sample date

	CONDITION			
SAMPLE #	GOOD	POOR	DEAD	TOTALS
1g Day 3	66	14	21	100
expected	*54.25*	*9.00*	*36.75*	
1g Day 5	80	4	16	100
expected	*54.25*	*9.00*	*36.75*	
1g Day 7	42	11	47	100
expected	*54.25*	*9.00*	*36.75*	
1g Day 10	30	7	63	100
expected	*54.25*	*9.00*	*36.75*	
TOTALS	217	36	147	400

Test statistic	Value	df	Prob
Log-Likelihood Ratio (G)	76.312	6	0.000

$\therefore$Reject H_0, and conclude that larval condition is dependent upon sample date.

during the flight experiment. Only three larvae were found to be swimming on Flight Day One in this chamber, and no larval swimming activity was observed in any video recording session for this SCA thereafter.

Among the larvae in the ARF MS-1 1g SCA test chambers, there was a similar tendency towards declining proportions of larvae in good condition as the experiment progressed (Fig. 4.3.1). On Day 5, 80% of the larvae were found to be in good condition, but by Day 10 only 30% of the larvae were deemed to be in good condition. This range of 50 percentage points was higher than that seen in the 0g treatment (36%). The proportion of larvae in poor condition remained relatively constant throughout the experiment, between 4% and 14%, while the percentage of dead larvae increased from 21% on Day 3 to 63% in the Day 10 sample. Again, this trend is similar to that seen with the 0g treatment larvae. Table 4.3.5 outlines the contingency table analysis used to test the null hypothesis of independence between sample date and condition of larvae reared in the 1g control experiment. As was the case in the microgravity treatment, the null hypothesis was rejected and it was concluded that larval condition was dependent upon the time at which the larvae were sampled ($P < 0.05$). The frequency distribution of larvae in the different condition categories changed significantly as the experiment progressed.

Comparing the larvae reared in microgravity with those raised in a unit gravity environment, there was a trend indicating a higher proportion of larvae in good condition in the 1g treatment samples than in the 0g samples (Fig. 4.3.1). On all sample dates, the number of larvae in good condition was higher in the 1g SCA test chambers than in the 0g chambers. Concomitant with the greater percentage of larvae in good condition in all

four of the 1g samples was a smaller proportion of larvae that were in poor condition or dead. Most samples of larvae reared in microgravity had a higher proportion of larvae that were dead or in poor condition than was observed in the corresponding 1g treatment samples. Table 4.3.6 outlines a series of 2 x 3 contingency tables that tests the independence of larval condition from gravity for each of the four sample dates. On Day 3 and Day 5, the null hypothesis of independence was rejected, meaning that the frequency distribution of larvae within each of the three condition classes was dependent upon gravity on those two dates. However, this situation was reversed on Day 7 and on Day 10, where larval condition was found to be independent of gravity on those days; that is, there was no significant difference between the 0g and 1g samples in the relative proportions of larvae in each condition category on Day 7 and Day 10.

Table 4.3.2 and Fig. 4.3.2 summarise the recovery data and larval condition assessment results for the larvae from the ARF Main System 2 Ground Control experiment, conducted in KSC's Orbiter Environmental Simulator (OES) on May 20-30, 1996. As was the case with the ARF MS-1 Flight Experiment, there was generally a decline in the numbers of larvae recovered from the "0g" SCA test chambers that were fixed later in the experimental schedule. In the "1g" treatment, however, the larval recovery rate was high, between 77% and 87%, in all but one of the SCA test chambers. In the sample fixed on Day 7 in the "1g" centrifuge, only 29 of the original 100 larvae were recovered at the end of the experiment. This low recovery rate may be explained by loss of larvae during recovery operations, but it is likely that much of the loss is due to early mortality in this container. Of the larvae that were recovered, 18 were dead and

Table 4.3.6. Two-way contingency tables used in analyses of larval mussel condition data from the microgravity (0g) and normal gravity (1g) SCA test chambers in ARF Main System #1 during Space Shuttle Mission STS-77, May 19-29, 1996. One hundred larvae were initially loaded into each SCA test chamber before launch.

H_0: Larval condition is independent of gravity on sample date indicated
H_A: Larval condition is not independent of gravity on sample date indicated

	CONDITION			
SAMPLE #	GOOD	POOR	DEAD	TOTALS
0g Day 3	61	29	20	100
expected	*58.0*	*21.5*	*20.5*	
1g Day 3	55	14	21	100
expected	*58.0*	*21.5*	*20.5*	
TOTALS	116	43	41	200

Test statistic	Value	df	Prob
Log-Likelihood Ratio (G)	7.062	2	0.029

∴Reject H_0, and conclude that larval condition is dependent upon gravity on Day 3.

	CONDITION			
SAMPLE #	GOOD	POOR	DEAD	TOTALS
0g Day 5	59	17	24	100
Expected	*69.5*	*10.5*	*20.0*	
1g Day 5	80	4	16	100
expected	*69.5*	*10.5*	*20.0*	
TOTALS	139	21	40	200

Test statistic	Value	df	Prob
Log-Likelihood Ratio (G)	13.468	2	0.001

∴Reject H_0, and conclude that larval condition is dependent upon gravity on Day 5.

	CONDITION			
SAMPLE #	GOOD	POOR	DEAD	TOTALS
0g Day 7	36	16	48	100
expected	*39.0*	*13.5*	*47.5*	
1g Day 7	42	11	47	100
expected	*39.0*	*13.5*	*47.5*	
TOTALS	78	27	95	200

Test statistic	Value	df	Prob
Log-Likelihood Ratio (G)	1.464	2	0.496

∴Accept H_0, and conclude that larval condition is independent of gravity on Day 7.

	CONDITION			
SAMPLE #	GOOD	POOR	DEAD	TOTALS
0g Day 10	23	8	69	100
expected	*26.5*	*7.5*	*66.0*	
1g Day 10	30	7	63	100
expected	*26.5*	*7.5*	*66.0*	
TOTALS	53	15	132	200

Test statistic	Value	Df	Prob
Log-Likelihood Ratio (G)	1.267	2	0.531

∴Accept H_0, and conclude that larval condition is independent of gravity on Day 10.

only 10 were considered to be in good condition at the time of fixation. This situation is similar to that seen in the ARF MS-1 0g Day 3 sample, where the proportion of larvae in good condition was unexpectedly low.

Larval survival data from the ARF MS-2 Ground Control experiment are shown in Table 4.3.2. In Fig. 4.3.2., survival data in each of the eight SCA test chambers are depicted as the total of the good and poor condition larvae. Mortality increased throughout the early part of the experiment at similar rates in both treatments, with the notable exception of the anomalous "1g" Day 7 sample. On Day 3, 81 live larvae were found in the "0g" sample, and 80 survivors were in the "1g" container, while after five days, 76 larvae were alive in the "0g" treatment, and 72 larvae survived the "1g" hypergravity exposure. By Day 10, however, there were significantly fewer (34) larvae in the "0g" SCA test chamber than in the "1g" container ($P < 0.05$), which had an unexpectedly high number of survivors at 73. The results of the series of pairwise contingency tables presented in Table 4.3.7 reveal that significant differences in survival between the two treatments occur only on Day 7 and on Day 10.

In the ARF MS-2 "0g" SCA test chambers, there was a general trend towards decreasing proportions of larvae that were in good condition at the time of fixation. Larvae in good condition comprised 72% of the total larvae recovered in the "0g" Day 3 sample, increased slightly to 76% in the "0g" Day 5 sample, and declined to 40% and 27% in the Day 7 and Day 10 samples, respectively. The percentage of dead larvae found in the SCA test chambers increased from 19% and 24% in the early samples, to 55% in the "0g" Day 7 sample, and 66% on Day 10. Throughout the experiment, the

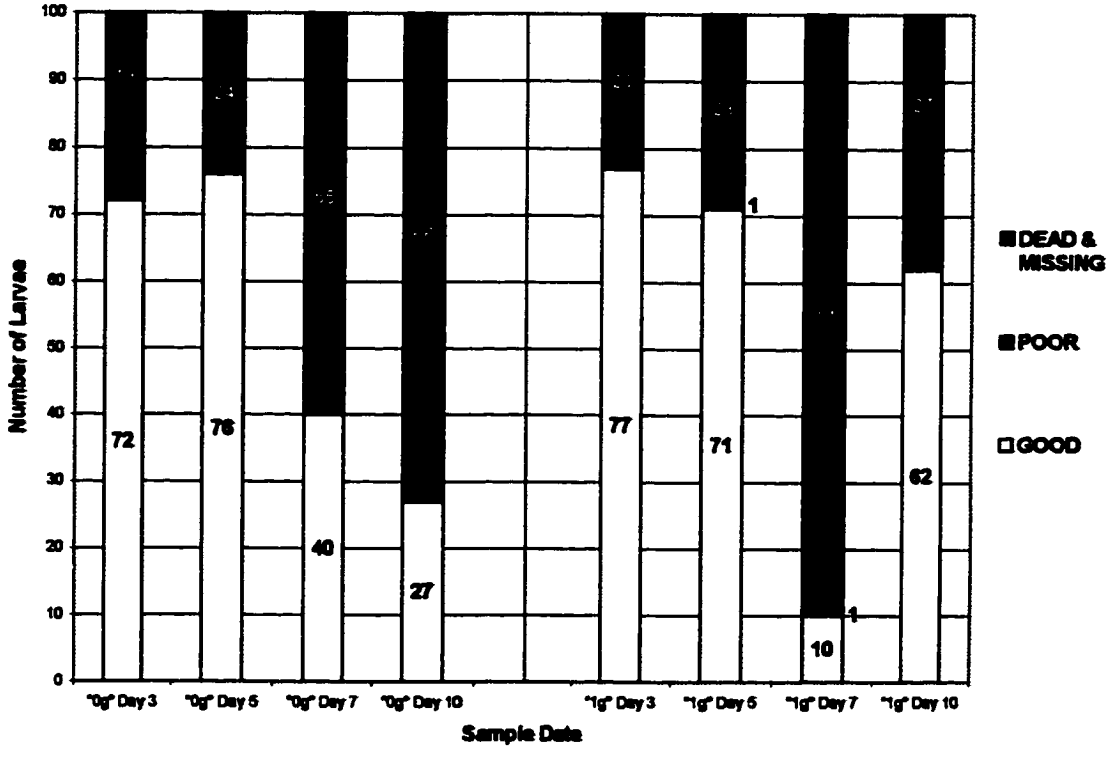

Fig. 4.3.2. Stacked bar graph summarising condition of mussel larvae from ARF Main System #2 SCA test chambers during hypergravity ("1g") and normal gravity ("0g") exposures in Orbiter Environmental Simulator (OES) during Space Shuttle Mission STS-77, May 20-30, 1996. The numbers of larvae in each condition category are superimposed on each bar segment. One hundred larvae were initially loaded into each SCA test chamber before launch. Data are from Table 4.3.2.

Table 4.3.7. Two-way contingency tables used in analyses of larval mussel survival data from ARF Main System #2 Ground Control experiment during hypergravity ("1g") and normal gravity ("0g") exposures in Orbiter Environmental Simulator (OES) during Space Shuttle Mission STS-77, May 20-30, 1996. One hundred larvae were initially loaded into each SCA test chamber before launch.

H_0: Larval survival is independent of gravity on sample date indicated
H_A: Larval survival is not independent of gravity on sample date indicated

SAMPLE #	ALIVE	DEAD	TOTALS
"0g" Day 3	81	19	100
expected	*80.5*	*19.5*	
"1g" Day 3	80	20	100
expected	*80.5*	*19.5*	
TOTALS	161	39	200

Test statistic	Value	df	Prob
Log-Likelihood Ratio (G)	0.032	1	0.858

∴Accept H_0, and conclude that larval survival is independent of gravity on Day 3.

SAMPLE #	ALIVE	DEAD	TOTALS
"0g" Day 5	76	24	100
Expected	*74*	*26*	
"1g" Day 5	72	28	100
expected	*74*	*26*	
TOTALS	148	52	200

Test statistic	Value	df	Prob
Log-Likelihood Ratio (G)	0.416	1	0.519

∴Accept H_0, and conclude that larval survival is independent of gravity on Day 5.

SAMPLE #	ALIVE	DEAD	TOTALS
"0g" Day 7	45	55	100
expected	*28*	*72*	
"1g" Day 7	11	89	100
expected	*28*	*72*	
TOTALS	56	144	200

Test statistic	Value	df	Prob
Log-Likelihood Ratio (G)	30.259	1	0.000

∴Reject H_0, and conclude that larval survival is dependent upon gravity on Day 7.

SAMPLE #	ALIVE	DEAD	TOTALS
"0g" Day 10	34	66	100
expected	*53.5*	*46.5*	
"1g" Day 10	73	27	100
expected	*53.5*	*46.5*	
TOTALS	107	93	200

Test statistic	Value	df	Prob
Log-Likelihood Ratio (G)	31.419	1	0.000

∴ Reject H_0, and conclude that larval survival is dependent upon gravity on Day 10.

amount of larvae in poor condition remained fairly constant, ranging between 0% and 9%, with the highest amount being found on Day 3. Table 4.3.8 outlines a two-way contingency table analysis which tested the hypothesis of independence between sample date and the distribution of larvae amongst the three condition categories. The rejection of this hypothesis led to the conclusion that larval condition in the "0g" treatment varied significantly with sample date ($P < 0.05$).

The "1g" treatment samples from the ARF MS-2 Ground Control experiment were notable in that most of the larvae retrieved from the majority of the chambers were in good condition, except for the unique case of the Day 7 sample. On Day 3, 77% of the recovered larvae were in good condition, 71% were rated as good in the chamber fixed on Day 5, and 62% of the larvae in the Day 10 sample were in good shape. In all three of these samples, the proportion of dead larvae remained relatively low, between 20% and 27%. Larvae in poor condition comprised only 3% and 1% of the sample on Days 3 and 5, and 11% on Day 10. As was the case with the "0g" and ARF MS-1 SCA test samples, contingency table analysis revealed significant differences in the frequency distribution of larvae within the three condition categories among the four sample dates (Table 4.3.9).

When the results from the "0g" and "1g" treatments in the ARF MS-2 Ground Control experiment are compared, some general trends are observed. The percentage of larvae considered to be in good condition was similar in both treatments on Day 3 and Day 5, while the "1g" sample had a higher proportion of larvae in good condition on Day 10. Dead larvae as a proportion of the sample generally increased throughout the experiment in the "0g" treatment, but remained relatively constant in the "1g" samples, except for the Day 7 sample. On Day 3 and Day 5, however, the amount of dead larvae

Table 4.3.8. Two-way contingency tables used in analyses of larval mussel condition data from ARF Main System #2 Ground Control experiment during normal gravity ("0g") exposures in Orbiter Environmental Simulator (OES) during Space Shuttle Mission STS-77, May 20-30, 1996. One hundred larvae were initially loaded into each SCA test chamber before launch.

H_0: Larval condition is independent of sample date
H_A: Larval condition is not independent of sample date

	CONDITION			
SAMPLE #	**GOOD**	**POOR**	**DEAD**	**TOTALS**
"0g" Day 3	**72**	**9**	**19**	**100**
expected	*53.75*	*5.25*	*41.00*	
"0g" Day 5	**76**	**0**	**24**	**100**
expected	*53.75*	*5.25*	*41.00*	
"0g" Day 7	**40**	**5**	**55**	**100**
expected	*53.75*	*5.25*	*41.00*	
"0g" Day 10	**27**	**7**	**66**	**100**
expected	*53.75*	*5.25*	*41.00*	
TOTALS	**215**	**21**	**164**	**400**

Test statistic	**Value**	**df**	**Prob**
Log-Likelihood Ratio (G)	**87.395**	**6**	**0.000**

∴Reject H_0, and conclude that larval condition is dependent upon sample date.

Table 4.3.9. Two-way contingency tables used in analyses of larval mussel survival data from ARF Main System #2 Ground Control experiment during hypergravity ("1g") exposures in Orbiter Environmental Simulator (OES) during Space Shuttle Mission STS-77, May 20-30, 1996. One hundred larvae were initially loaded into each SCA test chamber before launch.

H_0: Larval condition is independent of sample date
H_A: Larval condition is not independent of sample date

	CONDITION			
SAMPLE #	**GOOD**	**POOR**	**DEAD**	**TOTALS**
"1g" Day 3	**77**	**3**	**20**	**100**
expected	*55*	*4*	*41*	
"1g" Day 5	**71**	**1**	**28**	**100**
expected	*55*	*4*	*41*	
"1g" Day 7	**10**	**1**	**89**	**100**
expected	*55*	*4*	*41*	
"1g" Day 10	**62**	**11**	**27**	**100**
expected	*55*	*4*	*41*	
TOTALS	**220**	**16**	**164**	**400**

Test statistic	**Value**	**df**	**Prob**
Log-Likelihood Ratio (G)	**149.154**	**6**	**0.000**

∴Reject H_0, and conclude that larval condition is dependent upon sample date.

in the samples was approximately the same in both treatments. Larvae in poor condition comprised a low proportion of both the "0g" and "1g" samples, but were slightly more prevalent in the "0g" treatment. Table 4.3.10 includes a series of four pairwise contingency tables that compare the "0g" and "1g" samples in terms of the numbers of larvae in each of the condition categories for each sample date. On Day 3 and Day 5, these analyses found no significant differences ($P > 0.05$) between the two gravity treatments, but larval condition was found to be dependent upon gravity in the Day 7 and Day 10 samples.

Although the ARF Main System 2 experiment conducted in Kennedy Space Center's Orbiter Environmental Simulator (OES) was a pseudoreplicate of the ARF Main System 1 experiment that flew in space, some comparisons between the two datasets can be made. There was a trend towards increasing mortality as both experiments progressed, with the only exception being found in the ARF MS-2 "1g" hypergravity treatment, where there was an unexpectedly high number of live larvae in the Day 10 sample. On any given sample day, the amount of live larvae in each of the four SCA test chambers was approximately equal, with the exceptions being the Day 7 and Day 10 samples from the ARF MS-2 "1g" containers. As noted earlier, these samples had abnormally low and high numbers of live larvae, respectively. Larvae reared in microgravity in the ARF MS-1 0g treatment appeared to have the lowest overall amount of larvae in good condition, while the numbers of good-condition larvae in the other treatments was roughly equal, again with the exception of the ARF MS-2 "1g" Day 7 and Day 10 samples. Larvae in poor condition were most numerous in the ARF MS-1 microgravity containers, followed by the 1g treatment in the same experiment.

Table 4.3.10. Two-way contingency tables used in analyses of larval mussel condition data from ARF Main System #2 Ground Control experiment during hypergravity ("1g") and normal gravity ("0g") exposures in Orbiter Environmental Simulator (OES) during Space Shuttle Mission STS-77, May 20-30, 1996. One hundred larvae were initially loaded into each SCA test chamber before launch.

H_0: Larval condition is independent of gravity on sample date indicated
H_A: Larval condition is not independent of gravity on sample date indicated

	CONDITION			
SAMPLE #	GOOD	POOR	DEAD	TOTALS
"0g" Day 3	72	9	19	100
expected	*74.5*	*6.0*	*19.5*	
"1g" Day 3	77	3	20	100
expected	*74.5*	*6.0*	*19.5*	
TOTALS	149	12	39	200

Test statistic	Value	df	Prob
Log-Likelihood Ratio (G)	3.333	2	0.189

∴Accept H_0, and conclude that larval condition is independent of gravity on Day 3.

	CONDITION			
SAMPLE #	GOOD	POOR	DEAD	TOTALS
"0g" Day 5	76	0	24	100
Expected	*73.5*	*0.5*	*26.0*	
"1g" Day 5	71	1	28	100
expected	*73.5*	*0.5*	*26.0*	
TOTALS	147	1	52	200

Test statistic	Value	df	Prob
Log-Likelihood Ratio (G)	1.864	2	0.394

∴ Accept H_0, and conclude that larval condition is independent of gravity on Day 5.

	CONDITION			
SAMPLE #	GOOD	POOR	DEAD	TOTALS
"0g" Day 7	40	5	55	100
expected	*25*	*3*	*72*	
"1g" Day 7	10	1	89	100
expected	*25*	*3*	*72*	
TOTALS	50	6	144	200

Test statistic	Value	df	Prob
Log-Likelihood Ratio (G)	30.290	2	0.000

∴Reject H_0, and conclude that larval condition is dependent upon gravity on Day 7.

	CONDITION			
SAMPLE #	GOOD	POOR	DEAD	TOTALS
"0g" Day 10	27	7	66	100
expected	*44.5*	*9.0*	*46.5*	
"1g" Day 10	62	11	27	100
expected	*44.5*	*9.0*	*46.5*	
TOTALS	89	18	93	200

Test statistic	Value	Df	Prob
Log-Likelihood Ratio (G)	31.911	2	0.000

∴ Reject H_0, and conclude that larval condition is dependent upon gravity on Day 10.

4.3.3 Larval Growth

Morphometric data describing the size and shell properties of mussel larvae from the ARF Main System 1 Flight experiment at the time of fixation are summarised in Table 4.3.11. Shell length, height, and square area data from larvae in good condition only are included in this table and the subsequent figures and analyses. In the case of a few individual larvae, shell length was the only parameter that could be measured, owing to problems with orientation of the larva on the microscope slide. Shell birefringence as tabulated here is used as an index of larval shell calcification and thickness (see Section 4.2.3).

Larval growth in all SCA test chambers was minimal during the ARF MS-1 experiment, as can be seen in Fig. 4.3.3, 4.3.4, and 4.3.5. The size of mussel larvae from all samples was assessed by measuring three related morphological parameters (shell length, height, and square area), and analyses of all three indicated that the larvae did not grow much during the Space Shuttle experiment, regardless of the gravity treatment.

Fig. 4.3.3 summarises the larval mussel shell length data from both the microgravity treatment and the normal gravity control for all sample dates. The two scatterplots in this figure show the shell length distributions of all individual larval measurements, and also include the linear regression lines for these datasets. The regression equation for the larvae raised in microgravity shows that these animals only grew at an average rate of 0.088 μm/day. Analysis of variance testing of this regression revealed that the slope of this equation was not significantly different from zero, confirming that the growth rate, as measured in terms of shell length, was negligible.

Table 4.3.11. Summary of growth data of mussel (*Mytilus edulis*) larvae from ARF Main System #1 during microgravity (0g) and normal gravity (1g) exposures on board Space Shuttle Mission STS-77, May 19-29, 1996

SHELL LENGTH (µm)

FLIGHT DAY#	0g				1g			
	MEAN	n	St. Dev.	St. Error	MEAN	n	St. Dev.	St. Error
0	110.7	30	4.5	0.8	110.7	30	4.5	0.8
3	109.7	51	5.8	0.8	108.8	65	5.3	0.7
5	110.5	59	5.9	0.8	111.9	80	4.2	0.5
7	111.2	36	6.3	1.0	111.1	42	5.9	0.9
10	110.9	11	6.7	2.0	113.0	30	4.3	0.8

SHELL HEIGHT (µm)

FLIGHT DAY#	0g				1g			
	MEAN	n	St. Dev.	St. Error	MEAN	n	St. Dev.	St. Error
0	81.6	30	3.6	0.7	81.6	30	3.6	0.7
3	80.1	48	3.9	0.6	80.1	65	4.2	0.5
5	80.3	58	4.6	0.6	81.6	79	3.2	0.4
7	80.8	36	4.9	0.8	81.1	42	4.4	0.7
10	81.3	11	4.5	1.4	81.1	30	3.5	0.6

SHELL AREA (µm²)

FLIGHT DAY#	0g				1g			
	MEAN	n	St. Dev.	St. Error	MEAN	n	St. Dev.	St. Error
0	7496	30	576.6	105.3	7496	30	576.6	105.3
3	7340	48	737.4	106.4	7274	65	696.7	86.4
5	7452	58	791.3	103.9	7618	79	556.8	62.6
7	7557	36	825.2	137.5	7568	42	771.6	119.1
10	7564	11	858.7	258.9	7702	30	602.4	110.0

SHELL BIREFRINGENCE (Integrated Digital Grey Value)

FLIGHT DAY#	0g				1g			
	MEAN	n	St. Dev.	St. Error	MEAN	n	St. Dev.	St. Error
3	298873	24	42948.0	8766.7	280153	44	64329.3	9696.0
5	346465	45	63737.2	9501.4	395887	48	71907.4	10378.9
7	205148	36	95511.4	15918.6	395507	40	91373.1	14447.4
10	528244	11	166178.1	50104.6	543583	28	67535.3	12763.0

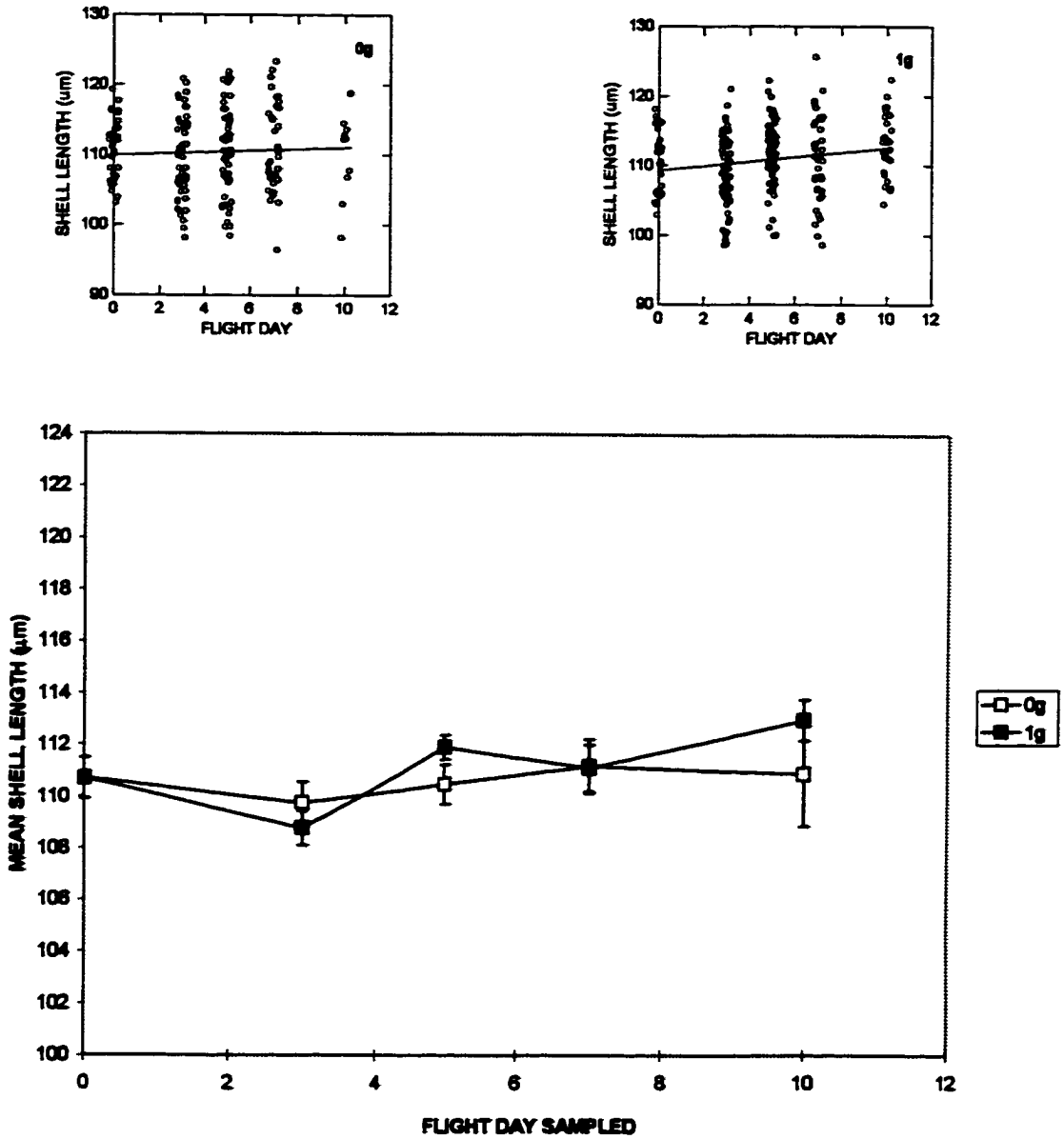

Fig. 4.3.3. Size of mussel (*Mytilus edulis*) larvae from ARF Main System #1 during microgravity (0g) and normal gravity (1g) exposures on board Space Shuttle Mission STS-77, May 19-29, 1996. TOP- scatterplots of individual shell length measurements, with regression lines (0g Length = 110.09 + 0.09×Day, r^2=0.002; 1g Length = 109.33 + 0.33×Day, r^2=0.034). BOTTOM- Line graph, measured as sample date vs. mean shell length ± standard error. Data are from Table 4.3.11.

Table 4.3.12. Two-way Analysis of Variance (ANOVA) for larval mussel (*Mytilus edulis*) shell length data from ARF Main System #1 during Space Shuttle Mission STS-77, May 19-29, 1996.

Source	Sum-of-Squares	df	Mean-Square	F-ratio	P
SAMPLE DATE	338.649	4	84.662	3.018	0.018
GRAVITY	19.748	1	19.748	0.704	0.402
SAMPLE DATE * GRAVITY	119.823	4	29.956	1.068	0.372
Error	11895.648	424	28.056		

Table 4.3.13. Two-way Analysis of Variance (ANOVA) for larval mussel (*Mytilus edulis*) shell height data from ARF Main System #1 during Space Shuttle Mission STS-77, May 19-29, 1996.

Source	Sum-of-Squares	df	Mean-Square	F-ratio	P
SAMPLE DATE	106.222	4	26.556	1.636	0.164
GRAVITY	5.863	1	5.863	0.361	0.548
SAMPLE DATE * GRAVITY	33.255	4	8.314	0.512	0.727
Error	6799.441	419	16.228		

Table 4.3.14. Two-way Analysis of Variance (ANOVA) for larval mussel (*Mytilus edulis*) shell square area data from ARF Main System #1 during Space Shuttle Mission STS-77, May 19-29, 1996.

Source	Sum-of-Squares	df	Mean-Square	F-ratio	P
SAMPLE DATE	5008769.04	4	1252192.258	2.599	0.036
GRAVITY	199384.432	1	199384.432	0.414	0.520
SAMPLE DATE * GRAVITY	950800.881	4	237700.220	0.493	0.741
Error	$2.02 \cdot 10^{5}$	419	481889.918		

Table 4.3.15. Two-way Analysis of Variance (ANOVA) for larval mussel (*Mytilus edulis*) shell calcification (optical birefringence) data from ARF Main System #1 during Space Shuttle Mission STS-77, May 19-29, 1996.

Source	Sum-of-Squares	df	Mean-Square	F-ratio	P
SAMPLE DATE	$1.55 \cdot 10^{12}$	3	$5.19 \cdot 10^{11}$	82.423	0.000
GRAVITY	$1.98 \cdot 10^{11}$	1	$1.98 \cdot 10^{11}$	31.541	0.000
SAMPLE DATE * GRAVITY	$4.24 \cdot 10^{11}$	3	$1.41 \cdot 10^{11}$	22.469	0.000
Error	$1.69 \cdot 10^{12}$	268	$6.29 \cdot 10^{9}$		

Larvae grown in the normal gravity chambers grew at a slightly higher rate of 0.332 μm/day over the course of the experiment; the slope for this equation was significantly greater than zero ($P = 0.004$). A two-way analysis of variance (ANOVA) model for the combined ARF MS-1 larval shell length dataset (see Table 4.3.12) revealed that the gravity treatment had no significant effect upon larval mussel shell length, but sample date had a slight effect ($P = 0.018$). Post-hoc Tukey's pairwise comparisons found that the mean shell length for larvae from the 1g Day 3 sample was significantly smaller than larvae from the 1g Day 5 and 1g Day 10 samples, but found no significant differences between any other possible pairwise combinations. When the 1g Day3 sample was removed from the analysis, a one-way ANOVA comparing the remaining larval samples found no significant differences in larval shell length due to either gravity or sample date.

Shell height data for larvae from the ARF MS-1 experiment are shown in Fig. 4.3.4. Average rates of change in the shell height dimension were only 0.022 μm/day for the larvae reared in normal gravity, and -0.038 μm/day for the animals from the microgravity treatment. Analysis of variance testing of these regressions reveal that neither of these slopes were significantly different from zero, meaning that there was no significant change in shell height throughout the course of the experiment. This conclusion is further supported by the results of the two-way ANOVA shown in Table 4.3.13, which shows that neither gravity treatment, sample date, nor the interaction term had any significant effect upon the shell height of the larvae in this experiment. There were no significant differences in the mean shell heights amongst any of the experimental groups of larvae.

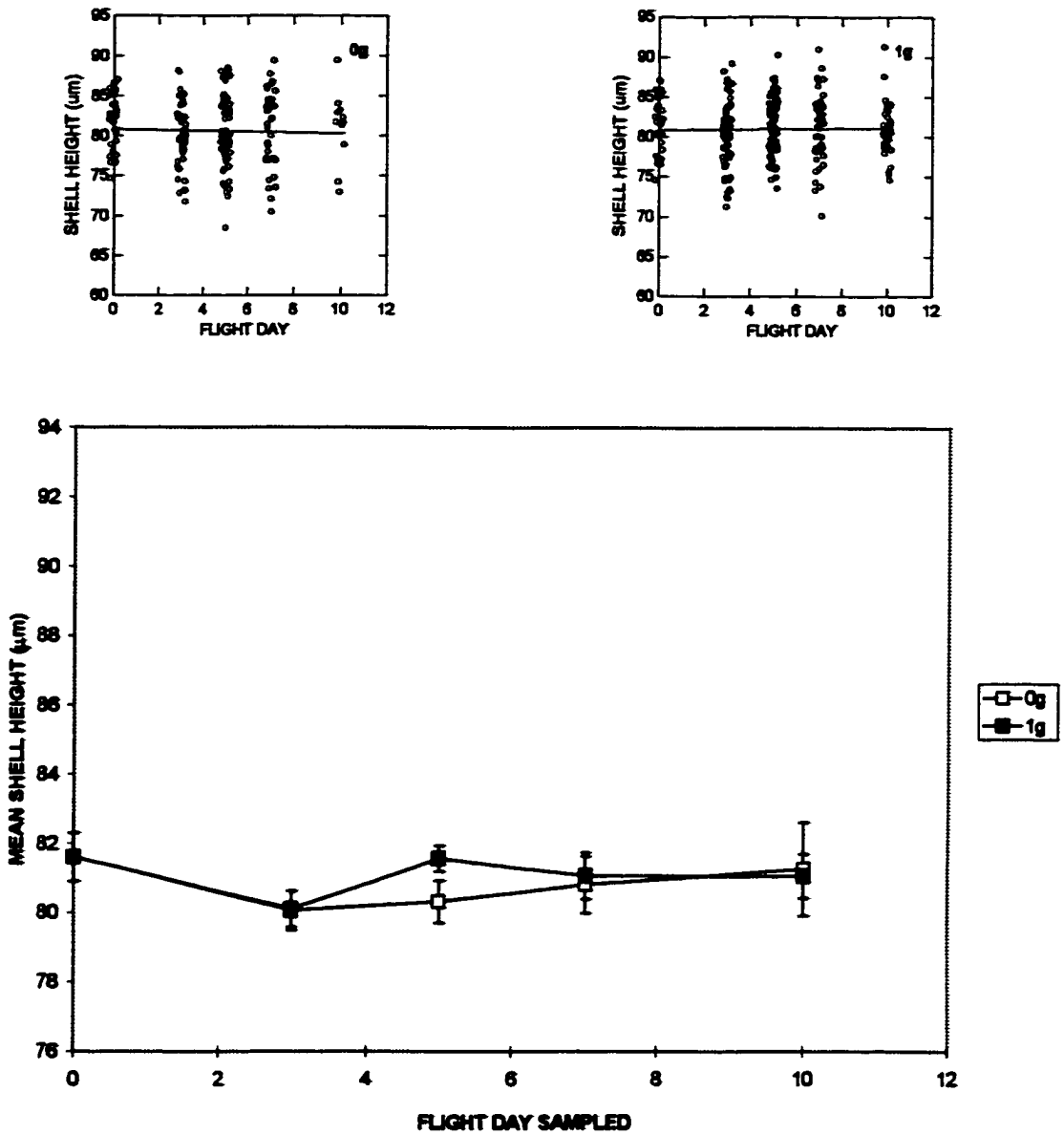

Fig. 4.3.4. Size of mussel (*Mytilus edulis*) larvae from ARF Main System #1 during microgravity (0g) and normal gravity (1g) exposures on board Space Shuttle Mission STS-77, May 19-29, 1996. TOP- scatterplots of individual shell height measurements, with regression lines (0g Height = 80.78 - 0.04xDay, r^2= 0.001; 1g Height = 80.93 + 0.02xDay, r^2=0.000). BOTTOM- Line graph, measured as mean shell height ± standard error. Data are from Table 4.3.11.

Fig. 4.3.5 shows scatterplots and a line graph representing the growth of larvae in the ARF MS-1 experiment in terms of increase in shell square area. Larvae reared in microgravity added new shell material to their margins at an average rate of 14.433 μm^2/day, a rate which was determined by analysis of variance to be not significantly different from a zero growth rate. Larvae in the normal gravity treatment grew their shells at a rate of 34.739 μm^2/day; this rate was significantly greater than zero. As was the case with the shell length data, a two-way ANOVA model (see Table 4.3.14) found that gravity had no significant influence upon larval shell square area, but sample date did influence shell area ($P = 0.036$). However, a matrix of post-hoc Tukey's pairwise comparisons failed to identify which sample means were responsible for this significant result. A one-way ANOVA that compared the data from each sample independently of gravity treatment or sample date also did not find any significant differences in mean square area between all samples from the ARF MS-1 experiment ($P > 0.05$).

Shell calcification data from the ARF MS-1 experiment are presented in Fig. 4.3.6 as the integrated digital grey value (IGV) of shell birefringence. In the normal gravity treatment, there was a general trend towards higher IGV values in the larvae sampled later in the experiment, meaning that these larvae developed thicker shells as the experiment progressed. The slope of the regression line for these data was significantly greater than zero ($P = 0.000$); however, this was not the case for the regression of the data from the larvae raised in microgravity ($P = 0.056$). Larvae sampled on Day 7 in the microgravity treatment had much lower IGV values than the corresponding sample from the control normal gravity sample. A two-way ANOVA (Table 4.3.15) found significant

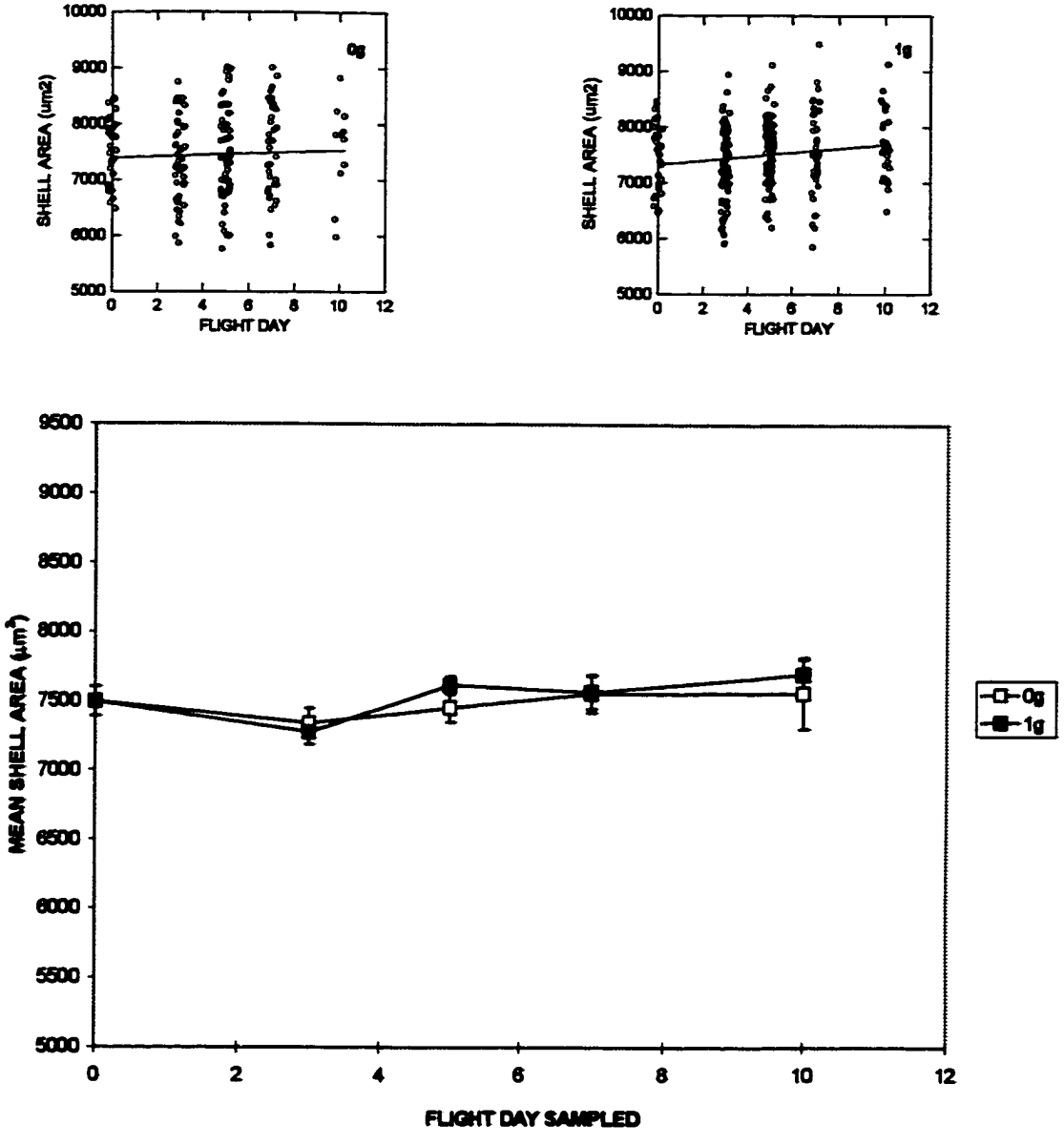

Fig. 4.3.5. Size of mussel (*Mytilus edulis*) larvae from ARF Main System #1 during microgravity (0g) and normal gravity (1g) exposures on board Space Shuttle Mission STS-77, May 19-29, 1996. TOP- scatterplots of individual shell square area measurements, with regression lines (0g Area =7394.4 + 14.4xDay, r^2=0.003; 1g Area = 7346.4 + 34.7xDay, r^2=0.022). BOTTOM- Line graph, measured as mean shell square area ± standard error. Data are from Table 4.3.11.

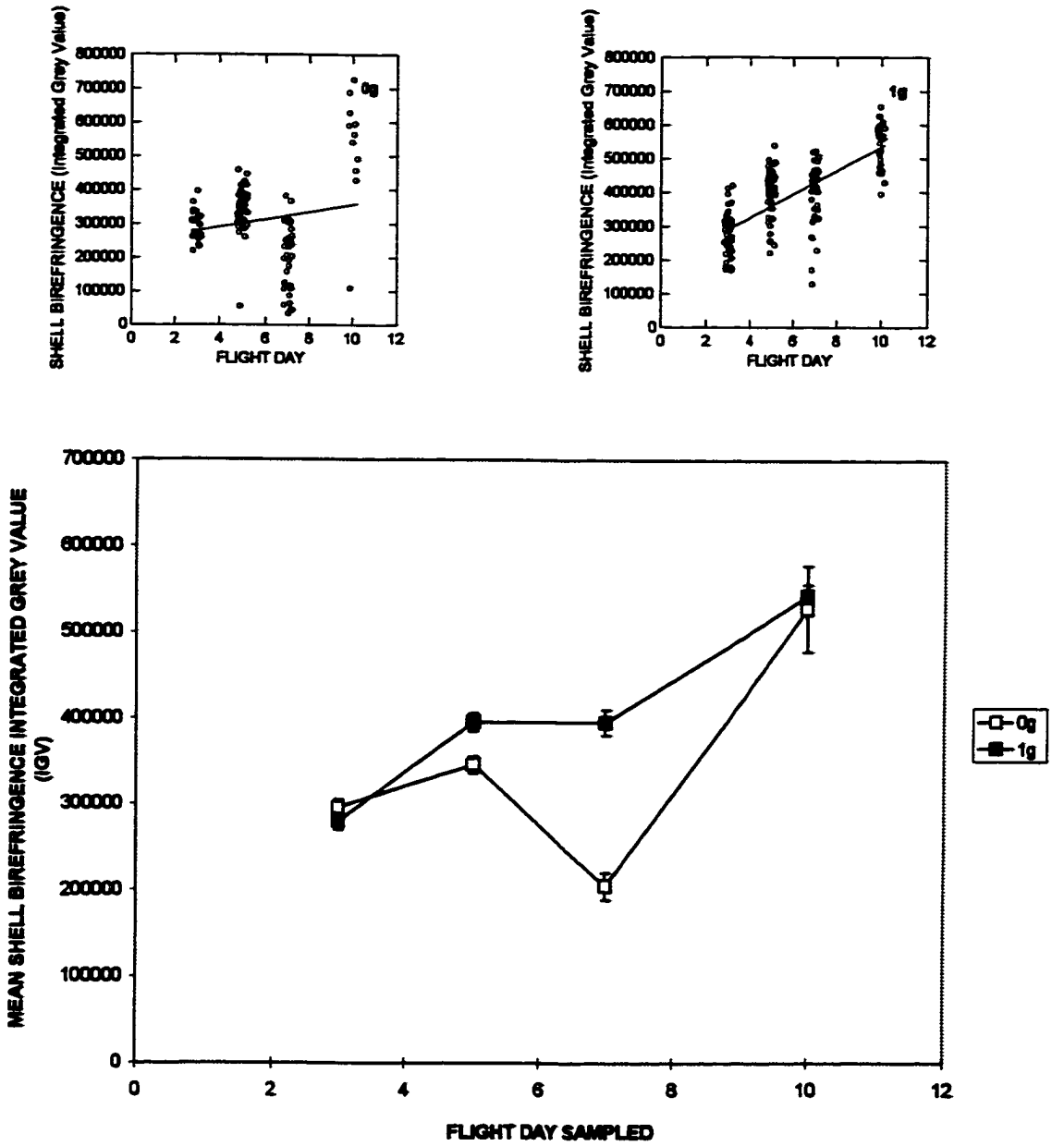

Fig. 4.3.6. Changes in mussel (*Mytilus edulis*) larval shell calcification from ARF Main System #1 during microgravity (0g) and normal gravity (1g) exposures on board Space Shuttle Mission STS-77, May 19-29, 1996. TOP- scatterplots of individual shell birefringence measurements (integrated digital grey value-IGV), with regression lines (0g IGV = 246354.9 + 11122.8xDay, r^2=0.032; 1g IGV = 191057.2 + 34120.9xDay, r^2=0.523). BOTTOM- Line graph, measured as mean shell IGV ± standard error. Data are from Table 4.3.11.

differences in the IGV dataset due to the sample date and gravity treatment factors, as well as the interaction term ($P = 0.000$). Comparing IGV values between the two gravity treatments on each sample date, a matrix of post-hoc Tukey's pairwise comparisons revealed significant differences in IGV values only on Day 7 ($P < 0.05$). However, the probability of the Day 5 samples being similar to each other was very low ($P = 0.054$), and would have been rejected if a significance level of $\alpha = 0.10$ had been chosen.

Larval size data from the ARF Main System 2 Ground Control experiment are recorded in Table 4.3.16, and illustrated in Figs. 4.3.7, 4.3.8, and 4.3.9. Following the same criteria that were used with the ARF MS-1 data, only larvae that were considered to be in good condition at the time of fixation were included in this dataset. In contrast to the ARF MS-1 results, there was significant growth of larvae in the ARF MS-2 experiment. For all three morphometric parameters measured (shell length, height, and square area), the slopes of regression lines fitting the data from the "0g" treatment (which in fact is a 1g treatment in this ground-based study - see Section 4.2.2) were significantly greater than zero ($P < 0.05$). Growth rates for larvae in the "1g" treatment (which is really ~1.4g - see Section 4.2.2) were not significantly different from zero growth rates ($P > 0.05$), as determined by analysis of variance testing of the regressions for the shell length, height, and square area datasets.

Shell length data from the ARF MS-2 experiment are shown in Fig. 4.3.7. Larvae in the "0g" treatment grew at an average rate of 0.93 μm/day, while the average rate of larval shell length growth in the "1g" treatment was determined by linear regression analysis to be only 0.18 μm/day. A two-way ANOVA model, using gravity, sample date, and an interaction term of gravity x treatment, found significant differences ($P < 0.05$)

Table 4.3.16. Summary of growth data of mussel (*Mytilus edulis*) larvae from ARF Main System #2 during hypergravity ("1g") and normal gravity ("0g") exposures in Orbiter Environmental Simulator (OES) during Space Shuttle Mission STS-77, May 20-30, 1996.

SHELL LENGTH (µm)

FLIGHT	"0g"				"1g"			
DAY#	MEAN	n	St. Dev.	St. Error	MEAN	n	St. Dev.	St. Error
0	110.7	30	4.5	0.8	110.7	30	4.5	0.8
3	112.8	72	7.1	0.8	113.5	77	6.5	0.7
5	115.7	76	8.5	1.0	116.1	71	8.9	1.1
7	114.8	39	6.9	1.1	112.9	10	4.6	1.5
10	120.9	27	8.2	1.6	113.8	62	5.7	0.7

SHELL HEIGHT (µm)

FLIGHT	"0g"				"1g"			
DAY#	MEAN	n	St. Dev.	St. Error	MEAN	n	St. Dev.	St. Error
0	81.6	30	3.6	0.7	81.6	30	3.6	0.7
3	83.1	72	5.5	0.6	83.6	77	5.6	0.6
5	85.5	76	7.4	0.8	87.5	71	7.3	0.9
7	84.1	39	5.6	0.9	84.1	10	4.4	1.4
10	90.6	27	8.0	1.5	83.3	62	4.3	0.5

SHELL AREA (µm²)

FLIGHT	"0g"				"1g"			
DAY#	MEAN	n	St. Dev.	St. Error	MEAN	n	St. Dev.	St. Error
0	7496	30	576.6	105.3	7496	30	576.6	105.3
3	7857	72	955.8	112.6	7962	76	959.8	110.1
5	8276	76	1285.8	147.5	8522	71	1320.3	156.7
7	8090	39	973.5	155.9	7959	10	688.4	217.7
10	9207	27	1422.8	273.8	7919	62	781.7	99.3

SHELL BIREFRINGENCE (Integrated Digital Grey Value)

FLIGHT	"0g"				"1g"			
DAY#	MEAN	n	St. Dev.	St. Error	MEAN	n	St. Dev.	St. Error
3	334811	42	51832.9	7998.0	384028	49	61973.4	8853.3
5	335652	47	92309.3	13464.7	433349	44	70218.2	10585.8
7	403061	32	94838.5	16765.2	328298	10	74336.4	23507.2
10	647714	12	74609.6	21537.9	630133	39	98675.0	15800.6

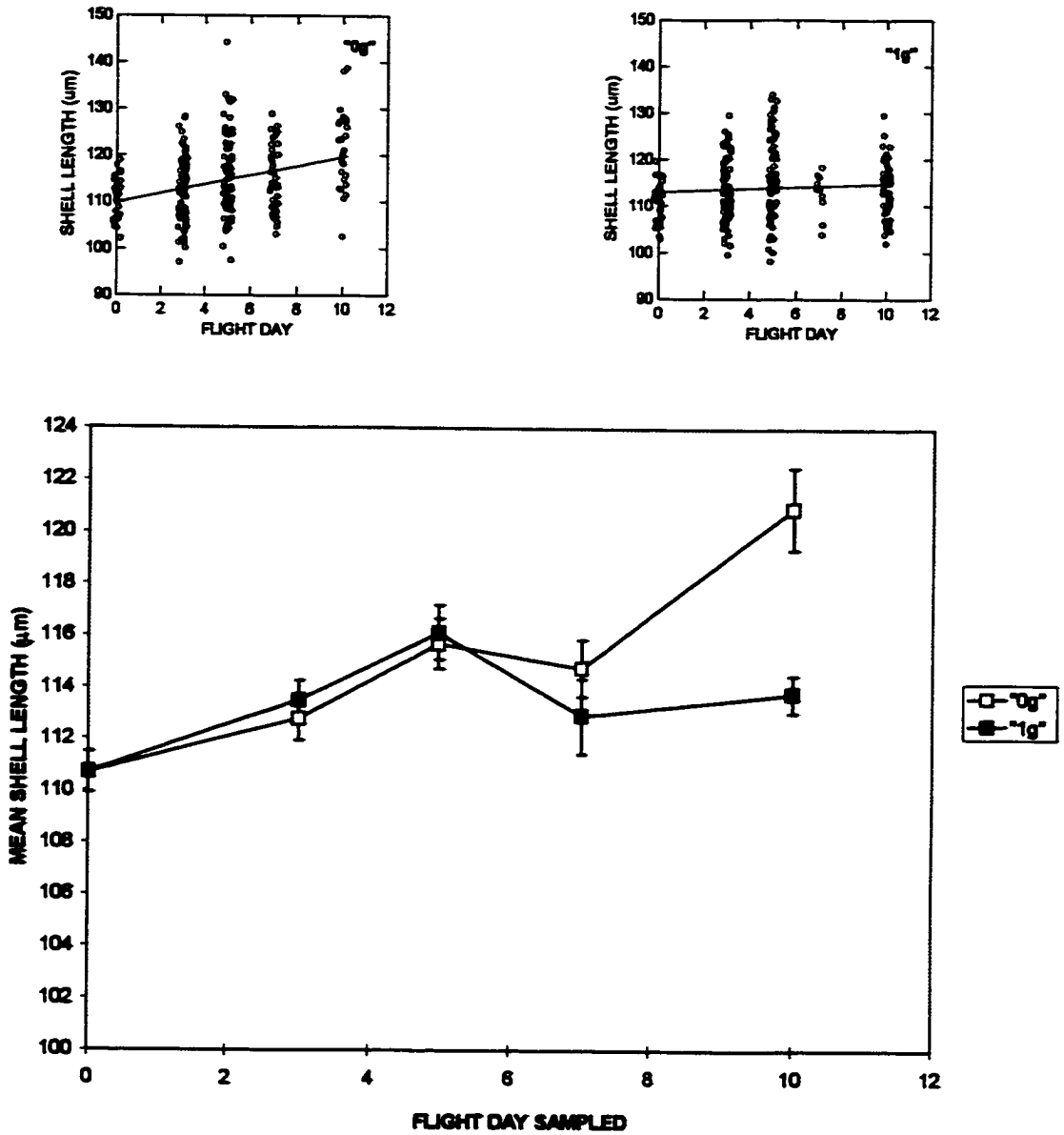

Fig. 4.3.7. Size of mussel (*Mytilus edulis*) larvae from ARF Main System #2 during hypergravity ("1g") and normal gravity ("0g") exposures in Orbiter Environmental Simulator (OES) during Space Shuttle Mission STS-77, May 20-30, 1996. TOP- scatterplots of individual shell length measurements, with regression lines ("0g" Length = 110.3+ 0.931xDay, r^2=0.107; "1g" Length = 113.03 + 0.18xDay, r^2=0.007). BOTTOM- Line graph, measured as sample date vs. mean shell length ± standard error. Data are from Table 4.3.16.

within the shell length dataset due to all three factors (see Table 4.3.17). A post-hoc Tukey's matrix of all possible pairwise comparisons revealed significant differences between mean shell lengths between the "0g" and "1g" samples only on Day 10; on all other sample dates, no significant differences in shell length due to gravity treatment were found.

Fig. 4.3.8 shows the mean shell height data for larvae from the ARF MS-2 ground control experiment. In the "0g" treatment, shell height increased at an average rate of 0.076 μm/day, and the rate of shell height increase in larvae from the "1g" samples was 0.077 μm/day. The results of the two-way ANOVA model shown in Table 4.3.18 found significant differences due to both the flight day factor and the flight day x gravity interaction term ($P < 0.05$). Tukey's post-hoc comparisons found significant differences between the sample means of the Day 10 samples, but not between "0g" and "1g" samples on any of the other sample dates.

The size of larvae from the MS-2 experiment as measured by shell square area are shown in Fig. 4.3.9. Larvae from the "0g" treatment added new material to their shells at a rate of 150.2 μm^2/day, while shell area growth rate in the "1g" samples was only 19.74 μm^2/day. Significant differences in this dataset were due to the flight day factor and the flight day x gravity interaction term ($P < 0.05$), as shown by the two-way ANOVA model outlined in Table 4.3.19. Post-hoc Tukey's comparisons detected significant differences in mean shell area between the samples collected on Flight Day 10, but no differences were found between matching "0g" and "1g" samples on any other sample date.

Table 4.3.17. Two-way Analysis of Variance (ANOVA) for larval mussel (*Mytilus edulis*) shell length data from ARF Main System #2 during Space Shuttle Mission STS-77, May 19-29, 1996.

Source	Sum-of-Squares	df	Mean-Square	F-ratio	P
SAMPLE DATE	2050.298	4	512.575	10.092	0.000
GRAVITY	205.844	1	205.844	4.053	0.045
SAMPLE DATE * GRAVITY	911.513	4	227.878	4.487	0.001
Error	24582.207	484	50.790		

Table 4.3.18. Two-way Analysis of Variance (ANOVA) for larval mussel (*Mytilus edulis*) shell height data from ARF Main System #2 during Space Shuttle Mission STS-77, May 19-29, 1996.

Source	Sum-of-Squares	df	Mean-Square	F-ratio	P
SAMPLE DATE	1715.631	4	428.908	11.969	0.000
GRAVITY	72.736	1	72.736	2.030	0.155
SAMPLE DATE * GRAVITY	1126.014	4	281.503	7.856	0.000
Error	17343.373	484	35.833		

Table 4.3.19. Two-way Analysis of Variance (ANOVA) for larval mussel (*Mytilus edulis*) shell square area data from ARF Main System #2 during Space Shuttle Mission STS-77, May 19-29, 1996.

Source	Sum-of-Squares	df	Mean-Square	F-ratio	P
SAMPLE DATE	$5.604 \cdot 10^{7}$	4	$1.401 \cdot 10^{7}$	12.791	0.000
GRAVITY	$3.723 \cdot 10^{6}$	1	$3.723 \cdot 10^{6}$	3.399	0.066
SAMPLE DATE * GRAVITY	$3.284 \cdot 10^{7}$	4	$8.209 \cdot 10^{6}$	7.494	0.000
Error	$5.302 \cdot 10^{8}$	484	$1.095 \cdot 10^{6}$		

Table 4.3.20. Two-way Analysis of Variance (ANOVA) for larval mussel (*Mytilus edulis*) shell calcification (optical birefringence) data from ARF Main System #2 during Space Shuttle Mission STS-77, May 19-29, 1996.

Source	Sum-of-Squares	df	Mean-Square	F-ratio	P
SAMPLE DATE	$2.274 \cdot 10^{12}$	3	$7.580 \cdot 10^{11}$	122.041	0.000
GRAVITY	$9.067 \cdot 10^{9}$	1	$9.067 \cdot 10^{9}$	1.460	0.228
SAMPLE DATE * GRAVITY	$2.081 \cdot 10^{11}$	3	$6.937 \cdot 10^{10}$	11.170	0.000
Error	$1.658 \cdot 10^{12}$	267	$6.211 \cdot 10^{9}$		

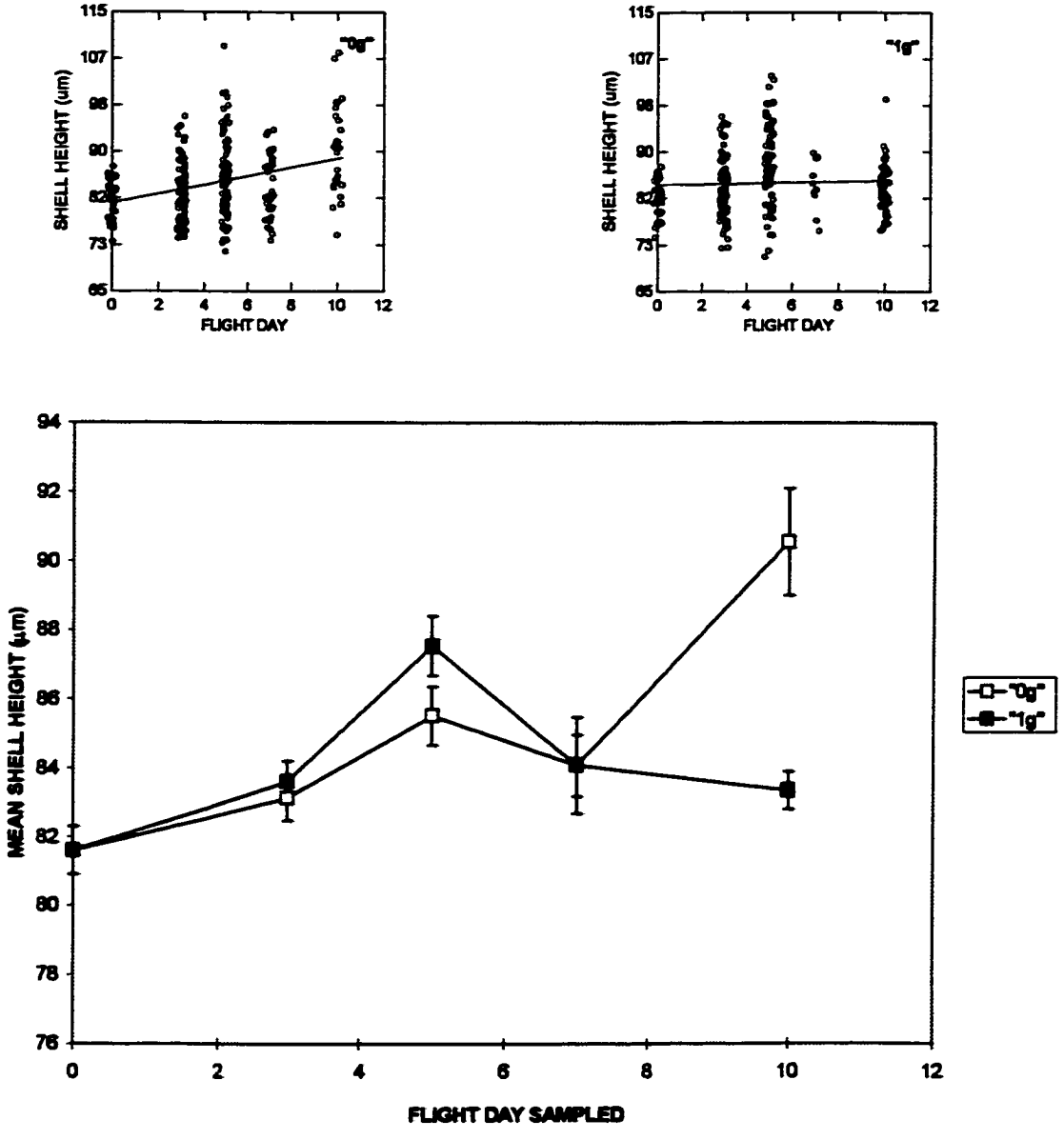

Fig. 4.3.8. Size of mussel (*Mytilus edulis*) larvae from ARF Main System #2 during hypergravity ("1g") and normal gravity ("0g") exposures in Orbiter Environmental Simulator (OES) during Space Shuttle Mission STS-77, May 20-30, 1996. TOP- scatterplots of individual shell height measurements, with regression lines ("0g" Height = 81.03+ 0.076xDay, r^2=0.101; "1g" Height = 84.05 + 0.077xDay, r^2=0.002). BOTTOM- Line graph, measured as sample date vs. mean shell height ± standard error. Data are from Table 4.3.16.

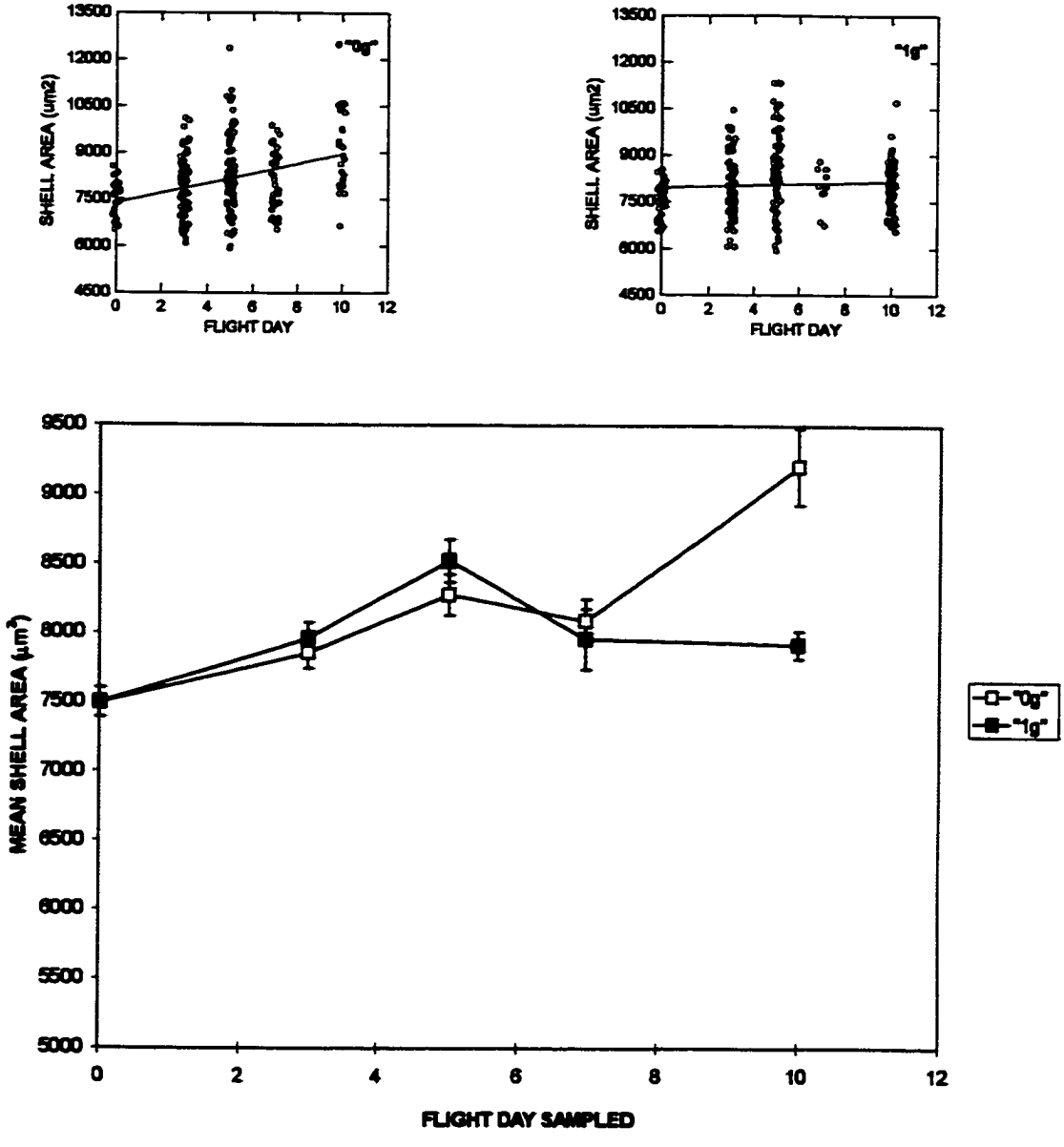

Fig. 4.3.9. Size of mussel (*Mytilus edulis*) larvae from ARF Main System #2 during hypergravity ("1g") and normal gravity ("0g") exposures in Orbiter Environmental Simulator (OES) during Space Shuttle Mission STS-77, May 20-30, 1996. TOP- scatterplots of individual shell square area measurements, with regression lines ("0g" Area = 74.42+ 150.20×Day, r^2=0.123; "1g" Area = 7956.94 + 19.74×Day, r^2=0.004). BOTTOM- Line graph, measured as sample date vs. mean shell square area ± standard error. Data are from Table 4.3.16.

Shell calcification data for the ARF MS-2 experiment are summarised in Fig. 4.3.10. Throughout the experiment, a general trend towards thickening shells can be seen in both the "0g" treatment and the "1g" samples. The slopes of the regression equations for both the "0g" and "1g" datasets were determined by analysis of variance to be significantly greater than zero ($P < 0.05$). A two -way ANOVA model shown in Table 4.3.20 revealed that the gravity factor did not significantly influence the shell calcification of the larvae in this experiment, but the flight day and flight day x gravity interaction term did have an effect upon shell calcification ($P < 0.05$). A matrix of Tukey's post-hoc pairwise comparisons detected significant differences between the "0g" and "1g" samples collected on Day 5, but not between matching samples on any other day of the experiment.

Larval growth data from the so-called "ideal condition control" experiment conducted in a seawater lab facility at Dalhousie University during the Space Shuttle mission study are plotted in Fig. 4.3.11. Larvae in this experiment grew at an average rate of 6.2 μm/day, as measured by shell length. This rate of growth was much higher than that seen in the ARF MS-1 and MS-2 experiments. Results from the lab control experiments conducted at Kennedy Space Center's Space Station Processing Facility (SSPF) are shown in Fig. 4.3.12. For these larvae, shell length increased at a rate of 0.467 μm/day, and shell height increased at a rate of 0.720 μm/day; analysis of variance of both of these regressions revealed that the slopes were significantly greater than zero.

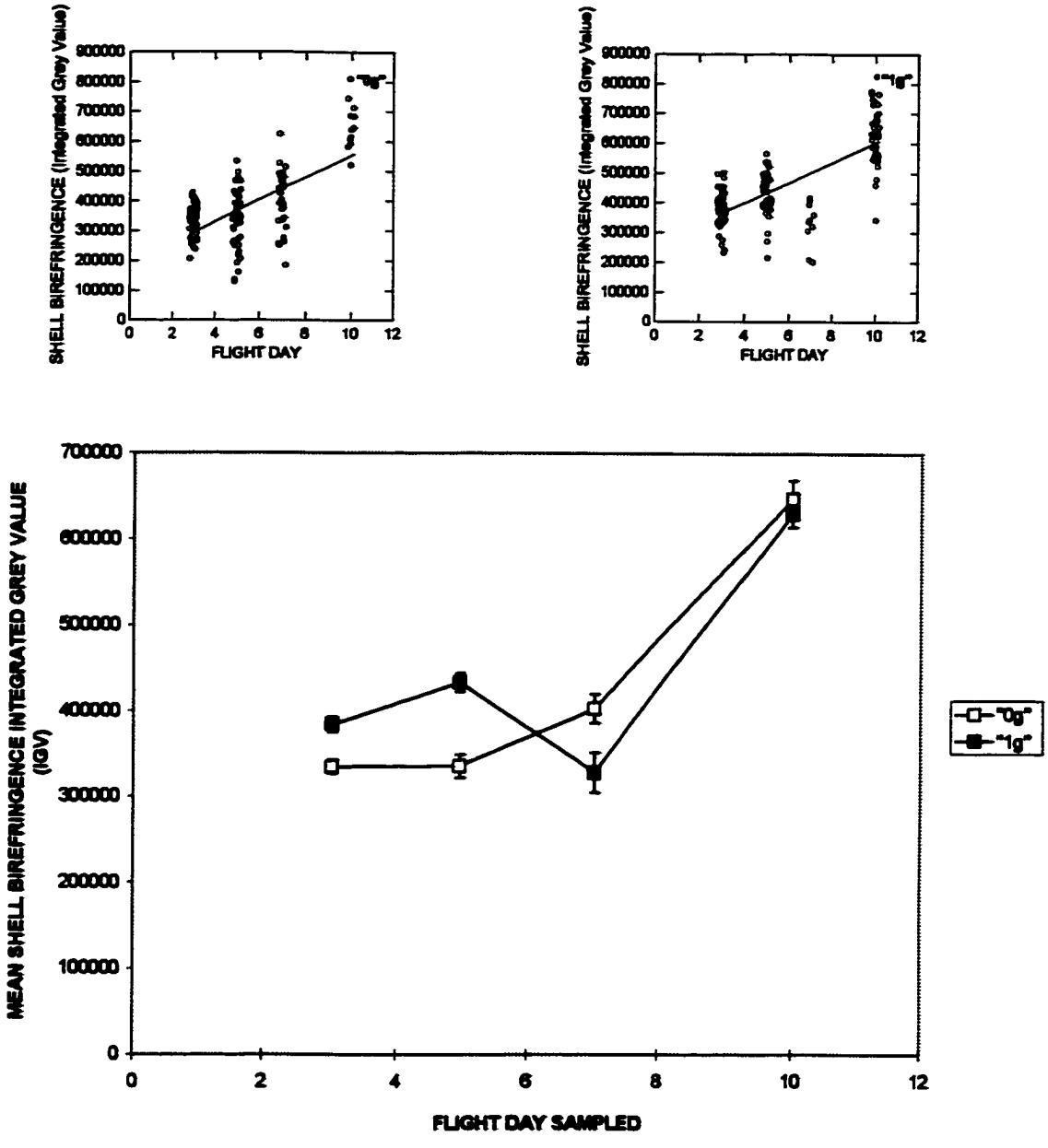

Fig. 4.3.10. Changes in mussel (*Mytilus edulis*) larval shell calcification from ARF Main System #2 during hypergravity ("1g") and normal gravity ("0g") exposures in Orbiter Environmental Simulator (OES) during Space Shuttle Mission STS-77, May 20-30, 1996. TOP- scatterplots of individual shell birefringence measurements (integrated digital grey value-IGV), with regression lines ("0g" IGV = 186018.3+ 36550.0xDay, r^2=0.411; "1g" IGV = 266310.9 + 33768.8xDay, r^2=0.523). BOTTOM- Line graph, measured as sample date vs. mean shell IGV ± standard error. Data are from Table 4.3.16.

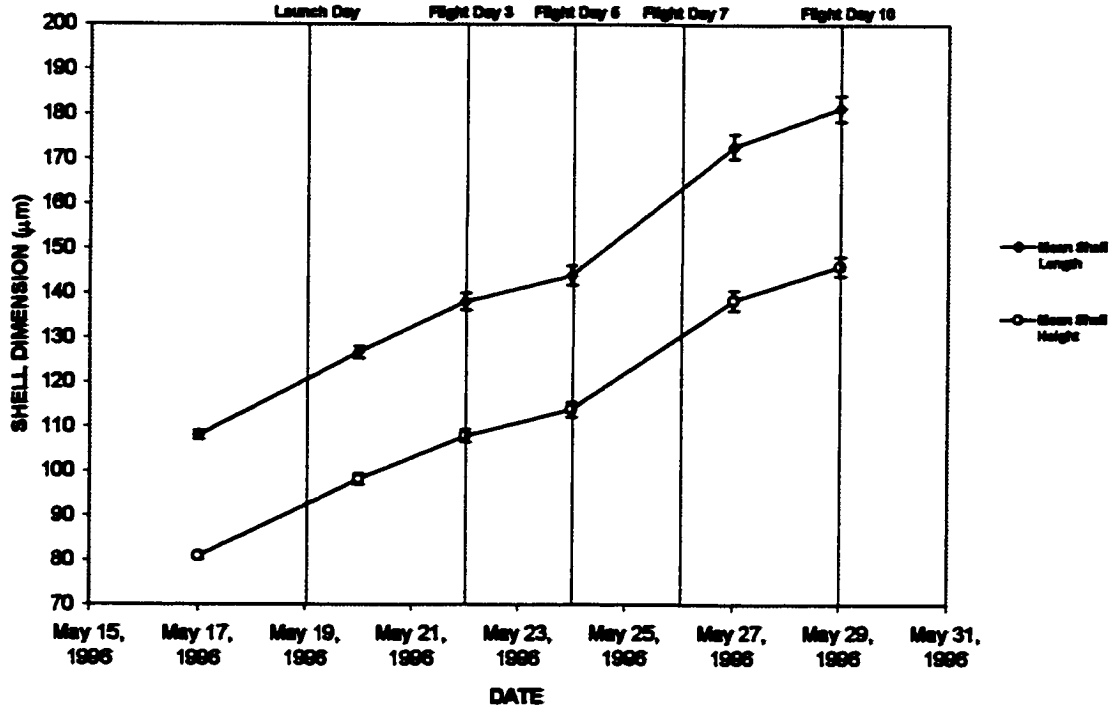

Fig. 4.3.11. Growth of mussel larvae (*Mytilus edulis*) in the "Ideal Conditions" control experiment conducted at Dalhousie University during the Space Shuttle Mission STS-77, May 19-29, 1996. Larvae were held in a 1000-litre tank, fed 25 000 cells/ml *Isochrysis galbana* (clone ISO), and seawater was changed and food was replenished every two days. Data are plotted as mean shell length ± standard error and mean shell height ± standard error. Regression equations: Length = 82.260 + 6.190 x Age; Height = 58.260 + 5.484 x Age. Sample dates for the ARF MS-1 Flight experiment are indicated.

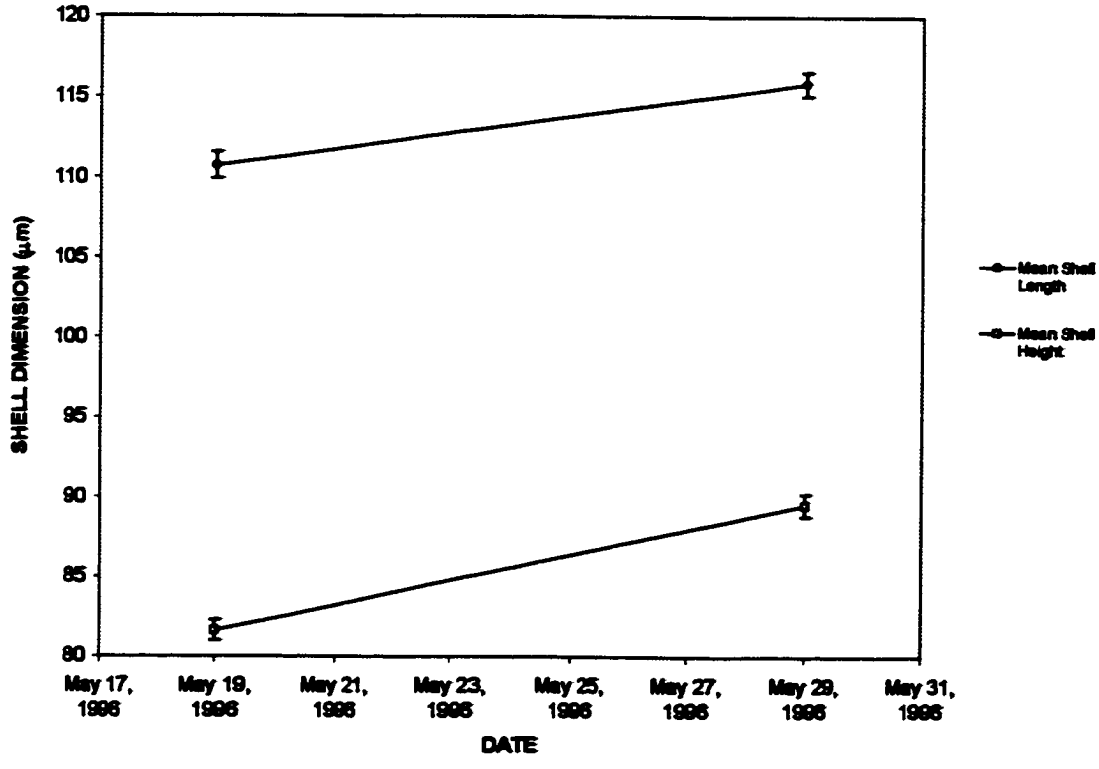

Fig. 4.3.12. Growth of mussel larvae (*Mytilus edulis*) in the lab control experiments conducted at Kennedy Space Center's Space Station Processing Facility during the Space Shuttle Mission STS-77, May 19-29, 1996. Larvae were held in small containers, each of which contained the same volume of seawater and the same algal food density (25 000 cells/ml *Isochrysis galbana*) as was used in the ARF experiments. Data are plotted as mean shell length ± standard error and mean shell height ± standard error. Regression equations: Length = 108.385 + 0.467 x Age; Height = 78.024 + 0.720 x Age. The two dates indicated are the launch date and landing date.

4.3.4 Algal Cell Population Data

On Landing Day, May 29, 1996, the algae samples from MS-1 SCA test chamber #3L0 and MS-1 SCA test chamber # 3L1 were examined on an epifluorescence microscope, and the cells examined were found to be still alive after 10 days in orbit. Individual algal cells were observed to be emitting red fluorescence, due to the presence of active chlorophyll. The algae/seawater samples from all MS-1 and MS-2 SCA test chambers were divided between two sample vials, fixed in glutaraldehyde, and transported back to Halifax and stored at 5°C until they were counted. Each of the two samples from each SCA test chamber were subjected to two replicate counts, and these data are summarised below in Table 4.3.21 and Table 4.3.22. Unfortunately, the Algae Measurement Unit (AMU) did not function properly during the STS-77 mission, and AMU data recorded during the flight were discounted as unreliable.

Fig. 4.3.13 illustrates the concentration of algae (*Isochrysis galbana*) as measured on each of the sample dates in the ARF MS-1 flight experiment, while Fig. 4.3.14 combines these data with a representation of the numbers of larvae deemed to be in good condition and capable of feeding at the time of sampling. The Day 0 samples for this experiment represent the concentration of algae in the SCA test chambers on the day of loading, which was one day before the launch of the Space Shuttle on Sunday, May 16, 1996. By Day 3, the concentration of *Isochrysis galbana* had increased from nearly 23000 cells/ml to approximately 32 000 cells/ml in the two SCA test chambers sampled on that day. Between Day 3 and the final day of the experiment, the algal concentration in both the 0g and 1g SCA test chambers decreased, presumably the result of larval grazing rates being greater than algal growth rates. Algal concentrations were higher in

the 0g chambers than in the 1g chambers for the remainder of the experiment, indicating that larvae in normal gravity conditions may have ingested more algal cells than those in microgravity. Alternatively, the algae population may have grown more in microgravity. The two-way ANOVA model shown in Table 4.3.23 shows that both sample date and the gravity treatment had significant influences upon the concentration of algae within the SCA test chambers. A post-hoc Tukey's matrix of pairwise comparisons revealed a significant difference between the concentration of algae in 0g and 1g samples on Day 5 of the experiment ($P = 0.055$), but not between gravity-paired samples on any other sample date.

The concentrations of algae in the samples from the ARF MS-2 ground control experiment are recorded in Table 4.3.22 and illustrated in Figs. 4.3.15 and 4.3.16. Unlike the ARF MS-1 experiment, there was no significant increase in algal concentration between the time at which the SCA test chambers were loaded and Day 3 of the experiment. The concentration of algae did not change much in either the 0g or the 1g samples throughout the experiment, and no distinctive pattern of grazing rates was discernible. The results of a two-way ANOVA model (see Table 4.3.24) found significant differences amongst these samples due to gravity, flight day, and the interaction term of these two factors ($P < 0.05$). Post-hoc Tukey's comparisons did not detect any significant differences between any of the paired samples on any of the sample dates, except for the Day 10 samples, where the algae concentration in the "0g" SCA test chamber was significantly greater than that found the in "1g" sample ($P < 0.05$).

Table 4.3.21. Summary of algae (*Isochrysis galbana* clone ISO) cell count data from ARF Main System #1 during microgravity (0g) and normal gravity (1g) exposures on board Space Shuttle Mission STS-77, May 19-29, 1996.

SAMPLE #	SCA #	MEAN ALGAL COUNT (cells/ml)	stan. dev.	stan. error	REPLICATE #			
					A-1	B-1	A-2	B-2
0g Day 0	-	22951	1430	715	22202	22306	25094	22202
0g Day 3	4R0	31946	3558	2054	30785	29113	N/A	35939
0g Day 5	4L0	30158	2639	1320	29671	29531	33850	27581
0g Day 7	3R0	24099	377	189	23959	23959	23820	24656
0g Day 10	3L0	26142	1264	730	25631	27581	N/A	25213
1g Day 0	-	22951	1430	715	22202	22306	25094	22202
1g Day 3	4R1	32017	2996	1498	34459	32317	33571	27720
1g Day 5	4L1	25701	1076	538	25770	25213	24656	27163
1g Day 7	3R1	22636	800	400	22845	22009	23681	22009
1g Day 10	3L1	21974	954	477	23402	21452	21591	21452

Table 4.3.22. Summary of algae (*Isochrysis galbana* clone ISO) cell count data from ARF Main System #2 during hypergravity ("1g") and normal gravity ("0g") exposures in Orbiter Environmental Simulator (OES) during Space Shuttle Mission STS-77, May 20-30, 1996

SAMPLE #	SCA #	MEAN ALGAL COUNT (cells/ml)	stan. dev.	stan. error	REPLICATE #			
					A-1	B-1	A-2	B-2
"0g" Day 0	-	23257	1029	541	22547	24612	22374	23493
"0g" Day 3	4R0	20094	627	313	19223	20059	20477	20616
"0g" Day 5	4L0	23193	1372	686	23124	21452	24795	23402
"0g" Day 7	3R0	20860	637	319	21173	21313	21034	19920
"0g" Day 10	3L0	21870	972	486	21870	20616	22009	22984
"1g" Day 0	-	23257	1029	541	22547	24612	22374	23493
"1g" Day 3	4R1	20129	995	497	19084	19502	20755	21173
"1g" Day 5	4L1	21173	1011	505	19780	22148	21173	21591
"1g" Day 7	3R1	22636	927	464	22566	23959	22148	21870
"1g" Day 10	3L1	14766	796	398	15184	13651	14766	15462

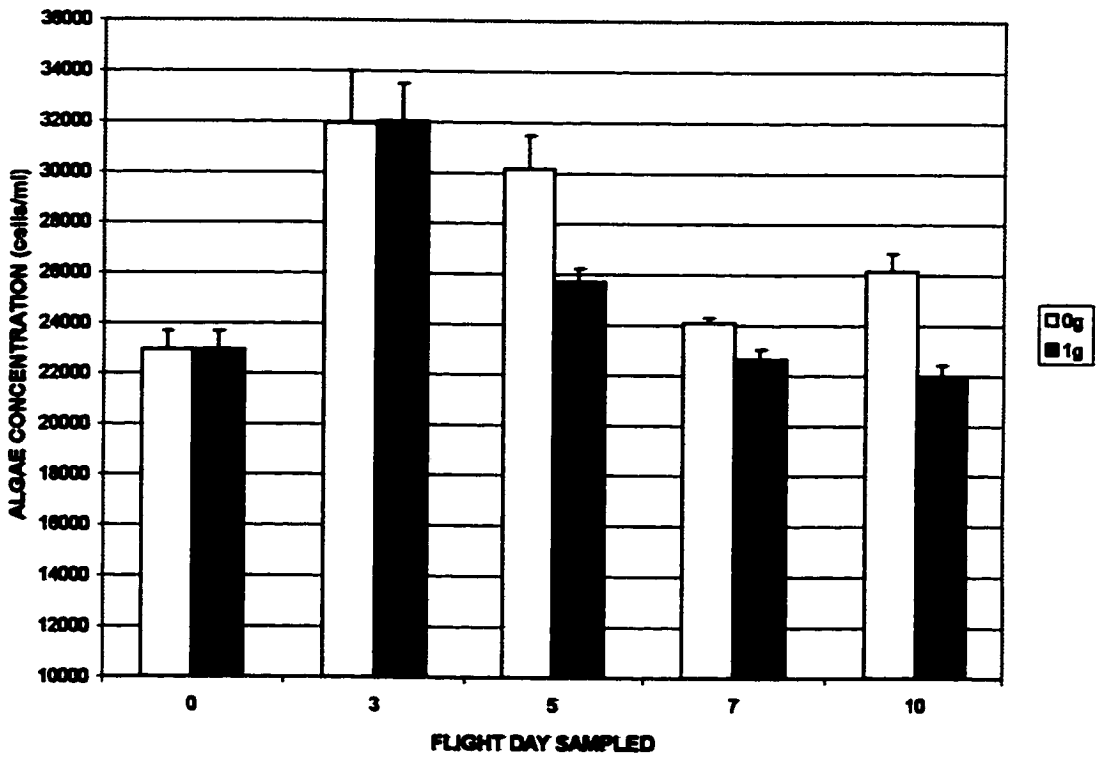

Fig. 4.3.13. Changes in algae (*Isochrysis galbana* clone ISO) cell concentration from ARF Main System #1 during microgravity (0g) and normal gravity (1g) exposures on board Space Shuttle Mission STS-77, May 19-29, 1996. Initial cell count at time of specimen loading on May 18, 1996 was 22 951 cells/ml. Measured as mean algal cell concentration + standard error.

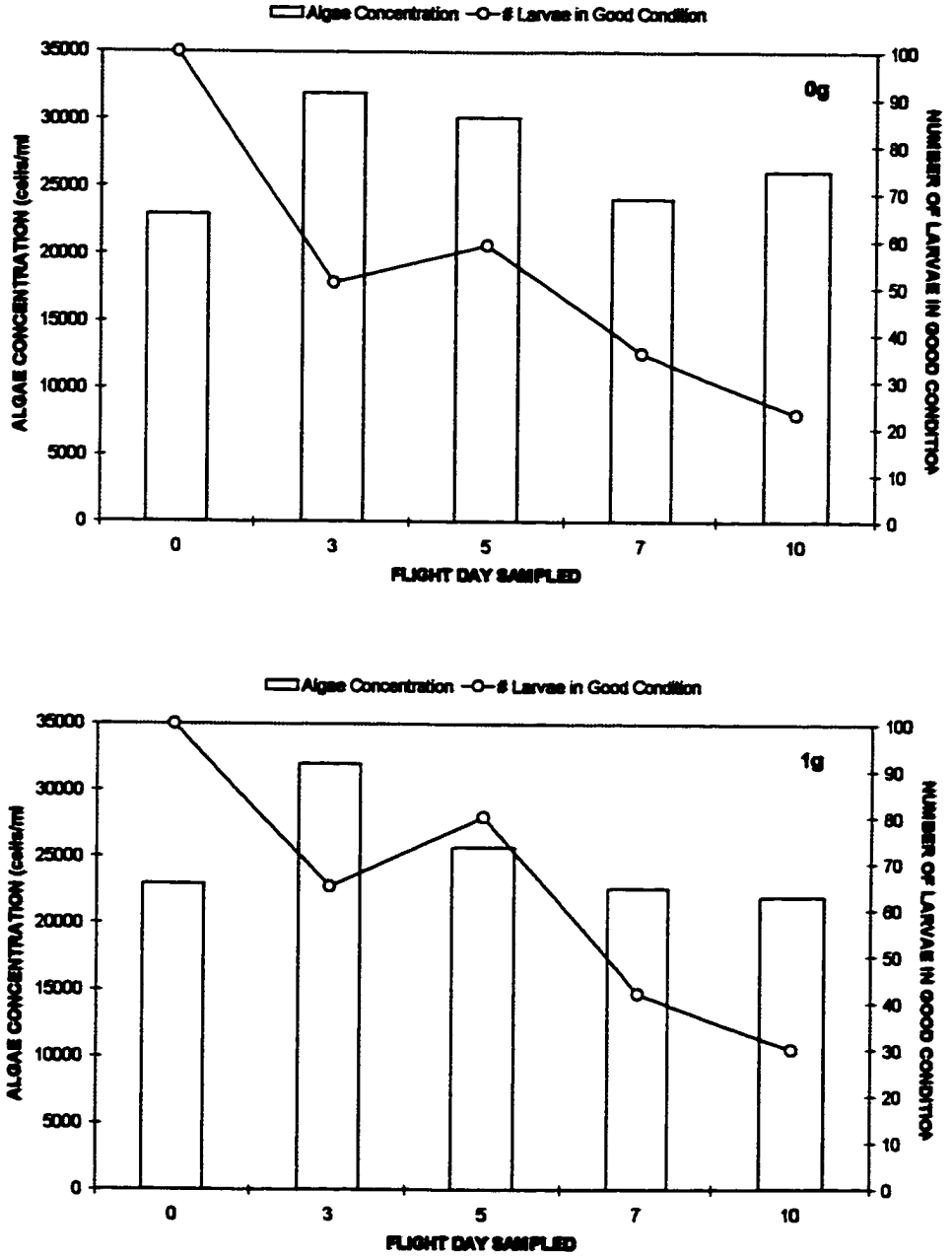

Fig. 4.3.14. Changes in algae (*Isochrysis galbana* clone ISO) cell concentration from ARF Main System #1 during microgravity (0g, top graph) and normal gravity (1g, bottom graph) exposures on board Space Shuttle Mission STS-77, May 19-29, 1996. The numbers of larvae deemed to be in good condition and capable of feeding at the time of sampling are superimposed.

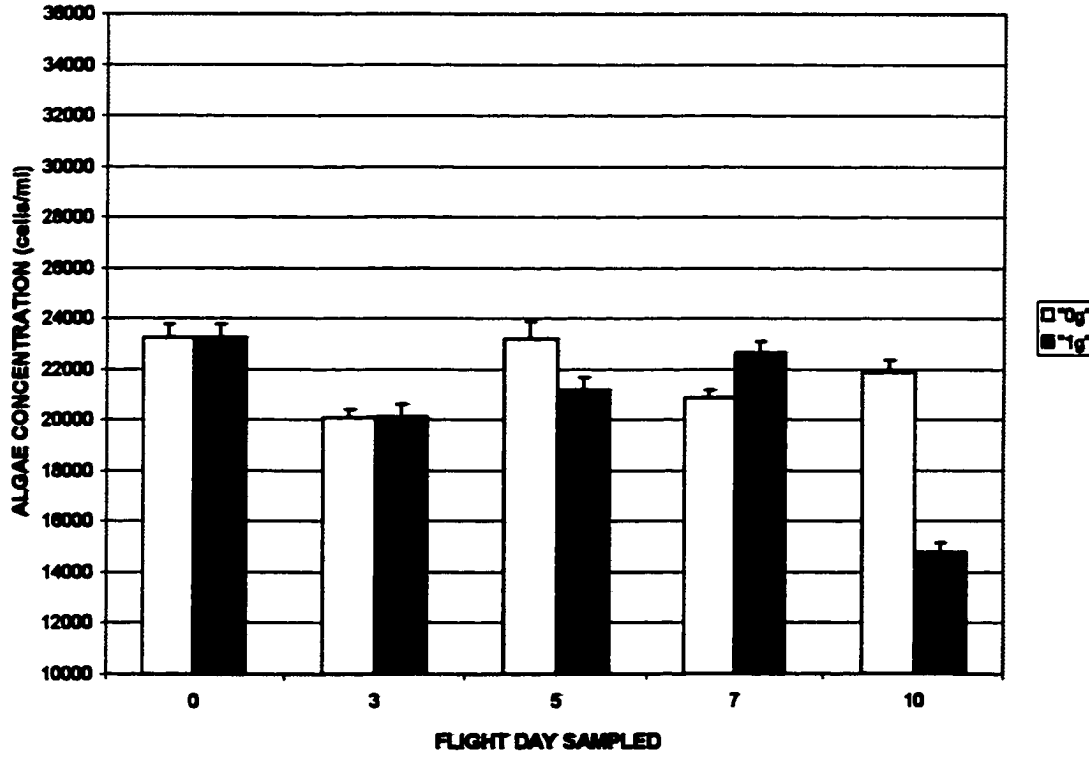

Fig. 4.3.15. Changes in algae (*Isochrysis galbana* clone ISO) cell concentration from ARF Main System #2 during normal gravity ("0g") and hypergravity ("1g") exposures in Orbiter Environmental Simulator (OES) during Space Shuttle Mission STS-77, May 20-30, 1996. Initial cell count at time of specimen loading on May 19, 1996 was 23 257 cells/ml. Measured as mean algal cell concentration ± standard error.

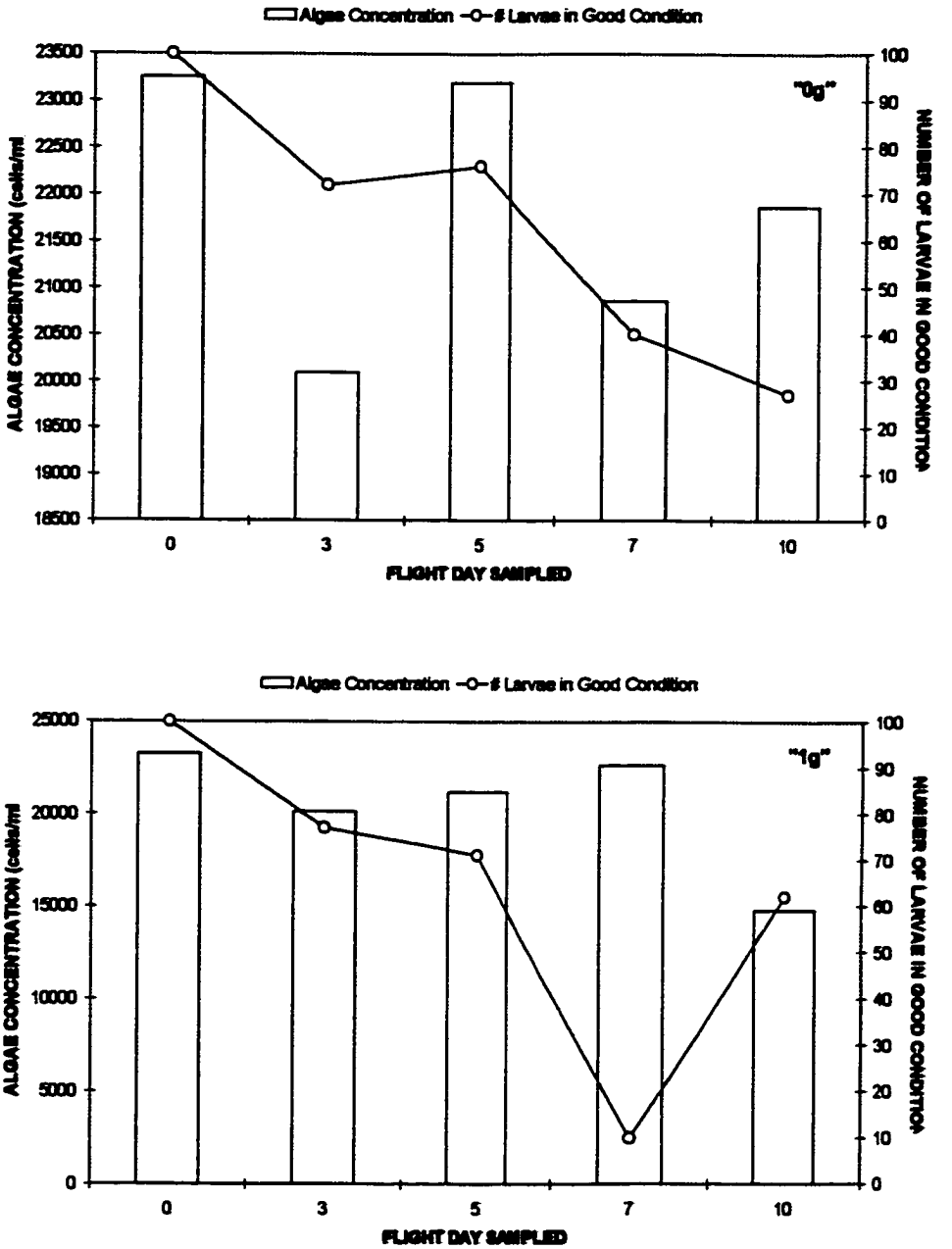

Fig. 4.3.16. Changes in algae (*Isochrysis galbana* clone ISO) cell concentration from ARF Main System #2 during normal gravity ("0g", top graph) and hypergravity ("1g", bottom graph) exposures in Orbiter Environmental Simulator (OES) during Space Shuttle Mission STS-77, May 20-30, 1996. The numbers of larvae deemed to be in good condition and capable of feeding at the time of sampling are superimposed.

Table 4.3.23. Two-way Analysis of Variance (ANOVA) for algae (*Isochrysis galbana* clone ISO) concentration data from ARF Main System #1 during Space Shuttle Mission STS-77, May 19-29, 1996.

Source	Sum-of-Squares	df	Mean-Square	F-ratio	P
SAMPLE DATE	$4.306 \cdot 10^8$	4	$1.077 \cdot 10^8$	31.025	0.000
GRAVITY	$3.762 \cdot 10^7$	1	$3.762 \cdot 10^7$	10.843	0.003
SAMPLE DATE * GRAVITY	$3.607 \cdot 10^7$	4	$9.016 \cdot 10^6$	2.598	0.058
Error	$9.716 \cdot 10^7$	28	$3.470 \cdot 10^6$		

Table 4.3.24. Two-way Analysis of Variance (ANOVA) for algae (*Isochrysis galbana* clone ISO) concentration data from ARF Main System #2 during Space Shuttle Mission STS-77, May 19-29, 1996.

Source	Sum-of-Squares	df	Mean-Square	F-ratio	P
SAMPLE DATE	$1.197 \cdot 10^8$	4	$2.992 \cdot 10^7$	32.355	0.000
GRAVITY	$2.140 \cdot 10^7$	1	$2.140 \cdot 10^7$	23.139	0.000
SAMPLE DATE * GRAVITY	$9.401 \cdot 10^7$	4	$2.350 \cdot 10^7$	25.416	0.000
Error	$2.774 \cdot 10^7$	30	924704.225		

4.4 DISCUSSION

4.4.1 The Role of Gravity in Food Capture and Growth in Marine Bivalve Larvae

4.4.1.1 Larval Growth

Growth and feeding processes in larval *Mytilus edulis* have been thoroughly studied over the years, often using the same algal food type as that used in this study. In 1965, Bayne reared the larvae of *Mytilus edulis* at 16°C and fed the flagellate alga *Isochrysis galbana* at a ration of 2.5×10^4 cells/ml, a concentration similar to that used in the current investigation. The growth rate of those larvae was approximately 5.6 μm/day, as measured by increase in shell length. In an extensive investigation involving three culture temperatures and six feeding levels, Sprung (1984a) recorded the highest growth rates (almost 12 μm/day) in blue mussel larvae reared at 18°C and a food concentration of 4×10^4 cells/ml of *Isochrysis galbana* (clone T-ISO). Larvae reared at 12°C and fed rations of 2×10^4 cells/ml and 4×10^4 cells/ml grew at rates of 7.8 μm/day and 6.8 μm/day, respectively (Sprung, 1984a). Pechenik *et al.* (1990) raised *Mytilus edulis* larvae at two temperatures and six different concentrations of *Isochrysis galbana* (clone T-ISO). Growth rates ranged between 1 and 8 μm/day, with the higher growth rates being recorded at 16°C and at the highest food rations (15 and 30×10^4 cells/ml). For larvae fed a ration of 1×10^4 cells/ml, growth rates were between 1.3 and 2.7 μm/day, and larvae reared on 3×10^4 cells/ml grew at average rates of approximately 3 μm/day. Other investigations using different algal diets have reported similar growth rates, with estimates ranging from 4.3 μm/day (Beaumont and Budd, 1982) to 8.7 μm/day (Jespersen and Olsen, 1982).

All of these estimates for *Mytilus edulis* larvae are much greater than the growth rates observed in the current study. In the ARF MS-1 experiment, the estimate for larval growth in the microgravity containers was only 0.09 μm/day, while the larvae in the control normal gravity treatment grew at a slightly higher rate of 0.33 μm/day. Although these results may appear to support Hypothesis B1 by suggesting that larvae in normal gravity were capable of greater ingestion and growth rates, the difference in growth rates between the two treatments was insignificant. After ten days in space, the final size of larvae in the microgravity chambers was not significantly different from their size at the start of the experiment. The larvae reared in normal gravity were only 2.3 μm longer than when they started; again, not a significant change from their size at Day 0. Larval growth was also poor in the ARF MS-2 ground control experiment; the "0g" treatment had a growth rate of 0.93 μm/day, and the rate of shell length growth in the "1g" hypergravity-reared larvae was only 0.18 μm/day. Taken together, the results of these experiments appear to show a slight trend towards higher growth rates for larvae reared in unit gravity, and lower growth rates when larvae are reared under conditions of different gravitational forces (microgravity and hypergravity). However, since larval growth rates in the ARF MS-1 experiment were so poor and were not significantly different from each other, decisive conclusions regarding the testing of Hypothesis B1 cannot be made based upon these data.

There are at least four possible explanations for the low growth rates observed in this study. It has long been a general observation among hatchery workers that bivalve larvae exhibit poor growth when they are confined in small containers (Couturier, pers. comm.). This is believed to be related to the increased incidence of contact with chamber

walls and with other larvae, which interferes with feeding mechanisms and behaviour. The small size of the SCA test chambers (~32 ml) was necessary for a multitude of engineering considerations pertaining to NASA's size and weight restrictions. They were also designed to be small enough to allow sufficient numbers of replicate containers to be carried into space. The observation of poor larval growth (0.47 μm/day) in the SSPF lab control experiments using containers of a size similar to the SCA test chambers lends further support to the argument that container volume has a strong influence on larval growth. In contrast, larvae from the same spawning batch that were grown in a large container at the Dalhousie University Aquatron lab as the so-called "ideal condition control" had a much higher growth rate of 6.2 μm/day.

Another factor that may have contributed to low growth rates may be the temperature regimen that the larvae were subjected to in the hours before the start of the experiment. Since the ARF MS-1 was occupied by another experiment during the first 24 hours after launch, it was necessary to delay the start of the bivalve larvae experiment by keeping the larvae at a low temperature of 5°C in order to slow down their metabolism and thereby limit growth. Due to NASA's requirement that the ARF be loaded in the Space Shuttle fourteen hours before launch, all pre-launch loading operations were also conducted at 6°C. This extended period of time in which the larvae were kept at a low temperature may have impacted upon their ability to grow after they were transferred to the ARF Main System at 12°C. A third possible explanation for poor growth may be related to the physical forces encountered during launch. Gravitational accelerations of approximately 3g are experienced during a Space Shuttle launch, accompanied by excessive vibrations. It is conceivable that these forces may have induced stress in the

animals that persisted long after orbit was achieved. Finally, since it was not possible to replenish the larval cultures with fresh algae and seawater during the Space Shuttle mission, there remains a possibility that animal waste products and algal exudates may have accumulated in the chambers and contributed to impaired larval growth responses. In particular, *Isochrysis galbana* has been noted to occasionally produce substances that are known to be toxic to larval bivalves (Guillard, 1958; Sprung, 1984a).

4.4.1.2 Larval Feeding

It is difficult to draw firm conclusions regarding larval feeding in the absence of gravity based upon the data collected in this study. Any investigation of feeding rates in animals requires that the feeding ration be firmly established. These data were not available in this study for two reasons. A decision made early in the development of the ARF program to limit the number of SCA test chambers available for this experiment meant that a control container dedicated to monitoring the effects of microgravity on algal growth could not be included in the experimental design. The addition of the Algae Measurement Unit (AMU) to the ARF hardware was a compromise solution, and was intended to monitor the algal concentration in each SCA test chamber throughout the course of the experiment. The failure of the AMU to function properly during the STS-77 mission meant that the growth of the algal population during the experiment could not be assessed. Since the effects of microgravity on the rate of algal growth are unknown, the rates of ingestion by the larvae could not be calculated.

Some insights into larval feeding can be drawn with the data that remain, however. A general decline in algal concentration throughout the ARF MS-1 experiment,

accompanied with the observation of algal cells in the guts of the animals (see Section 4.4.3.1), suggests that the larvae were indeed feeding during their time in space. This observation also means that the rate of larval ingestion exceeded the rate of algal cell division. There is also a general trend towards higher algal concentrations in the microgravity chambers than in the normal gravity containers, which is statistically significant on Day 5. This indicates that the larvae that were reared in normal gravity may have been ingesting algae at a higher rate than the larvae in the microgravity containers, thereby lending support to Hypothesis B1. The influence of hypergravity on larval feeding could not be assessed, as no clear patterns could be seen in the algal population data for the ARF MS-2 experiment.

4.4.1.3 Summary

Definitive conclusions regarding the validity of Hypothesis B1 cannot be made based upon the results of the ARF experiment. The test of larval feeding capacity in the absence of gravity was confounded by the inability to accurately assess algal population growth independent of larval grazing. Measurement of larval growth as an indirect method of assessing feeding ability did not yield very useful data, in that growth rates of all larvae, regardless of gravity treatment, were very poor. On the other hand, although there were no statistically significant differences in growth rates between larvae reared in microgravity and normal gravity, there was a slight trend towards better larval growth from the normal gravity samples. When considered along with the observation of a possible tendency towards higher feeding rates in larvae reared in normal gravity, these data lend some support to the hypothesis that gravity is essential for normal feeding

processes in marine bivalve larvae. Further investigation is clearly required, as the results of this experiment neither confirm nor reject Hypothesis B1.

4.4.2 Buoyancy Regulation in Marine Bivalve Larvae

4.4.2.1 Buoyant Density

There are few studies of buoyancy regulation in marine bivalve larvae. In a comprehensive examination of locomotor energetics and buoyancy control in marine bivalve larvae, Gallager (1992) monitored changes in the density of *Bankia gouldi* larvae throughout development and also through periods of imposed starvation. Egg density was found to be 1.036 $g \cdot cm^{-3}$ and larval density increased to 1.135 $g \cdot cm^{-3}$ as the prodissoconch I shell was formed, and eventually leveled out at around 1.202 $g \cdot cm^{-3}$. The density of well-fed larvae did not change throughout the remainder of the planktonic period, but larvae deprived of particulate food for two or three day periods exhibited an increase in density at a rate of approximately 0.035 $g \cdot cm^{-3}$ per day. Concomitant with the increased density during the starvation periods was a decline in the amount of lipid reserves stored by the larvae. These results led the author to conclude that the larvae of *Bankia gouldi* store lipids as a means of regulating buoyancy.

Jackson (1992) presented data on the changes in larval density and lipid utilization throughout early development for the sea scallop *Placopecten magellanicus*. The density of the eggs was reported as 1.02 $g \cdot cm^{-3}$ and larval density increased to between 1.28 and 1.30 $g \cdot cm^{-3}$ as the veliger stage was reached and the shell was formed. A period followed in which larval density was too high to be measured by the

methodology used, but by the time the larvae reached a size of 130 μm shell length, density had decreased to 1.26 $g \cdot cm^{-3}$. Periods of starvation resulted in stunted growth rates and the catabolism of lipid reserves, as was also observed in Gallager's 1992 study.

In the present study, there is no evidence from the density measurement data to support the hypothesis that mussel larvae actively regulate their buoyancy in order to optimise feeding efficiency or to conserve locomotor energy. There were no differences in buoyant density between larvae reared under different gravity conditions; the specific gravity of larvae from both the microgravity and normal gravity treatments was approximately 1.35 to 1.36 $g \cdot cm^{-3}$. These measurements are consistent with previous measurements of larval density for *Mytilus edulis* grown under laboratory conditions (Jackson, unpub. data), but are greater than those reported by Jackson (1992) for *Placopecten magellanicus* and those reported by Gallager (1992) for *Bankia gouldi*. Since larval density was similar in both gravity treatments, the data from this experiment do not support the prediction based upon Hypothesis B2 that larvae reared in microgravity would compensate for the absence of gravity by increasing their overall density.

4.4.2.2 Lipids

There was no apparent effect of spaceflight on the amount of neutral lipid in the mussel larvae returned from space on May 29, 1996. In both the microgravity and normal gravity treatments, live larvae stained with the lipophilic vital stain Nile Red showed an abundance of small lipid globules distributed throughout the tissues of the animals, with no noticeable differences in the amount of lipid between the two groups.

This pattern of neutral lipid distribution is typical of small, young bivalve veligers (Jackson, 1992; Jackson, 1993). When initially released from the parent, bivalve eggs contain a large amount of lipid in the form of triacylglycerol, which the developing embryos catabolise as an energy source (Holland, 1978). This lipid is the principal source of energy for larvae until the feeding organs and digestive system are fully developed, at which point surplus ingested food energy is stored as triglyceride globules in the digestive gland.

The larvae used in this experiment were only six days old at the time of launch, and throughout the experiment they were using both their maternally-derived lipid reserves as well as ingested food as sources of energy. By the end of the spaceflight experiment, the pattern of lipid distribution in the larvae suggested that the lipid globules that were initially provided by the parent had not been fully utilised. Any potential influence that microgravity may have had upon the manner in which bivalve larvae allocate ingested energy to lipid deposition was masked by the preponderance of maternal lipid that was distributed throughout the larval tissues. This made it difficult to determine if larvae reared in microgravity were actively adjusting their buoyancy by allocating less energy to the production of lipid reserves. As such, evidence to either support or reject the hypothesis that bivalve larvae are capable of regulating their own buoyancy in response to their environment (Hypothesis B2) cannot be established from the observations of lipid distribution in the mussel larvae that developed in space.

4.4.2.3 Shell Calcification

The results from the ARF MS-1 shell calcification measurements contradict the Hypothesis B2 prediction, in that there is a tendency towards more heavily mineralised shells in larvae reared in normal gravity than in larvae from the microgravity samples. Larvae raised in the normal gravity SCA test chambers showed a progressive increase in the degree of shell birefringence as the experiment progressed. This was not the case for the larvae from the microgravity samples, where shell birefringence did not change significantly over the ten day course of the experiment. While statistically significant differences in shell birefringence only existed between the two treatments on Flight Day 7, shells from microgravity-raised larvae were less calcified than those from the control treatment larvae for the last 7 days of the Space Shuttle experiment. A trend towards divergence in mean birefringence measurements between the two groups on Day 5 and Day 7 was lost by the time the experiment was concluded, when larvae from both treatments sampled on Day 10 had similar degrees of shell mineralisation. These data suggest that larvae in microgravity do not increase their shell mass as a means of increasing their density.

Shell birefringence measurements of larvae from the ARF MS-2 ground control experiment did not show any clear trend towards a relationship between gravity and shell calcification. Larval shell mineralisation increased throughout the experiment in both the "0g" normal gravity and "1g" hypergravity treatments. With the exception of the Day 5 samples, there were no significant differences in shell birefringence between the two groups. Whereas the results from the ARF MS-1 flight experiment suggest that gravity may be required in order for normal shell mineralisation to occur (see Section 4.4.3.4),

the MS-2 data would suggest that increased gravity does not result in increased shell density.

The ARF MS-1 Day 10 microgravity sample appeared to have been a possible anomaly, or it may have been an artifact resulting from the post-flight handling procedures. The larvae returned from space were living in a normal gravity environment for several hours before they were fixed in preparation for shell birefringence measurements. After the shuttle Endeavour landed at Kennedy Space Center, three hours passed before the ARF was delivered to the lab at the Space Station Processing Facility for unloading of live specimens. Several more hours passed while the larvae were examined in detail and videotaped. If gravity is indeed required for normal shell calcification, as the ARF MS-1 results suggest, it is possible that the larvae reared in microgravity added new calcium to their shells during this extended exposure to a normal gravity environment.

4.4.2.4 Summary

To summarise, the data collected in this experiment do not lend support to the hypothesis that bivalve larvae actively regulate their buoyancy as a means of optimising feeding efficiency or to conserve energy allocated to swimming processes. Comparisons of specific gravity measurements, lipid content, and shell calcification data between groups of larvae raised under different gravity environments in this experiment do not provide any evidence to suggest that the buoyant density of bivalve larvae is the result of an actively regulated process.

4.4.3 The Influence of Gravity on Development of Marine Bivalve Larvae

4.4.3.1 Qualitative Observations of Live Larvae Returned From Space

Post-flight examination of the larvae returned alive to KSC after 10 days in space revealed that the larvae raised in microgravity had apparently developed normally. The general shape of the shells and the vela of these larvae were typical of mussel larvae of that size and age; no deformities were observed. Internal organs appeared to be normal and the guts of many of the animals contained algal food, indicating that the digestive tract and feeding mechanisms had developed and functioned in the same manner as larvae from the unit gravity control treatment. Most microgravity-reared larvae were actively swimming in a typical helical pattern, indicating that ciliary function and control of locomotor processes had also developed normally. Some mortalities were observed, but these were relatively few in number compared to active, surviving larvae. These general observations supported the hypothesis that gravity does not affect the normal development of early veliger stage larvae of *Mytilus edulis*.

4.4.3.2 General Condition

The condition of mussel larvae as reported here for the ARF experiment was a simple qualitative assessment, using broad criteria of general appearance as an index of overall larval health. As such, there is no basis for making comparisons of these data with results from larval condition indices reported in the literature, such as those described by Gallager *et al.* (1986), Fraser (1989) or Jackson (1993). Even so, the visual assessment of larval condition as performed in this investigation provided an additional method of interpreting the results from the Space Shuttle experiment, thereby maximising

the amount of data that could be extracted from the rather valuable samples collected in this study.

There was a tendency for larvae exposed to microgravity to be in poorer condition than those reared in normal gravity. On all sample dates, the ARF MS-1 unit gravity samples had a higher proportion of larvae deemed to be in good condition, and a lower proportion of larvae in poor condition, than the samples from the microgravity treatment. Larvae from both of the ARF MS-2 treatments also had higher proportions of good condition larvae. There are two possible explanations for these observations. If the larvae reared in microgravity had encountered difficulties in feeding (see Section 4.4.1.1 above), then the poor appearance of these larvae could reflect a lack of sufficient energy intake. Alternatively, it may be indicative of abnormalities associated with development in the absence of gravity. For instance, measurements of shell calcification revealed that the shells of larvae in the microgravity treatment were not as heavily mineralised as those raised in normal gravity (see Section 4.4.3.4 below). In either case, the observations of larval condition would suggest that mussel larvae require gravity in order to develop properly, a conclusion inconsistent with Hypothesis B3 .

4.4.3.3 Lipid Utilisation

As discussed in Section 4.4.2.2, gravity did not appear to have an influence on the manner in which lipid is utilised in marine bivalve larvae. In all larvae returned from space, lipid globules were dispersed throughout the tissues of the larvae and were not concentrated in any particular area. Neutral lipid distributed in this manner is characteristic of early bivalve veligers (Jackson, 1992, 1993). Regardless of the gravity

treatment in which larvae were raised, the amount of neutral lipid globules present in the animals was similar and there were no apparent differences between the two groups in terms of the localisation of lipid. This suggests that larvae in both gravity treatments apparently catabolised and deposited lipid in a similar manner. Since the patterns of lipid distribution were similar in both the microgravity and normal gravity-reared larvae, it can be surmised that the normal process of early development and lipid catabolism in mussel larvae was not affected by the absence of gravity.

4.4.3.4 Shell Formation

The study of larval invertebrate calcification processes in microgravity is a new science, and as such there are few data with which to compare the results of the current investigation. Marthy *et al.* (1996) undertook a study in which larvae of the sea urchin *Sphaerechinus granularis* were fertilised on the ground but allowed to develop from blastula stage through to pluteus in microgravity aboard the space shuttle Columbia. After fourteen days in space, calcified skeletal structures had formed in these larvae as expected. Some abnormalities were noted, but since the normal gravity control larvae also had "sub-normal" skeletons, these were attributed to a pre-flight handling irregularity. A parallel experiment with plutei that had formed skeletons on the ground was also conducted to determine if decalcification of skeletal tissues would take place in the absence of gravity; these larvae showed no signs of skeletal demineralisation after fourteen days in microgravity. The authors concluded that the absence of gravity does not impair the normal biomineralization process in larval echinoderm skeletons.

Results from the current study do not necessarily agree with the conclusions of Marthy *et al.* (1996). Although the general morphology of the bivalve larvae reared in microgravity indicated that their shells developed normally, they did not appear to mineralise their shells at the same rate as larvae grown under conditions of normal gravity. As an indicator of the amount of aragonitic calcium carbonate in the larval shells, birefringence measurements showed that shell calcification in the microgravity-reared larvae did not change much throughout the experiment; it even declined somewhat between Flight Day 5 and Flight Day 7. On the other hand, birefringence was observed in surviving larvae from all microgravity samples, indicating that the larval mussel shells did not decalcify in the absence of gravity. So, whereas Marthy *et al.* (1996) concluded normal biomineralisation processes occurred for sea urchin larvae in microgravity, the data from this study suggest that while the absence of gravity does not precipitate the loss of calcified shell tissue, gravity does appear to be required in order for normal shell growth to occur. This is a field of study that should be investigated further in microgravity experiments dedicated to a more detailed examination of calcification processes in molluscan larvae.

4.4.3.5 Larval Survival

Gravity did not appear to have much of an influence upon larval survival in this study. In general, larval mortality increased at similar rates in all gravity treatments. In the ARF Main System 1 experiment that flew aboard the Space Shuttle, there were no significant differences in the numbers of live larvae found in SCA test chambers from the two gravity treatments sampled on any given day. Neither were any significant differences found in larval survival rates from the first two sample dates in the ARF Main

System 2 ground control experiment. However, on Day 7 in the MS-2 "1g" sample, there was an unexpectedly high number of dead larvae, and the Day 10 "1g" sample had a significantly greater proportion of live larvae than the corresponding "0g" sample. The higher number of larvae in the Day 10 "1g" sample may be an anomaly, or it may be indicative of a trend towards greater overall survival in this hypergravity treatment. Unfortunately, the unusually high mortality observed in the Day 7 "1g" sample confounds any efforts to ascertain if there was a clear trend towards lower mortality in the MS-2 hypergravity treatment.

The high mortality in the Day 7 "1g" sample, and the poor condition of the surviving larvae raises the possibility that these larvae were exposed to a toxic substance that may have been present in that SCA test chamber. Although the pre-launch SCA cleaning and rinsing procedures were very rigorous and were inspected by NASA Quality Assurance inspectors at every step (see Appendix 2 for details), there remains a possibility that some of the materials used in construction leached or offgassed noxious substances into that particular chamber. It is also possible that a source of contamination may have been the glutaraldehyde fixative. Although the design of the test chambers included barriers and buffer zones between the fixative and the specimen chamber, any small leak in the fixative containment bag or burstable membrane (see Fig. 2.4) could have allowed glutaraldehyde to slowly leach into the chamber. In a pre-launch toxicity test, mussel larvae were shown to be able to tolerate glutaraldehyde concentrations of 2.5 x 10^{-3} % (w/v) and below for at least several hours (Jackson, unpub. data). Long exposures to low, sublethal concentrations of glutaraldehyde may have eventually led to the death of many of the larvae in this chamber, and left the survivors in very poor

condition. Sublethal effects of trace levels of glutaraldehyde may also explain the poor condition and absence of swimming activity observed in the MS-1 0g Day3 sample, where a high proportion of dead and poor larvae were found in the sample.

Although it has been acknowledged since the pioneering work of Thorson (1950) that planktonic invertebrate larvae have high natural mortality rates, data regarding survival and mortality of marine bivalve larvae are rare in the literature. The scarcity of studies relating to larval mortality in the field is due in part to the inherent problems associated with tracking and sampling larvae from the same cohort throughout time (Rumrill, 1990; Levin, 1990; Morgan, 1995). However, in a unique study that followed a cohort of *Mytilus edulis* larvae throughout planktonic development, Jørgensen (1981) reported a daily mortality rate of approximately 14% for early stage larvae. In a laboratory-based study, Wang and Widdows (1991) reported mortality rates for *Mytilus edulis* larvae of approximately 10% per day, and Hansen *et al.* (1997) found larval mussel mortalities in their experiments to be on the order of 8% per day. The instantaneous mortality rates for the ARF Main System 1 and 2 experiments listed in Table 4.4.1 are consistent with those reported by these authors, ranging from a low of approximately 3% per day to a high of about 11% per day. The conditions prevalent in the ARF system hardware apparently did not contribute to higher than normal mortality rates for the larvae of *Mytilus edulis*.

Table 4.4.1. Summary of larval mussel instantaneous mortality rates from ARF Main System #1 and Main System #2 SCA test chambers during Space Shuttle Mission STS-77, May 19-29, 1996. Calculated as $M = \ln (N_0 / N_t) / -t$, where N_0 = initial # of larvae, and N_t is # of larvae at time t (Rumrill, 1990).

SAMPLE #	INSTANTANEOUS MORTALITY (# larvae / day)
0g Day 3	-0.074
0g Day 5	-0.055
0g Day 7	-0.093
0g Day 10	-0.117
1g Day 3	-0.079
1g Day 5	-0.035
1g Day 7	-0.091
1g Day 10	-0.099
"0g" Day 3	-0.070
"0g" Day 5	-0.055
"0g" Day 7	-0.114
"0g" Day 10	-0.108
"1g" Day 3	-0.074
"1g" Day 5	-0.066
"1g" Day 7	-0.315
"1g" Day 10	-0.031

4.4.3.6 Summary

Differing results have been found in previous studies of early development in microgravity. The African clawed frog *Xenopus laevis* has been shown to be able to complete embryogenesis in microgravity, producing nearly normal larvae and only a few abnormalities (Souza *et al.*, 1995). Amongst invertebrates, Spooner *et al.* (1994) found that the brine shrimp *Artemia* developed normally in the absence of gravity, but the rate of development was considerably accelerated in comparison to ground controls. The ephyra stage of the jellyfish *Aurelia aurita* that were in space for fourteen days had a higher incidence of abnormal arm development than normal gravity controls (Spangenberg et al., 1995). In contrast, Crawford and Martin (1998) reported that a microgravity exposure of seven days did not significantly affect the morphological development of embryos of the sea star *Pisaster ochraceus*, and Marthy *et al.* (1996) found that skeletal development of the sea urchin *Sphaerechinus granularis* proceeded normally in the absence of gravity. It is apparent that the effect of gravity on larval invertebrate development varies widely among species.

In this investigation, there also appeared to be inconsistencies in the data collected to support the testing of Hypothesis B3. Some data tend to support the hypothesis that gravity does not influence larval bivalve development, while other results suggest that gravity is required in order for normal bivalve development to occur. Observations of larvae made at KSC immediately after the return of the Space Shuttle revealed that larvae had appeared to have developed normally in space, and gravity did not seem to have an influence on larval lipid usage. Larval survival was also independent of gravity treatment. However, closer examination of all larvae retrieved from the SCA test

chambers revealed that larvae reared in microgravity were generally in poorer condition than larvae from the normal gravity treatment. The poor appearance of many of the microgravity-reared larvae included shells that were apparently thinner and less mineralised than those of their unit gravity counterparts. Taking all of these results into consideration, it can be stated that some processes of early larval bivalve development, and shell formation in particular, may require gravity in order to proceed normally.

4.4.4 Overall Summary

This study was designed to use the microgravity environment of a Space Shuttle laboratory as a means of investigating the role that gravity plays in the feeding, growth, and development of marine bivalve larvae. To this end, three hypotheses were tested and some overall conclusions can be drawn from the results of these experiments. Although conclusive evidence supporting the hypothesis that gravity acts as a restraining force that enhances larval bivalve feeding mechanisms was not gathered in this study, the data are not inconsistent with the premise that gravity might affect feeding in this manner. The data collected in this experiment do not support the hypothesis that bivalve larvae actively regulate their buoyancy as a means of optimising feeding efficiency. And finally, gravity has been shown to be required for some aspects of normal bivalve development, especially the process of shell mineralisation. The results of these experiments will be further discussed in context with the results of the behavioural studies from Chapter 3 in the final chapter of this thesis.

CHAPTER 5

Discussion - The Forces Acting on Swimming Bivalve Larvae

5. THE FORCES ACTING ON SWIMMING BIVALVE LARVAE

A detailed kinematic analysis of the forces involved in larval bivalve locomotion and feeding was conducted for the larvae of *Cerastoderma edule* by Jonsson *et al.* (1991). Wang and Xu (1997) used a similar approach in their analysis of the swimming patterns of larval *Sinonovacula constricta*, an infaunal bivalve. These authors calculated the total amount of power that is produced by swimming veligers, using estimates of the drag and gravity forces acting upon the larvae. These analyses were based upon the premise of Newton's third law, which states that any body exerting a force upon another experiences an equal and opposite force that is exerted by the second body. In terms of swimming bivalve larvae, the drag and gravitational forces acting upon the larvae are counteracted equally by the total amount of force produced by the larvae themselves. Since the drag and gravitational forces acting upon swimming bivalve larvae can be calculated based upon easily measurable parameters such as body size, density, and swimming speed, the amount of force expended by the larvae to counteract these forces can be estimated.

The data collected in the experiments on larval *Mytilus edulis* conducted in the Aquatic Research Facility and its related ground-based study are amenable to this same form of kinematic analysis. The unique advantage of studying locomotor patterns in the absence of gravity makes this approach a valuable contribution to the study of zooplankton energetics, since drag is the only force that the larvae are working against. An understanding of the role that gravity plays in the cost of locomotion is particularly important in the assessment of whether gravity is used as a tethering force by zooplankton as a means of maximising feeding success (Emlet and Strathmann, 1985).

An analysis of the locomotion of small aquatic organisms must consider the low Reynolds number nature of the planktonic environment. For small organisms moving at relatively slow speeds, the seawater surrounding them is perceived as being very thick and sticky; viscous forces predominate, and inertia is negligible (Vogel, 1981). At low Reynolds numbers, estimates of the drag force acting on swimming bivalve larvae can be calculated using Stokes' law for the drag of a sphere:

$$F_{Drag} = 6 \pi \mu a U \qquad \text{(eq. 5.1)}$$

where μ is the dynamic viscosity of seawater at the experimental temperature of 12°C ($1.327 \cdot 10^{-3}$ kg·m^{-1}·s^{-1}), a is the radius of the organism in question, and U is the animal's swimming velocity. Since bivalve larvae are not spherical, an estimate of the value of a can be obtained by calculating the value for their equivalent "Stokes' radius" (Vogel, 1981), based upon the equation for small objects falling at terminal velocity:

$$a = \sqrt{\frac{9 \mu U_{term.}}{2g(\rho - \rho_0)}} \qquad \text{(eq. 5.2)}$$

where $U_{term.}$ is the terminal falling velocity of the animal, ρ is the density of the larva ($1.35 \cdot 10^{3}$ kg·m^{-3}), ρ_0 is the density of seawater ($1.024 \cdot 10^{3}$ kg·m^{-3}), and g is the gravitational acceleration constant (9.8 m·s^{-2}). Although terminal falling velocity data for *Mytilus edulis* larvae were unavailable, the value for $U_{term.}$ ($1.06 \cdot 10^{-3}$ m·s^{-1}) was obtained from measurements of larvae of the sea scallop, *Placopecten magellanicus*, that were the same size and density as the mussel larvae used in these experiments. Solving this equation results in a value of 44.8 µm, which was used as the value for larval size in the

calculations for both drag and gravitational forces. For larvae swimming in microgravity, drag is the only force to be considered, and the values obtained for the Stokes' law equation explain the total amount of force that is produced by those larvae.

When larvae are swimming in a normal, earthbound environment, they are subject to gravitational forces as well as the force of drag. The effect of gravity on swimming larvae can be calculated using the equation for "net body force," which is the difference between weight and buoyancy (Vogel, 1981):

$$F_{Gravity} = (\rho - \rho_0)\, 4/3\, \pi\, a^3\, g \qquad \text{(eq. 5.3)}$$

This value was determined to be $1.180 \cdot 10^{-9}$ Newtons. Finally, the total force produced by larvae in normal gravity is obtained by resolving the individual force vectors (drag and gravity) acting on a larva swimming in a helix, as demonstrated by Jonsson *et al.* (1991):

$$|F_{TOTAL}| = \sqrt{|F_{DRAG}|^2 + |F_{GRAVITY}|^2 - 2 \times |F_{DRAG}| \times |F_{GRAVITY}| \times \cos\theta} \qquad \text{(eq. 5.4)}$$

where θ is the helix pitch angle. The amount of force generated by larvae in the presence of gravity is strongly influenced by the angle of helical pitch, as can be clearly seen in Fig. 5.1. As the pitch of the helix angle increased through 90° (horizontal) and became steeper as the larvae climbed higher, the total amount of force required for swimming increased. Larvae swimming in microgravity, however, exhibited no such dependence of force upon helix pitch angle since gravity was not present to pull against the animal and displace its forward motion towards the horizontal (see Section 3.4.1). In the absence of

gravity, larvae generated significantly less force than larvae swimming in normal gravity. The largest forces calculated were among the upward swimming larvae, with values in the range of $1.27 \cdot 10^{-9}$ Newtons to $1.65 \cdot 10^{-9}$ Newtons. These values are lower than those reported by Jonsson *et al.* (1991) for upward swimming larvae of *Cerastoderma edule* ($5.8 \cdot 10^{-9}$ N), but the larvae in their experiment were much larger than the *Mytilus edulis* used in this study (Stokes' radius of 120 μm versus 45 μm). As both drag force and net body force are sensitive to the animal's size (see eq. 5.1.and 5.3), larger larvae would have to generate more force in order to swim upwards.

As discussed in Section 3.4.1, downward swimming larvae had faster linear swimming speeds than upward swimmers and larvae in microgravity, as can be seen in Fig. 5.2. However, this graph also shows that these larvae were not generating as much force as upward swimmers in order to achieve these speeds; upward swimming required that a greater amount of force be generated. For upward swimmers, the amount of force produced was directly proportional to the linear swimming speed (Fig. 5.2), as well as the angle of helix pitch (Fig. 5.1). Conversely, force was not dependent upon linear swimming speed for downward swimming larvae; the slope of the regression indicated in Fig. 5.2 was not significantly different from zero. Force was a linear function of instantaneous linear swimming velocity for the larvae in microgravity, however, since Stokes' law for drag explains all of the force under those conditions.

The range of speeds observed in the microgravity dataset reflected larvae that would be swimming both upwards and downwards if they were in normal gravity. The microgravity larvae with the lowest linear swimming speeds would probably have been

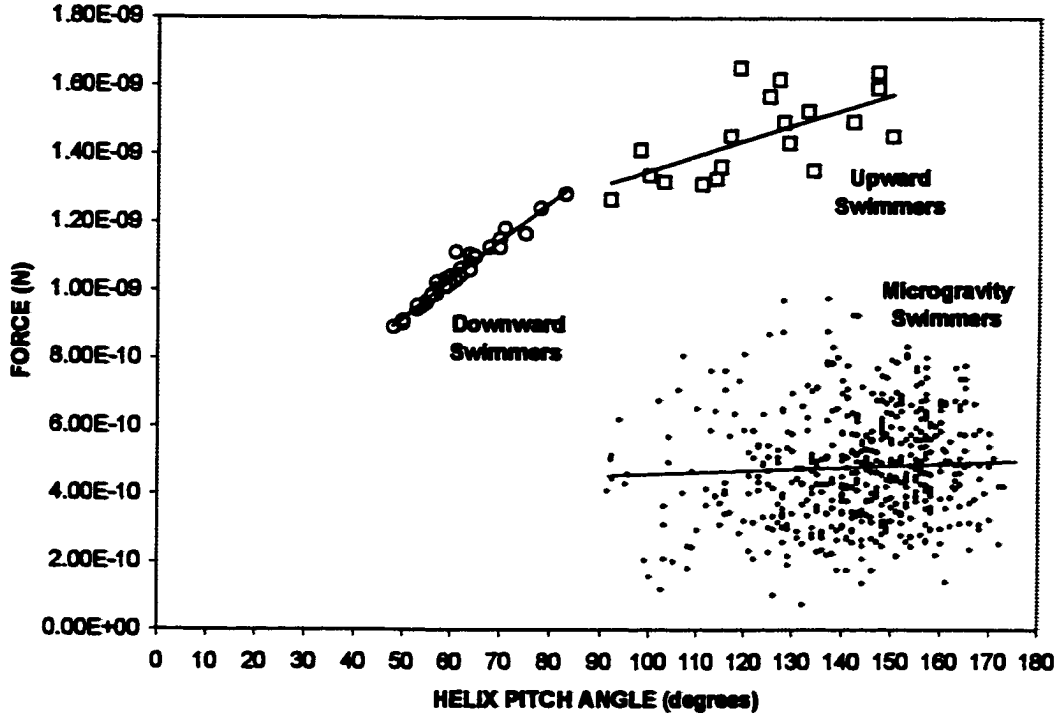

Fig. 5.1. The relationship between helix pitch angle and the total amount of force generated by mussel larvae (*Mytilus edulis*) swimming in normal gravity and microgravity.

downward swimmers under normal conditions, since they would not have been swimming fast enough and generating enough force to overcome the pull of gravity. The fastest microgravity swimmers swam at greater speeds than the fastest upward swimming larvae in normal gravity, but exerted a significantly lower amount of force in order to do so. Fig. 5.2 also reveals that the fastest downward swimmers had similar speeds to the fastest microgravity swimmers, but again, the larvae in normal gravity required more force in order to reach those speeds.

The large differences in the amount of force required to generate similar swimming speeds between microgravity and normal gravity swimmers emphasises the importance of gravity as a force governing the locomotion of bivalve larvae. This force differential may even imply that larvae in microgravity should have had a "reserve" amount of energy that could have been spent to make them swim even faster. However, there is evidence suggesting that there may be a maximum possible speed at which mussel larvae of this size can swim. Gallager (1993) reported that the swimming speed of bivalve larvae increased with the frequency of ciliary beating up to a maximum level, at which point increased beat frequency did not produce faster speeds. It was suggested that this maximum swimming speed occurred when the combination of restraining forces acting on the larva (gravity and drag) exceeded the maximum amount of force that could be generated by the velar cilia. At beat frequencies beyond this maximum, the cilia would bend or slip through the fluid and thereby lose propulsive efficiency. If this hypothesis is correct, the fastest swimming speeds recorded for mussel larvae in microgravity may represent larvae whose cilia were beating at maximum beat frequency, and therefore were swimming as fast as larvae of this size possibly can.

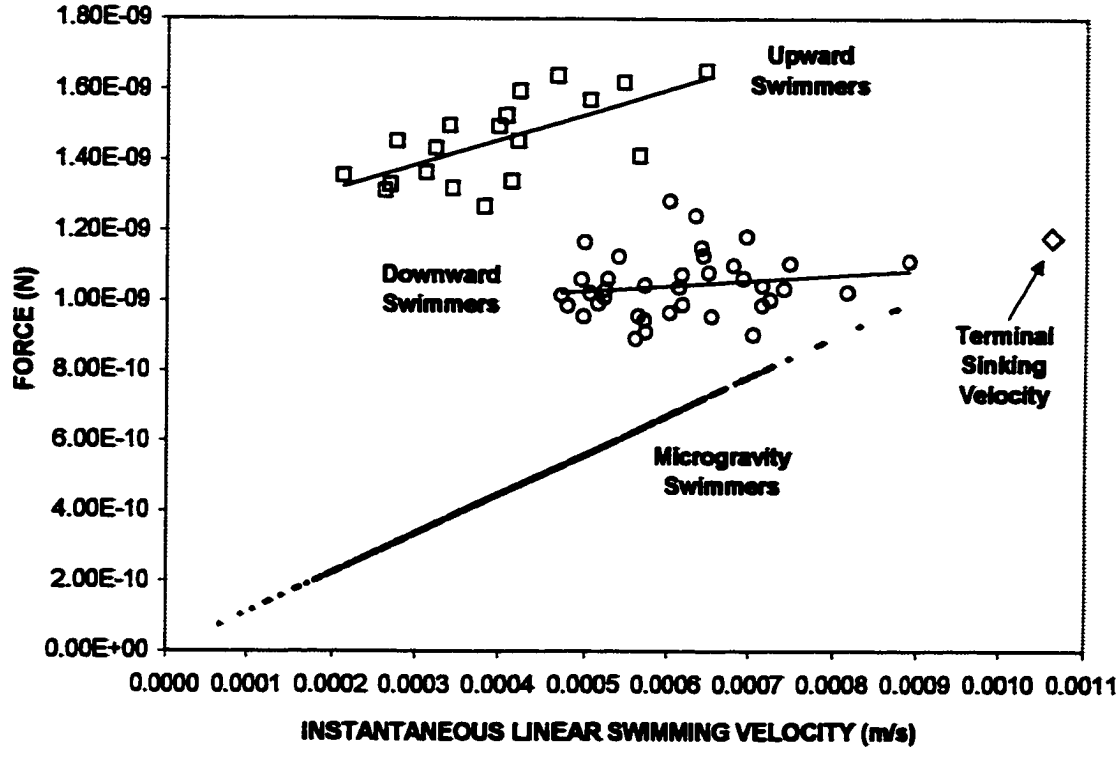

Fig. 5.2. The relationship between instantaneous linear swimming velocity and the total amount of force required by mussel larvae (*Mytilus edulis*) swimming in normal gravity and microgravity.

An overlooked aspect of vertical migration amongst analyses of bivalve veligers to date is that these animals accumulate potential energy as they swim upwards, which can be recovered and utilised as they sink or otherwise move downwards. The possibility that heavy zooplankters use potential energy in this way encourages a reassessment of energy usage in bivalve larvae. As a means of addressing this question, the calculated forces and velocities of larvae swimming in microgravity and normal gravity were resolved into their constituent *x*-axis and *y*-axis components, and then compared to estimates of total metabolism to derive an index of locomotor efficiency. In the larva's frame of reference, the *y*-components of force and velocity were defined as those along the vertical swimming direction (parallel to the helix axis for larvae swimming in microgravity), and the *x*-axis represented the horizontal component of motion (normal to the *y*-axis in the microgravity situation). The amount of power generated by larvae in the vertical and horizontal planes was then calculated as the product of the *x* and *y* components of force and velocity. For the larvae swimming upwards or downwards in normal gravity, the rates of gain or loss of potential energy were calculated as the product of net body force ($1.18 \cdot 10^{-9}$ N) and vertical velocity; these were then added algebraically to the *y*-component of power.

Fig. 5.3 illustrates the results of this analysis, by plotting the total power output of each larva against the *x*-component of its own power output. In this representation, it appears that the downward swimming larvae are, in effect, "gliding" as they move downwards. A greater proportion of their power is spent moving in the horizontal plane, a behaviour which Gallager (1993) has implicated as an adaptation for increasing the size of the flow field and maximising food particle encounter rate, thereby enhancing feeding

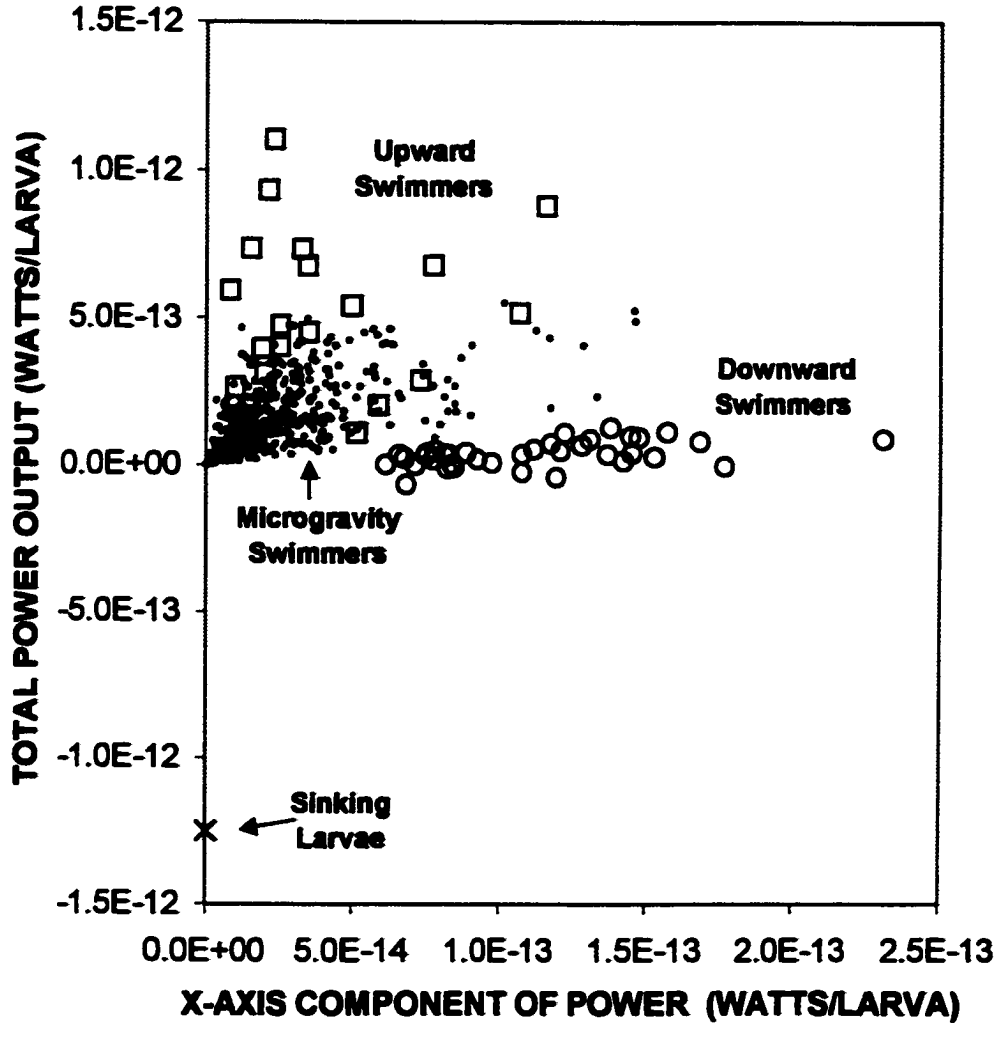

Fig. 5.3. The relationship between the horizontal component of power and the total amount of power expended by mussel larvae (*Mytilus edulis*) swimming in normal gravity and microgravity. The scale of the *x*-axis in this representation is tenfold greater than the scale of the *y*-axis.

efficiency. As these larvae are moving downward they are reducing their expenditure of metabolic power, and are instead making use of the potential energy they acquired during upward swimming. The helical descent is well controlled by the larvae, since the rate of power dissipation never reaches that experienced by larvae falling straight downwards at terminal sinking velocity. The observation that larvae in microgravity also allocate a higher proportion of their total power output along the *x*-axis may indicate an attempt at optimising feeding efficiency, but it is difficult to confirm this without greater knowledge of the interaction between the velar cilia and food particles in the surrounding fluid. Further pursuit along this avenue of investigation would require detailed observations of feeding mechanics and behaviour using high magnification, high resolution, high speed imaging and tracking technology.

The amount of energy accumulated by larvae swimming upwards in the presence of gravity more than doubled the power outputs of larvae swimming against only the force of drag in microgravity. The average total power output for upward-swimming larvae was $5.4 \cdot 10^{-13}$ W·larva^{-1}, while larvae in microgravity had an average power expenditure of only $2.3 \cdot 10^{-13}$ W·larva^{-1}. The mean power output of larvae swimming downwards in normal gravity was over an order of magnitude lower, at only $3.8 \cdot 10^{-14}$ W·larva^{-1}. Since bivalve larvae divide their time between energetically expensive upward swimming and more economical downward motion in roughly equal proportions, it is possible that their overall energy consumption may be similar to that seen in microgravity where the range of power outputs reflects larvae that would be swimming in both directions if they were in normal gravity. Fig. 5.4 shows the relationship between the power expenditures of mussel larvae and their vertical swimming velocities (forward

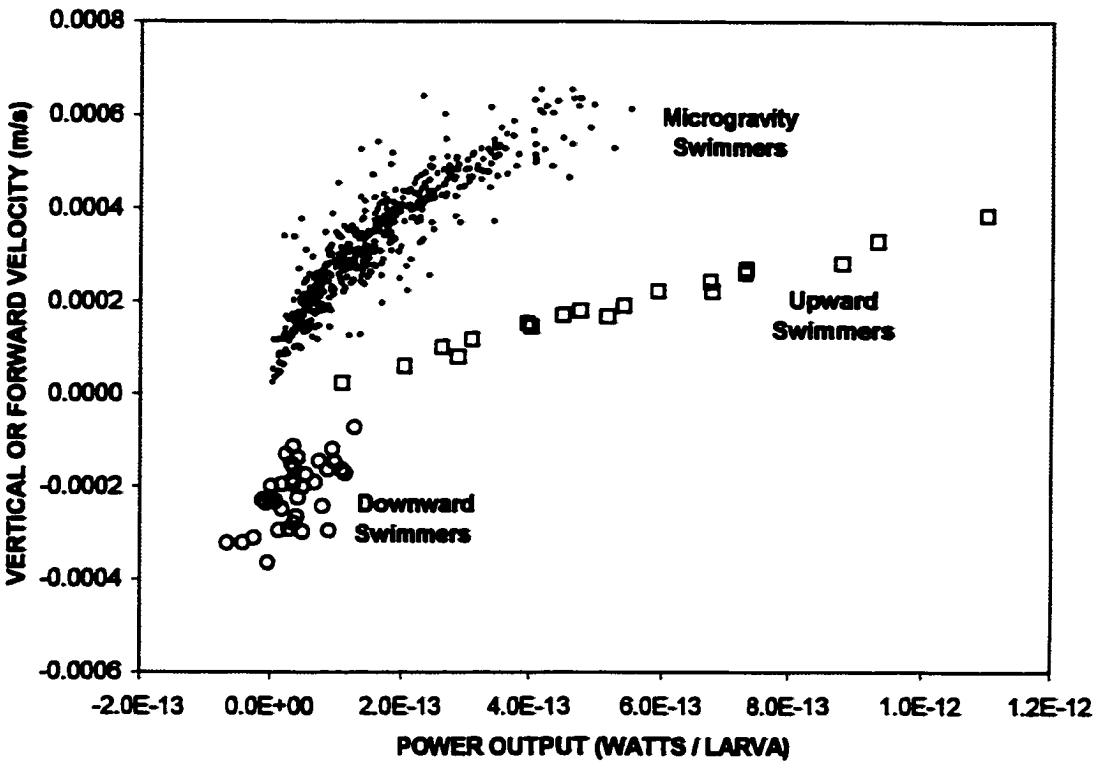

Fig. 5.4. The relationship between energy expenditure (power output) and vertical swimming velocity of mussel larvae (*Mytilus edulis*) swimming in normal gravity and microgravity. Vertical velocity of downward swimmers are indicated as negative values.

velocities in the case of larvae in microgravity). Larvae swimming in microgravity generally spent less energy to move forward than upward swimmers in normal gravity, but were able to move forward at a much faster rate. The relationship between power expenditure and swimming velocity for the microgravity larvae strongly resembles that described by Gallager (1993) for the dependence of vertical velocity upon ciliary beat frequency in the larvae of the bivalve *Lyrodus pedicellatus*. Gallager's relationship showed that below a certain beat frequency (~12 Hz), larvae started to move downwards. Since mussel larvae swimming in microgravity could not fall, the entire range of ciliary beat frequencies available to mussel larvae results in forward locomotion. In this way, the data from the microgravity experiment clearly show the relationship between power output due to ciliary beat frequency and the resultant forward velocity, without the confounding effects caused by gravity.

In their kinematic analysis of swimming in *Sinonovacula constricta*, Wang and Xu (1997) reported that the cost of locomotion for larvae 133 μm in shell length was $7.3 \cdot 10^{-13}$ W·larva^{-1}. This value is similar to the mean theoretical energy expenditure as calculated in this study for *Mytilus edulis* larvae swimming upwards in normal gravity ($5.4 \cdot 10^{-13}$ W·larva^{-1}). The mean net cost of locomotion for mussel larvae in the absence of gravity was much lower at only $2.3 \cdot 10^{-13}$ W·larva^{-1}, but this value may more truly reflect the actual metabolic costs since it incorporates the full suite of behaviours and the entire range of ciliary power outputs. Using data for metabolic rates of *Mytilus edulis* larvae from Wang and Widdows (1991), Wang and Xu (1997) estimated that the cost of locomotion comprised a negligible proportion of the total energy expenditure for *Sinonovacula constricta* veligers, at only 0.05%. This number is similar to that obtained

by Sprung (1984c), who concluded that the cost of locomotion for larvae of *Mytilus edulis* accounted for less than 1% of the total energy expenditure. However, both of these reports neglected to consider the inherent hydrodynamic and metabolic inefficiencies of converting ingested and stored energy into movement. The values obtained by using a kinematic analysis of locomotion represent the theoretical amount of energy required to overcome gravity and drag forces and propel the larva forward, a process which is the end result of a long metabolic chain with energy losses at each stage. By comparing the respiratory rates of resting and actively swimming *Mytilus edulis* larvae, Zeuthen (1947) estimated the real cost of locomotion at 50%, and Gallager (1992) obtained a similar value using an estimate of 10% for the overall efficiency of converting chemical energy into usable energy for veliger locomotion. The lower power requirements for locomotion amongst larvae in microgravity warrant a re-examination of these locomotor cost and efficiency estimates.

Gallager (1992) described a relationship between ciliary beat frequency and the respiratory rate of *Bankia gouldi* larvae that suggests that the resting metabolism in these animals comprises approximately one third of the active, routine metabolism. Using this estimate of resting metabolism in conjunction with Wang and Widdows' (1991) calculation of routine total energy metabolism for small *Mytilus edulis* veligers ($1.5 \cdot 10^{-9}$ $W \cdot larva^{-1}$), the active metabolism of these larvae can be estimated as $1.0 \cdot 10^{-9}$ $W \cdot larva^{-1}$. If this amount of metabolic energy is ultimately responsible for the $2.3 \cdot 10^{-13}$ $W \cdot larva^{-1}$ expressed as the swimming power output of larvae in microgravity, the overall conversion efficiency amounts to only 0.02%. This is much lower than the 10% figure suggested by Gallager (1992), but Gallager acknowledged that this estimate may be high.

Even if the actual conversion efficiencies are as low as 1%, however, the cost of locomotion in small bivalve larvae is probably relatively low as suggested by Sprung (1984c) and Wang and Xu (1997). Clearly, a better understanding of locomotor and feeding physiology in bivalve larvae requires more accurate estimates of conversion efficiencies and locomotor costs that can only be obtained through more detailed examination of the relationship between feeding and locomotor mechanisms at the level of cilia-fluid interactions.

The results from the feeding and growth experiments outlined in Chapter 4 appeared to indicate that the absence of gravity did not significantly impact upon the effectiveness of larval feeding. This may seem to contradict the hypothesis proposed by Emlet and Strathmann (1985) that indicates that optimal feeding in small plankters requires the restraining force of gravity, but the model as presented here provides an explanation for this apparent discrepancy. This analysis of power outputs suggests that larvae are capable of altering their swimming behaviours and power expenditures between upward motion, which places more power into the y-component, and horizontal and downward motion, where more power is expended along the x-axis. Gallager (1993) implicated the horizontal motion observed during hovering behaviour as an adaptation to increase the size of the flow field generated by the actions of the velar cilia, thereby maximising feeding efficiency. In the absence of gravity many of the larvae allocated more power to motion in the x-axis, perhaps in an attempt to enhance feeding efficiency. Indeed, the behaviour of larvae in microgravity actually changed over the ten day course of the experiment, in that they increased the diameter of their helices and decreased rotational velocity in an apparent attempt to increase feeding effort. This evidence

implies that mussel larvae have a hitherto undescribed degree of control over their behavioural repertoire that may have enabled them to counter any diminished feeding efficiency due to loss of gravity by altering their feeding behaviour and thereby adapting to a weightless environment. Recent observations of a complex nervous system in bivalve larvae (Croll *et al.*, 1997) and control over a wide range of behaviours suggests that bivalve veligers are more complicated than previously believed; they are not merely passive particles in the water column, but they are ideally adapted to their function as "tiny feeding machines which convert small eggs into larger juveniles" (Strathmann and Leise, 1979).

APPENDIX 1

Digitised Tracks and Trajectory Measurements of *Mytilus edulis* Larvae Swimming in Microgravity

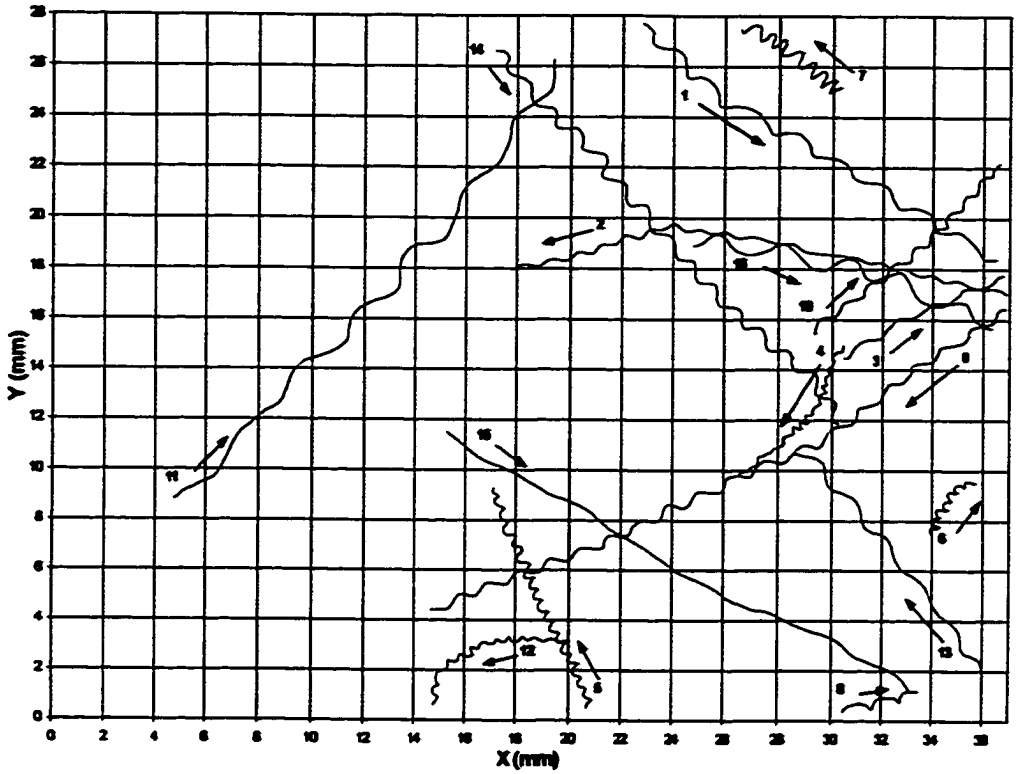

Fig A1.1. Reconstructed tracks of swimming mussel larvae (*Mytilus edulis*) from SCA# 3L0, Day 1 Day recording session, May 20, 1996. Track direction indicated by arrows.

Table A1.1. Trajectory measurement data from tracks of swimming mussel larvae (*Mytilus edulis*) from SCA# 3L0, Day 1 Day recording session, May 20, 1996.

LARVAL TRACK #	HELIX HEIGHT (mm)	HELIX DIAMETER (mm)	HELIX PITCH ANGLE	TIME (s)	ANGULAR VELOCITY (rad/s)	LINEAR VELOCITY (mm/s)	FORWARD VELOCITY (mm/s)	NGDR	TRACK DIRECTION (degrees) *
1	1.9	0.5	52	73.0	0.76	0.30	0.23	0.84	325
2	1.0	0.3	50	105.0	1.26	0.27	0.19	0.88	168, 196 (177)
3	1.6	0.3	60	21.0	1.38	0.41	0.35	0.92	249, 220 (28)
4	0.3	0.2	13	183.8	0.93	0.11	0.04	0.50	234
5	0.5	0.3	27	70.0	1.83	0.31	0.14	0.58	114
6	0.4	0.3	19	30.0	1.31	0.22	0.09	0.44	242
7	0.5	0.6	13	91.5	0.58	0.19	0.05	0.40	139
8	1.2	0.5	56	17.7	0.97	0.30	0.18	0.80	15
9	1.3	0.3	53	73.0	1.63	0.44	0.35	0.88	208
10	1.2	0.4	52	53.0	1.02	0.27	0.19	0.82	29
11	3.2	0.8	58	55.0	0.84	0.53	0.42	0.91	49
12	0.5	0.2	36	50.5	1.61	0.23	0.14	0.58	73, 28, 359 (206)
13	2.1	0.5	59	40.0	0.90	0.38	0.30	0.91	128
14	1.3	0.5	50	101.0	0.98	0.31	0.20	0.78	312
15	2.9	0.3	75	50.0	N/A	0.43	0.42	0.96	150
16	2.5	0.7	45	40.0	0.80	0.41	0.31	0.83	344
MEAN	1.4	0.4	46.1	66.1	1.12	0.32	0.22	0.75	134.9
s.d.	0.9	0.2	17.4	63.2	0.36	0.11	0.12	0.19	78.6
N	16	16	16	16	15	16	16	16	16

* Reference line, 0°, is the horizontal axis. For larvae that change track direction, net resultant track direction is recorded in parentheses.

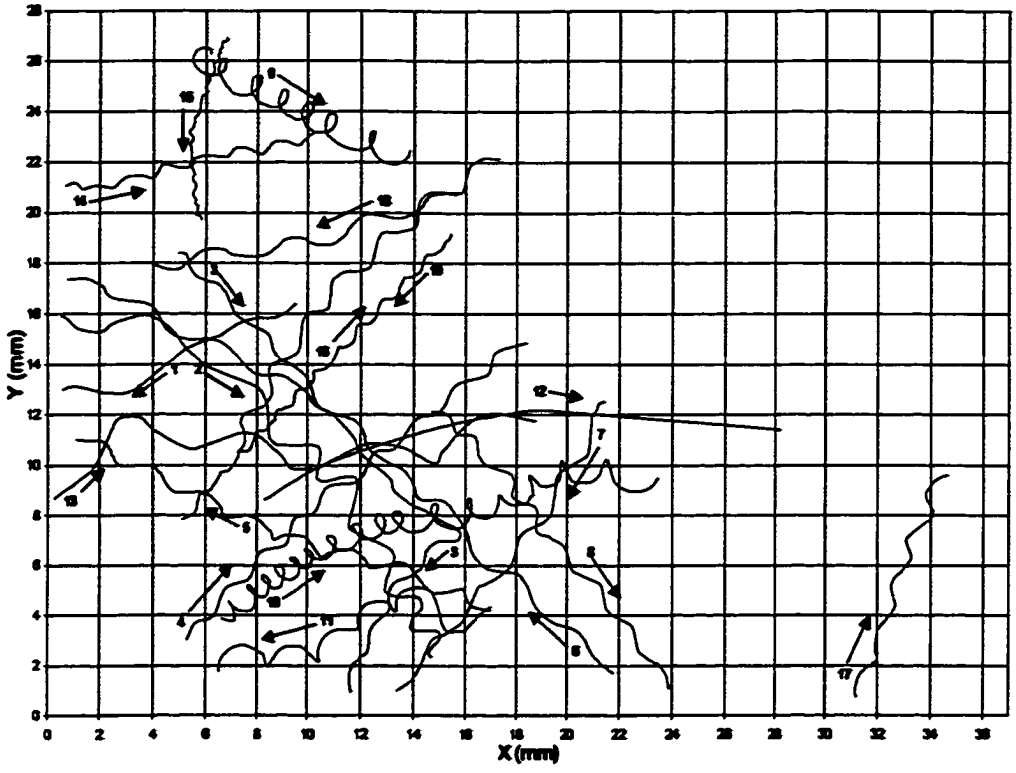

Fig A1.2. Reconstructed tracks of swimming mussel larvae (Mytilus edulis) from SCA# 3R0, Day 1 Day recording session, May 20, 1996. Track direction indicated by arrows.

Table A1.2. Trajectory measurement data from tracks of swimming mussel larvae (Mytilus edulis) from SCA# 3R0, Day 1 Day recording session, May 20, 1996.

LARVAL TRACK #	HELIX HEIGHT (mm)	HELIX DIAMETER (mm)	HELIX PITCH ANGLE	TIME (s)	ANGULAR VELOCITY (rad/s)	LINEAR VELOCITY (mm/s)	FORWARD VELOCITY (mm/s)	NGDR	TRACK DIRECTION (degrees)*
1	N/A	N/A	N/A	20.0	N/A	N/A	0.48	0.94	207
2	2.0	1.0	37	81.0	N/A	N/A	0.26	0.74	355, 315, 296 (316)
3	1.9	0.3	65	60.0	1.24	0.43	0.38	0.75	312, 241 (291)
4	1.9	0.4	65	59.0	0.98	0.35	0.30	0.92	42
5	2.0	0.5	52	59.0	0.91	0.38	0.29	0.87	157
6	3.3	0.6	60	59.7	0.85	0.50	0.44	0.92	137, 152 (143)
7	3.0	0.6	64	28.0	1.07	0.59	0.50	0.93	234
8	1.9	0.4	63	47.0	1.00	0.35	0.31	0.88	310
9	1.1	0.9	19	59.0	0.85	0.42	0.15	0.40	332
10	1.1	0.8	20	178.3	0.58	0.26	0.10	0.45	34, 16, 351 (18)
11	1.9	0.8	37	59.0	N/A	N/A	0.19	0.67	208, 110, 210, 183 (194)
12	0.5	N/A	N/A	59.0	N/A	N/A	0.35	0.97	23, 10, 355 (8)
13	4.4	1.1	60	63.0	0.44	0.39	0.31	0.83	34, 353, 22 (9)
14	1.6	0.4	50	23.0	1.71	0.52	0.42	0.89	13
15	0.5	0.2	58	38.0	2.66	0.30	0.20	0.88	250, 278 (263)
16	1.1	0.2	65	39.0	2.27	0.45	0.39	0.89	47
17	2.0	0.4	59	33.0	0.89	0.34	0.29	0.90	71
18	3.0	0.7	55	32.0	0.77	0.45	0.37	0.91	194
19	2.4	0.7	55	54.0	0.77	0.38	0.29	0.83	221, 239 (229)
MEAN	**2.0**	**0.6**	**52.2**	**55.3**	**1.13**	**0.41**	**0.32**	**0.82**	**317.9**
s.d.	**1.0**	**0.3**	**14.4**	**33.9**	**0.62**	**0.09**	**0.11**	**0.16**	**73.9**
N	**18**	**17**	**17**	**19**	**16**	**16**	**19**	**19**	**19**

* Reference line, 0°, is the horizontal axis. For larvae that change track direction, net resultant track direction is recorded in parentheses.

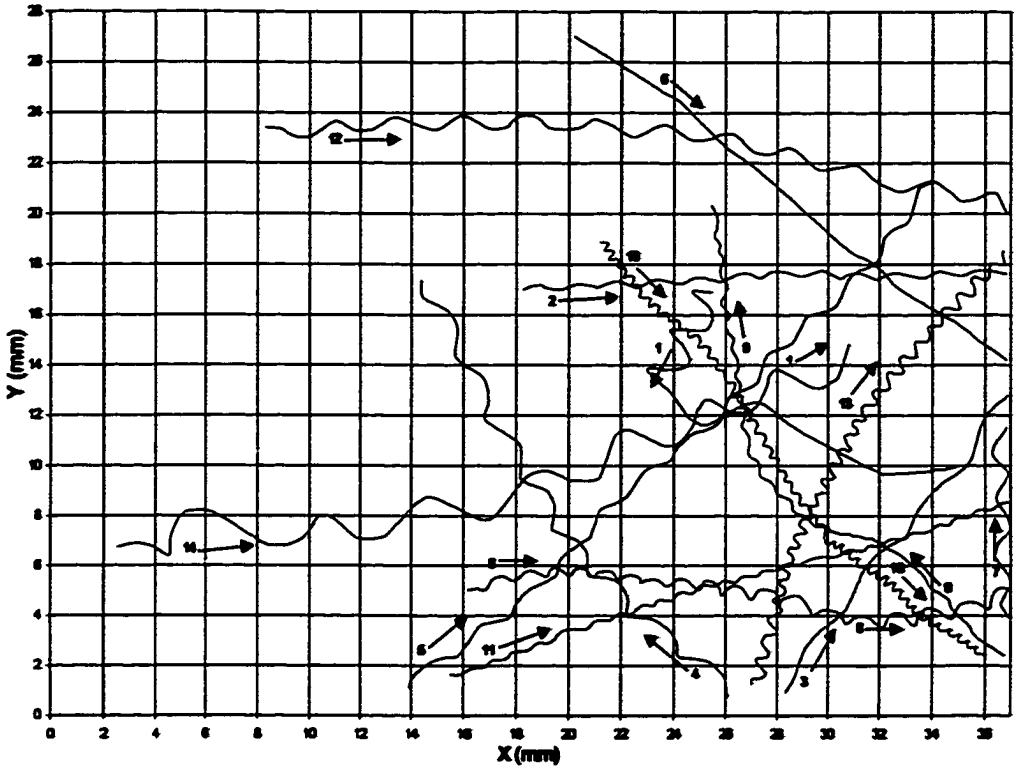

Fig A1.3a. Reconstructed tracks of swimming mussel larvae (Mytilus edulis) from SCA# 4L0, Day 1 Day recording session, May 20, 1996. Track direction indicated by arrows. Larvae #1-14.

Table A1.3a. Trajectory measurement data from tracks of swimming mussel larvae (Mytilus edulis) from SCA# 4L0, Day 1 Day recording session, May 20, 1996. Larvae #1-14.

LARVAL TRACK #	HELIX HEIGHT (mm)	HELIX DIAMETER (mm)	HELIX PITCH ANGLE	TIME (s)	ANGULAR VELOCITY (rad/s)	LINEAR VELOCITY (mm/s)	FORWARD VELOCITY (mm/s)	NGDR	TRACK DIRECTION (degrees) *
1	1.8	1.2	16	62.0	N/A	N/A	0.27	0.56	241, 343 (324)
2	1.6	0.3	67	51.5	1.39	0.41	0.36	0.95	2
3	4.3	0.3	75	25.0	0.86	0.60	0.59	0.97	52
4	2.7	0.6	61	40.0	1.19	0.63	0.52	0.87	153
5	2.3	0.3	74.0	93.0	0.85	0.33	0.31	0.94	44
6	N/A	N/A	N/A	34.0	N/A	0.62	0.62	1.00	321
7	1.8	0.5	56	20.0	1.31	0.53	0.38	0.86	92
8	1.3	0.6	44	79.0	1.32	0.45	0.27	0.76	5, 346, 13 (1)
9	1.1	0.2	59	53.0	2.52	0.52	0.44	0.87	132, 164, 99 (122)
10	0.6	0.2	54	154.0	1.47	0.22	0.15	0.64	313, 302, 322 (312)
11	0.8	0.1	68	54.5	3.19	0.47	0.41	0.94	18
12	2.5	0.5	56.0	73.0	1.01	0.47	0.40	0.90	1, 347 (353)
13	0.7	0.4	36	129.5	1.45	0.30	0.16	0.64	73, 50 (61)
14	4.4	1.4	48	59.0	0.72	0.70	0.51	0.78	7, 24 (16)
MEAN	**2.0**	**0.5**	**54.6**	**69.8**	**1.39**	**0.47**	**0.38**	**0.86**	**38.9**
s.d.	**1.2**	**0.3**	**18.6**	**35.6**	**0.68**	**0.13**	**0.16**	**0.21**	**67.3**
N	**26**	**26**	**26**	**28**	**24**	**26**	**28**	**28**	**28**

* Reference line, 0°, is the horizontal axis. For larvae that change track direction, net resultant track direction is recorded in parentheses.

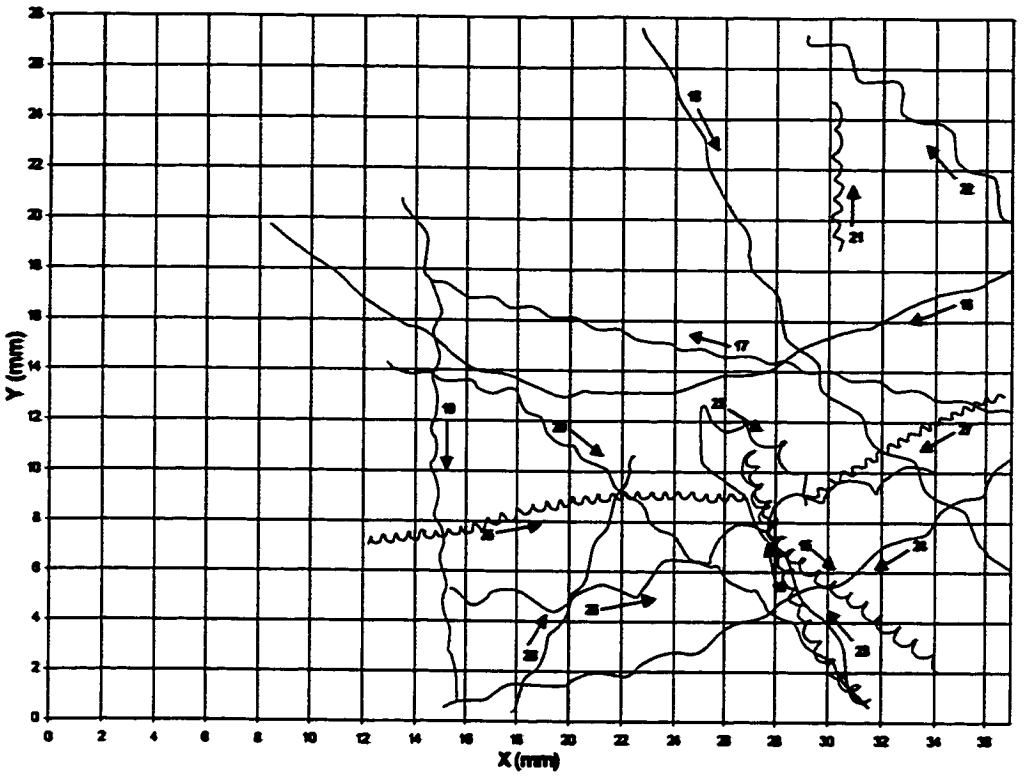

Fig A1.3b. Reconstructed tracks of swimming mussel larvae (*Mytilus edulis*) from SCA# 4L0, Day 1 Day recording session, May 20, 1996. Track direction indicated by arrows. Larvae #15-28.

Table A1.3b. Trajectory measurement data from tracks of swimming mussel larvae (*Mytilus edulis*) from SCA# 4L0, Day 1 Day recording session, May 20, 1996. Larvae #15-28.

LARVAL TRACK #	HELIX HEIGHT (mm)	HELIX DIAMETER (mm)	HELIX PITCH ANGLE	TIME (s)	ANGULAR VELOCITY (rad/s)	LINEAR VELOCITY (mm/s)	FORWARD VELOCITY (mm/s)	NGDR	TRACK DIRECTION (degrees) *
15	0.8	0.4	61	144.0	1.27	0.31	0.16	0.07	126, 107, 290, 321 (21)
16	N/A	N/A	N/A	44.0	N/A	0.72	0.72	0.90	198, 145 (177)
17	1.8	0.2	73	61.5	1.33	0.39	0.38	0.97	167
18	2.9	0.5	60	49.5	1.15	0.61	0.53	0.94	132, 114 (304)
19	1.8	0.2	72	43.0	1.64	0.50	0.47	0.95	274
20	1.9	0.3	70	75.0	1.04	0.35	0.32	0.92	348, 317 (324)
21	0.8	0.3	55	29.6	1.59	0.30	0.20	0.81	92
22	3.0	0.7	50	26.0	0.86	0.52	0.41	0.93	136
23	4.2	0.5	69	80.0	N/A	N/A	0.24	0.39	120, 327 (106)
24	3.0	0.3	2	55.5	0.92	0.46	0.44	0.94	212, 194 (205)
25	0.7	0.4	26	78.0	1.78	0.37	0.19	0.59	10, 358 (8)
26	3.2	0.8	58	40.0	0.97	0.62	0.49	0.81	333, 2 (14)
27	0.5	0.3	24	48.0	2.31	0.35	0.18	0.65	210
28	2.0	0.3	75	26.0	1.34	0.47	0.43	0.97	66
MEAN	**2.0**	**0.5**	**54.6**	**60.8**	**1.39**	**0.47**	**0.38**	**0.80**	**30.9**
s.d.	**1.2**	**0.3**	**18.6**	**36.6**	**0.58**	**0.13**	**0.16**	**0.21**	**67.3**
N	**26**	**26**	**26**	**28**	**24**	**26**	**28**	**28**	**28**

* Reference line, 0°, is the horizontal axis. For larvae that change track direction, net resultant track direction is recorded in parentheses.

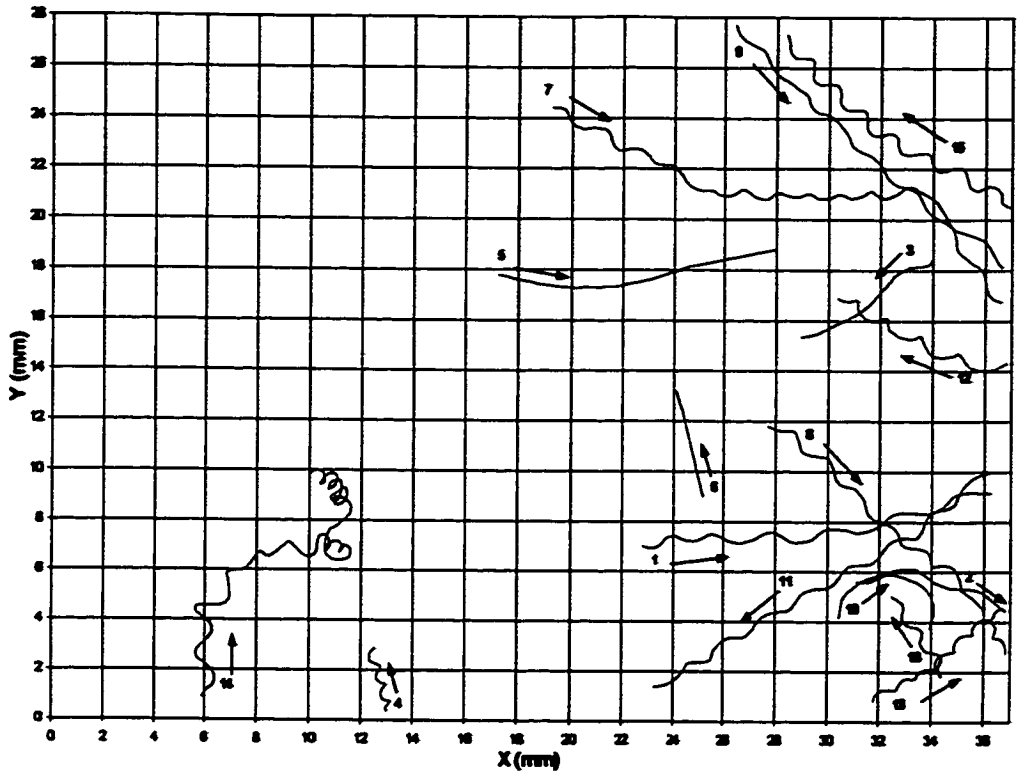

Fig A1.4. Reconstructed tracks of swimming mussel larvae (*Mytilus edulis*) from SCA# 3L0, Day 2 Night recording session, May 21, 1996. Track direction indicated by arrows.

Table A1.4. Trajectory measurement data from tracks of swimming mussel larvae (*Mytilus edulis*) from SCA# 3L0, Day 2 Night recording session, May 21, 1996.

LARVAL TRACK #	HELIX HEIGHT (mm)	HELIX DIAMETER (mm)	HELIX PITCH ANGLE	TIME (s)	ANGULAR VELOCITY (rad/s)	LINEAR VELOCITY (mm/s)	FORWARD VELOCITY (mm/s)	NGDR	TRACK DIRECTION (degrees)*
1	2.3	0.5	60	52.0	0.75	0.32	0.27	0.92	3, 19 (9)
2	2.8	0.3	71	51.5	0.27	0.13	0.12	0.92	2, 339 (349)
3	N/A	N/A	N/A	191.5	N/A	N/A	0.03	N/A	211
4	0.7	0.3	40	15.0	1.53	0.31	0.18	0.73	107
5	0.3	0.4	26	116.7	N/A	N/A	0.10	N/A	349, 1, 15 (5)
6	0.3	0.4	13	191.5	N/A	N/A	0.02	N/A	104
7	1.7	0.5	55	70.0	N/A	N/A	0.28	0.86	332, 1, 319 (340)
8	1.8	0.5	58	66.0	0.70	0.25	0.20	0.88	317, 302 (315)
9	2.0	0.3	61	52.0	0.94	0.33	0.30	0.93	313
10	N/A	0.2	N/A	191.5	N/A	N/A	0.03	N/A	(clockwise)
11	2.0	0.4	68	62.0	0.83	0.31	0.26	0.91	213
12	1.5	0.5	37	38.0	0.82	0.28	0.19	0.81	151
13	1.0	0.3	49	38.0	1.06	0.24	0.17	0.83	36
14	N/A	N/A	N/A	164.9	N/A	N/A	0.10	0.35	83, 20, 324, 98, 128 (65)
15	1.5	0.6	46	53.0	0.92	0.36	0.22	0.77	142
16	1.3	0.4	51	23.6	0.81	0.24	0.16	0.84	121
MEAN	**1.5**	**0.4**	**48.5**	**86.1**	**0.86**	**0.28**	**0.17**	**0.81**	**69.8**
s.d.	**0.8**	**0.1**	**27.4**	**63.2**	**0.32**	**0.07**	**0.09**	**0.16**	**71.4**
N	**13**	**14**	**13**	**16**	**10**	**10**	**16**	**12**	**16**

* Reference line, 0°, is the horizontal axis. For larvae that change track direction, net resultant track direction is recorded in parentheses.

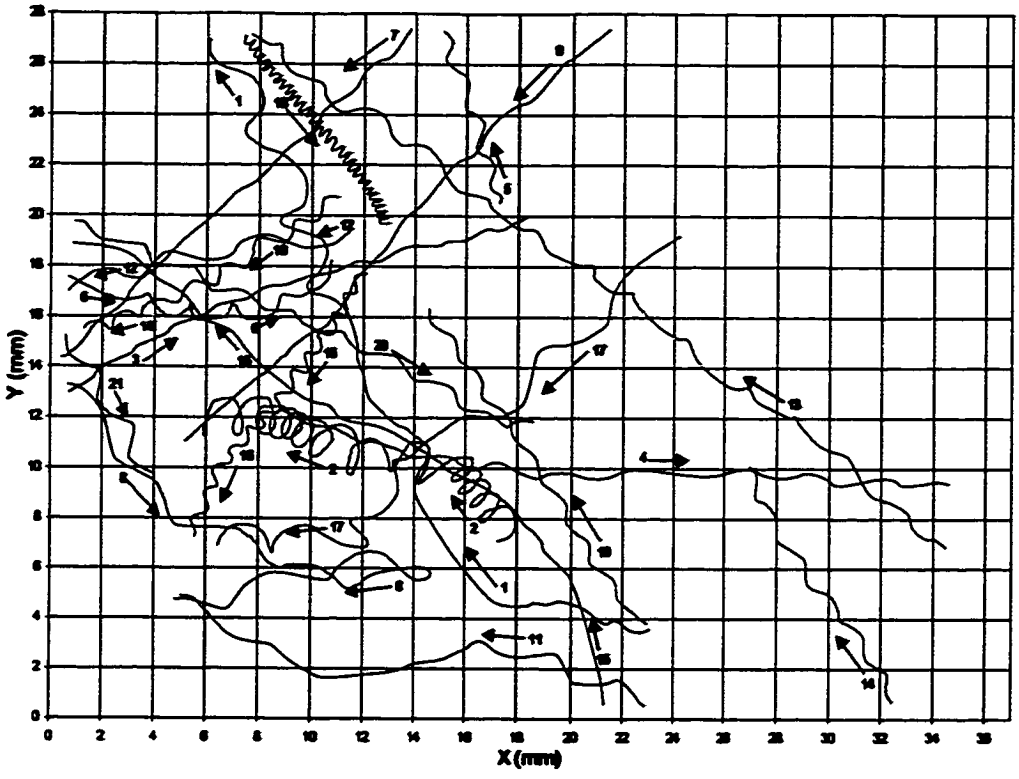

Fig A1.5. Reconstructed tracks of swimming mussel larvae (*Mytilus edulis*) from SCA# 3R0, Day 2 Night recording session, May 21, 1996. Track direction indicated by arrows.

Table A1.5. Trajectory measurement data from tracks of swimming mussel larvae (*Mytilus edulis*) from SCA# 3R0, Day 2 Night recording session, May 21, 1996.

LARVAL TRACK #	HELIX HEIGHT (mm)	HELIX DIAMETER (mm)	HELIX PITCH ANGLE	TIME (s)	ANGULAR VELOCITY (rad/s)	LINEAR VELOCITY (mm/s)	FORWARD VELOCITY (mm/s)	NGDR	TRACK DIRECTION (degrees)*
1	3.4	1.2	17	81.0	N/A	N/A	0.38	0.80	166, 115 (126)
2	0.7	1.1	33	172.0	N/A	N/A	0.07	0.25	128, 166 (160)
3	2.2	0.3	73	55.0	0.96	0.37	0.35	0.97	30, 15 (22)
4	2.5	0.3	71	47.0	1.41	0.60	0.56	0.96	343, 358 (353)
5	1.7	0.5	68	24.0	1.10	0.41	0.30	0.86	109
6	1.6	0.8	33	40.0	1.07	0.49	0.28	0.71	347, 28 (4)
7	2.6	0.4	74	31.0	1.46	0.66	0.60	0.98	224
8	4.2	0.8	63	79.0	0.52	0.41	0.35	0.32	307, 338, 12, 197 (298)
9	N/A	N/A	N/A	46.0	N/A	0.51	0.50	0.98	225
10	2.0	0.3	73	28.5	1.66	0.60	0.53	0.93	123
11	2.8	0.6	64	45.0	N/A	N/A	0.43	0.90	161, 192, 151 (166)
12	3.1	0.6	56	21.0	1.06	0.62	0.53	0.90	193
13	2.6	0.3	6	89.0	0.91	0.41	0.38	0.92	143
14	1.9	0.4	60	29.0	1.24	0.45	0.38	0.91	121
15	N/A	N/A	N/A	73.0	N/A	0.40	0.40	0.94	104, 129, 149 (138)
16	1.0	0.3	36	67.5	1.10	0.27	0.18	0.70	237
17	4.0	1.1	60	98.0	N/A	N/A	0.24	0.78	220, 243, 181 (214)
18	0.3	0.4	15	194.0	0.99	0.18	0.05	0.36	309, 291 (307)
19	1.4	0.5	36	46.0	1.07	0.37	0.24	0.77	213, 198 (208)
20	2.0	0.6	59	51.0	1.20	0.51	0.38	0.90	335
21	2.6	0.7	54	27.0	0.58	0.30	0.24	0.86	301
MEAN	**2.3**	**0.6**	**50.4**	**64.8**	**1.09**	**0.46**	**0.35**	**0.89**	**190.1**
s.d.	**1.8**	**0.3**	**28.7**	**46.5**	**0.3**	**0.13**	**0.16**	**0.22**	**71.3**
N	**19**	**19**	**19**	**21**	**16**	**17**	**21**	**21**	**21**

* Reference line, 0°, is the horizontal axis. For larvae that change track direction, net resultant track direction is recorded in parentheses.

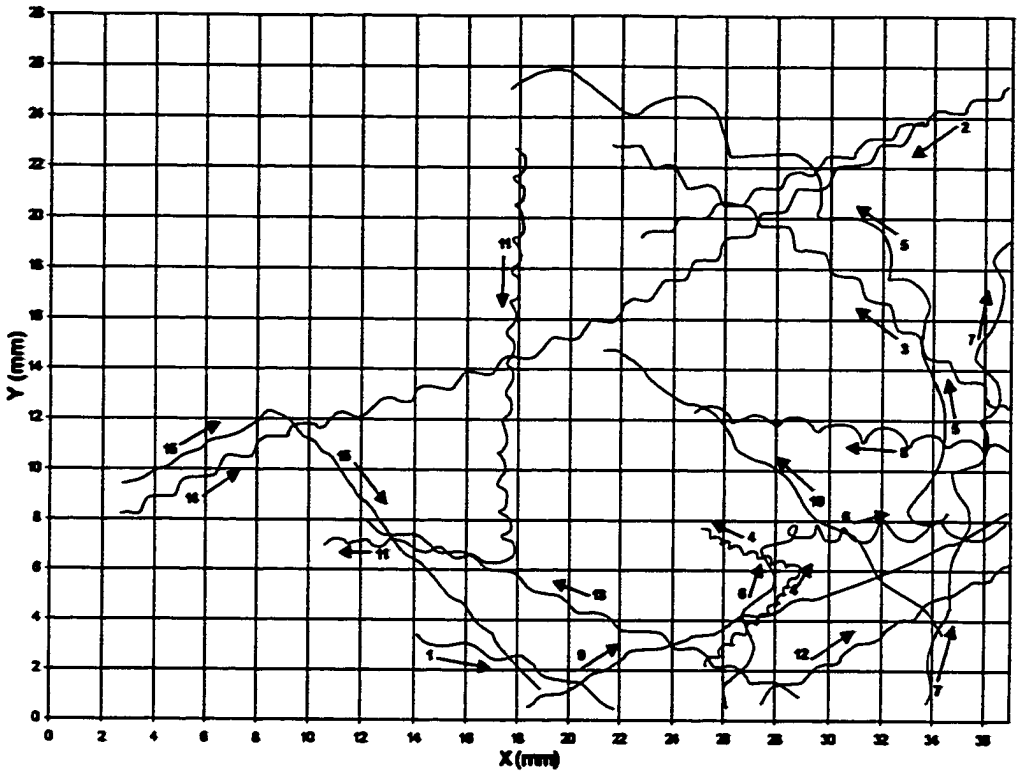

Fig A1.6a. Reconstructed tracks of swimming mussel larvae (*Mytilus edulis*) from SCA# 4L0, Day 2 Night recording session, May 21, 1996. Track direction indicated by arrows. Larvae #1-15.

Table A1.6a. Trajectory measurement data from tracks of swimming mussel larvae (*Mytilus edulis*) from SCA# 4L0, Day 2 Night recording session, May 21, 1996. Larvae #1-15.

LARVAL TRACK #	HELIX HEIGHT (mm)	HELIX DIAMETER (mm)	HELIX PITCH ANGLE	TIME (s)	ANGULAR VELOCITY (rad/s)	LINEAR VELOCITY (mm/s)	FORWARD VELOCITY (mm/s)	NGDR	TRACK DIRECTION (degrees) *
1	2.3	0.4	67	21.0	1.07	0.45	0.39	0.93	340
2	1.7	0.4	62	36.5	1.51	0.53	0.42	0.89	203
3	1.8	0.4	49	40.0	1.66	0.58	0.47	0.86	140, 152 (146)
4	0.7	0.3	45	44.0	1.88	0.33	0.22	0.43	44, 156 (92)
5	3.7	1.2	38	67.0	N/A	N/A	0.42	0.71	210, 61, 113, 143, 175 (135)
6	1.5	0.7	32	72.5	N/A	N/A	0.22	0.61	73, 3 (35)
7	2.4	0.8	50	43.0	N/A	N/A	0.44	0.89	80
8	1.6	0.4	52	50.0	0.95	0.31	0.24	0.82	174
9	N/A	N/A	N/A	36.5	N/A	0.57	0.55	0.98	23
10	3.9	0.5	70	34.0	0.82	0.55	0.51	0.96	137
11	1.4	0.3	51	76.0	1.40	0.38	0.31	0.82	267, 174 (245)
12	2.0	0.3	67	17.5	1.97	0.72	0.63	0.94	30
13	2.0	0.2	336	57.0	1.04	0.35	0.32	0.94	158
14	1.7	0.4	53	77.0	1.66	0.56	0.45	0.88	22, 33 (27)
15	N/A	N/A	N/A	63.5	N/A	0.35	0.34	0.82	26, 312 (333)
MEAN	**2.1**	**0.5**	**64.2**	**48.9**	**1.37**	**0.47**	**0.39**	**0.86**	**86.1**
s.d.	**0.9**	**0.3**	**21.8**	**22.9**	**0.68**	**0.14**	**0.12**	**0.15**	**66.3**
N	**26**	**26.0**	**26**	**30**	**23**	**27**	**30**	**30**	**30**

* Reference line, 0°, is the horizontal axis. For larvae that change track direction, net resultant track direction is recorded in parentheses.

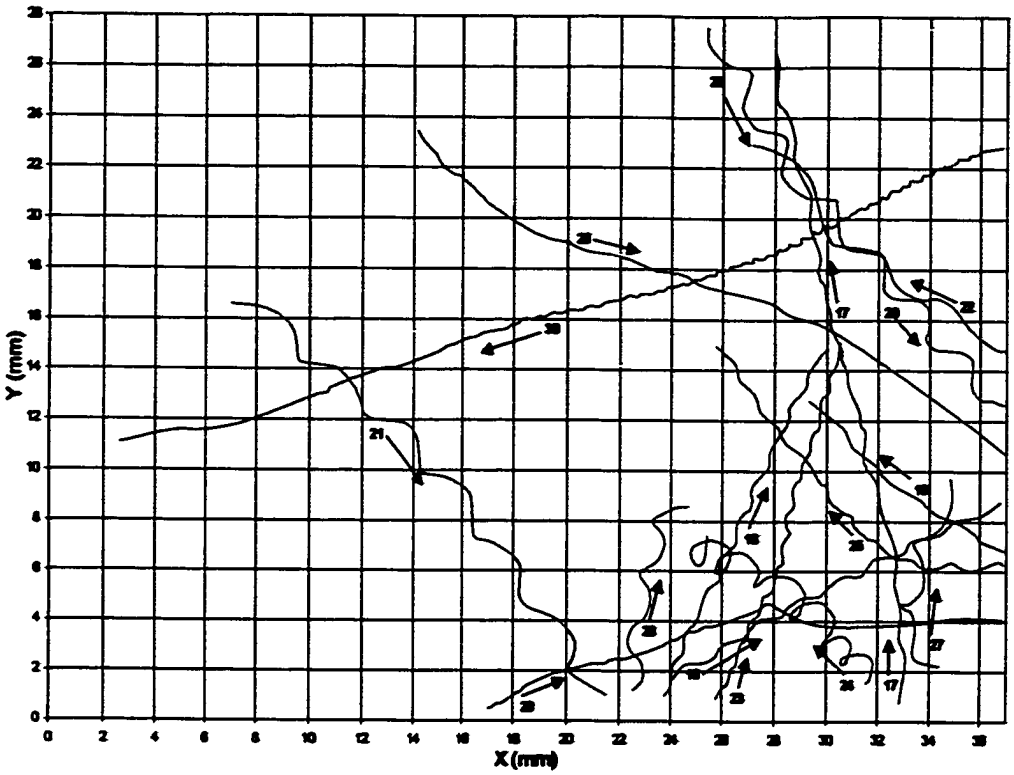

Fig A1.6b. Reconstructed tracks of swimming mussel larvae (*Mytilus edulis*) from SCA# 4L0, Day 2 Night recording session, May 21, 1996. Track direction indicated by arrows. Larvae #16-30.

Table A1.6b. Trajectory measurement data from tracks of swimming mussel larvae (*Mytilus edulis*) from SCA# 4L0, Day 2 Night recording session, May 21, 1996. Larvae #16-30.

LARVAL TRACK #	HELIX HEIGHT (mm)	HELIX DIAMETER (mm)	HELIX PITCH ANGLE	TIME (s)	ANGULAR VELOCITY (rad/s)	LINEAR VELOCITY (mm/s)	FORWARD VELOCITY (mm/s)	NGDR	TRACK DIRECTION (degrees) *
16	1.8	0.3	71	34.0	1.49	0.47	0.43	0.94	29
17	1.3	0.2	82	75.0	1.77	0.38	0.35	0.97	103
18	1.6	0.3	70	39.5	1.50	0.44	0.39	0.96	65
19	2.2	0.2	77	17.0	1.63	0.60	0.57	0.98	141
20	3.2	1.1	43	42.5	0.87	0.64	0.44	0.82	308
21	3.3	0.9	53	35.0	1.18	0.83	0.61	0.87	319, 305 (313)
22	3.5	0.7	58	37.0	0.62	0.41	0.34	0.92	145
23	1.3	0.2	73	45.0	1.67	0.38	0.33	0.95	71
24	1.6	1.1	13	62.0	0.55	0.33	0.14	0.42	137, 157 (136)
25	1.8	0.3	67	60.5	0.90	0.28	0.25	0.89	177, 129 (142)
26	N/A	N/A	N/A	65.0	N/A	0.41	0.41	0.97	317, 343, 323 (331)
27	2.5	0.7	45	17.0	1.19	0.64	0.48	0.77	79
28	2.6	0.6	46	36.0	0.51	0.26	0.21	0.80	78
29	N/A	N/A	N/A	41.5	N/A	0.51	0.50	0.95	20, 336, 4 (10)
30	0.5	0.1	76	125.5	3.77	0.33	0.29	0.94	206, 196 (199)
MEAN	**2.1**	**0.5**	**54.2**	**48.9**	**1.37**	**0.47**	**0.39**	**0.85**	**86.1**
s.d.	**0.9**	**0.3**	**21.0**	**22.9**	**0.68**	**0.14**	**0.12**	**0.16**	**66.3**
N	**26**	**26.0**	**26**	**30**	**23**	**27**	**30**	**30**	**30**

* Reference line, 0°, is the horizontal axis. For larvae that change track direction, net resultant track direction is recorded in parentheses.

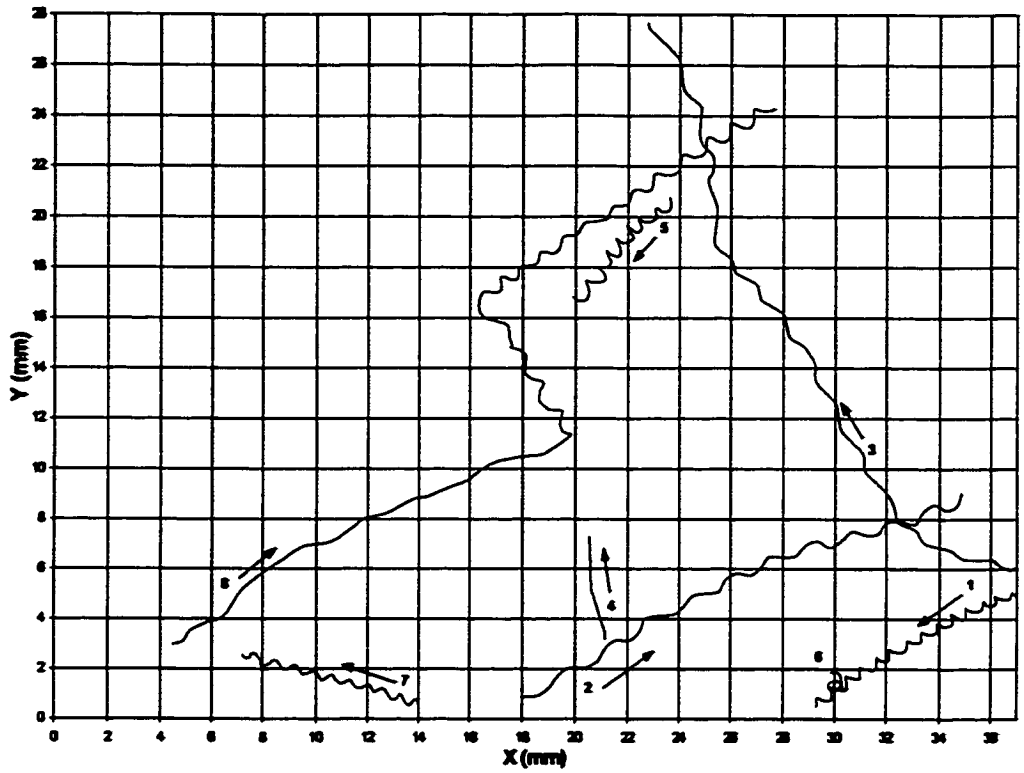

Fig A1.7. Reconstructed tracks of swimming mussel larvae (*Mytilus edulis*) from SCA# 3L0, Day 2 Day recording session, May 21, 1996. Track direction indicated by arrows.

Table A1.7. Trajectory measurement data from tracks of swimming mussel larvae (*Mytilus edulis*) from SCA# 3L0, Day 2 Day recording session, May 21, 1996.

LARVAL TRACK #	HELIX HEIGHT (mm)	HELIX DIAMETER (mm)	HELIX PITCH ANGLE	TIME (s)	ANGULAR VELOCITY (rad/s)	LINEAR VELOCITY (mm/s)	FORWARD VELOCITY (mm/s)	NGDR	TRACK DIRECTION (degrees) *
1	0.7	0.4	54	63.0	1.25	0.29	0.14	0.64	210
2	1.7	0.5	50	68.0	1.05	0.38	0.28	0.84	32, 20 (26)
3	2.1	0.3	67	105.0	0.77	0.28	0.26	0.89	160, 122, 95, 122 (123)
4	N/A	N/A	N/A	266.7	N/A	N/A	0.02	N/A	105, 90 (98)
5	0.7	0.5	32	54.2	0.99	0.28	0.10	0.49	224
6	N/A	0.4	N/A	156.1	N/A	N/A	N/A	0.34	(clockwise)
7	0.8	0.3	39	57.0	1.05	0.20	0.13	0.73	163
8	1.3	0.5	42	123.4	N/A	N/A	0.30	0.74	29, 124, 34 (43)
MEAN	**1.2**	**0.4**	**48.4**	**111.7**	**1.02**	**0.29**	**0.18**	**0.67**	**128.5**
s.d.	**0.6**	**0.1**	**34.9**	**72.5**	**0.17**	**0.07**	**0.11**	**0.20**	**64.6**
N	**6**	**7**	**6**	**8**	**5**	**5**	**7**	**7**	**7**

* Reference line, 0°, is the horizontal axis. For larvae that change track direction, net resultant track direction is recorded in parentheses.

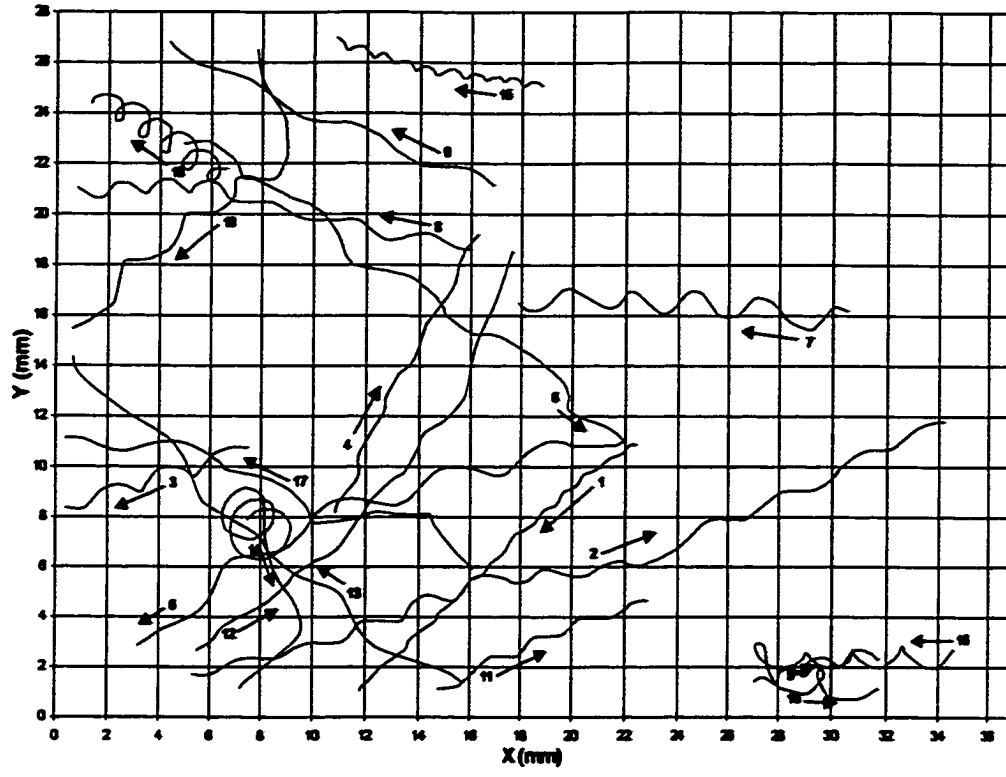

Fig A1.8a. Reconstructed tracks of swimming mussel larvae (*Mytilus edulis*) from SCA# 3R0, Day 2 Day recording session, May 21, 1996. Track direction indicated by arrows. Larvae #1-18.

Table A1.8a. Trajectory measurement data from tracks of swimming mussel larvae (*Mytilus edulis*) from SCA# 3R0, Day 2 Day recording session, May 21, 1996. Larvae #1-18.

LARVAL TRACK #	HELIX HEIGHT (mm)	HELIX DIAMETER (mm)	HELIX PITCH ANGLE	TIME (s)	ANGULAR VELOCITY (rad/s)	LINEAR VELOCITY (mm/s)	FORWARD VELOCITY (mm/s)	NGDR	TRACK DIRECTION (degrees) *
1	1.1	0.2	70	28.0	2.94	0.58	0.52	0.97	223
2	2.4	0.6	68	72.5	1.12	0.55	0.43	0.93	20
3	2.2	0.7	39	20.0	1.06	0.52	0.38	0.88	200
4	2.5	0.3	74	22.0	1.39	0.59	0.56	0.96	64
5	1.2	0.5	26	22.5	1.15	0.36	0.21	0.74	17
6	4.3	0.9	56	99.0	0.61	0.50	0.42	0.45	323, 196, 212 (265)
7	2.5	1.0	41	47.0	0.69	0.43	0.27	0.80	177
8	1.7	0.5	50	59.0	0.95	0.36	0.26	0.90	167, 184 (171)
9	4.7	0.5	74	28.0	0.66	0.52	0.49	0.97	157
10	3.1	0.7	58	36.0	0.85	0.52	0.43	0.79	281, 219 (237)
11	2.0	0.4	63	26.0	1.05	0.39	0.34	0.94	24
12	3.3	0.2	80	43.5	0.90	0.48	0.47	0.96	37, 61 (53)
13	4.5	0.6	69	42.0	0.66	0.51	0.47	0.96	140
14	N/A	2.0	N/A	60.0	N/A	N/A	N/A	0.29	N/A
15	0.8	0.3	50	39.0	1.67	0.31	0.21	0.83	172, 159 (166)
16	1.8	0.8	42	57.0	0.76	0.39	0.22	0.18	182, 344 (206)
17	4.1	0.6	63	53.0	0.49	0.35	0.32	0.91	162
18	1.1	1.0	26	59.5	0.57	0.31	0.10	0.37	147
MEAN	**2.7**	**0.6**	**59.6**	**46.9**	**1.04**	**0.46**	**0.38**	**0.82**	**197.5**
s.d.	**1.2**	**0.4**	**16.9**	**19.5**	**0.56**	**0.09**	**0.11**	**0.29**	**78.9**
N	**30**	**31**	**30**	**35**	**29**	**30**	**34**	**35**	**34**

* Reference line, 0°, is the horizontal axis. For larvae that change track direction, net resultant track direction is recorded in parentheses.

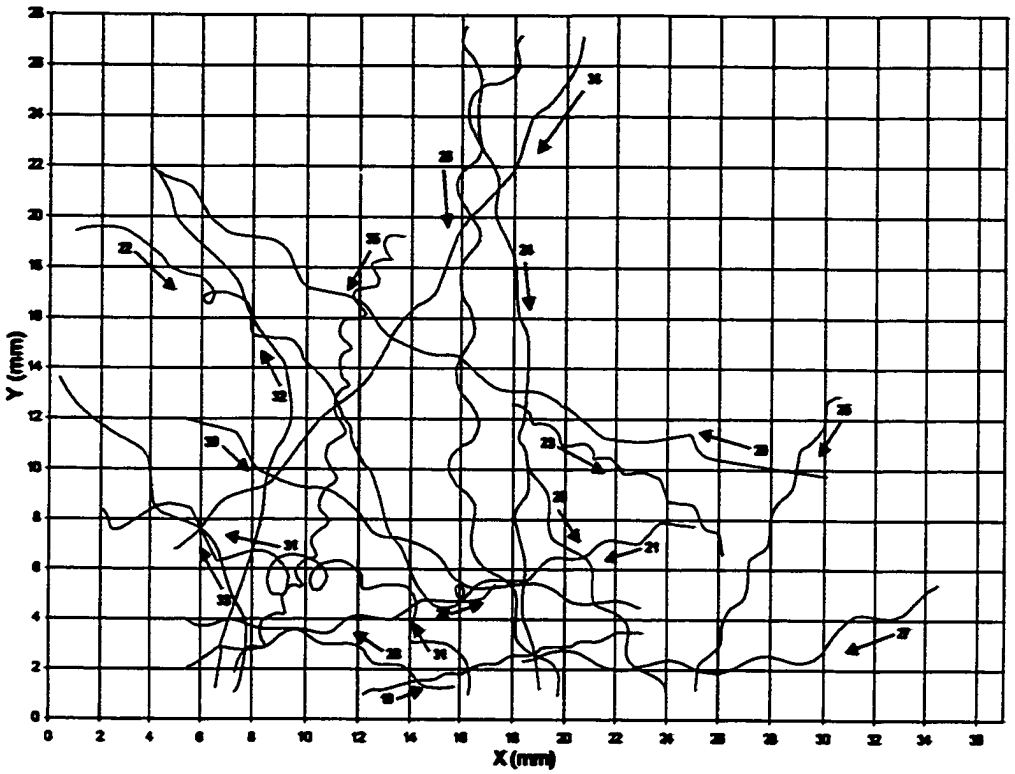

Fig A1.8b. Reconstructed tracks of swimming mussel larvae (*Mytilus edulis*) from SCA# 3R0, Day 2 Day recording session, May 21, 1996. Track direction indicated by arrows. Larvae #19-35.

Table A1.8b. Trajectory measurement data from tracks of swimming mussel larvae (*Mytilus edulis*) from SCA# 3R0, Day 2 Day recording session, May 21, 1996. Larvae #19-35.

LARVAL TRACK #	HELIX HEIGHT (mm)	HELIX DIAMETER (mm)	HELIX PITCH ANGLE	TIME (s)	ANGULAR VELOCITY (rad/s)	LINEAR VELOCITY (mm/s)	FORWARD VELOCITY (mm/s)	NGDR	TRACK DIRECTION (degrees) *
19	1.4	0.2	74	20.5	2.51	0.58	0.54	0.97	14
20	4.4	0.6	66	81.5	0.51	0.38	0.35	0.93	165, 148 (155)
21	2.6	0.4	68	45.5	1.09	0.50	0.45	0.94	196
22	N/A	N/A	N/A	72.5	N/A	N/A	0.33	0.76	328, 295, 23 (320)
23	1.5	0.4	61	32.0	1.36	0.40	0.32	0.86	330
24	N/A	N/A	N/A	53.0	N/A	N/A	0.50	0.97	276
25	2.6	0.3	74	30.0	1.05	0.45	0.43	0.94	246
26	3.8	1.0	51	64.0	0.70	0.57	0.43	0.85	247, 270, 298 (273)
27	3.8	0.4	67	47.0	0.60	0.38	0.36	0.91	207, 179 (191)
28	2.0	0.4	63	25.5	1.34	0.50	0.44	0.94	160, 178 (166)
29	3.1	0.7	54	26.5	0.82	0.49	0.40	0.91	301
30	4.0	0.5	65	57.0	0.53	0.37	0.34	0.94	329, 349 (337)
31	2.8	1.3	33	68.0	N/A	N/A	0.25	0.59	134, 179, 162 (153)
32	N/A	N/A	N/A	62.0	N/A	0.37	0.37	0.70	76, 121 (97)
33	N/A	N/A	N/A	34.0	N/A	N/A	0.45	0.90	122
34	4.4	0.4	75	42.0	0.89	0.64	0.62	0.97	236
35	1.4	0.4	83	66.5	1.27	0.38	0.28	0.76	256, 232 (250)
MEAN	**2.7**	**0.6**	**59.6**	**46.9**	**1.04**	**0.46**	**0.38**	**0.82**	**197.5**
s.d.	**1.2**	**0.4**	**16.9**	**19.5**	**0.56**	**0.09**	**0.11**	**0.26**	**78.9**
N	**38**	**31**	**38**	**35**	**29**	**38**	**34**	**35**	**34**

* Reference line, 0°, is the horizontal axis. For larvae that change track direction, net resultant track direction is recorded in parentheses.

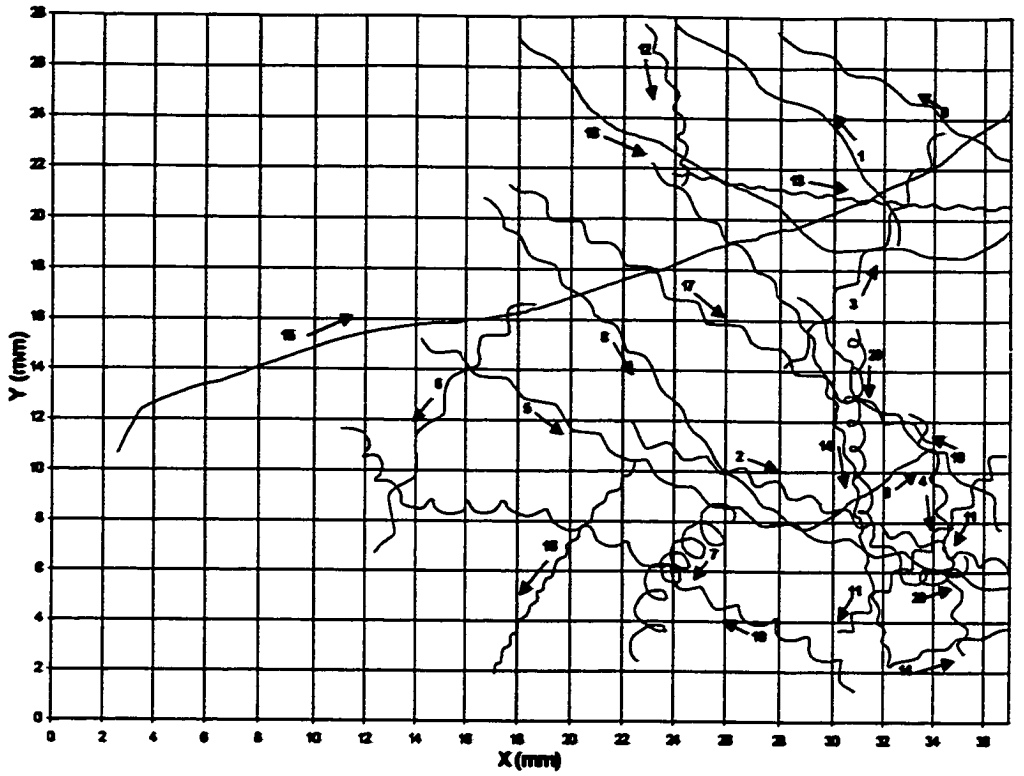

Fig A1.9a. Reconstructed tracks of swimming mussel larvae (*Mytilus edulis*) from SCA# 4L0, Day 2 Day recording session, May 21, 1996. Track direction indicated by arrows. Larvae #1-20.

Table A1.9a. Trajectory measurement data from tracks of swimming mussel larvae (*Mytilus edulis*) from SCA# 4L0, Day 2 Day recording session, May 21, 1996. Larvae #1-20.

LARVAL TRACK #	HELIX HEIGHT (mm)	HELIX DIAMETER (mm)	HELIX PITCH ANGLE	TIME (s)	ANGULAR VELOCITY (rad/s)	LINEAR VELOCITY (mm/s)	FORWARD VELOCITY (mm/s)	NGDR	TRACK DIRECTION (degrees) *
1	N/A	N/A	N/A	28.5	N/A	0.45	0.43	0.94	138
2	1.4	0.5	47	34.5	2.15	0.70	0.47	0.81	340
3	1.7	0.4	55	28.0	1.49	0.51	0.40	0.85	57
4	1.4	0.5	41	36.0	1.24	0.40	0.28	0.79	280
5	2.0	0.4	65.0	59.0	1.36	0.50	0.42	0.92	330, 345 (337)
6	2.4	0.6	55	34.0	0.92	0.45	0.35	0.84	239
7	0.7	1.1	N/A	52.0	1.10	0.62	0.13	0.28	224, 285 (240)
8	1.7	0.3	67	42.5	2.05	0.67	0.57	0.80	312, 34 (330)
9	2.3	0.3	70	19.0	1.53	0.60	0.55	0.96	152
10	2.6	0.5	68	43.0	0.68	0.32	0.29	0.90	136
11	1.2	0.4	1	36.0	1.28	0.37	0.26	0.75	228
12	1.2	0.3	55.0	23.0	1.45	0.34	0.29	0.84	282
13	0.9	0.1	66	22.0	4.39	0.65	0.60	0.95	354
14	1.4	0.3	64	62.0	2.03	0.52	0.44	0.78	312, 283, 18 (307)
15	N/A	N/A	N/A	72.0	N/A	0.53	0.52	0.97	58, 17, 34 (22)
16	0.9	0.2	70	51.0	1.41	0.23	0.20	0.89	238
17	2.0	0.6	51	42.0	1.42	0.61	0.46	0.87	328
18	N/A	N/A	N/A	42.0	N/A	N/A	0.51	0.91	324, 3 (336)
19	1.6	0.5	45	76.0	1.20	0.43	0.31	0.75	148, 172, 120 (152)
20	1.0	0.6	23	54.0	1.47	0.53	0.24	0.43	274, 6 (296)
MEAN	**1.6**	**0.5**	**49.9**	**59.7**	**1.46**	**0.48**	**0.37**	**0.79**	**311.3**
s.d.	**0.7**	**0.2**	**17.8**	**23.6**	**0.65**	**0.14**	**0.13**	**0.17**	**78.9**
N	**32**	**36**	**31**	**40**	**31**	**36**	**40**	**40**	**40**

* Reference line, 0°, is the horizontal axis. For larvae that change track direction, net resultant track direction is recorded in parentheses.

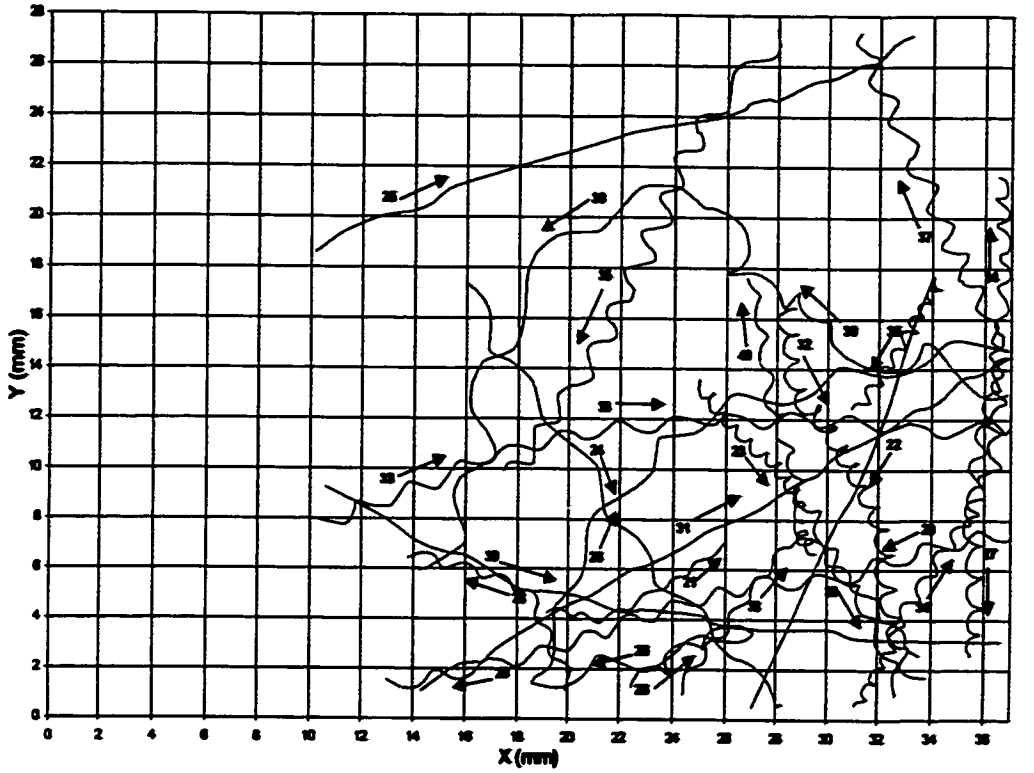

Fig A1.9b. Reconstructed tracks of swimming mussel larvae (*Mytilus edulis*) from SCA# 4L0, Day 2 Day recording session, May 21, 1996. Track direction indicated by arrows. Larvae #21-40.

Table A1.9b. Trajectory measurement data from tracks of swimming mussel larvae (*Mytilus edulis*) from SCA# 4L0, Day 2 Day recording session, May 21, 1996. Larvae #21-40.

LARVAL TRACK #	HELIX HEIGHT (mm)	HELIX DIAMETER (mm)	HELIX PITCH ANGLE	TIME (s)	ANGULAR VELOCITY (rad/s)	LINEAR VELOCITY (mm/s)	FORWARD VELOCITY (mm/s)	NGDR	TRACK DIRECTION (degrees) *
21	1.3	0.2	74	23.0	1.61	0.38	0.34	0.87	346, 38 (23)
22	N/A	N/A	N/A	40.0	N/A	0.47	0.47	1.00	248
23	0.8	0.4	45	49.5	1.35	0.31	0.17	0.50	312, 281 (303)
24	3.9	0.6	89	43.0	0.78	0.54	0.48	0.93	306
25	N/A	N/A	N/A	48.5	N/A	0.52	0.51	0.98	20
26	1.7	0.7	23	112.0	N/A	N/A	0.34	0.45	27, 194, 62, 15 (43)
27	1.4	0.6	35	50.5	1.08	0.38	0.24	0.70	265
28	1.5	0.4	49	44.0	0.86	0.26	0.20	0.76	113, 163 (140)
29	2.1	0.6	59	58.0	1.25	0.57	0.43	0.85	195
30	N/A	N/A	N/A	129.0	N/A	N/A	0.27	0.56	160, 134, 230, 252 (197)
31	N/A	N/A	N/A	68.0	N/A	0.39	0.39	0.99	30
32	1.2	0.6	25	87.0	0.92	0.33	0.18	0.55	281, 305, 284 (289)
33	2.6	0.5	67	56.5	1.18	0.56	0.49	0.86	20, 358 (8)
34	1.3	0.5	38	97.5	1.13	0.35	0.23	0.71	62, 89 (76)
35	1.6	0.7	47	44.0	1.78	0.79	0.47	0.75	241
36	0.8	0.4	13	43.0	1.10	0.28	0.14	0.62	240
37	1.8	0.7	38	28.0	1.72	0.78	0.49	0.74	114
38	1.5	0.5	53	36.0	1.64	0.55	0.40	0.57	56, 313 (10)
39	N/A	N/A	N/A	54.0	N/A	N/A	0.50	0.97	333, 355 (347)
40	1.5	0.5	60	57.0	1.32	0.44	0.31	0.81	117, 101 (110)
MEAN	**1.6**	**0.5**	**49.9**	**59.7**	**1.46**	**0.48**	**0.37**	**0.79**	**311.3**
s.d.	**0.7**	**0.2**	**17.8**	**23.6**	**0.66**	**0.14**	**0.13**	**0.17**	**78.9**
N	**32**	**36**	**31**	**40**	**31**	**36**	**40**	**40**	**40**

* Reference line, 0°, is the horizontal axis. For larvae that change track direction, net resultant track direction is recorded in parentheses.

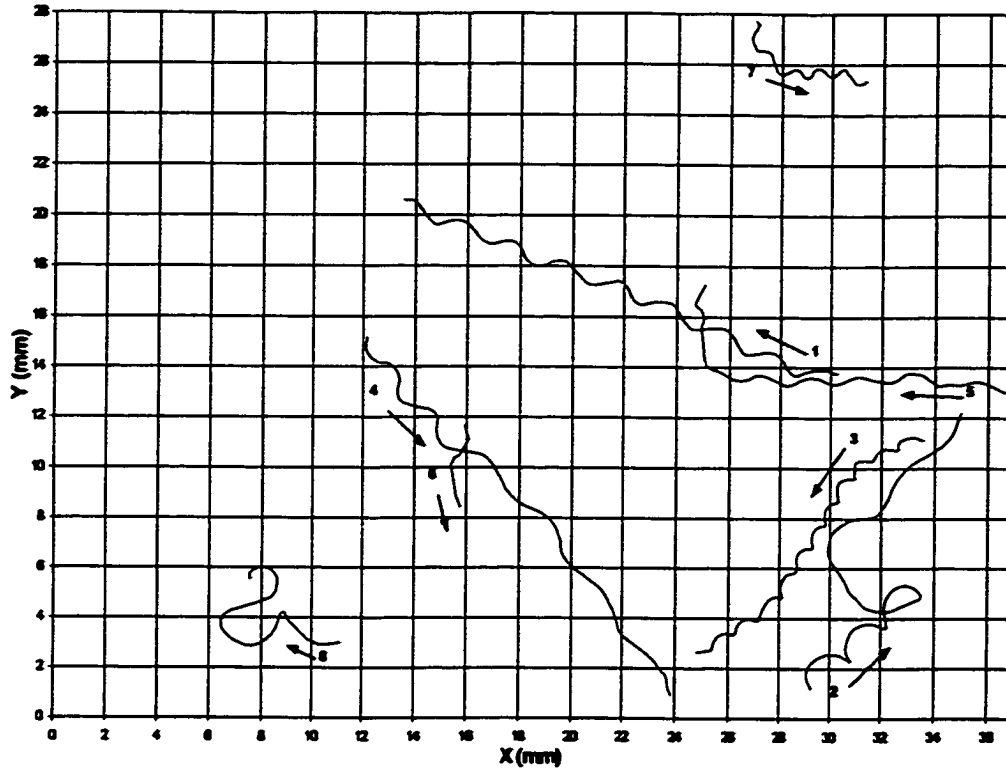

Fig A1.10. Reconstructed tracks of swimming mussel larvae (*Mytilus edulis*) from SCA# 3L0, Day 3 Night recording session, May 22, 1996. Track direction indicated by arrows.

Table A1.10. Trajectory measurement data from tracks of swimming mussel larvae (*Mytilus edulis*) from SCA# 3L0, Day 3 Night recording session, May 22, 1996.

LARVAL TRACK #	HELIX HEIGHT (mm)	HELIX DIAMETER (mm)	HELIX PITCH ANGLE	TIME (s)	ANGULAR VELOCITY (rad/s)	LINEAR VELOCITY (mm/s)	FORWARD VELOCITY (mm/s)	NGDR	TRACK DIRECTION (degrees) *
1	2.3	0.6	55	54.0	0.95	0.44	0.34	0.87	157
2	2.0	0.9	66	136.0	N/A	N/A	0.14	0.57	41, 199, 122, 42 (83)
3	1.2	0.3	50	50.0	1.42	0.35	0.26	0.78	208, 238, 213 (224)
4	2.0	0.3	67	45.0	N/A	N/A	0.42	0.90	309
5	2.0	0.3	67	74.8	0.66	0.23	0.21	0.77	177, 93 (160)
6	N/A	0.4	N/A	237.4	N/A	N/A	0.01	N/A	284, 230, 283 (277)
7	1.0	0.3	54	73.1	0.52	0.12	0.08	0.65	297, 358 (332)
8	N/A	N/A	N/A	59.3	N/A	N/A	N/A	0.37	N/A
MEAN	**1.8**	**0.5**	**58.4**	**91.2**	**0.88**	**0.29**	**0.21**	**0.70**	**243.9**
s.d.	**0.6**	**0.2**	**33.7**	**65.7**	**0.4**	**0.14**	**0.14**	**0.19**	**71.8**
N	**6**	**7**	**6**	**8**	**4**	**4**	**7**	**7**	**7**

* Reference line, 0°, is the horizontal axis. For larvae that change track direction, net resultant track direction is recorded in parentheses.

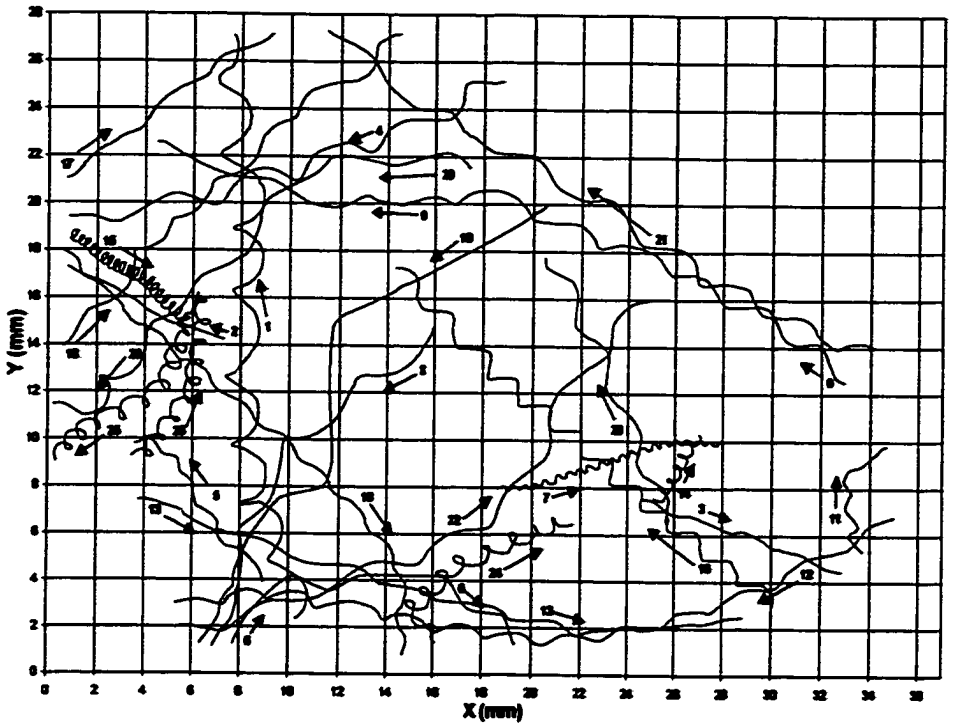

Fig A1.11. Reconstructed tracks of swimming mussel larvae (*Mytilus edulis*) from SCA# 3R0, Day 3 Night recording session, May 22, 1996. Track direction indicated by arrows.

Table A1.11. Trajectory measurement data from tracks of swimming mussel larvae (*Mytilus edulis*) from SCA# 3R0, Day 3 Night recording session, May 22, 1996.

LARVAL TRACK #	HELIX HEIGHT (mm)	HELIX DIAMETER (mm)	HELIX PITCH ANGLE	TIME (s)	ANGULAR VELOCITY (rad/s)	LINEAR VELOCITY (mm/s)	FORWARD VELOCITY (mm/s)	NGDR	TRACK DIRECTION (degrees) *
1	2.6	1.2	299	66.0	0.89	0.66	0.37	0.80	109, 93 (96)
2	N/A	N/A	N/A	15.0	N/A	0.48	0.46	0.99	156
3	2.7	0.2	74	22.0	0.94	0.41	0.40	0.97	339
4	3.5	0.9	46	54.0	0.63	0.45	0.35	0.87	203, 189 (196)
5	1.9	0.4	68	27.0	1.01	0.36	0.30	0.88	127
6	2.8	0.5	69	53.5	N/A	N/A	0.26	0.78	50, 358, 325 (1)
7	0.5	0.3	45	54.0	2.12	0.32	0.18	0.70	4, 19, 1 (12)
8	4.0	0.7	67	41.0	0.65	0.47	0.41	0.90	222, 251 (237)
9	3.1	0.8	57	59.0	1.06	0.69	0.53	0.90	154, 179, 157 (160)
10	N/A	N/A	N/A	66.0	N/A	N/A	0.36	0.90	209, 270, 196, 242 (233)
11	1.3	0.3	63	19.5	1.33	0.33	0.27	0.76	100, 35 (78)
12	2.3	0.4	58	59.0	1.46	0.61	0.53	0.90	206, 170, 192 (188)
13	3.3	0.4	77	54.0	0.91	0.52	0.48	0.96	343, 6 (349)
14	0.5	0.5	22	26.8	1.51	0.37	0.12	0.42	58
15	0.4	0.4	18	140.0	0.73	0.16	0.05	0.26	327, 312 (325)
16	1.8	0.7	2	76.0	0.97	0.45	0.28	0.77	139
17	3.6	0.4	4	20.0	0.91	0.55	0.53	0.97	37
18	2.6	0.4	71	47.0	1.00	0.45	0.41	0.92	45
19	2.2	0.3	61	59.0	1.15	0.44	0.39	0.91	317, 277 (309)
20	3.0	0.8	58	59.5	N/A	N/A	0.36	0.82	180, 225 (210)
21	2.8	0.6	50	49.0	1.20	0.66	0.54	0.91	150
22	4.8	0.5	72	60.0	0.55	0.44	0.42	0.89	20, 57 (36)
23	3.3	0.7	58	27.0	0.87	0.54	0.46	0.90	116
24	1.1	0.7	10	142.0	0.36	0.14	0.07	0.40	128, 38, 22 (42)
25	1.0	0.6	34	125.0	0.83	0.30	0.14	0.06	48, 84, 249, 210 (184)
MEAN	2.4	0.6	47.1	57.9	1.01	0.45	0.35	0.78	96.3
s.d.	1.2	0.2	28.7	34.3	0.38	0.15	0.15	0.24	73.1
N	20	23	23	25	21	22	25	25	25

* Reference line, 0°, is the horizontal axis. For larvae that change track direction, net resultant track direction is recorded in parentheses.

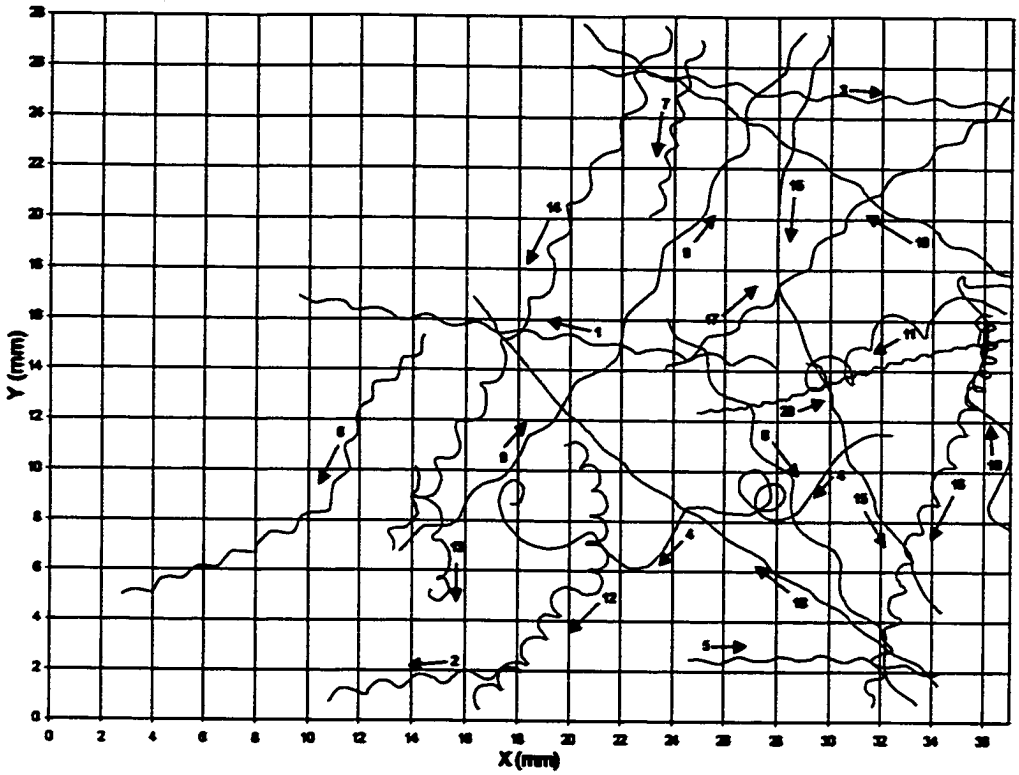

Fig A1.12a. Reconstructed tracks of swimming mussel larvae (*Mytilus edulis*) from SCA# 4L0, Day 3 Night recording session, May 22, 1996. Track direction indicated by arrows. Larvae #1-20.

Table A1.12a. Trajectory measurement data from tracks of swimming mussel larvae (*Mytilus edulis*) from SCA# 4L0, Day 3 Night recording session, May 22, 1996. Larvae #1-20.

LARVAL TRACK #	HELIX HEIGHT (mm)	HELIX DIAMETER (mm)	HELIX PITCH ANGLE	TIME (s)	ANGULAR VELOCITY (rad/s)	LINEAR VELOCITY (mm/s)	FORWARD VELOCITY (mm/s)	NGDR	TRACK DIRECTION (degrees) *
1	1.9	0.2	82	44.0	1.38	0.45	0.42	0.93	172
2	1.7	0.4	54	29.5	0.94	0.32	0.25	0.84	189
3	1.8	0.3	67	32.5	1.72	0.56	0.51	0.95	355
4	N/A	N/A	N/A	69.0	N/A	N/A	0.29	0.50	205, 144 (191)
5	1.6	0.2	73	26.0	1.45	0.39	0.37	0.95	359
6	1.6	0.3	63	46.0	1.36	0.40	0.34	0.84	240, 204 (222)
7	1.4	0.4	48	30.5	1.09	0.32	0.24	0.83	257
8	2.9	0.6	58	49.5	0.79	0.44	0.37	0.90	301
9	3.1	0.4	66	54.0	0.99	0.52	0.48	0.94	46, 59 (53)
10	4.9	1.2	55	26.0	N/A	N/A	0.41	0.88	100
11	2.2	1.1	35	52.0	N/A	N/A	0.16	0.52	199
12	1.2	0.6	33	66.5	1.00	0.37	0.20	0.51	301, 267, 231 (253)
13	1.6	0.6	39	26.0	N/A	N/A	0.22	0.60	293, 264 (277)
14	1.8	0.8	38	44.0	1.82	0.87	0.53	0.80	62
15	2.8	0.4	78	62.0	0.90	0.43	0.40	0.93	257, 295 (281)
16	1.3	0.5	33	67.0	1.16	0.39	0.24	0.57	282, 252 (254)
17	2.0	0.4	67	32.0	1.66	0.62	0.53	0.93	39
18	2.2	0.2	77	70.0	N/A	0.34	0.34	0.98	145, 129 (139)
19	2.4	0.4	67	37.0	1.33	0.58	0.52	0.97	150
20	0.7	0.2	64	39.5	2.67	0.43	0.31	0.91	14
MEAN	**2.1**	**0.5**	**55.7**	**41.4**	**1.35**	**0.51**	**0.40**	**0.82**	**29.7**
s.d.	**0.8**	**0.3**	**14.1**	**16.8**	**0.52**	**0.16**	**0.14**	**0.14**	**75.2**
N	**38**	**38**	**38**	**40**	**33**	**35**	**40**	**40**	**40**

* Reference line, 0°, is the horizontal axis. For larvae that change track direction, net resultant track direction is recorded in parentheses.

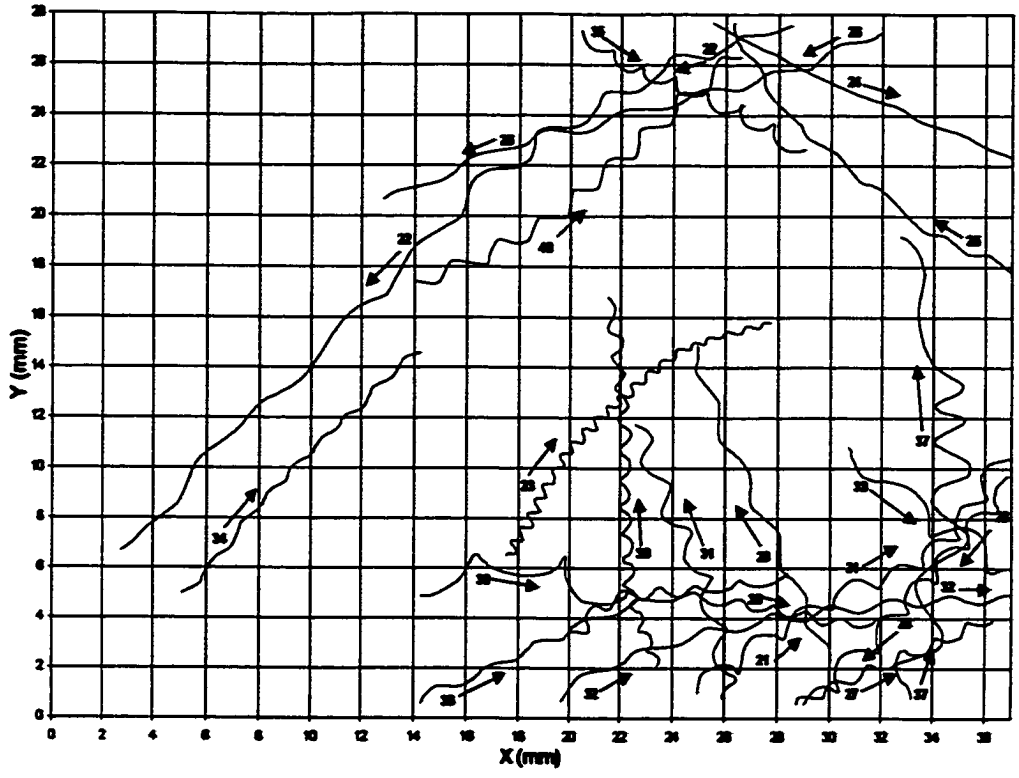

Fig A1.12b. Reconstructed tracks of swimming mussel larvae (*Mytilus edulis*) from SCA# 4L0, Day 3 Night recording session, May 22, 1996. Track direction indicated by arrows. Larvae #21-40.

Table A1.12b. Trajectory measurement data from tracks of swimming mussel larvae (*Mytilus edulis*) from SCA# 4L0, Day 3 Night recording session, May 22, 1996. Larvae #21-40.

LARVAL TRACK #	HELIX HEIGHT (mm)	HELIX DIAMETER (mm)	HELIX PITCH ANGLE	TIME (s)	ANGULAR VELOCITY (rad/s)	LINEAR VELOCITY (mm/s)	FORWARD VELOCITY (mm/s)	NGDR	TRACK DIRECTION (degrees) *
21	2.3	0.7	48	29.0	1.45	0.75	0.54	0.77	30, 53 (38)
22	3.0	0.5	57	52.0	N/A	N/A	0.65	0.93	205, 226 (219)
23	0.6	0.4	60	85.0	1.64	0.35	0.17	0.68	60, 41, 15 (43)
24	N/A	N/A	N/A	21.5	N/A	0.60	0.59	0.99	335
25	2.6	0.3	80	36.0	0.98	0.43	0.41	0.95	152, 128 (137)
26	2.7	0.3	75	31.0	1.51	0.70	0.65	0.96	198
27	1.5	0.4	51	18.5	1.89	0.61	0.45	0.84	25
28	1.8	0.7	35	23.5	1.77	0.78	0.51	0.75	230
29	2.9	0.5	66	39.0	0.81	0.42	0.37	0.94	113
30	1.1	0.3	38	34.0	2.54	0.58	0.44	0.78	107, 93 (97)
31	2.3	0.7	47	23.0	1.34	0.71	0.50	0.79	109
32	2.4	0.4	63	27.5	1.68	0.73	0.65	0.93	21, 4 (14)
33	2.7	1.1	35	30.5	0.61	0.42	0.26	0.80	324
34	1.7	0.2	78	50.0	0.97	0.28	0.27	0.94	47
35	1.5	0.6	45	35.0	1.21	0.44	0.28	0.76	332
36	2.1	0.3	67	29.5	1.51	0.57	0.51	0.93	25, 11 (20)
37	3.0	1.4	38	59.0	0.70	0.58	0.33	0.70	70, 95, 113 (91)
38	1.4	0.4	51	72.0	0.79	0.24	0.17	0.80	42, 351 (3)
39	3.5	0.8	55	24.0	0.67	0.46	0.37	0.74	13, 340 (1)
40	1.8	0.6	52	27.0	1.95	0.83	0.57	0.82	39
MEAN	**2.1**	**0.5**	**56.7**	**41.4**	**1.35**	**0.51**	**0.40**	**0.82**	**29.7**
s.d.	**0.8**	**0.3**	**14.1**	**16.8**	**0.52**	**0.16**	**0.14**	**0.14**	**75.2**
N	**38**	**38**	**38**	**40**	**33**	**35**	**40**	**40**	**40**

* Reference line, 0°, is the horizontal axis. For larvae that change track direction, net resultant track direction is recorded in parentheses.

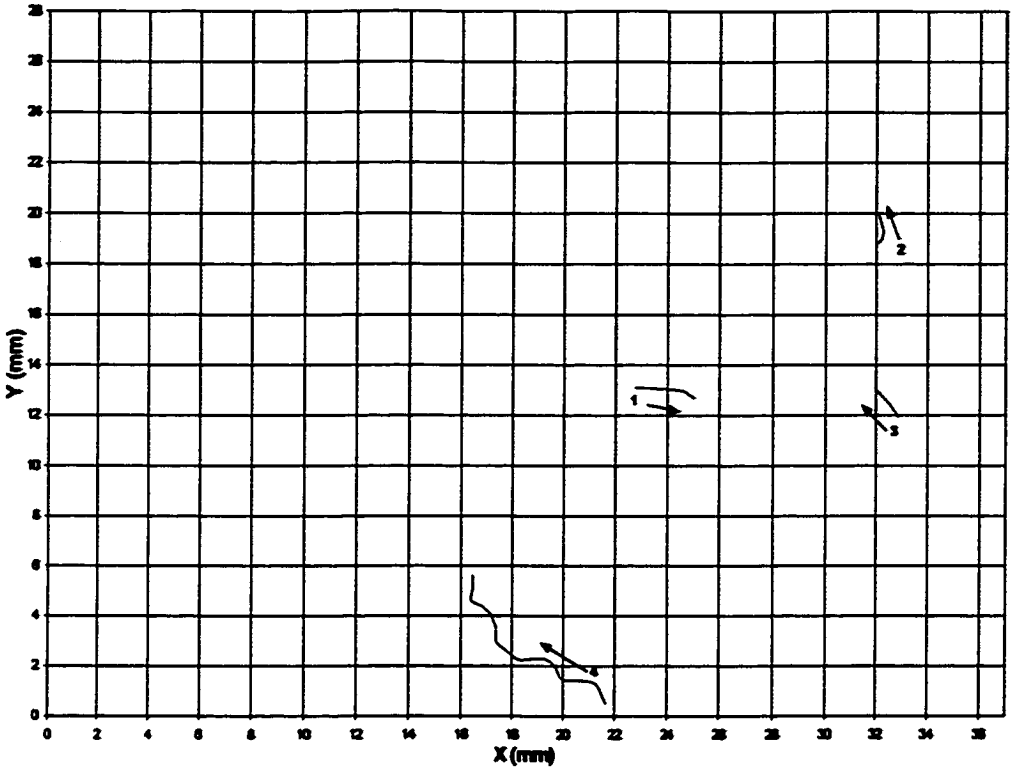

Fig A1.13. Reconstructed tracks of swimming mussel larvae (*Mytilus edulis*) from SCA# 3L0, Day 3 Day recording session, May 22, 1996. Track direction indicated by arrows.

Table A1.13. Trajectory measurement data from tracks of swimming mussel larvae (*Mytilus edulis*) from SCA# 3L0, Day 3 Day recording session, May 22, 1996.

LARVAL TRACK #	HELIX HEIGHT (mm)	HELIX DIAMETER (mm)	HELIX PITCH ANGLE	TIME (s)	ANGULAR VELOCITY (rad/s)	LINEAR VELOCITY (mm/s)	FORWARD VELOCITY (mm/s)	NGDR	TRACK DIRECTION (degrees) *
1	N/A	N/A	N/A	211.9	N/A	N/A	N/A	N/A	348
2	N/A	N/A	N/A	211.9	N/A	N/A	N/A	N/A	88
3	N/A	N/A	N/A	211.9	N/A	N/A	N/A	N/A	129
4	2.0	0.6	55	22.0	1.12	0.48	0.36	0.84	135
MEAN	**2.0**	**0.6**	**55.0**	**164.4**	**1.12**	**0.48**	**0.36**	**0.84**	**98.1**
s.d.	**N/A**	**N/A**	**N/A**	**96.0**	**N/A**	**N/A**	**N/A**	**N/A**	**52.8**
N	**1**	**1**	**1**	**4**	**1**	**1**	**1**	**1**	**4**

* Reference line, 0°, is the horizontal axis. For larvae that change track direction, net resultant track direction is recorded in parentheses.

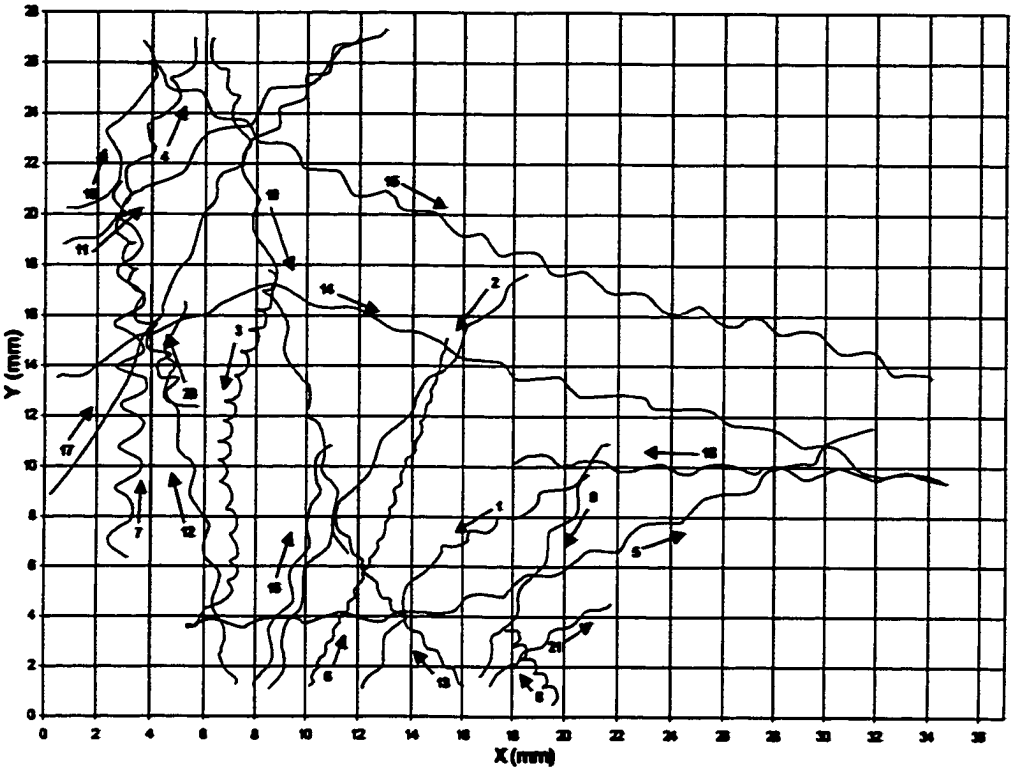

Fig A1.14. Reconstructed tracks of swimming mussel larvae (*Mytilus edulis*) from SCA# 3R0, Day 3 Day recording session, May 22, 1996. Track direction indicated by arrows.

Table A1.14. Trajectory measurement data from tracks of swimming mussel larvae (*Mytilus edulis*) from SCA# 3R0, Day 3 Day recording session, May 22, 1996.

LARVAL TRACK #	HELIX HEIGHT (mm)	HELIX DIAMETER (mm)	HELIX PITCH ANGLE	TIME (s)	ANGULAR VELOCITY (rad/s)	LINEAR VELOCITY (mm/s)	FORWARD VELOCITY (mm/s)	NGDR	TRACK DIRECTION (degrees) *
1	1.3	0.4	61	47.0	1.47	0.40	0.30	0.87	209, 249 (226)
2	2.8	0.3	78	52.0	0.83	0.40	0.38	0.95	231, 252 (239)
3	0.9	0.4	44	76.0	1.47	0.36	0.20	0.66	253, 276, 222 (257)
4	1.9	0.6	52	19.0	1.23	0.52	0.37	0.84	67
5	2.5	0.4	66	55.0	1.29	0.58	0.51	0.93	4, 23 (17)
6	0.7	0.1	67	53.0	2.53	0.32	0.28	0.93	70
7	1.6	1.0	17	43.0	1.24	0.72	0.32	0.66	90
8	0.8	0.4	43	19.5	1.40	0.34	0.18	0.59	123
9	2.2	0.4	63	14.5	1.80	0.75	0.63	0.93	241
10	3.7	1.0	65	22.0	0.55	0.43	0.33	0.82	69
11	3.0	0.7	65	29.0	1.07	0.65	0.52	0.93	35
12	2.1	0.3	65	32.0	1.46	0.53	0.49	0.91	101
13	1.0	0.2	67	24.0	2.30	0.41	0.35	0.91	127
14	2.8	0.3	75	74.0	1.09	0.51	0.49	0.91	25, 342 (353)
15	2.1	0.5	60	71.0	1.43	0.57	0.47	0.89	331, 343 (338)
16	2.4	0.5	67	32.0	0.81	0.37	0.32	0.92	72
17	1.7	0.5	65	52.0	N/A	N/A	0.42	0.93	62, 48 (57)
18	2.4	0.3	70	35.0	1.26	0.52	0.48	0.94	177
19	2.4	0.5	59	41.7	1.35	0.60	0.51	0.91	284
20	1.0	0.4	51	41.0	1.39	0.34	0.23	0.66	106
21	1.3	0.3	68	27.0	1.02	0.27	0.21	0.93	37
MEAN	**1.9**	**0.5**	**60.6**	**46.9**	**1.36**	**0.48**	**0.38**	**0.86**	**69.6**
s.d.	**0.8**	**0.2**	**12.8**	**18.3**	**0.46**	**0.14**	**0.12**	**0.11**	**68.1**
N	**21**	**21**	**21**	**21**	**20**	**20**	**21**	**21**	**21**

* Reference line, 0°, is the horizontal axis. For larvae that change track direction, net resultant track direction is recorded in parentheses.

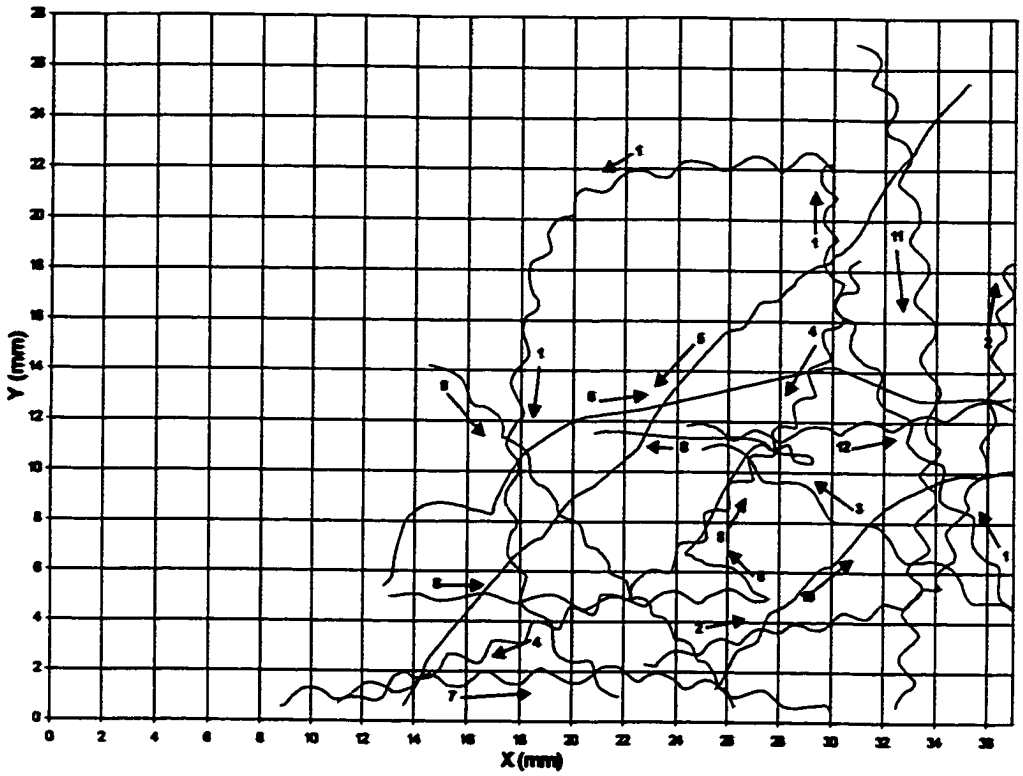

Fig A1.15a. Reconstructed tracks of swimming mussel larvae (*Mytilus edulis*) from SCA# 4L0, Day 3 Day recording session, May 22, 1996. Track direction indicated by arrows. Larvae #1-12.

Table A1.15a. Trajectory measurement data from tracks of swimming mussel larvae (*Mytilus edulis*) from SCA# 4L0, Day 3 Day recording session, May 22, 1996. Larvae #1-12.

LARVAL TRACK #	HELIX HEIGHT (mm)	HELIX DIAMETER (mm)	HELIX PITCH ANGLE	TIME (s)	ANGULAR VELOCITY (rad/s)	LINEAR VELOCITY (mm/s)	FORWARD VELOCITY (mm/s)	NGDR	TRACK DIRECTION (degrees) *
1	2.4	0.7	54	104.5	N/A	N/A	0.49	0.26	121, 95, 185, 229, 264, 286, 316 (194)
2	1.8	0.4	59	82.0	1.09	0.38	0.31	0.74	14, 81 (49)
3	3.3	0.7	58	30.0	0.86	0.53	0.45	0.90	149
4	1.6	0.6	48	86.0	1.26	0.49	0.33	0.74	250, 233, 200 (222)
5	N/A	N/A	N/A	76.0	N/A	0.44	0.43	0.98	229
6	5.0	1.7	48	52.5	N/A	N/A	0.50	0.88	35, 3 (18)
7	2.2	0.5	44	58.5	1.04	0.46	0.36	0.87	6, 355 (360)
8	2.8	0.4	63	154.0	N/A	N/A	0.22	0.28	359, 150, 57, 344, 174 (40)
9	1.6	0.3	67	41.5	1.67	0.50	0.43	0.91	310
10	2.0	0.3	66	30.0	1.57	0.56	0.49	0.94	47, 12 (37)
11	1.9	0.6	47	69.0	1.27	0.55	0.39	0.81	282, 263 (274)
12	2.2	0.5	58	23.0	1.56	0.67	0.55	0.90	5
MEAN	**2.1**	**0.6**	**52.5**	**67.2**	**1.21**	**0.51**	**0.37**	**0.71**	**21.1**
s.d.	**0.9**	**0.3**	**12.6**	**31.4**	**0.33**	**0.10**	**0.12**	**0.26**	**67.5**
N	**21**	**21**	**21**	**23**	**16**	**17**	**23**	**23**	**23**

* Reference line, 0°, is the horizontal axis. For larvae that change track direction, net resultant track direction is recorded in parentheses.

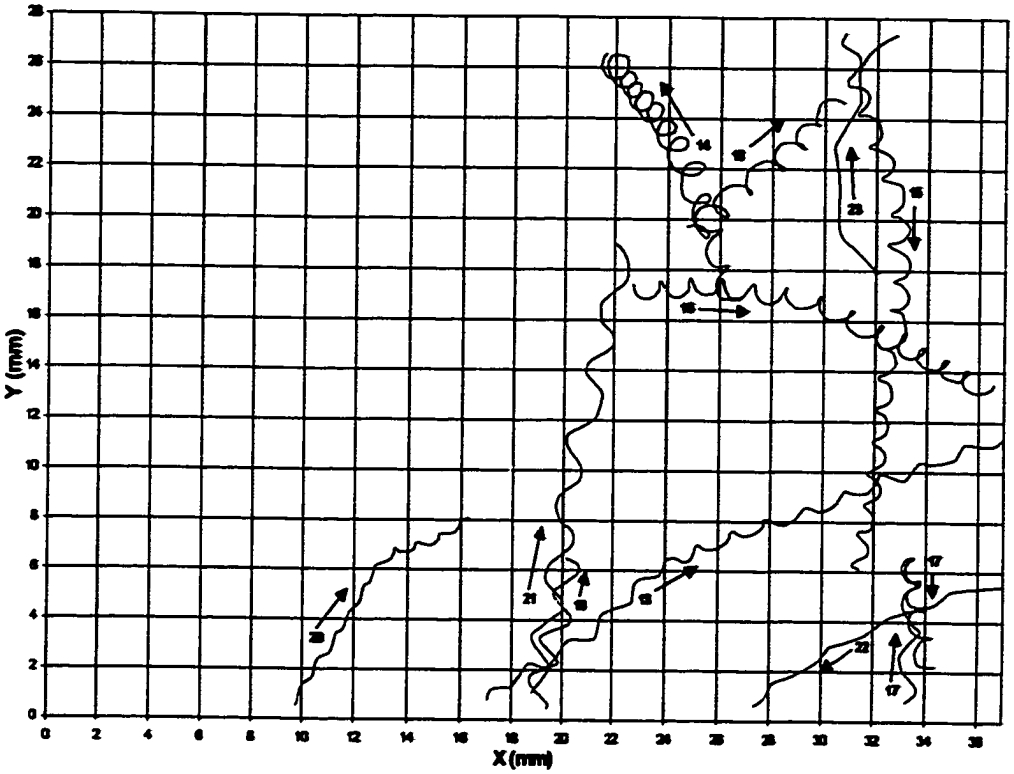

Fig A1.15b. Reconstructed tracks of swimming mussel larvae (*Mytilus edulis*) from SCA# 4L0, Day 3 Day recording session, May 22, 1996. Track direction indicated by arrows. Larvae #13-23.

Table A1.15b. Trajectory measurement data from tracks of swimming mussel larvae (*Mytilus edulis*) from SCA# 4L0, Day 3 Day recording session, May 22, 1996. Larvae #13-23.

LARVAL TRACK #	HELIX HEIGHT (mm)	HELIX DIAMETER (mm)	HELIX PITCH ANGLE	TIME (s)	ANGULAR VELOCITY (rad/s)	LINEAR VELOCITY (mm/s)	FORWARD VELOCITY (mm/s)	NGDR	TRACK DIRECTION (degrees)*
13	1.6	0.4	56	60.0	1.47	0.50	0.38	0.85	35, 21 (28)
14	1.6	0.8	39	78.5	0.57	0.27	0.14	0.34	308, 289 (298)
15	1.4	0.6	34	79.0	1.25	0.44	0.28	0.68	286, 262 (272)
16	1.3	0.7	24	50.5	1.42	0.58	0.29	0.53	4, 345, 333 (344)
17	2.0	0.6	57	42.0	N/A	N/A	0.25	0.12	89, 280 (51)
18	1.6	0.8	51	44.0	0.94	0.46	0.24	0.50	43
19	2.1	1.2	32	24.0	0.77	0.53	0.25	0.67	61
20	1.2	0.2	70	33.0	N/A	N/A	0.31	0.87	59, 27 (49)
21	3.0	0.9	51	39.0	0.99	0.64	0.47	0.81	78
22	2.6	0.2	75	17.0	1.56	0.66	0.64	0.96	196, 215 (207)
23	N/A	N/A	N/A	41.0	N/A	N/A	0.25	0.87	128, 92, 62 (86)
MEAN	**2.1**	**0.6**	**52.5**	**57.2**	**1.21**	**0.51**	**0.37**	**0.71**	**21.1**
s.d.	**0.9**	**0.3**	**12.6**	**31.4**	**0.33**	**0.10**	**0.12**	**0.25**	**67.5**
N	**21**	**21**	**21**	**23**	**16**	**17**	**23**	**23**	**23**

* Reference line, 0°, is the horizontal axis. For larvae that change track direction, net resultant track direction is recorded in parentheses.

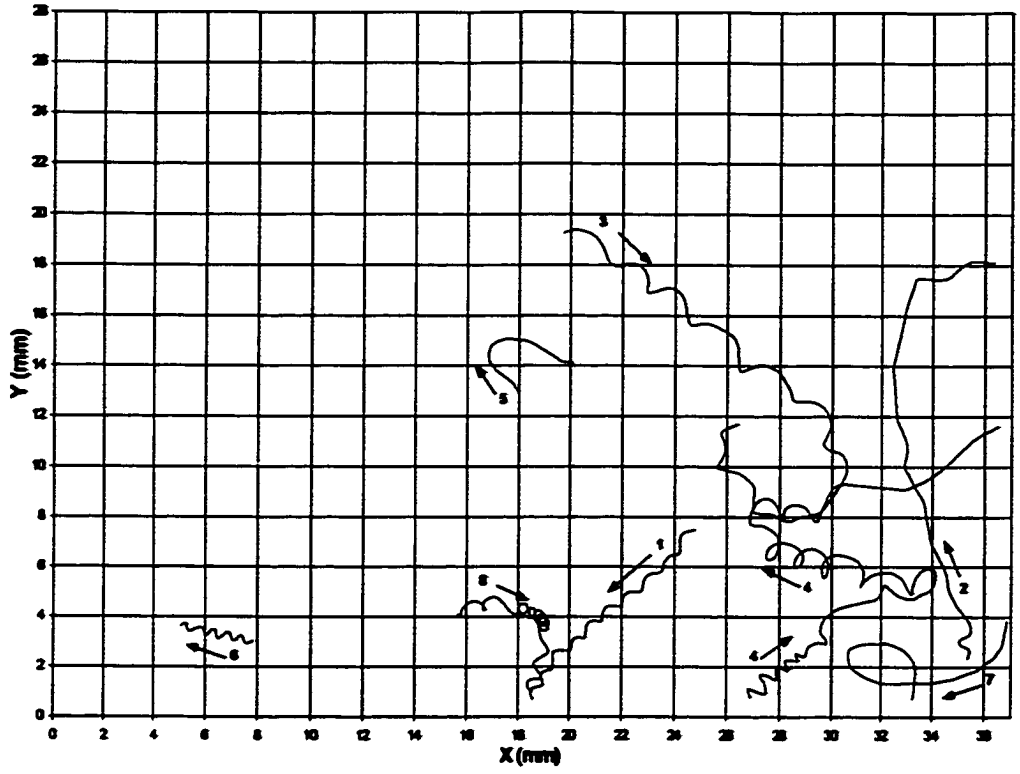

Fig A1.16. Reconstructed tracks of swimming mussel larvae (*Mytilus edulis*) from SCA# 3L0, Day 4 Night recording session, May 23, 1996. Track direction indicated by arrows.

Table A1.16. Trajectory measurement data from tracks of swimming mussel larvae (*Mytilus edulis*) from SCA# 3L0, Day 4 Night recording session, May 23, 1996.

LARVAL TRACK #	HELIX HEIGHT (mm)	HELIX DIAMETER (mm)	HELIX PITCH ANGLE	TIME (s)	ANGULAR VELOCITY (rad/s)	LINEAR VELOCITY (mm/s)	FORWARD VELOCITY (mm/s)	NGDR	TRACK DIRECTION (degrees) *
1	1.0	0.3	47	40.0	1.45	0.31	0.23	0.78	225
2	N/A	N/A	N/A	61.0	N/A	N/A	0.31	0.78	86, 108, 77, 19 (86)
3	2.0	0.8	29	149.0	N/A	N/A	0.21	0.51	321, 240, 168, 181, 355, 21 (336)
4	0.7	0.6	22	196.0	N/A	N/A	0.11	0.30	38, 202, 162, 114 (93)
5	N/A	0.3	N/A	211.7	N/A	N/A	0.03	N/A	(clockwise)
6	0.6	0.3	30	22.0	1.46	0.29	0.13	0.64	166
7	N/A	N/A	N/A	88.0	N/A	N/A	N/A	0.39	222
8	1.0	0.5	30.0	81.0	N/A	N/A	0.08	0.29	9, 330, 257 (313)
MEAN	**1.1**	**0.5**	**31.6**	**106.1**	**1.46**	**0.30**	**0.16**	**0.53**	**199.1**
s.d.	**0.6**	**0.2**	**8.2**	**71.2**	**0.01**	**0.01**	**0.10**	**0.21**	**76.9**
N	**5**	**6**	**5**	**8**	**2**	**2**	**7**	**7**	**7**

* Reference line, 0°, is the horizontal axis. For larvae that change track direction, net resultant track direction is recorded in parentheses.

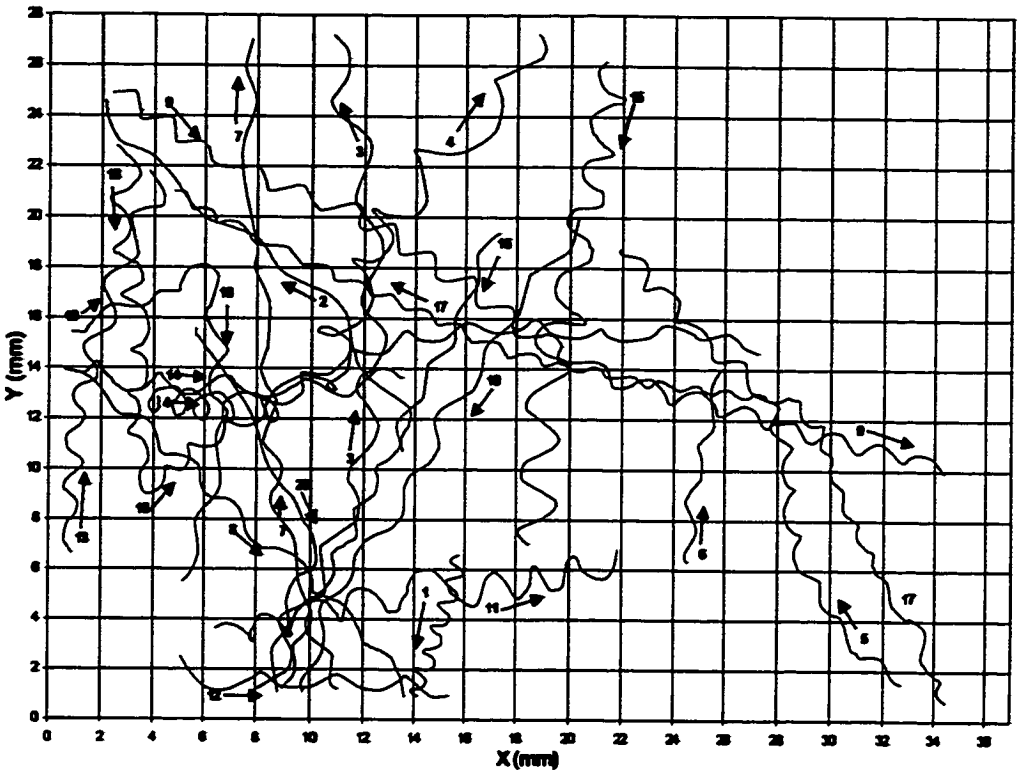

Fig A1.17. Reconstructed tracks of swimming mussel larvae (*Mytilus edulis*) from SCA# 3R0, Day 4 Night recording session, May 23, 1996. Track direction indicated by arrows.

Table A1.17. Trajectory measurement data from tracks of swimming mussel larvae (*Mytilus edulis*) from SCA# 3R0, Day 4 Night recording session, May 23, 1996.

LARVAL TRACK #	HELIX HEIGHT (mm)	HELIX DIAMETER (mm)	HELIX PITCH ANGLE	TIME (s)	ANGULAR VELOCITY (rad/s)	LINEAR VELOCITY (mm/s)	FORWARD VELOCITY (mm/s)	NGDR	TRACK DIRECTION (degrees) *
1	1.0	0.5	27	23.0	1.69	0.51	0.26	0.57	254
2	4.3	0.5	76	44.0	0.60	0.44	0.41	0.91	119, 138 (129)
3	3.1	0.9	54	58.0	0.94	0.64	0.47	0.84	67, 89, 105 (84)
4	2.2	1.2	25	84.0	N/A	N/A	0.28	0.47	357, 63 (45)
5	1.8	0.4	61	44.0	1.65	0.59	0.48	0.82	134, 92, 136 (213)
6	2.3	0.4	66	15.0	1.43	0.60	0.53	0.92	79
7	2.9	0.5	71	72.0	N/A	N/A	0.36	0.95	105, 92 (97)
8	2.4	0.7	51	37.0	1.32	0.70	0.50	0.89	316
9	1.9	0.8	40	112.0	1.03	0.52	0.32	0.77	330, 345 (335)
10	2.0	0.4	70	53.0	1.11	0.42	0.35	0.52	25, 269, 245 (293)
11	1.9	1.2	42	57.0	0.91	0.59	0.28	0.59	11
12	2.7	0.6	58	25.0	0.97	0.52	0.42	0.86	358
13	2.0	0.7	37	50.5	0.97	0.47	0.31	0.79	86, 67 (79)
14	2.7	0.8	44	45.1	0.85	0.38	0.28	0.81	359
15	2.1	1.1	30	52.0	1.10	0.73	0.37	0.63	260
16	2.1	0.6	61	44.0	1.38	0.59	0.45	0.92	244
17	1.5	0.4	50	108.0	1.49	0.46	0.36	0.82	115, 174, 155 (146)
18	2.1	0.5	55	114.0	1.04	0.44	0.34	0.53	278, 34, 4, 356 (342)
19	3.1	0.5	65	35.0	1.25	0.69	0.62	0.93	239
20	2.7	0.5	50	36.0	N/A	N/A	0.44	0.91	300, 254 (282)
MEAN	**2.3**	**0.7**	**51.7**	**55.4**	**1.16**	**0.55**	**0.39**	**0.77**	**337.7**
s.d.	**0.7**	**0.3**	**14.4**	**28.8**	**0.31**	**0.11**	**0.10**	**0.16**	**72.9**
N	**20**	**20**	**20**	**20**	**17**	**17**	**20**	**20**	**20**

* Reference line, 0°, is the horizontal axis. For larvae that change track direction, net resultant track direction is recorded in parentheses.

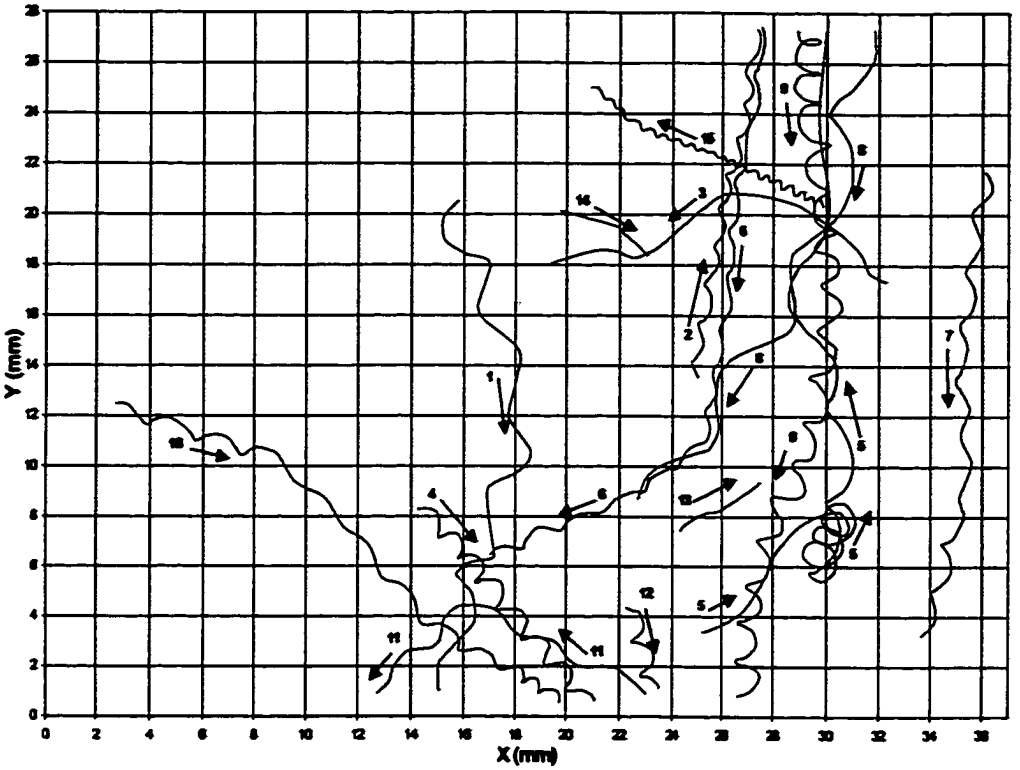

Fig A1.18. Reconstructed tracks of swimming mussel larvae (*Mytilus edulis*) from SCA# 4L0, Day 4 Night recording session, May 23, 1996. Track direction indicated by arrows.

Table A1.18. Trajectory measurement data from tracks of swimming mussel larvae (*Mytilus edulis*) from SCA# 4L0, Day 4 Night recording session, May 23, 1996.

LARVAL TRACK #	HELIX HEIGHT (mm)	HELIX DIAMETER (mm)	HELIX PITCH ANGLE	TIME (s)	ANGULAR VELOCITY (rad/s)	LINEAR VELOCITY (mm/s)	FORWARD VELOCITY (mm/s)	NGDR	TRACK DIRECTION (degrees) *
1	3.9	1.1	53	33.0	N/A	N/A	0.63	0.80	292, 254 (268)
2	1.6	0.3	68	44.5	1.22	0.37	0.32	0.89	80
3	N/A	N/A	N/A	56.0	N/A	N/A	0.26	0.85	146, 200 (177)
4	1.5	0.8	37	42.5	0.99	0.45	0.24	0.66	309
5	N/A	N/A	N/A	101.5	N/A	N/A	N/A	0.53	43, 249, 85, 130, 81 (79)
6	2.0	0.3	72	82.0	0.96	0.35	0.32	0.84	262, 208 (243)
7	2.4	0.4	58	39.0	1.27	0.56	0.48	0.89	263
8	5.9	1.5	44	43.0	0.52	0.63	0.49	0.88	280, 234 (244)
9	1.9	0.8	34	80.0	1.13	0.57	0.34	0.63	276, 253, 282 (265)
10	1.9	0.5	50	88.0	N/A	N/A	0.24	0.84	342, 318 (325)
11	2.6	0.4	68	51.5	0.58	0.26	0.24	0.76	152, 223 (180)
12	1.4	0.6	33	12.5	1.25	0.48	0.28	0.70	284
13	N/A	N/A	N/A	212.9	N/A	N/A	0.02	0.98	31
14	N/A	N/A	N/A	212.9	N/A	N/A	0.02	0.97	344, 313 (332)
15	0.6	0.2	56	86.0	1.25	0.16	0.12	0.77	157
MEAN	**2.3**	**0.6**	**52.1**	**79.8**	**1.02**	**0.43**	**0.29**	**0.80**	**266.9**
s.d.	**1.5**	**0.4**	**13.2**	**60.6**	**0.29**	**0.15**	**0.17**	**0.13**	**67.3**
N	**11**	**11**	**11**	**15**	**9**	**9**	**14**	**15**	**15**

* Reference line, 0°, is the horizontal axis. For larvae that change track direction, net resultant track direction is recorded in parentheses.

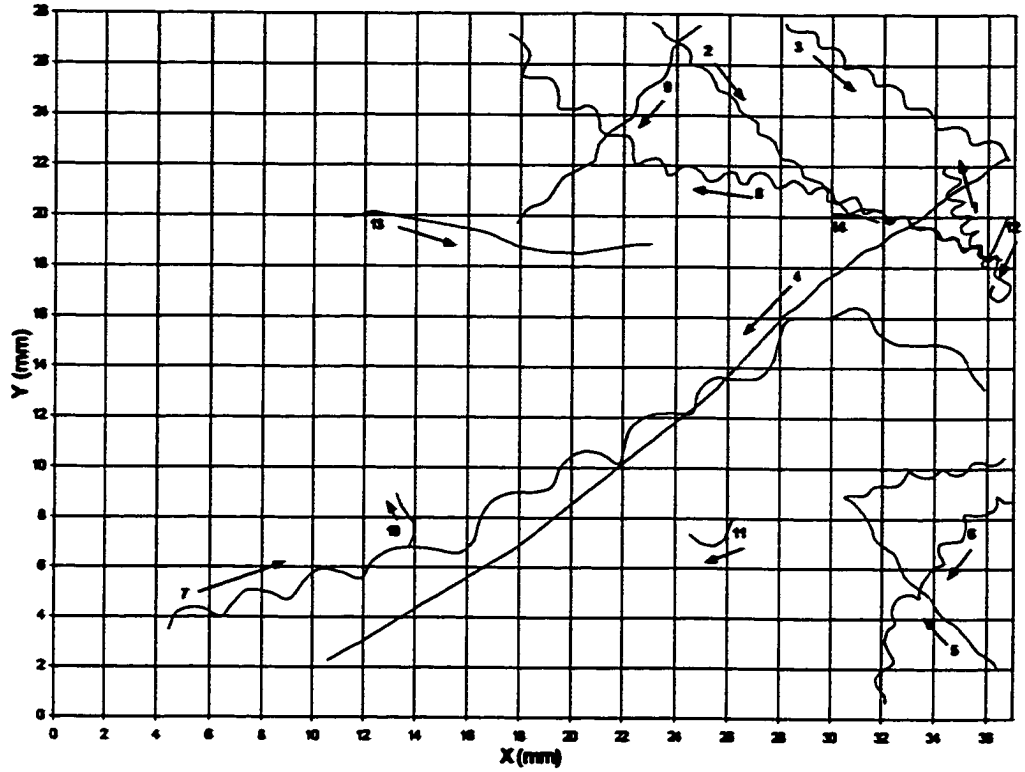

Fig A1.19. Reconstructed tracks of swimming mussel larvae (*Mytilus edulis*) from SCA# 3L0, Day 4 Day recording session, May 23, 1996. Track direction indicated by arrows.

Table A1.19. Trajectory measurement data from tracks of swimming mussel larvae (*Mytilus edulis*) from SCA# 3L0, Day 4 Day recording session, May 23, 1996.

LARVAL TRACK #	HELIX HEIGHT (mm)	HELIX DIAMETER (mm)	HELIX PITCH ANGLE	TIME (s)	ANGULAR VELOCITY (rad/s)	LINEAR VELOCITY (mm/s)	FORWARD VELOCITY (mm/s)	NGDR	TRACK DIRECTION (degrees)*
1	0.6	0.6	17	60.5	N/A	N/A	0.07	0.51	110
2	1.0	0.4	48	49.0	2.35	0.58	0.36	0.83	316, 336 (325)
3	1.6	0.5	57	39.0	1.08	0.36	0.27	0.82	328
4	N/A	N/A	N/A	122.0	N/A	0.28	0.28	0.99	218
5	1.9	0.2	69	76.0	N/A	N/A	0.20	0.50	130, 15 (86)
6	1.6	0.5	49	87.0	0.46	0.16	0.12	0.71	222, 262 (239)
7	3.5	1.3	42	131.0	0.50	0.43	0.28	0.36	26, 331 (17)
8	1.7	0.6	46	154.0	0.58	0.24	0.15	0.63	102, 162, 141 (152)
9	2.1	0.4	26	35.0	0.91	0.36	0.31	0.95	229
10	N/A	N/A	N/A	212.4	N/A	N/A	N/A	N/A	71, 118 (103)
11	N/A	N/A	N/A	212.4	N/A	N/A	N/A	N/A	246, 147 (202)
12	N/A	N/A	N/A	212.4	N/A	N/A	N/A	N/A	245
13	N/A	0.4	N/A	212.4	N/A	N/A	0.06	N/A	355
14	N/A	N/A	N/A	212.4	N/A	N/A	N/A	N/A	349
MEAN	**1.7**	**0.6**	**44.3**	**129.7**	**0.98**	**0.34**	**0.21**	**0.76**	**263.9**
s.d.	**0.9**	**0.3**	**16.3**	**72.4**	**0.71**	**0.14**	**0.10**	**0.21**	**77.4**
N	**8**	**9**	**8**	**14**	**6**	**7**	**10**	**9**	**14**

* Reference line, 0°, is the horizontal axis. For larvae that change track direction, net resultant track direction is recorded in parentheses.

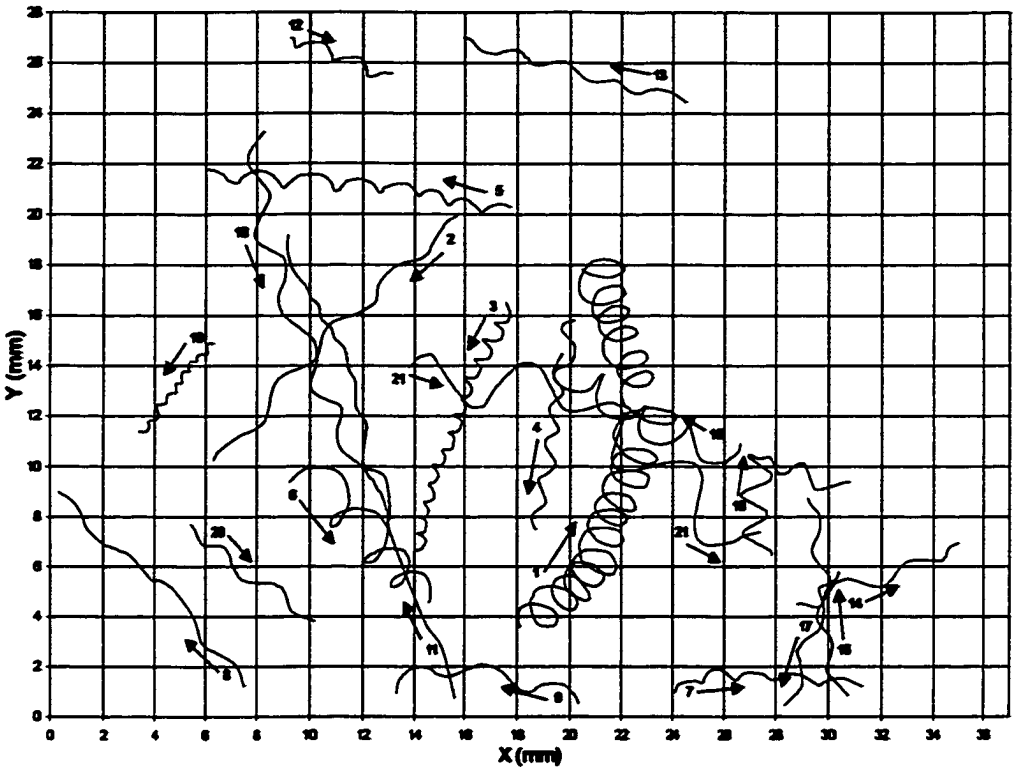

Fig A1.20. Reconstructed tracks of swimming mussel larvae (*Mytilus edulis*) from SCA# 3R0, Day 4 Day recording session, May 23, 1996. Track direction indicated by arrows.

Table A1.20. Trajectory measurement data from tracks of swimming mussel larvae (*Mytilus edulis*) from SCA# 3R0, Day 4 Day recording session, May 23, 1996.

LARVAL TRACK #	HELIX HEIGHT (mm)	HELIX DIAMETER (mm)	HELIX PITCH ANGLE	TIME (s)	ANGULAR VELOCITY (rad/s)	LINEAR VELOCITY (mm/s)	FORWARD VELOCITY (mm/s)	NGDR	TRACK DIRECTION (degrees) *
1	0.9	1.3	12	132.0	0.90	0.60	0.13	0.20	40, 69, 112 (61)
2	3.0	0.5	63	21.0	1.34	0.72	0.64	0.94	22
3	0.9	0.4	39	69.0	1.12	0.28	0.15	0.64	251
4	1.5	0.4	2	27.0	1.29	0.40	0.31	0.80	260
5	1.7	0.5	53	38.0	1.12	0.42	0.31	0.82	173
6	1.9	1.6	26	32.0	0.73	0.63	0.22	0.45	313
7	1.5	0.4	54	21.0	1.43	0.44	0.35	0.86	333, 18 (182)
8	3.5	0.5	66	23.0	0.82	0.50	0.46	0.95	134
9	3.1	0.7	53	23.0	0.65	0.40	0.32	0.81	169, 199 (356)
10	1.6	1.0	26	42.0	0.70	0.39	0.18	0.35	92, 338 (44)
11	2.1	0.3	80	41.0	1.42	0.52	0.48	0.97	110
12	1.6	0.5	49	10.5	N/A	N/A	0.38	0.79	336
13	1.9	0.4	61	18.5	1.60	0.56	0.49	0.90	164
14	2.8	0.7	57	14.0	1.08	0.61	0.48	0.87	20
15	2.1	1.2	14	37.0	0.65	0.44	0.22	0.55	154
16	2.7	0.6	62	17.5	1.09	0.58	0.46	0.91	97
17	2.8	0.5	61	17.0	0.76	0.40	0.34	0.90	250
18	2.8	0.9	53	40.5	0.90	0.56	0.40	0.86	283, 297 (287)
19	0.5	0.2	29	30.0	2.06	0.25	0.15	0.77	232
20	2.6	0.6	58	28.0	0.53	0.27	0.22	0.89	321
21	4.0	2.0	40	62.0	0.40	0.47	0.25	0.66	355, 317 (334)
MEAN	**2.2**	**0.7**	**46.9**	**36.4**	**1.03**	**0.47**	**0.33**	**0.76**	**389.5**
s.d.	**0.9**	**0.5**	**19.6**	**26.6**	**0.41**	**0.13**	**0.14**	**0.21**	**78.4**
N	**21**	**21**	**21**	**21**	**20**	**20**	**21**	**21**	**21**

* Reference line, 0°, is the horizontal axis. For larvae that change track direction, net resultant track direction is recorded in parentheses.

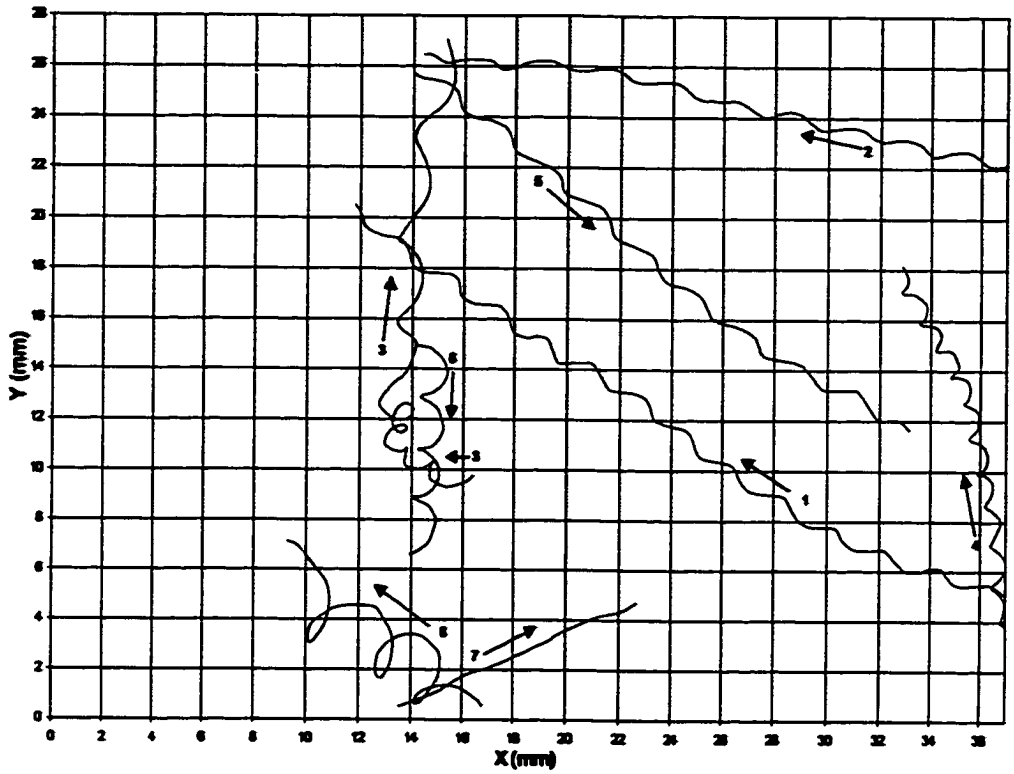

Fig A1.21. Reconstructed tracks of swimming mussel larvae (*Mytilus edulis*) from SCA# 4L0, Day 4 Day recording session, May 23, 1996. Track direction indicated by arrows.

Table A1.21. Trajectory measurement data from tracks of swimming mussel larvae (*Mytilus edulis*) from SCA# 4L0, Day 4 Day recording session, May 23, 1996.

LARVAL TRACK #	HELIX HEIGHT (mm)	HELIX DIAMETER (mm)	HELIX PITCH ANGLE	TIME (s)	ANGULAR VELOCITY (rad/s)	LINEAR VELOCITY (mm/s)	FORWARD VELOCITY (mm/s)	NGDR	TRACK DIRECTION (degrees) *
1	2.3	0.5	67	73.0	1.14	0.49	0.41	0.90	164, 145 (149)
2	2.4	0.3	66	59.0	1.04	0.43	0.39	0.95	168
3	3.4	0.9	52	95.0	N/A	N/A	0.21	0.63	153, 83 (94)
4	1.5	0.5	48	56.8	1.14	0.40	0.27	0.76	94, 116 (106)
5	2.5	0.5	58	51.0	1.18	0.54	0.47	0.92	323
6	2.0	0.9	30	27.0	0.96	0.53	0.31	0.68	266
7	N/A	N/A	N/A	22.0	N/A	0.46	0.46	1.00	25
8	3.2	2.4	16	40.0	0.49	0.63	0.25	0.48	147
MEAN	**2.4**	**0.8**	**48.3**	**53.0**	**1.00**	**0.50**	**0.35**	**0.79**	**123.7**
s.d.	**0.7**	**0.7**	**17.4**	**24.0**	**0.26**	**0.08**	**0.10**	**0.18**	**67.3**
N	**7**	**7**	**7**	**8**	**6**	**7**	**8**	**8**	**8**

* Reference line, 0°, is the horizontal axis. For larvae that change track direction, net resultant track direction is recorded in parentheses.

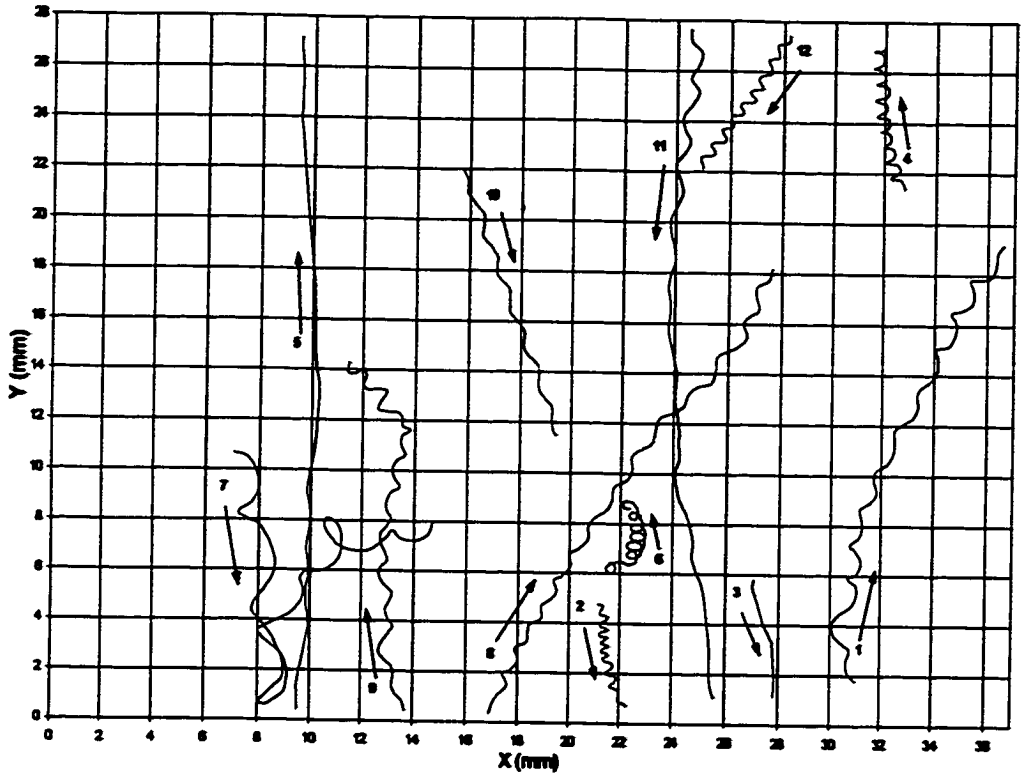

Fig A1.22. Reconstructed tracks of swimming mussel larvae (*Mytilus edulis*) from SCA# 3L0, Day 5 Night recording session, May 24, 1996. Track direction indicated by arrows.

Table A1.22. Trajectory measurement data from tracks of swimming mussel larvae (*Mytilus edulis*) from SCA# 3L0, Day 5 Night recording session, May 24, 1996.

LARVAL TRACK #	HELIX HEIGHT (mm)	HELIX DIAMETER (mm)	HELIX PITCH ANGLE	TIME (s)	ANGULAR VELOCITY (rad/s)	LINEAR VELOCITY (mm/s)	FORWARD VELOCITY (mm/s)	NGDR	TRACK DIRECTION (degrees) *
1	1.7	0.5	51	62.0	1.14	0.43	0.32	0.78	102, 72 (72)
2	0.4	0.3	35	51.0	1.37	0.20	0.09	0.55	282
3	N/A	0.2	N/A	183.8	N/A	N/A	0.03	N/A	279
4	0.7	0.5	18	71.0	0.84	0.22	0.09	0.50	99
5	N/A	N/A	N/A	106.0	N/A	0.26	0.26	0.99	90
6	0.4	0.4	N/A	50.4	0.99	0.20	0.06	0.19	26, 91 (69)
7	4.0	1.3	38	127.0	N/A	N/A	0.17	0.25	277, 79, 52, 9 (341)
8	1.1	0.4	40	85.0	1.44	0.39	0.25	0.81	59
9	1.3	0.4	46	78.0	0.91	0.25	0.19	0.71	102, 83, 134 (99)
10	1.6	0.3	71	23.0	1.95	0.60	0.50	0.94	290
11	N/A	N/A	N/A	73.0	N/A	N/A	0.38	0.94	273
12	0.7	0.4	39	74.0	0.77	0.17	0.09	0.67	237
MEAN	**1.3**	**0.5**	**42.2**	**82.9**	**1.16**	**0.30**	**0.20**	**0.67**	**17.9**
s.d.	**1.1**	**0.3**	**14.6**	**41.7**	**0.39**	**0.14**	**0.14**	**0.27**	**73.5**
N	**9**	**10**	**8**	**12**	**8**	**9**	**12**	**11**	**12**

* Reference line, 0°, is the horizontal axis. For larvae that change track direction, net resultant track direction is recorded in parentheses.

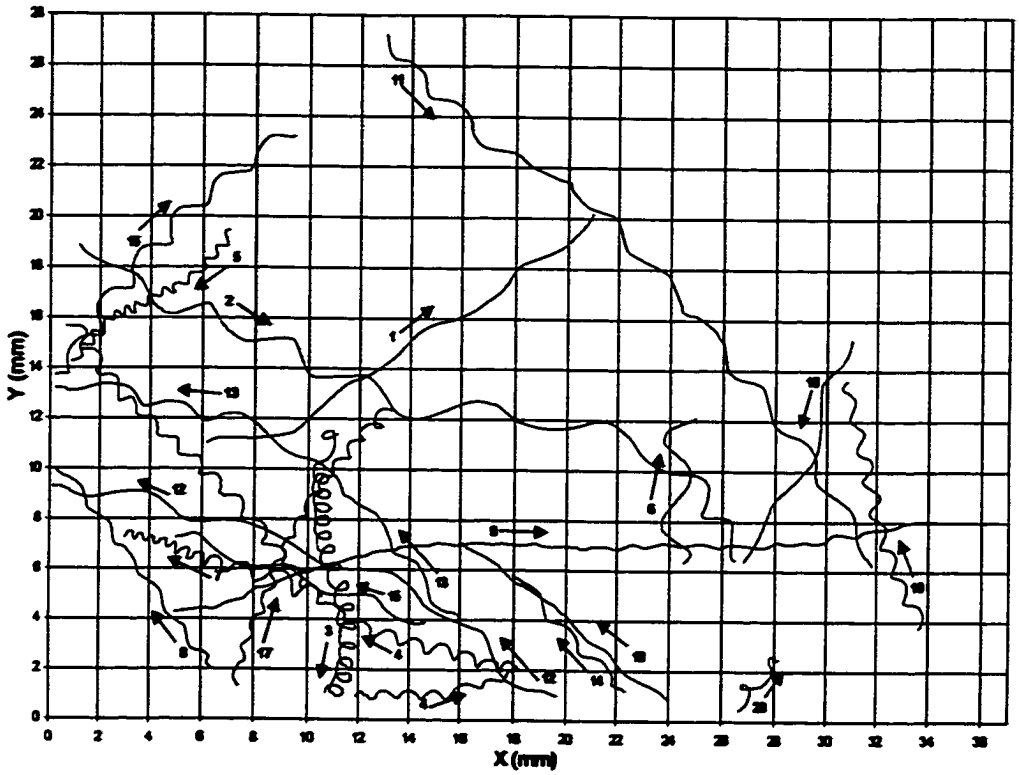

Fig A1.23. Reconstructed tracks of swimming mussel larvae (*Mytilus edulis*) from SCA# 3R0, Day 5 Night recording session, May 24, 1996. Track direction indicated by arrows.

Table A1.23. Trajectory measurement data from tracks of swimming mussel larvae (*Mytilus edulis*) from SCA# 3R0, Day 5 Night recording session, May 24, 1996.

LARVAL TRACK #	HELIX HEIGHT (mm)	HELIX DIAMETER (mm)	HELIX PITCH ANGLE	TIME (s)	ANGULAR VELOCITY (rad/s)	LINEAR VELOCITY (mm/s)	FORWARD VELOCITY (mm/s)	NGDR	TRACK DIRECTION (degrees) *
1	3.9	0.3	82	80.0	0.35	0.23	0.22	0.96	37
2	3.4	0.9	47	74.5	N/A	N/A	0.39	0.84	315, 333, 353 (334)
3	0.6	0.6	5	91.0	1.24	0.38	0.12	0.33	267, 286, 250 (268)
4	1.2	0.5	39	101.0	1.56	0.48	0.29	0.47	2, 23, 165, 132 (128)
5	0.6	0.3	36	154.0	0.52	0.09	0.05	0.66	226, 205, 227 (220)
6	3.5	1.0	57	21.0	0.50	0.38	0.28	0.74	89
7	0.8	0.6	34	47.0	N/A	N/A	0.17	0.60	161
8	1.7	0.3	64	46.0	0.79	0.25	0.22	0.93	126
9	1.3	0.1	80	106.0	1.39	0.29	0.28	0.97	18, 359, 12 (7)
10	1.2	0.4	52	31.5	1.68	0.47	0.33	0.79	105
11	2.9	0.7	58	64.0	0.96	0.55	0.44	0.91	319, 304 (312)
12	4.1	0.7	68	45.0	0.73	0.54	0.48	0.93	145, 169 (157)
13	3.0	0.4	73	51.0	0.80	0.41	0.38	0.89	134, 168 (150)
14	2.0	0.5	58	36.0	0.55	0.22	0.18	0.90	132
15	3.5	0.5	73	16.0	1.14	0.69	0.64	0.94	160
16	2.2	0.7	47	42.0	0.91	0.45	0.32	0.81	48
17	1.1	0.2	61	80.0	0.89	0.19	0.16	0.76	72, 50 (62)
18	5.1	0.8	70	41.0	0.29	0.27	0.24	0.96	245
19	2.0	0.2	79	30.0	1.08	0.36	0.34	0.98	141
20	1.6	0.6	53	13.0	0.78	0.31	0.19	0.63	55
MEAN	**2.3**	**0.5**	**57.1**	**58.5**	**0.90**	**0.36**	**0.29**	**0.80**	**114.6**
s.d.	**1.3**	**0.2**	**18.1**	**35.5**	**0.39**	**0.15**	**0.14**	**0.18**	**66.5**
N	**20**	**20**	**20**	**20**	**18**	**18**	**20**	**20**	**20**

* Reference line, 0°, is the horizontal axis. For larvae that change track direction, net resultant track direction is recorded in parentheses.

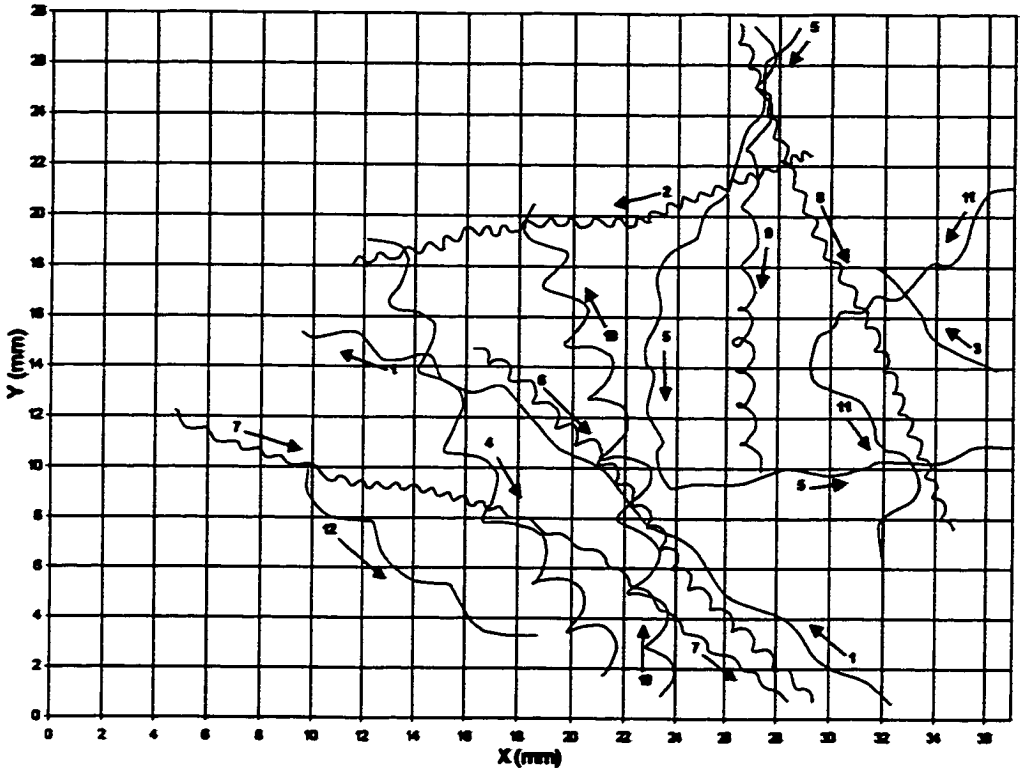

Fig A1.24. Reconstructed tracks of swimming mussel larvae (*Mytilus edulis*) from SCA# 4L0, Day 5 Night recording session, May 24, 1996. Track direction indicated by arrows.

Table A1.24. Trajectory measurement data from tracks of swimming mussel larvae (*Mytilus edulis*) from SCA# 4L0, Day 5 Night recording session, May 24, 1996.

LARVAL TRACK #	HELIX HEIGHT (mm)	HELIX DIAMETER (mm)	HELIX PITCH ANGLE	TIME (s)	ANGULAR VELOCITY (rad/s)	LINEAR VELOCITY (mm/s)	FORWARD VELOCITY (mm/s)	NGDR	TRACK DIRECTION (degrees) *
1	4.9	0.5	71	73.0	N/A	N/A	0.38	0.93	141, 159 (147)
2	0.7	0.3	43	60.0	2.75	0.53	0.31	0.71	203, 183, 195 (194)
3	N/A	0.2	N/A	221.7	N/A	N/A	0.03	0.97	152, 116, 135 (139)
4	3.2	1.3	40	51.0	0.74	0.62	0.38	0.68	296
5	3.7	0.5	73	105.0	N/A	N/A	0.31	0.54	242, 275, 8 (296)
6	1.0	0.5	31	93.0	1.26	0.36	0.21	0.71	312
7	0.8	0.4	47	58.0	3.84	0.87	0.46	0.86	338, 350, 323 (334)
8	0.9	0.4	28	66.0	2.31	0.57	0.33	0.78	293
9	2.4	0.7	50	68.0	N/A	N/A	0.26	0.72	269
10	2.4	1.4	26	60.8	0.87	0.68	0.33	0.65	106
11	N/A	N/A	N/A	77.0	N/A	N/A	0.26	0.70	218, 309, 221 (251)
12	3.8	0.9	60	26.0	0.70	0.54	0.43	0.88	322
MEAN	**2.4**	**0.6**	**46.8**	**80.8**	**1.78**	**0.58**	**0.31**	**0.76**	**276.1**
s.d.	**1.5**	**0.4**	**15.9**	**48.9**	**1.21**	**0.16**	**0.11**	**0.13**	**59.9**
N	**10**	**11**	**10**	**12**	**7**	**7**	**12**	**12**	**10**

* Reference line, 0°, is the horizontal axis. For larvae that change track direction, net resultant track direction is recorded in parentheses.

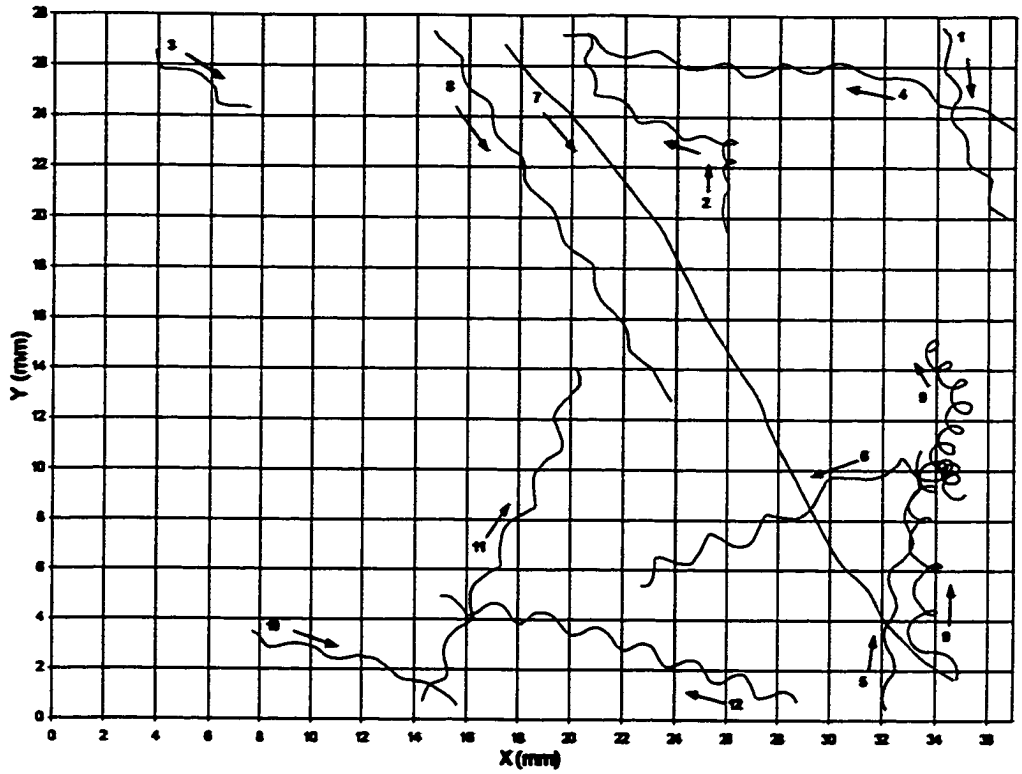

Fig A1.25. Reconstructed tracks of swimming mussel larvae (*Mytilus edulis*) from SCA# 3L0, Day 5 Day recording session, May 24, 1996. Track direction indicated by arrows.

Table A1.25. Trajectory measurement data from tracks of swimming mussel larvae (*Mytilus edulis*) from SCA# 3L0, Day 5 Day recording session, May 24, 1996.

LARVAL TRACK #	HELIX HEIGHT (mm)	HELIX DIAMETER (mm)	HELIX PITCH ANGLE	TIME (s)	ANGULAR VELOCITY (rad/s)	LINEAR VELOCITY (mm/s)	FORWARD VELOCITY (mm/s)	NGDR	TRACK DIRECTION (degrees) *
1	2.2	0.4	68	28.0	0.88	0.35	0.30	0.88	290
2	1.9	0.5	80	95.0	N/A	N/A	0.13	0.66	90, 155, 107 (124)
3	2.7	0.5	58	18.0	0.56	0.29	0.24	0.87	327
4	2.6	0.6	60	45.0	0.98	0.49	0.41	0.91	168
5	2.6	0.5	62	50.0	0.52	0.25	0.21	0.92	83
6	2.4	1.0	46	126.7	N/A	N/A	0.12	0.57	106, 158, 205 (197)
7	N/A	N/A	N/A	57.0	N/A	0.56	0.55	0.99	305
8	2.5	0.4	57	44.9	0.99	0.45	0.39	0.56	303
9	2.0	1.1	25	98.5	N/A	N/A	0.15	0.23	95, 67, 121 (95)
10	2.6	0.4	66	38.0	0.54	0.25	0.23	0.93	338
11	2.5	0.6	63	78.0	0.48	0.23	0.19	0.87	65
12	2.0	0.7	45	57.0	0.82	0.39	0.26	0.81	162
MEAN	**2.4**	**0.6**	**55.6**	**61.3**	**0.72**	**0.36**	**0.27**	**0.77**	**61.7**
s.d.	**0.3**	**0.2**	**11.8**	**32.1**	**0.22**	**0.12**	**0.13**	**0.22**	**79.4**
N	**11**	**11**	**11**	**12**	**8**	**9**	**12**	**12**	**12**

* Reference line, 0°, is the horizontal axis. For larvae that change track direction, net resultant track direction is recorded in parentheses.

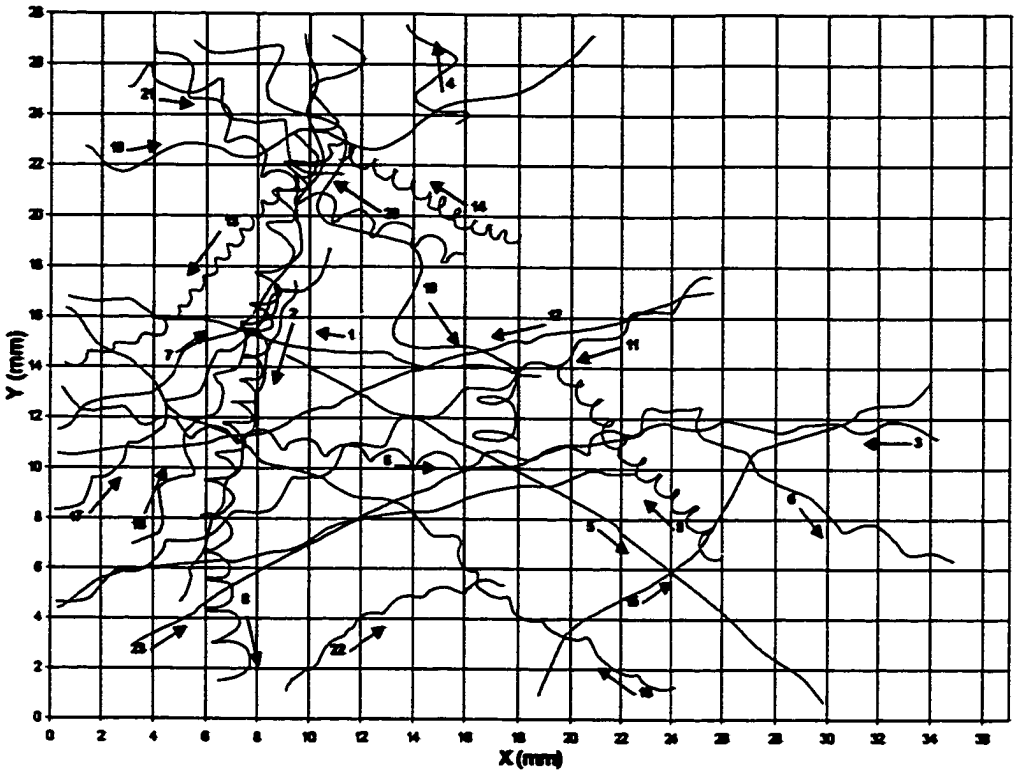

Fig A1.26. Reconstructed tracks of swimming mussel larvae (*Mytilus edulis*) from SCA# 3R0, Day 5 Day recording session, May 24, 1996. Track direction indicated by arrows.

Table A1.26. Trajectory measurement data from tracks of swimming mussel larvae (*Mytilus edulis*) from SCA# 3R0, Day 5 Day recording session, May 24, 1996.

LARVAL TRACK #	HELIX HEIGHT (mm)	HELIX DIAMETER (mm)	HELIX PITCH ANGLE	TIME (s)	ANGULAR VELOCITY (rad/s)	LINEAR VELOCITY (mm/s)	FORWARD VELOCITY (mm/s)	NGDR	TRACK DIRECTION (degrees) *
1	3.8	0.4	78	36.5	0.83	0.53	0.50	0.98	170
2	1.7	0.3	68	48.0	1.03	0.32	0.28	0.96	250
3	2.6	0.4	75	63.0	N/A	N/A	0.53	0.95	180, 196, 211 (195)
4	2.4	1.8	23	17.0	0.69	0.68	0.26	0.58	105
5	N/A	N/A	N/A	48.0	N/A	0.53	0.52	0.99	332, 312 (326)
6	1.7	0.6	50	121.0	1.11	0.45	0.31	0.80	350, 20, 329 (349)
7	3.9	0.8	55	47.0	0.70	0.51	0.44	0.85	32, 87 (59)
8	1.3	1.1	20	134.0	0.97	0.58	0.20	0.47	253, 278 (260)
9	0.9	0.7	14	52.0	1.31	0.51	0.19	0.79	131
10	4.6	0.8	60	33.0	0.85	0.71	0.62	0.98	5, 33 (13)
11	2.3	0.7	59	58.0	1.31	0.67	0.49	0.90	207
12	N/A	N/A	N/A	91.0	N/A	0.29	0.29	0.98	195, 202, 186 (194)
13	0.8	0.4	35	93.0	1.19	0.27	0.16	0.72	227, 201 (220)
14	0.9	0.6	25	59.0	0.85	0.28	0.13	0.45	150
15	10.0	1.3	73	50.0	0.25	0.44	0.40	0.94	43, 20 (40)
16	1.5	0.4	54	69.0	N/A	N/A	0.41	0.92	148
17	2.2	0.5	58	31.0	1.17	0.50	0.42	0.81	45
18	2.3	0.6	44	41.5	0.92	0.45	0.34	0.80	56
19	5.6	2.5	27	91.0	N/A	N/A	0.22	0.60	303, 270 (308)
20	1.8	0.8	36	70.5	0.76	0.36	0.21	0.65	158, 130 (145)
21	3.0	1.0	31	34.0	0.58	0.41	0.28	0.73	17, 325 (337)
22	1.7	0.4	67	34.0	1.05	0.34	0.29	0.88	43, 13 (27)
23	4.8	0.4	81	52.0	0.58	0.45	0.44	0.98	13
MEAN	**2.9**	**0.8**	**49.3**	**59.7**	**0.9**	**0.46**	**0.34**	**0.81**	**83.8**
s.d.	**2.1**	**0.5**	**28.1**	**29.2**	**0.28**	**0.13**	**0.14**	**0.17**	**77.5**
N	**21**	**21**	**21**	**23**	**18**	**20**	**23**	**23**	**23**

* Reference line, 0°, is the horizontal axis. For larvae that change track direction, net resultant track direction is recorded in parentheses.

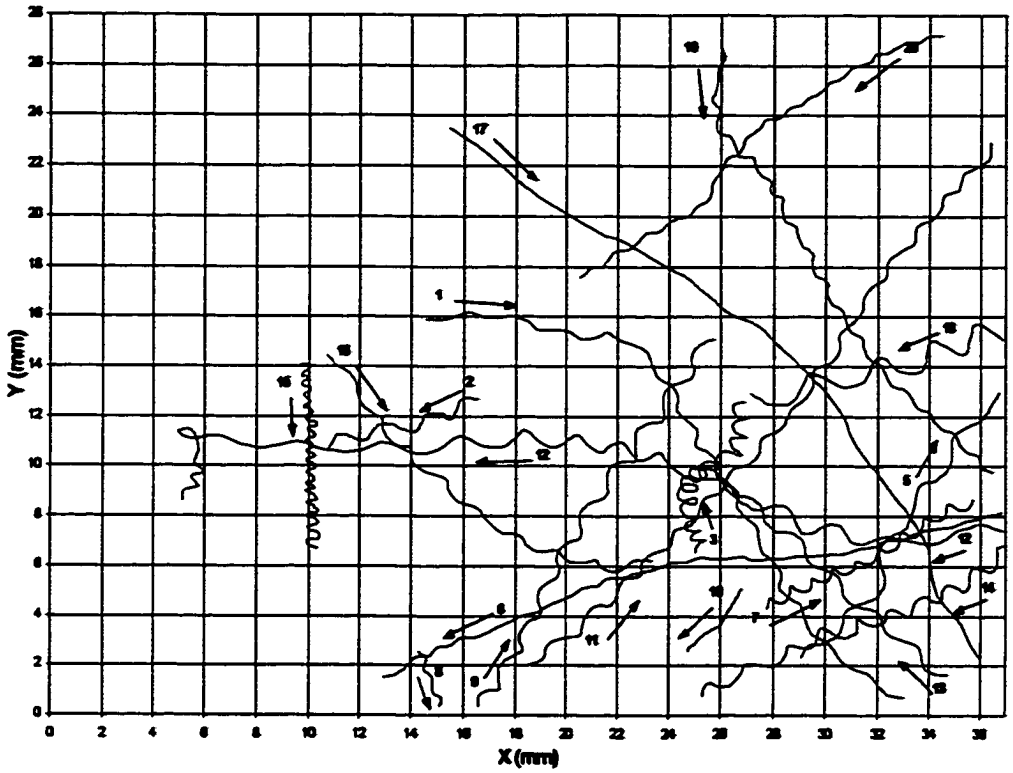

Fig A1.27. Reconstructed tracks of swimming mussel larvae (*Mytilus edulis*) from SCA# 3L0, Day 6 Night recording session, May 25, 1996. Track direction indicated by arrows.

Table A1.27. Trajectory measurement data from tracks of swimming mussel larvae (*Mytilus edulis*) from SCA# 3L0, Day 6 Night recording session, May 25, 1996.

LARVAL TRACK #	HELIX HEIGHT (mm)	HELIX DIAMETER (mm)	HELIX PITCH ANGLE	TIME (s)	ANGULAR VELOCITY (rad/s)	LINEAR VELOCITY (mm/s)	FORWARD VELOCITY (mm/s)	NGDR	TRACK DIRECTION (degrees) *
1	1.8	0.4	56	96.0	0.95	0.34	0.28	0.84	351, 300 (321)
2	1.9	0.6	52	37.7	0.57	0.23	0.17	0.80	200
3	0.8	0.7	13	138.0	N/A	N/A	0.05	0.33	104, 37, 87 (73)
5	2.7	0.5	50	43.0	0.74	0.37	0.32	0.89	54
6	1.4	0.3	65	89.0	1.31	0.34	0.29	0.93	196
7	1.0	0.4	44	37.7	1.59	0.42	0.25	0.66	27
8	0.8	0.2	56	11.0	1.67	0.28	0.22	0.70	290
9	1.8	0.5	41	99.6	0.61	0.24	0.18	0.80	57
10	1.3	0.3	60	94.0	1.13	0.29	0.22	0.82	264, 307 (302)
11	1.6	0.5	50	66.0	1.70	0.62	0.43	0.85	49
12	2.4	0.7	48	112.0	N/A	N/A	0.32	0.73	184, 157, 180, 256 (178)
13	2.1	0.5	58	76.0	0.52	0.22	0.17	0.89	137
14	1.3	0.6	31	49.0	1.30	0.47	0.28	0.72	204
15	0.4	0.3	17	51.3	2.07	0.36	0.15	0.48	272
16	1.5	0.4	62	46.0	1.41	0.46	0.34	0.85	313, 346 (327)
17	N/A	N/A	N/A	72.0	N/A	0.43	0.43	0.96	325, 298 (314)
18	2.8	1.0	34	35.0	0.67	0.43	0.29	0.72	196
19	N/A	N/A	N/A	220.9	N/A	N/A	N/A	N/A	232
20	1.0	0.2	54	104.0	1.06	0.19	0.17	0.87	208, 238, 208 (215)
MEAN	**1.6**	**0.5**	**46.7**	**77.9**	**1.16**	**0.36**	**0.26**	**0.77**	**264.9**
s.d.	**0.7**	**0.2**	**14.5**	**47.4**	**0.48**	**0.11**	**0.10**	**0.16**	**74.6**
N	**17**	**17**	**17**	**18**	**16**	**16**	**18**	**18**	**18**

* Reference line, 0°, is the horizontal axis. For larvae that change track direction, net resultant track direction is recorded in parentheses.

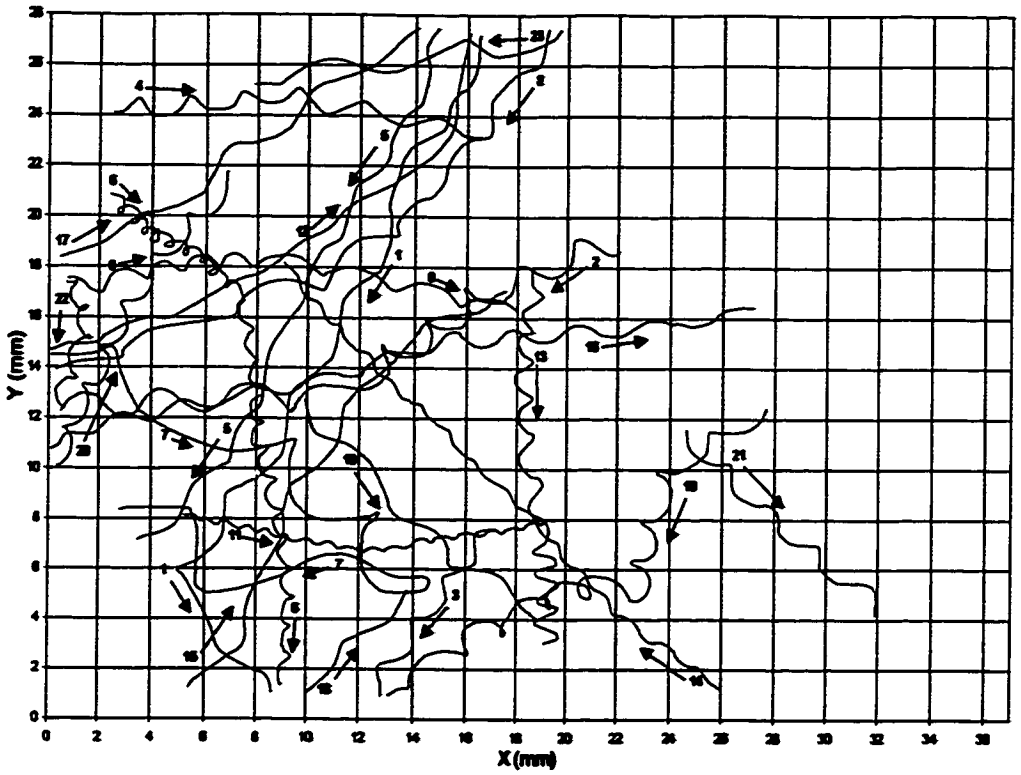

Fig A1.28. Reconstructed tracks of swimming mussel larvae (*Mytilus edulis*) from SCA# 3R0, Day 6 Night recording session, May 25, 1996. Track direction indicated by arrows.

Table A1.28. Trajectory measurement data from tracks of swimming mussel larvae (*Mytilus edulis*) from SCA# 3R0, Day 6 Night recording session, May 25, 1996.

LARVAL TRACK #	HELIX HEIGHT (mm)	HELIX DIAMETER (mm)	HELIX PITCH ANGLE	TIME (s)	ANGULAR VELOCITY (rad/s)	LINEAR VELOCITY (mm/s)	FORWARD VELOCITY (mm/s)	NGDR	TRACK DIRECTION (degrees) *
1	4.6	0.7	67	59.0	0.69	0.56	0.50	0.84	242, 301 (254)
2	2.4	1.1	37	75.0	N/A	N/A	0.31	0.71	206, 182 (197)
3	2.3	0.7	57	26.0	0.85	0.42	0.31	0.82	237
4	2.1	0.6	38	65.0	0.66	0.30	0.22	0.84	4, 345 (356)
5	3.4	0.5	68	46.0	0.90	0.54	0.49	0.95	244, 218 (241)
6	1.3	0.5	42	150.0	0.72	0.23	0.15	0.57	325, 278, 265 (289)
7	4.2	1.8	35	107.0	N/A	N/A	0.27	0.17	326, 265, 181, 133 (293)
8	3.5	0.7	52	50.0	0.87	0.57	0.46	0.87	229, 196 (216)
9	1.4	0.5	34	67.5	N/A	N/A	0.26	0.83	10, 348 (356)
10	2.0	0.8	32	72.5	0.87	0.45	0.28	0.62	213, 258, 207 (218)
11	0.9	0.2	61	66.0	1.20	0.20	0.16	0.88	347, 10 (360)
12	3.0	0.5	68	51.5	N/A	N/A	0.42	0.93	20, 37, 61 (39)
13	1.5	0.8	35	62.5	1.03	0.46	0.24	0.64	267, 278 (272)
14	1.8	0.2	76	91.0	1.04	0.28	0.26	0.95	135
15	4.2	0.6	70	35.0	N/A	N/A	0.59	0.92	60, 21 (53)
16	2.4	0.6	54	70.0	1.04	0.50	0.40	0.91	15, 4 (12)
17	4.1	0.8	61	27.0	0.93	0.71	0.61	0.95	33
18	3.5	0.6	65	15.5	0.65	0.41	0.36	0.98	48
19	4.5	0.7	63	42.0	0.42	0.33	0.30	0.92	315
20	2.0	0.7	47	44.0	0.96	0.46	0.31	0.78	64, 48 (61)
21	2.5	0.7	50	34.0	0.76	0.41	0.31	0.84	318
22	1.4	0.4	63	20.0	1.26	0.36	0.28	0.62	267, 246 (270)
23	4.5	0.7	67	19.5	0.86	0.69	0.62	0.93	186
MEAN	2.7	0.7	54.0	57.4	0.87	0.44	0.35	0.80	307.5
s.d.	1.2	0.3	13.5	31.7	0.21	0.14	0.14	0.18	68.5
N	23	23	23	23	18	18	23	23	23

* Reference line, 0°, is the horizontal axis. For larvae that change track direction, net resultant track direction is recorded in parentheses.

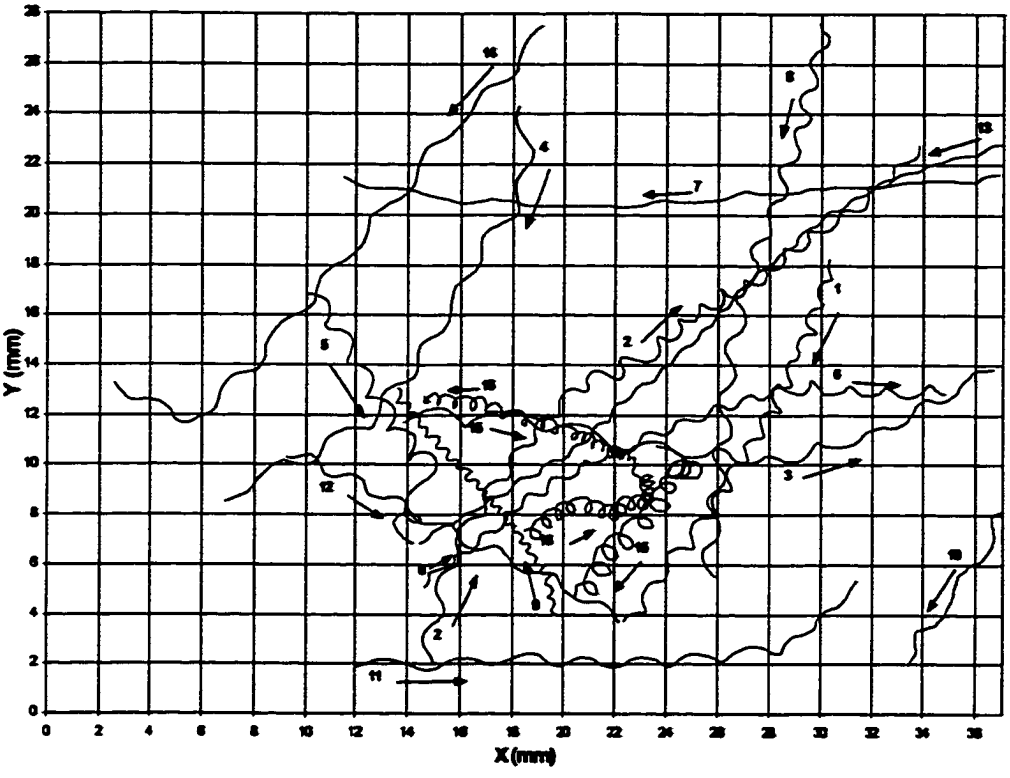

Fig A1.29. Reconstructed tracks of swimming mussel larvae (*Mytilus edulis*) from SCA# 3L0, Day 6 Day recording session, May 25, 1996. Track direction indicated by arrows.

Table A1.29. Trajectory measurement data from tracks of swimming mussel larvae (*Mytilus edulis*) from SCA# 3L0, Day 6 Day recording session, May 25, 1996.

LARVAL TRACK #	HELIX HEIGHT (mm)	HELIX DIAMETER (mm)	HELIX PITCH ANGLE	TIME (s)	ANGULAR VELOCITY (rad/s)	LINEAR VELOCITY (mm/s)	FORWARD VELOCITY (mm/s)	NGDR	TRACK DIRECTION (degrees) *
1	1.2	0.5	37	64.0	1.34	0.44	0.26	0.70	242
2	1.7	0.5	52	99.0	N/A	N/A	0.30	0.68	49, 37 (48)
3	1.9	0.6	48	70.0	0.66	0.27	0.20	0.87	353, 24 (13)
4	2.3	0.7	46	78.0	0.75	0.38	0.28	0.82	239, 209 (234)
5	1.7	0.8	30	114.0	N/A	N/A	0.10	0.56	301, 257 (293)
6	1.3	0.5	55	84.0	1.35	0.42	0.27	0.76	40, 21, 360 (21)
7	N/A	N/A	N/A	57.0	N/A	0.42	0.45	0.98	182
8	2.0	0.6	48	81.0	0.88	0.39	0.28	0.80	260
9	0.4	0.2	32	118.0	1.36	0.19	0.10	0.60	128
10	2.8	0.6	52	34.0	0.48	0.26	0.21	0.90	241
11	2.2	0.5	58	77.0	0.78	0.33	0.28	0.88	2, 41 (10)
12	2.3	0.5	57	38.0	1.07	0.47	0.39	0.87	332
13	1.2	0.2	59	84.0	1.80	0.40	0.34	0.91	200, 219 (215)
14	3.3	0.6	66	60.0	0.80	0.48	0.42	0.82	230, 150 (221)
15	3.0	0.8	54	125.0	N/A	N/A	0.15	0.25	350, 232 (313)
16	0.5	0.6	51	158.0	N/A	N/A	0.10	0.14	51, 174 (125)
MEAN	**1.9**	**0.5**	**49.6**	**83.8**	**1.02**	**0.37**	**0.26**	**0.72**	**270.8**
s.d.	**0.8**	**0.2**	**9.7**	**32.7**	**0.39**	**0.09**	**0.11**	**0.23**	**79.7**
N	**16**	**16**	**16**	**16**	**11**	**12**	**16**	**16**	**16**

* Reference line, 0°, is the horizontal axis. For larvae that change track direction, net resultant track direction is recorded in parentheses.

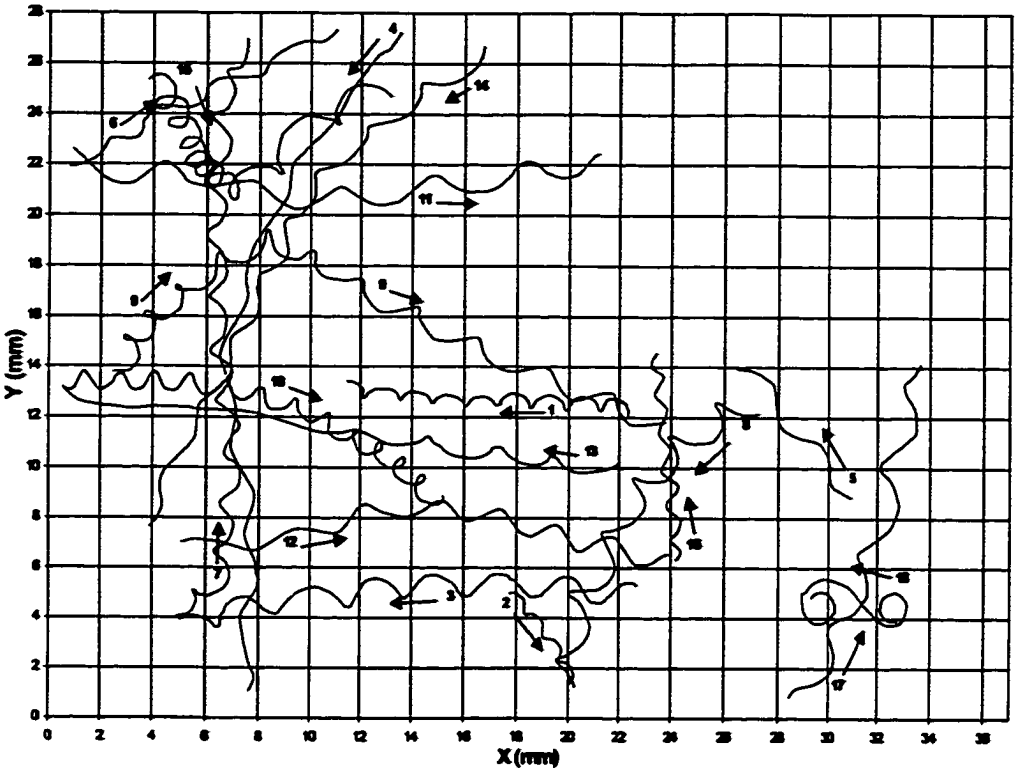

Fig A1.30. Reconstructed tracks of swimming mussel larvae (*Mytilus edulis*) from SCA# 3R0, Day 6 Day recording session, May 25, 1996. Track direction indicated by arrows.

Table A1.30. Trajectory measurement data from tracks of swimming mussel larvae (*Mytilus edulis*) from SCA# 3R0, Day 6 Day recording session, May 25, 1996.

LARVAL TRACK #	HELIX HEIGHT (mm)	HELIX DIAMETER (mm)	HELIX PITCH ANGLE	TIME (s)	ANGULAR VELOCITY (rad/s)	LINEAR VELOCITY (mm/s)	FORWARD VELOCITY (mm/s)	NGDR	TRACK DIRECTION (degrees)*
1	1.4	0.5	44	58.5	0.83	0.27	0.19	0.74	177
2	1.2	0.4	54	25.0	0.89	0.24	0.17	0.79	303
3	2.3	0.8	43	48.0	1.00	0.56	0.37	0.77	178, 192 (185)
4	3.7	0.6	70	52.0	0.90	0.59	0.54	0.92	238, 275 (257)
5	3.0	0.7	53	15.0	0.95	0.57	0.45	0.89	126
6	2.2	0.5	54	29.0	1.12	0.50	0.40	0.91	28
7	1.9	0.7	50	96.0	0.80	0.38	0.25	0.78	38, 89 (84)
8	2.2	1.0	35	49.0	0.80	0.49	0.28	0.63	221, 253 (237)
9	2.6	0.8	56	148.0	0.41	0.24	0.17	0.63	41, 334 (355)
10	1.4	0.7	33	71.0	0.98	0.41	0.22	0.57	358, 326 (344)
11	3.7	0.9	55	59.5	0.59	0.43	0.35	0.86	350, 9 (360)
12	2.4	0.7	53	56.0	0.91	0.46	0.34	0.85	9, 344 (359)
13	2.8	0.6	52	54.5	N/A	N/A	0.40	0.93	172
14	2.4	0.5	60	57.0	1.09	0.49	0.41	0.89	218, 245 (236)
15	1.0	1.0	33	114.0	N/A	N/A	0.11	0.32	300, 35 (356)
16	1.6	0.4	59	40.0	0.83	0.26	0.21	0.84	96
17	3.7	1.0	49	26.5	0.93	0.72	0.55	0.84	69
18	N/A	1.3	N/A	31.5	N/A	N/A	N/A	0.29	N/A
MEAN	**2.3**	**0.7**	**50.2**	**57.3**	**0.87**	**0.44**	**0.32**	**0.75**	**10.7**
s.d.	**0.9**	**0.3**	**9.6**	**33.3**	**0.18**	**0.14**	**0.13**	**0.19**	**76.4**
N	**17**	**18**	**17**	**18**	**16**	**16**	**17**	**18**	**17**

* Reference line, 0°, is the horizontal axis. For larvae that change track direction, net resultant track direction is recorded in parentheses.

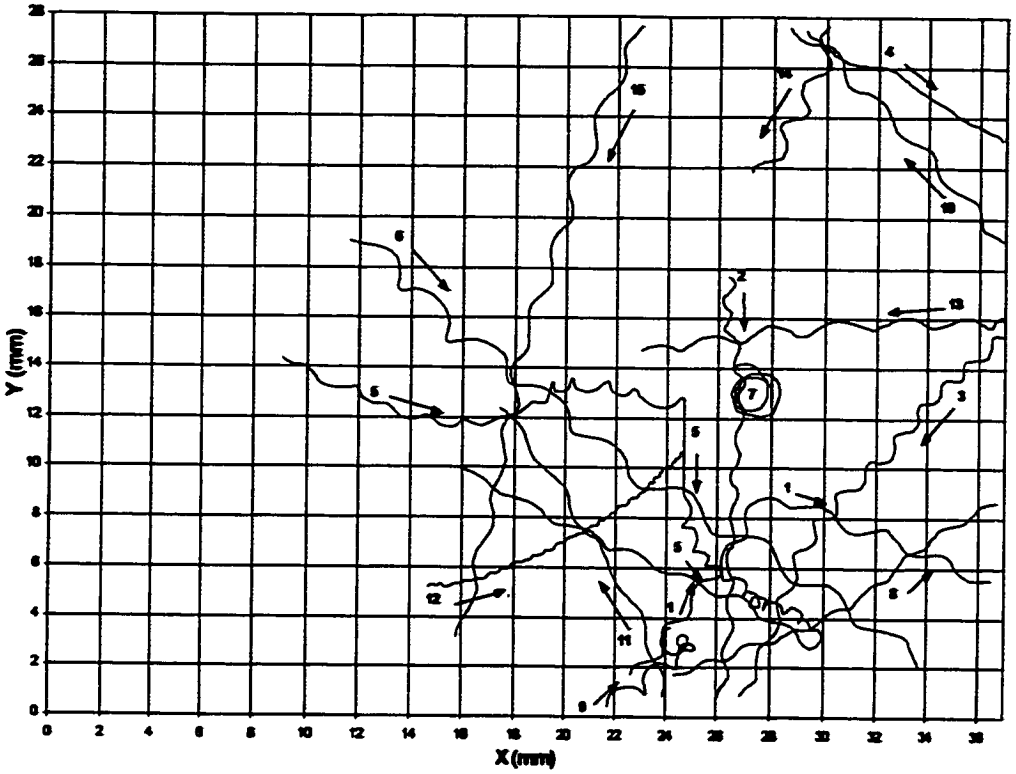

Fig A1.31. Reconstructed tracks of swimming mussel larvae (*Mytilus edulis*) from SCA# 3L0, Day 7 Night recording session, May 26, 1996. Track direction indicated by arrows.

Table A1.31. Trajectory measurement data from tracks of swimming mussel larvae (*Mytilus edulis*) from SCA# 3L0, Day 7 Night recording session, May 26, 1996.

LARVAL TRACK #	HELIX HEIGHT (mm)	HELIX DIAMETER (mm)	HELIX PITCH ANGLE	TIME (s)	ANGULAR VELOCITY (rad/s)	LINEAR VELOCITY (mm/s)	FORWARD VELOCITY (mm/s)	NGDR	TRACK DIRECTION (degrees) *
1	2.0	0.6	53	49.0	1.20	0.52	0.38	0.68	54, 337 (15)
2	1.7	0.3	64	81.0	0.77	0.25	0.21	0.88	269
3	1.5	0.6	44	69.0	1.14	0.44	0.27	0.79	227, 251 (235)
4	N/A	N/A	N/A	35.0	N/A	0.28	0.27	0.96	331
5	1.5	0.5	54	155.8	N/A	N/A	0.29	0.13	338, 22, 347, 270, 325, 154 (328)
6	3.7	0.9	54	77.0	0.63	0.47	0.37	0.83	322
7	N/A	0.2	N/A	221.2	N/A	N/A	N/A	N/A	Clockwise
8	1.8	0.2	78	59.0	0.86	0.27	0.25	0.94	29
9	1.6	0.8	40	113.0	N/A	N/A	0.05	0.41	34, 147 (52)
10	2.8	0.5	65	23.0	1.15	0.58	0.51	0.92	132
11	3.3	0.4	64	50.0	0.52	0.30	0.28	0.95	120
12	0.5	0.1	51	91.0	1.57	0.16	0.13	0.88	14, 29, 44 (29)
13	2.7	0.6	158	37.0	0.90	0.46	0.38	0.90	186
14	2.1	0.7	44	40.0	0.51	0.24	0.17	0.78	245
15	2.8	0.5	67	49.0	1.17	0.61	0.53	0.91	254
MEAN	**2.2**	**0.5**	**61.3**	**76.7**	**0.96**	**0.38**	**0.29**	**0.78**	**323.5**
s.d.	**0.9**	**0.2**	**26.3**	**52.7**	**0.33**	**0.16**	**0.14**	**0.24**	**72.0**
N	**13**	**14**	**13**	**15**	**11**	**12**	**14**	**14**	**14**

* Reference line, 0°, is the horizontal axis. For larvae that change track direction, net resultant track direction is recorded in parentheses.

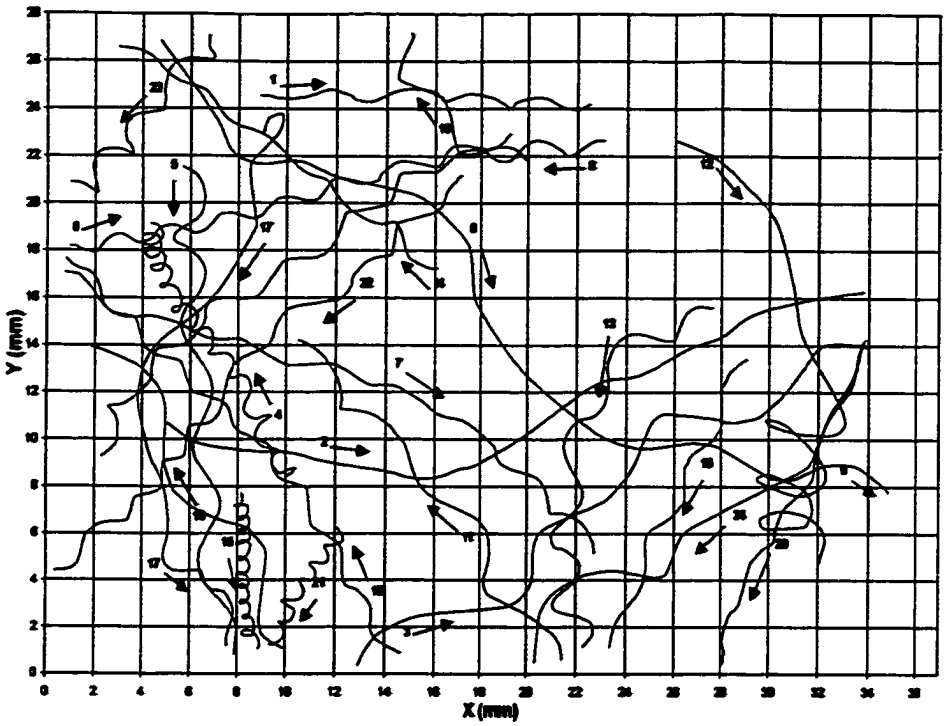

Fig A1.32. Reconstructed tracks of swimming mussel larvae (*Mytilus edulis*) from SCA# 3R0, Day 7 Night recording session, May 26, 1996. Track direction indicated by arrows.

Table A1.32. Trajectory measurement data from tracks of swimming mussel larvae (*Mytilus edulis*) from SCA# 3R0, Day 7 Night recording session, May 26, 1996.

LARVAL TRACK #	HELIX HEIGHT (mm)	HELIX DIAMETER (mm)	HELIX PITCH ANGLE	TIME (s)	ANGULAR VELOCITY (rad/s)	LINEAR VELOCITY (mm/s)	FORWARD VELOCITY (mm/s)	NGDR	TRACK DIRECTION (degrees) *
1	3.3	0.5	67	30.0	0.86	0.51	0.45	0.94	358
2	N/A	N/A	N/A	61.0	N/A	N/A	0.51	0.94	350, 24)11)
3	7.6	1.7	60	66.5	0.31	0.45	0.37	0.89	34
4	1.2	0.6	48	110.0	0.60	0.20	0.11	0.49	120
5	4.9	1.0	62	40.5	0.66	0.60	0.52	0.87	274
6	2.5	0.6	56	55.5	0.85	0.42	0.34	0.89	15
7	3.5	0.4	74	96.0	0.47	0.28	0.26	0.93	340, 313 (332)
8	3.4	0.6	62	104.0	0.46	0.28	0.25	0.84	186, 218, 247 (213)
9	N/A	N/A	N/A	97.0	N/A	N/A	0.38	0.90	302, 345, 313, 350 (328)
10	7.3	2.0	53	43.0	0.30	0.46	0.35	0.88	120
11	5.6	1.4	64	45.0	0.44	0.49	0.39	0.90	130
12	1.9	2.1	27	94.0	N/A	N/A	0.21	0.53	323, 288, 257 (288)
13	2.8	1.1	38	57.5	N/A	N/A	0.30	0.72	210, 289 (250)
14	3.0	0.4	74	39.5	0.84	0.44	0.41	0.95	144
15	0.7	0.4	38	45.0	1.29	0.32	0.15	0.44	273
16	3.5	0.6	65	22.5	1.07	0.66	0.60	0.94	245
17	N/A	N/A	N/A	106.0	N/A	N/A	0.23	0.77	45, 243, 277, 231, 281, 321, 255 (266)
18	2.9	0.6	67	51.0	0.94	0.51	0.43	0.91	118, 137 (130)
19	4.1	0.9	62	31.5	0.39	0.30	0.25	0.76	178, 120 (133)
20	N/A	N/A	N/A	36.0	N/A	N/A	0.42	0.97	247
21	0.9	0.5	40	24.0	1.61	0.47	0.24	0.63	241
22	2.6	0.8	62	52.0	1.02	0.60	0.46	0.89	225
23	2.3	0.9	44	54.5	0.42	0.25	0.16	0.69	229
24	N/A	N/A	N/A	51.5	N/A	N/A	0.38	0.89	247, 208, 285 (225)
MEAN	3.4	0.9	56.0	69.1	0.74	0.43	0.34	0.81	246.9
s.d.	1.9	0.5	12.8	27.5	0.37	0.14	0.13	0.15	69.7
N	19	19	19	24	17	17	24	24	24

* Reference line, 0°, is the horizontal axis. For larvae that change track direction, net resultant track direction is recorded in parentheses.

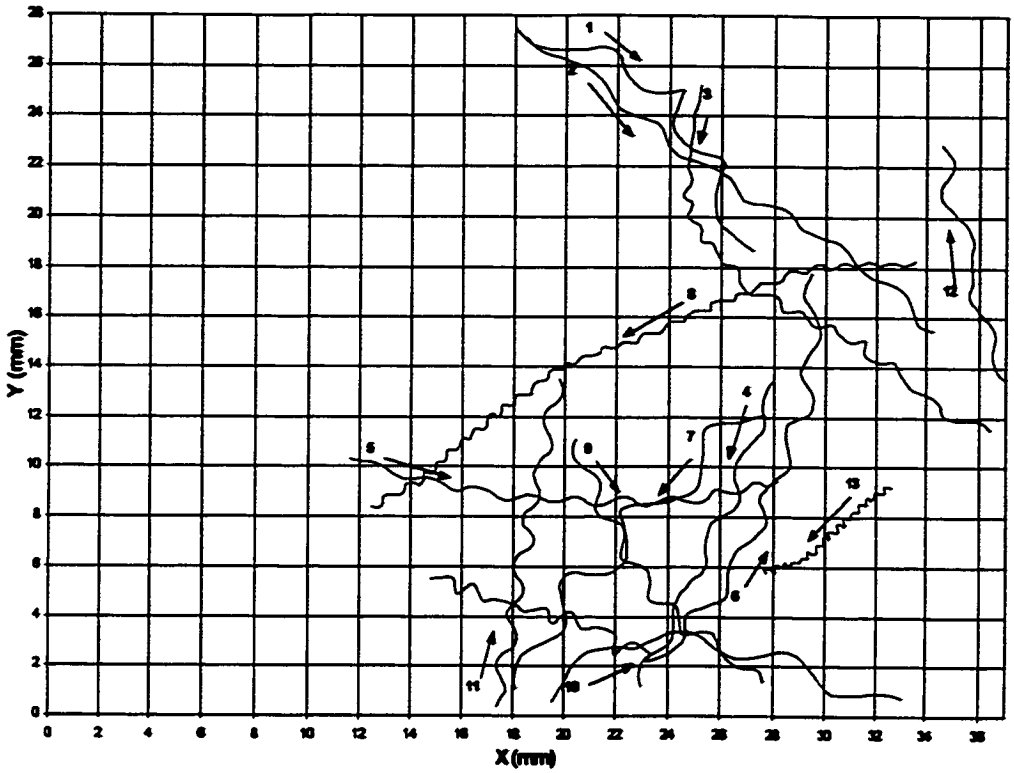

Fig A1.33. Reconstructed tracks of swimming mussel larvae (*Mytilus edulis*) from SCA# 3L0, Day 7 Day recording session, May 26, 1996. Track direction indicated by arrows.

Table A1.33. Trajectory measurement data from tracks of swimming mussel larvae (*Mytilus edulis*) from SCA# 3L0, Day 7 Day recording session, May 26, 1996.

LARVAL TRACK #	HELIX HEIGHT (mm)	HELIX DIAMETER (mm)	HELIX PITCH ANGLE	TIME (s)	ANGULAR VELOCITY (rad/s)	LINEAR VELOCITY (mm/s)	FORWARD VELOCITY (mm/s)	NGDR	TRACK DIRECTION (degrees) *
1	3.3	1.1	42	52.9	0.51	0.38	0.27	0.80	330, 295 (316)
2	2.9	0.6	62	38.9	1.13	0.62	0.52	0.94	324
3	1.3	0.4	51	76.9	1.35	0.37	0.27	0.72	267, 324, 325 (309)
4	3.2	0.6	53	42.1	0.63	0.37	0.32	0.91	249
5	2.0	0.4	64	83.4	0.66	0.25	0.21	0.88	351
6	1.5	0.7	52	137.6	N/A	N/A	0.19	0.81	338, 55, 70, 84 (40)
7	4.3	1.6	50	65.1	0.34	0.35	0.23	0.79	230
8	0.8	0.3	52	83.4	2.20	0.41	0.29	0.79	180, 203, 217 (204)
9	2.1	0.7	50	56.0	0.69	0.34	0.23	0.81	300, 321 (306)
10	4.0	0.7	62	44.9	0.54	0.39	0.34	0.84	30, 344 (1)
11	2.1	0.5	57	47.3	0.84	0.35	0.28	0.97	79
12	3.2	0.8	62	20.0	0.95	0.61	0.48	0.88	105
13	0.5	0.3	42	221.3	0.36	0.07	0.03	0.51	223
MEAN	**2.4**	**0.7**	**53.8**	**74.6**	**0.85**	**0.38**	**0.28**	**0.82**	**311.1**
s.d.	**1.2**	**0.4**	**7.0**	**62.8**	**0.52**	**0.14**	**0.12**	**0.12**	**66.5**
N	**13**	**13**	**13**	**13**	**12**	**12**	**13**	**13**	**13**

* Reference line, 0°, is the horizontal axis. For larvae that change track direction, net resultant track direction is recorded in parentheses.

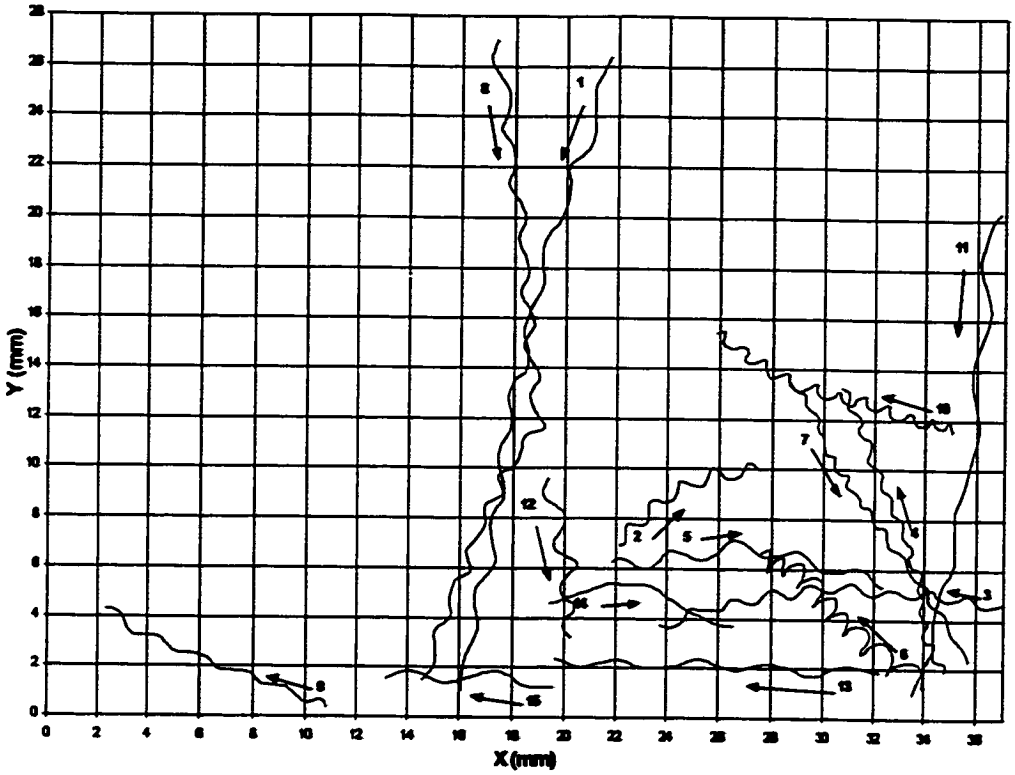

Fig A1.34. Reconstructed tracks of swimming mussel larvae (*Mytilus edulis*) from SCA# 3L0, Day 8 Night recording session, May 27, 1996. Track direction indicated by arrows.

Table A1.34. Trajectory measurement data from tracks of swimming mussel larvae (*Mytilus edulis*) from SCA# 3L0, Day 8 Night recording session, May 27, 1996.

LARVAL TRACK #	HELIX HEIGHT (mm)	HELIX DIAMETER (mm)	HELIX PITCH ANGLE	TIME (s)	ANGULAR VELOCITY (rad/s)	LINEAR VELOCITY (mm/s)	FORWARD VELOCITY (mm/s)	NGDR	TRACK DIRECTION (degrees) *
1	2.9	0.5	54	62.0	0.93	0.49	0.43	0.94	258
2	1.5	0.5	54	31.9	0.90	0.31	0.21	0.70	43, 18 (29)
3	1.6	0.5	56	44.6	1.25	0.44	0.31	0.84	175, 192 (184)
4	1.0	0.4	76	88.6	0.89	0.21	0.14	0.78	111
5	2.5	0.6	62	31.8	0.87	0.44	0.35	0.85	8, 345 (355)
6	1.1	0.9	9	127.5	0.39	0.18	0.07	0.39	139
7	0.9	0.4	53	60.2	1.63	0.39	0.23	0.87	301
8	2.2	0.6	36	109.3	N/A	N/A	0.24	0.85	276, 244 (264)
9	1.9	0.4	65	29.0	1.12	0.40	0.33	0.91	156
10	1.0	0.5	22	57.8	1.09	0.33	0.18	0.60	157
11	4.4	0.6	71	68.0	0.43	0.32	0.30	0.97	260
12	1.9	0.9	47	31.3	0.72	0.38	0.22	0.78	279
13	3.2	0.4	64	62.7	0.40	0.22	0.21	0.96	13
14	0.2	0.5	18	157.9	N/A	N/A	0.05	0.93	21, 358, 324, 348 (353)
15	3.3	0.5	67	31.4	0.40	0.24	0.21	0.93	177
MEAN	**2.0**	**0.5**	**50.6**	**66.3**	**0.85**	**0.33**	**0.23**	**0.82**	**245.0**
s.d.	**1.1**	**0.2**	**19.3**	**39.0**	**0.38**	**0.10**	**0.10**	**0.16**	**75.0**
N	**15**	**15**	**15**	**15**	**13**	**13**	**15**	**15**	**15**

* Reference line, 0°, is the horizontal axis. For larvae that change track direction, net resultant track direction is recorded in parentheses.

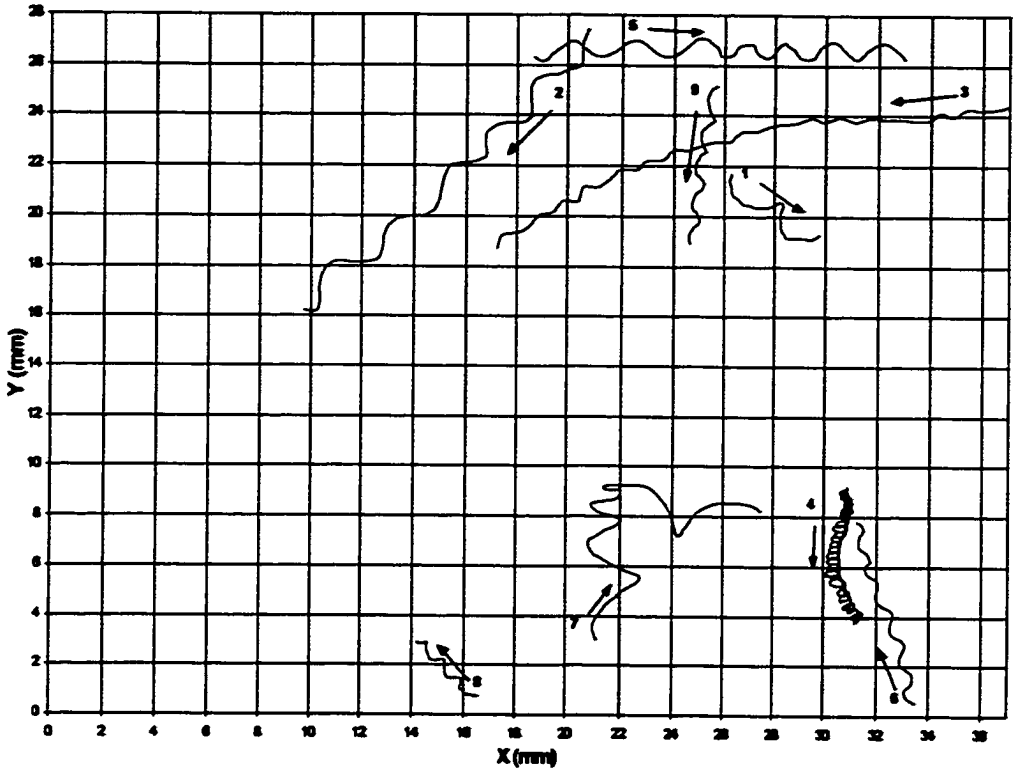

Fig A1.35. Reconstructed tracks of swimming mussel larvae (*Mytilus edulis*) from SCA# 3L0, Day 8 Day recording session, May 27, 1996. Track direction indicated by arrows.

Table A1.35. Trajectory measurement data from tracks of swimming mussel larvae (*Mytilus edulis*) from SCA# 3L0, Day 8 Day recording session, May 27, 1996.

LARVAL TRACK #	HELIX HEIGHT (mm)	HELIX DIAMETER (mm)	HELIX PITCH ANGLE	TIME (s)	ANGULAR VELOCITY (rad/s)	LINEAR VELOCITY (mm/s)	FORWARD VELOCITY (mm/s)	NGDR	TRACK DIRECTION (degrees) *
1	2.0	1.0	52	12.4	N/A	N/A	0.36	0.71	143
2	3.0	0.8	55	62.5	0.55	0.34	0.26	0.80	224
3	1.3	0.3	64	59.1	1.71	0.46	0.36	0.87	185, 196, 210 (196)
4	0.2	0.5	19	156.7	N/A	N/A	0.04	0.19	298, 255, 295 (276)
5	1.9	0.8	50	92.0	0.53	0.28	0.16	0.78	359
6	1.3	0.4	57	45.9	0.81	0.23	0.17	0.83	107
7	N/A	N/A	N/A	93.9	N/A	N/A	0.13	0.41	95, 82, 349 (39)
8	1.0	0.4	45	26.0	0.82	0.21	0.13	0.76	147
9	1.5	0.4	59	31.4	0.91	0.28	0.21	0.85	261
MEAN	**1.5**	**0.6**	**50.3**	**64.4**	**0.89**	**0.30**	**0.20**	**0.69**	**187.3**
s.d.	**0.8**	**0.2**	**12.8**	**44.4**	**0.43**	**0.09**	**0.11**	**0.23**	**72.6**
N	**8**	**8**	**8**	**9**	**6**	**6**	**9**	**9**	**9**

* Reference line, 0°, is the horizontal axis. For larvae that change track direction, net resultant track direction is recorded in parentheses.

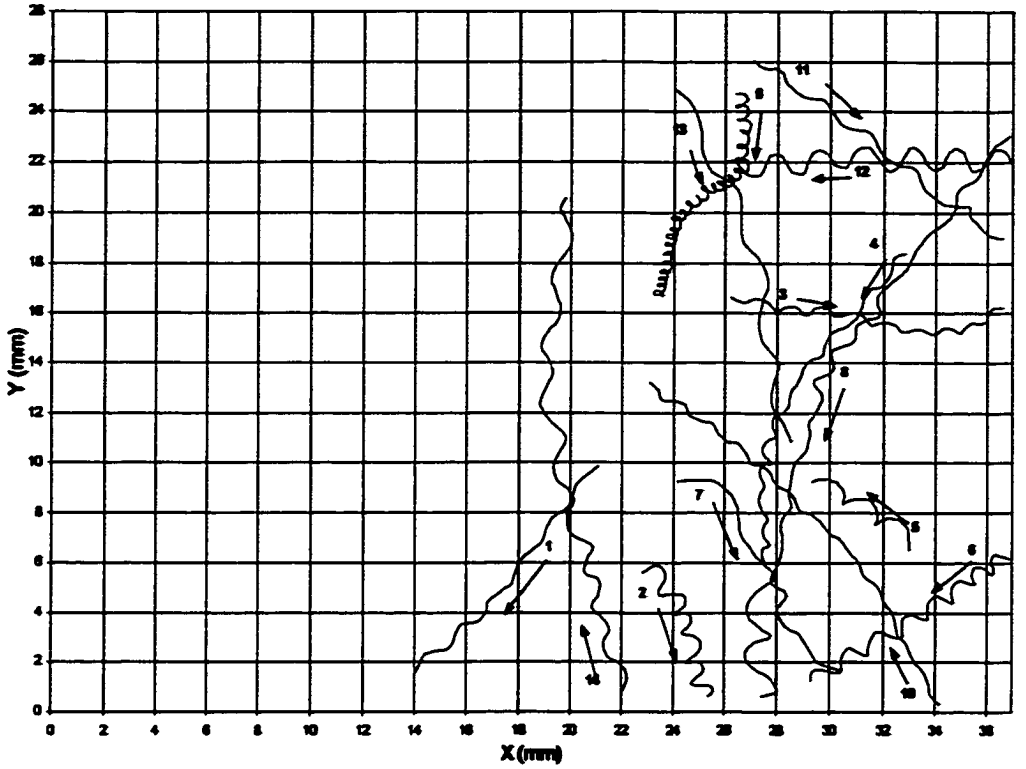

Fig A1.36. Reconstructed tracks of swimming mussel larvae (*Mytilus edulis*) from SCA# 3L0, Day 9 Night recording session, May 28, 1996. Track direction indicated by arrows.

Table A1.36. Trajectory measurement data from tracks of swimming mussel larvae (*Mytilus edulis*) from SCA# 3L0, Day 9 Night recording session, May 28, 1996.

LARVAL TRACK #	HELIX HEIGHT (mm)	HELIX DIAMETER (mm)	HELIX PITCH ANGLE	TIME (s)	ANGULAR VELOCITY (rad/s)	LINEAR VELOCITY (mm/s)	FORWARD VELOCITY (mm/s)	NGDR	TRACK DIRECTION (degrees) *
1	2.1	0.3	73	31.4	1.08	0.39	0.36	0.92	230
2	1.2	0.6	31	51.8	0.62	0.21	0.12	0.52	288
3	1.3	0.4	56	40.3	1.31	0.36	0.28	0.81	350, 24 (358)
4	1.1	0.6	41	62.8	1.28	0.42	0.23	0.80	236, 264 (247)
5	1.5	0.7	38	31.4	0.61	0.27	0.15	0.68	145
6	1.3	0.7	38	64.0	0.72	0.31	0.14	0.62	215
7	2.4	1.0	53	37.0	N/A	N/A	0.28	0.68	303, 270 (290)
8	1.2	0.4	46	187.3	0.72	0.21	0.14	0.65	233, 255, 296 (253)
9	0.5	0.5	60	220.2	N/A	N/A	0.04	0.33	271, 212, 258 (248)
10	1.5	0.3	69	100.3	0.74	0.20	0.17	0.89	118, 138 (131)
11	2.3	0.5	66	32.0	1.03	0.44	0.38	0.91	324
12	1.7	0.9	32	42.0	0.96	0.53	0.26	0.64	182
13	3.5	0.5	72	62.8	0.44	0.27	0.25	0.92	287
14	1.6	0.6	42	97.0	0.83	0.33	0.21	0.84	104, 101, 77 (97)
MEAN	**1.7**	**0.6**	**51.2**	**75.7**	**0.86**	**0.33**	**0.22**	**0.76**	**246.1**
s.d.	**0.7**	**0.2**	**14.3**	**58.9**	**0.27**	**0.10**	**0.10**	**0.13**	**61.9**
N	**14**	**14**	**14**	**14**	**12**	**12**	**14**	**13**	**14**

* Reference line, 0°, is the horizontal axis. For larvae that change track direction, net resultant track direction is recorded in parentheses.

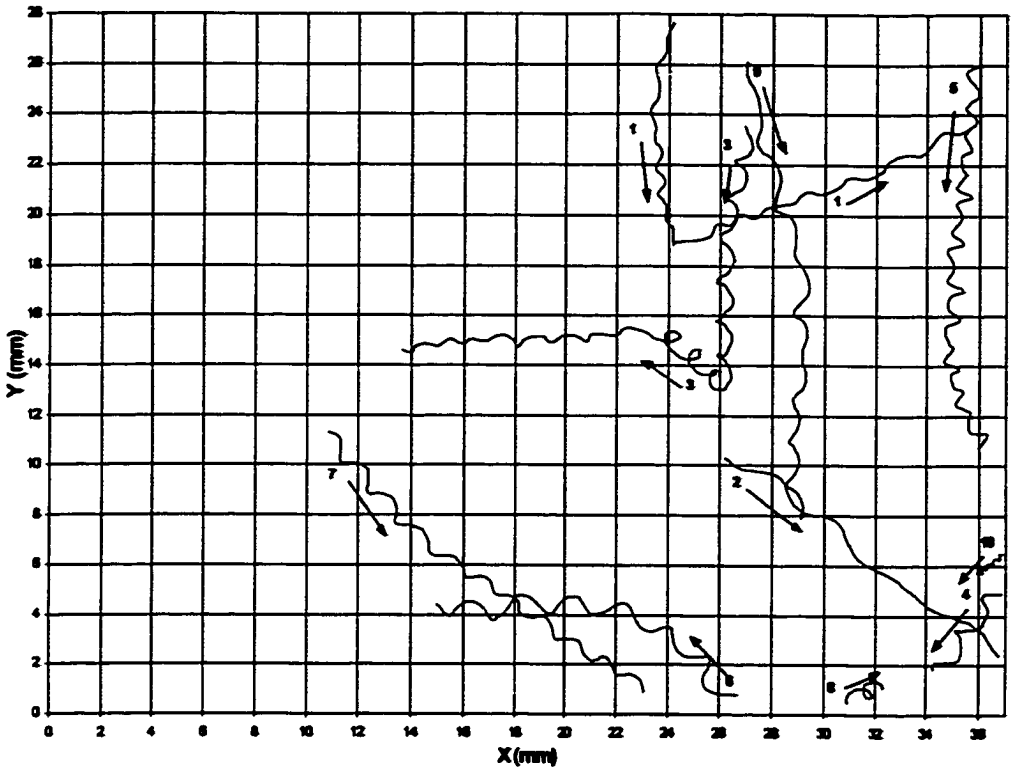

Fig A1.37. Reconstructed tracks of swimming mussel larvae (*Mytilus edulis*) from SCA# 3L0, Day 9 Day recording session, May 28, 1996. Track direction indicated by arrows.

Table A1.37. Trajectory measurement data from tracks of swimming mussel larvae (*Mytilus edulis*) from SCA# 3L0, Day 9 Day recording session, May 28, 1996.

LARVAL TRACK #	HELIX HEIGHT (mm)	HELIX DIAMETER (mm)	HELIX PITCH ANGLE	TIME (s)	ANGULAR VELOCITY (rad/s)	LINEAR VELOCITY (mm/s)	FORWARD VELOCITY (mm/s)	NGDR	TRACK DIRECTION (degrees)*
1	1.8	0.5	56	140.0	N/A	N/A	0.16	0.48	269, 24 (341)
2	3.0	0.7	65	38.0	N/A	N/A	0.35	0.91	323
3	1.6	0.5	51	113.4	N/A	N/A	0.21	0.56	266, 135, 183 (215)
4	1.7	0.8	37	21.0	0.70	0.33	0.19	0.68	232
5	0.9	0.6	24	112.0	0.99	0.35	0.14	0.57	285, 294 (270)
6	1.9	0.7	41	79.0	0.56	0.26	0.17	0.71	131, 151, 183 (163)
7	1.5	0.5	52	50.0	1.36	0.47	0.34	0.79	320
8	0.6	0.6	43	26.3	N/A	N/A	0.05	0.46	20
9	1.8	0.5	48	74.0	0.89	0.34	0.26	0.86	283, 267 (276)
10	0.3	0.2	41	56.8	N/A	N/A	0.02	0.54	223
MEAN	**1.5**	**0.6**	**46.8**	**71.3**	**0.90**	**0.35**	**0.19**	**0.66**	**276.9**
s.d.	**0.8**	**0.2**	**10.7**	**48.0**	**0.31**	**0.08**	**0.11**	**0.16**	**57.4**
N	**10**	**10**	**10**	**10**	**5**	**5**	**10**	**10**	**10**

* Reference line, 0°, is the horizontal axis. For larvae that change track direction, net resultant track direction is recorded in parentheses.

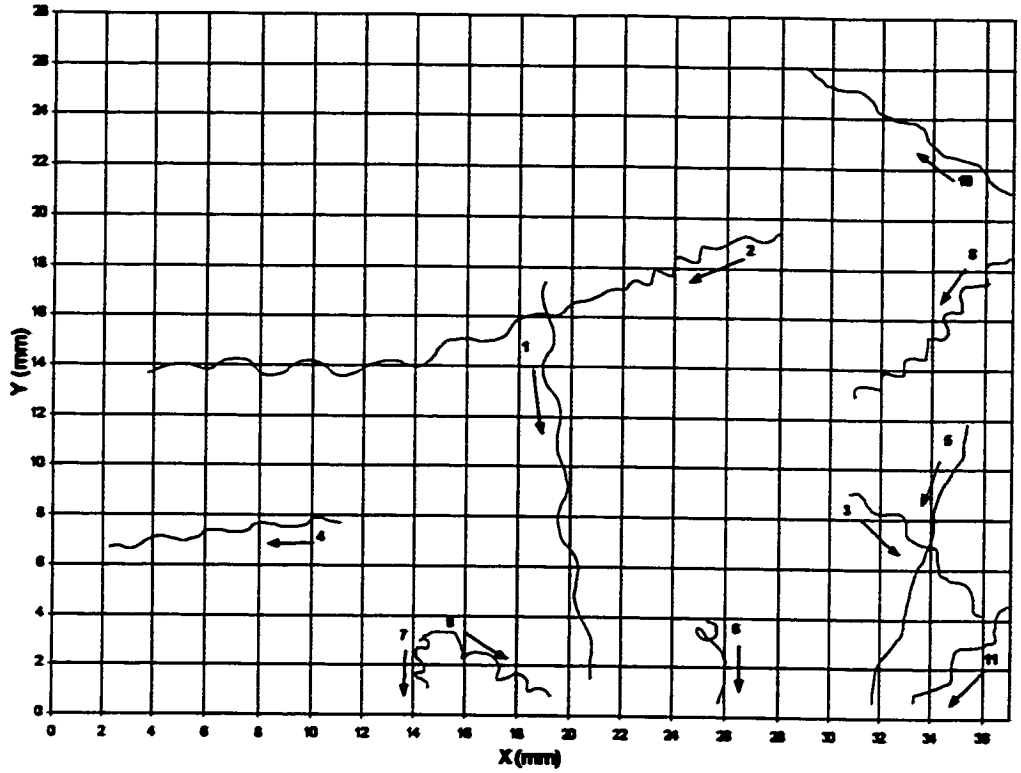

Fig A1.38. Reconstructed tracks of swimming mussel larvae (*Mytilus edulis*) from SCA# 3L0, Day 10 Night recording session, May 29, 1996. Track direction indicated by arrows.

Table A1.38. Trajectory measurement data from tracks of swimming mussel larvae (*Mytilus edulis*) from SCA# 3L0, Day 10 Night recording session, May 29, 1996.

LARVAL TRACK #	HELIX HEIGHT (mm)	HELIX DIAMETER (mm)	HELIX PITCH ANGLE	TIME (s)	ANGULAR VELOCITY (rad/s)	LINEAR VELOCITY (mm/s)	FORWARD VELOCITY (mm/s)	NGDR	TRACK DIRECTION (degrees) *
1	3.2	0.6	62	63.2	0.51	0.31	0.26	0.95	277
2	1.1	0.7	14	126.5	N/A	N/A	0.20	0.79	200, 180 (193)
3	1.9	0.5	53	31.6	0.79	0.30	0.24	0.85	317
4	2.0	0.3	62	20.0	1.41	0.49	0.45	0.94	186
5	3.7	0.5	71	26.0	N/A	0.48	0.46	0.97	252
6	N/A	N/A	N/A	30.0	N/A	N/A	0.12	0.63	277
7	1.0	0.4	47	157.9	N/A	N/A	0.01	0.67	267
8	1.4	0.6	47	73.0	0.53	0.20	0.12	0.71	225
9	1.7	0.7	43	31.4	0.67	0.30	0.18	0.69	332
10	2.6	0.4	59	38.5	0.59	0.27	0.25	0.93	147
11	2.4	0.8	47	26.0	0.55	0.31	0.21	0.89	226
MEAN	2.1	0.6	50.6	66.7	0.72	0.33	0.23	0.82	246.7
s.d.	0.9	0.2	14.6	46.8	0.32	0.10	0.14	0.13	49.7
N	10	10	10	11	7	8	11	11	11

* Reference line, 0°, is the horizontal axis. For larvae that change track direction, net resultant track direction is recorded in parentheses.

APPENDIX 2

Circular Scatter Diagrams Representing Swimming Directions of *Mytilus edulis* Larvae in Microgravity

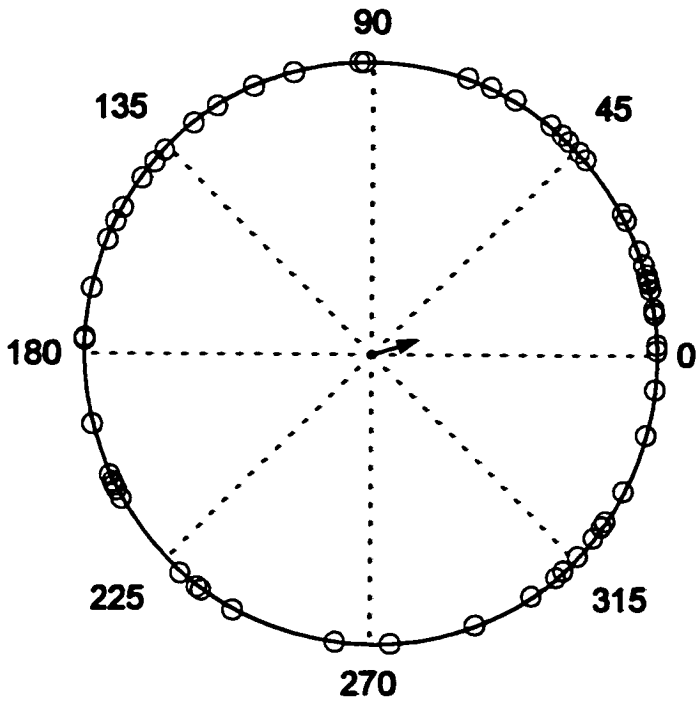

Sample size, *n*	63
Sample mean angle, $\bar{a}$	18°
Length of mean vector, *r*	0.15
Angular deviation, *s*	74.6
Rayleigh's z statistic (nr^2)	1.475
Uniform Distribution? (α= 0.05)	Yes

Fig A2.1. Scatter diagram illustrating track orientations of mussel larvae (*Mytilus edulis*) swimming in a microgravity environment. Data are pooled from all SCAs, Day 1 Day recording session, May 20, 1996. The arrow indicates the sample mean vector *m*, and descriptive statistics are tabulated. Rayleigh's z statistic tests the null hypothesis that larvae exhibit no preferred direction.

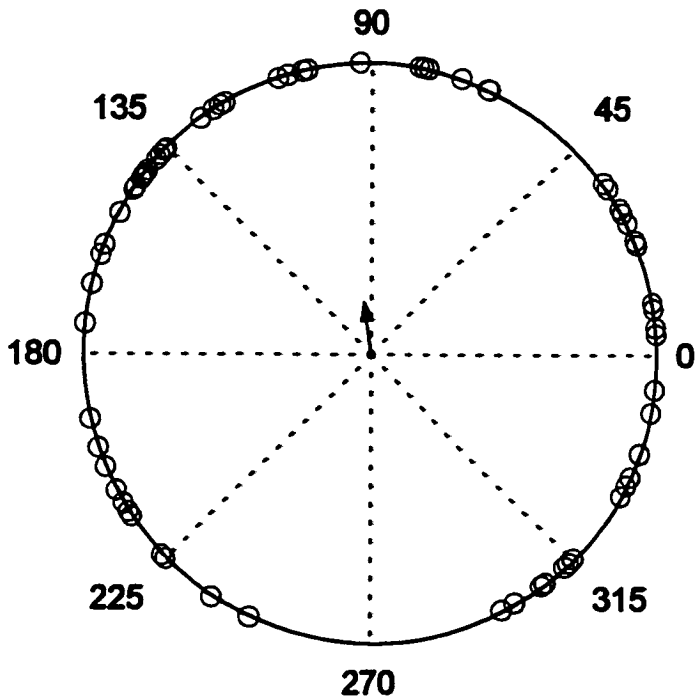

Sample size, *n*	66
Sample mean angle, $\bar{a}$	98°
Length of mean vector, *r*	0.18
Angular deviation, *s*	73.5
Rayleigh's z statistic (nr^2)	2.098
Uniform Distribution? (α= 0.05)	Yes

Fig A2.2. Scatter diagram illustrating track orientations of mussel larvae (*Mytilus edulis*) swimming in a microgravity environment. Data are pooled from all SCAs, Day 2 Night recording session, May 21, 1996. The arrow indicates the sample mean vector *m*, and descriptive statistics are tabulated. Rayleigh's z statistic tests the null hypothesis that larvae exhibit no preferred direction.

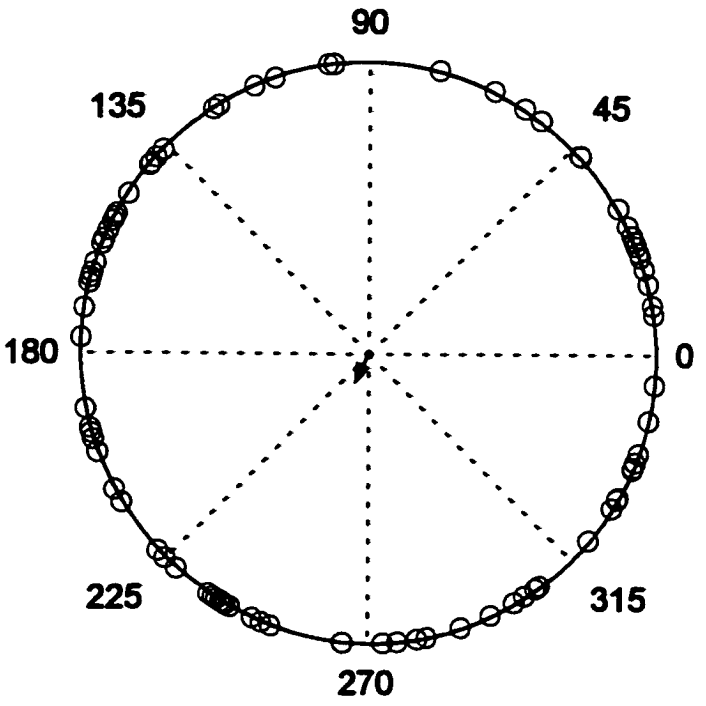

Sample size, *n*	81
Sample mean angle, $\bar{a}$	245°
Length of mean vector, *r*	0.10
Angular deviation, *s*	76.7
Rayleigh's z statistic (nr^2)	0.886
Uniform Distribution? (α= 0.05)	Yes

Fig A2.3. Scatter diagram illustrating track orientations of mussel larvae (*Mytilus edulis*) swimming in a microgravity environment. Data are pooled from all SCAs, Day 2 Day recording session, May 21, 1996. The arrow indicates the sample mean vector *m*, and descriptive statistics are tabulated. Rayleigh's z statistic tests the null hypothesis that larvae exhibit no preferred direction.

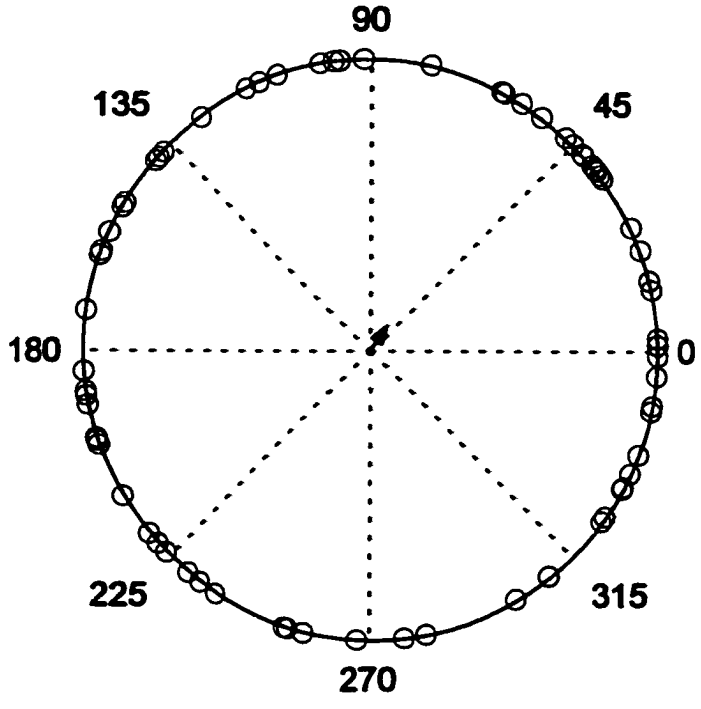

Sample size, *n*	72
Sample mean angle, $\bar{a}$	58°
Length of mean vector, *r*	0.10
Angular deviation, *s*	76.9
Rayleigh's z statistic (nr^2)	0.703
Uniform Distribution? (α= 0.05)	Yes

Fig A2.4. Scatter diagram illustrating track orientations of mussel larvae (*Mytilus edulis*) swimming in a microgravity environment. Data are pooled from all SCAs, Day 3 Night recording session, May 22, 1996. The arrow indicates the sample mean vector *m*, and descriptive statistics are tabulated. Rayleigh's z statistic tests the null hypothesis that larvae exhibit no preferred direction.

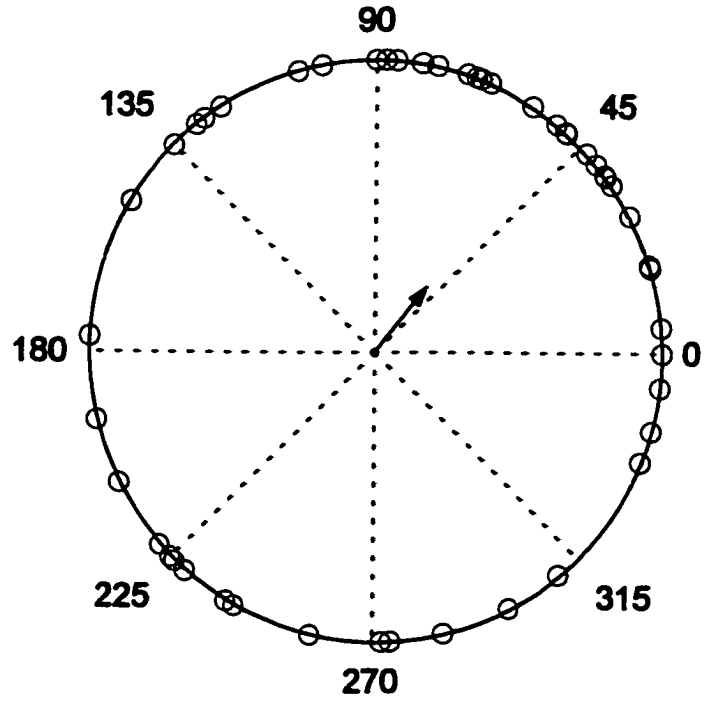

Sample size, *n*	48
Sample mean angle, $\bar{a}$	52°
Length of mean vector, *r*	0.28
Angular deviation, *s*	68.7
Rayleigh's z statistic (nr^2)	3.800
Uniform Distribution? (α= 0.05)	No

Fig A2.5. Scatter diagram illustrating track orientations of mussel larvae (*Mytilus edulis*) swimming in a microgravity environment. Data are pooled from all SCAs, Day 3 Day recording session, May 22, 1996. The arrow indicates the sample mean vector *m*, and descriptive statistics are tabulated. Rayleigh's z statistic tests the null hypothesis that larvae exhibit no preferred direction.

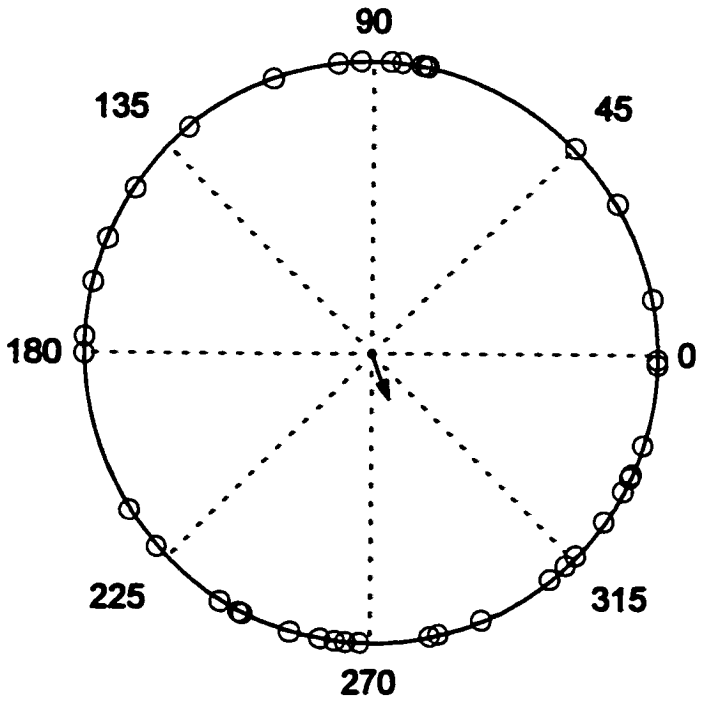

Sample size, *n*	42
Sample mean angle, $\bar{a}$	291°
Length of mean vector, *r*	0.16
Angular deviation, *s*	74.1
Rayleigh's z statistic (nr^2)	1.112
Uniform Distribution? (α= 0.05)	Yes

Fig A2.6. Scatter diagram illustrating track orientations of mussel larvae (*Mytilus edulis*) swimming in a microgravity environment. Data are pooled from all SCAs, Day 4 Night recording session, May 23, 1996. The arrow indicates the sample mean vector *m*, and descriptive statistics are tabulated. Rayleigh's z statistic tests the null hypothesis that larvae exhibit no preferred direction.

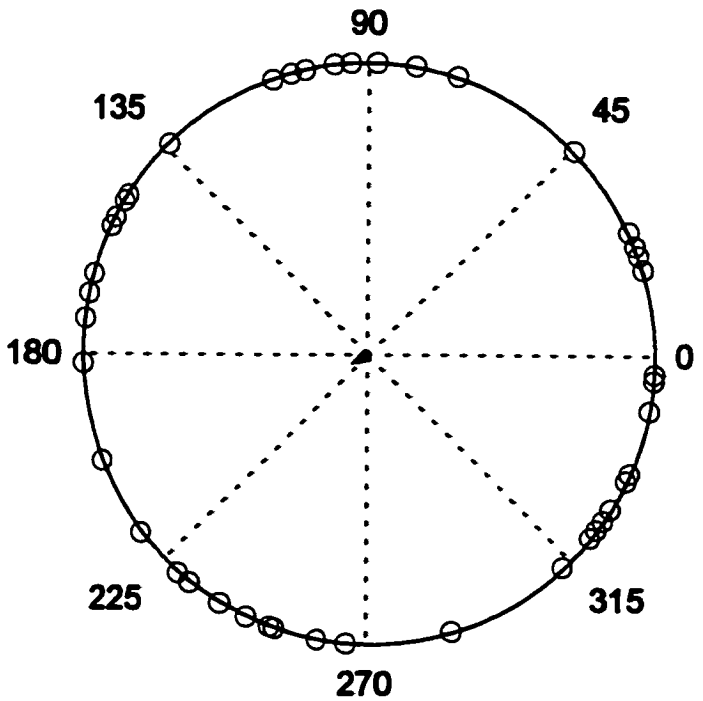

Sample size, *n*	43
Sample mean angle, $\bar{a}$	194°
Length of mean vector, *r*	0.02
Angular deviation, *s*	80.4
Rayleigh's z statistic (nr^2)	0.011
Uniform Distribution? (α= 0.05)	Yes

Fig A2.7. Scatter diagram illustrating track orientations of mussel larvae (*Mytilus edulis*) swimming in a microgravity environment. Data are pooled from all SCAs, Day 4 Day recording session, May 23, 1996. The arrow indicates the sample mean vector *m*, and descriptive statistics are tabulated. Rayleigh's z statistic tests the null hypothesis that larvae exhibit no preferred direction.

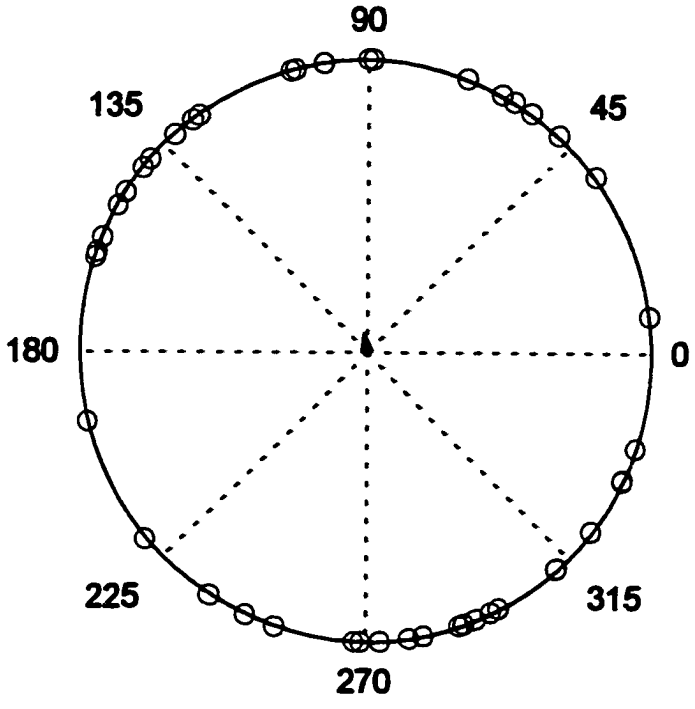

Sample size, n	44
Sample mean angle, $\bar{a}$	96
Length of mean vector, r	0.05
Angular deviation, s	79.1
Rayleigh's z statistic (nr^2)	0.098
Uniform Distribution? (α= 0.05)	Yes

Fig A2.8. Scatter diagram illustrating track orientations of mussel larvae (*Mytilus edulis*) swimming in a microgravity environment. Data are pooled from all SCAs, Day 5 Night recording session, May 24, 1996. The arrow indicates the sample mean vector m, and descriptive statistics are tabulated. Rayleigh's z statistic tests the null hypothesis that larvae exhibit no preferred direction.

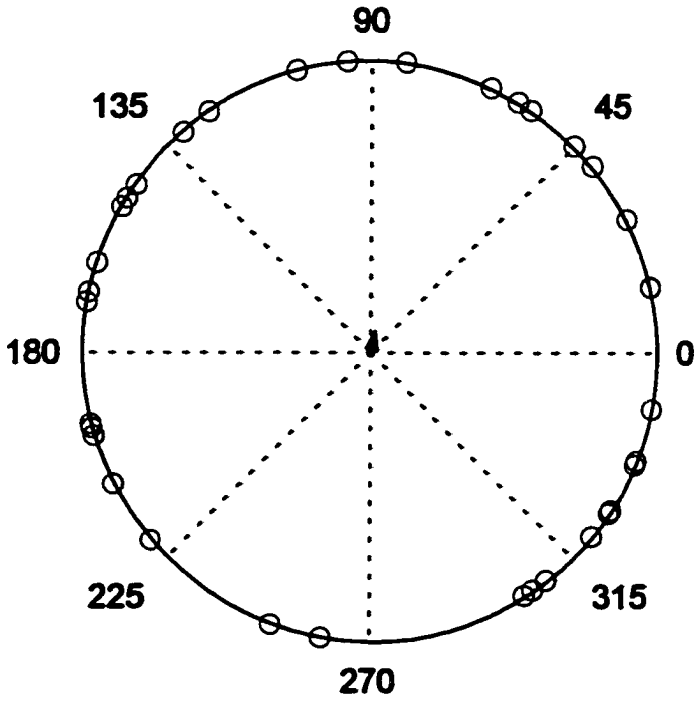

Sample size, *n*	35
Sample mean angle, $\bar{a}$	79°
Length of mean vector, *r*	0.07
Angular deviation, *s*	78.1
Rayleigh's z statistic (nr^2)	0.171
Uniform Distribution? (α= 0.05)	Yes

Fig A2.9. Scatter diagram illustrating track orientations of mussel larvae (*Mytilus edulis*) swimming in a microgravity environment. Data are pooled from all SCAs, Day 5 Day recording session, May 24, 1996. The arrow indicates the sample mean vector *m*, and descriptive statistics are tabulated. Rayleigh's z statistic tests the null hypothesis that larvae exhibit no preferred direction.

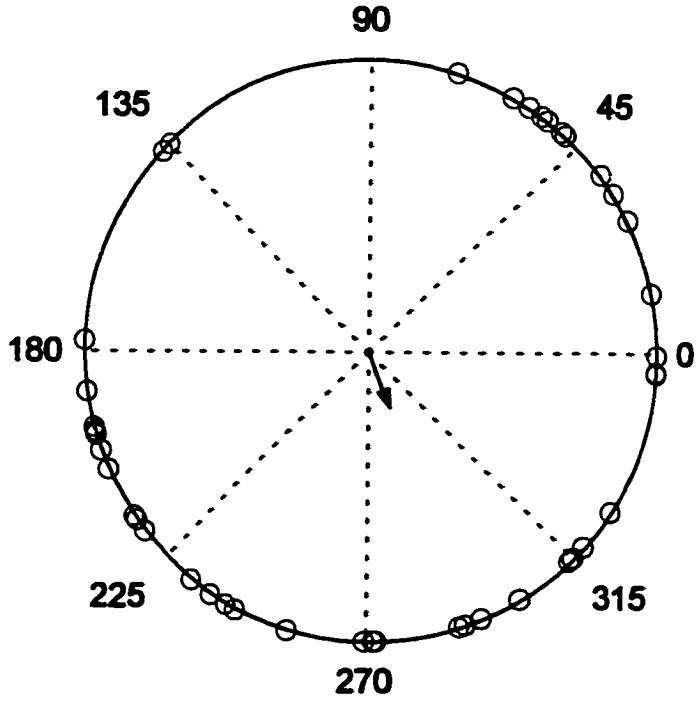

Sample size, *n*	42
Sample mean angle, $\bar{a}$	292°
Length of mean vector, *r*	0.21
Angular deviation, *s*	72.2
Rayleigh's z statistic (nr^2)	1.785
Uniform Distribution? (α= 0.05)	Yes

Fig A2.10. Scatter diagram illustrating track orientations of mussel larvae (*Mytilus edulis*) swimming in a microgravity environment. Data are pooled from all SCAs, Day 6 Night recording session, May 25, 1996. The arrow indicates the sample mean vector *m*, and descriptive statistics are tabulated. Rayleigh's z statistic tests the null hypothesis that larvae exhibit no preferred direction.

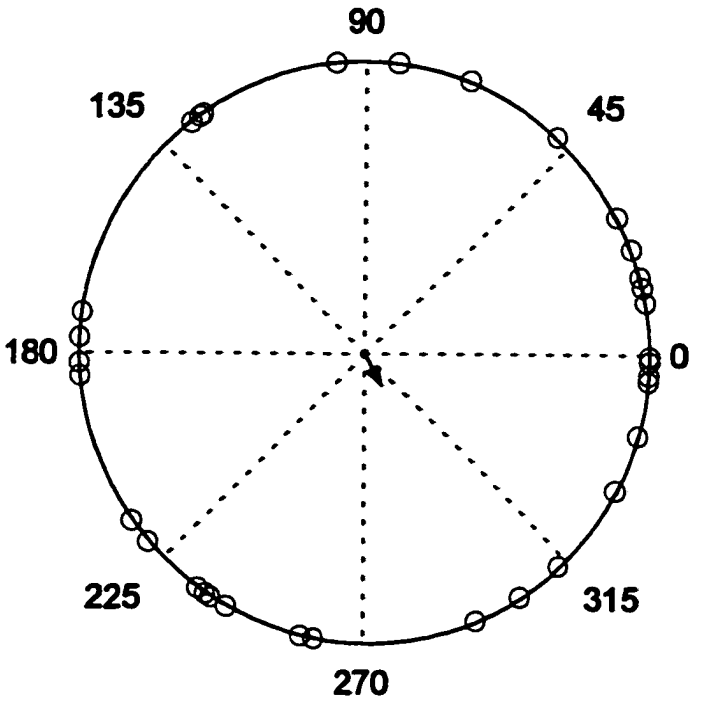

Sample size, *n*	33
Sample mean angle, $\bar{a}$	299°
Length of mean vector, *r*	0.12
Angular deviation, *s*	76.0
Rayleigh's z statistic (nr^2)	0.478
Uniform Distribution? (α= 0.05)	Yes

Fig A2.11. Scatter diagram illustrating track orientations of mussel larvae (*Mytilus edulis*) swimming in a microgravity environment. Data are pooled from all SCAs, Day 6 Day recording session, May 25, 1996. The arrow indicates the sample mean vector *m*, and descriptive statistics are tabulated. Rayleigh's z statistic tests the null hypothesis that larvae exhibit no preferred direction.

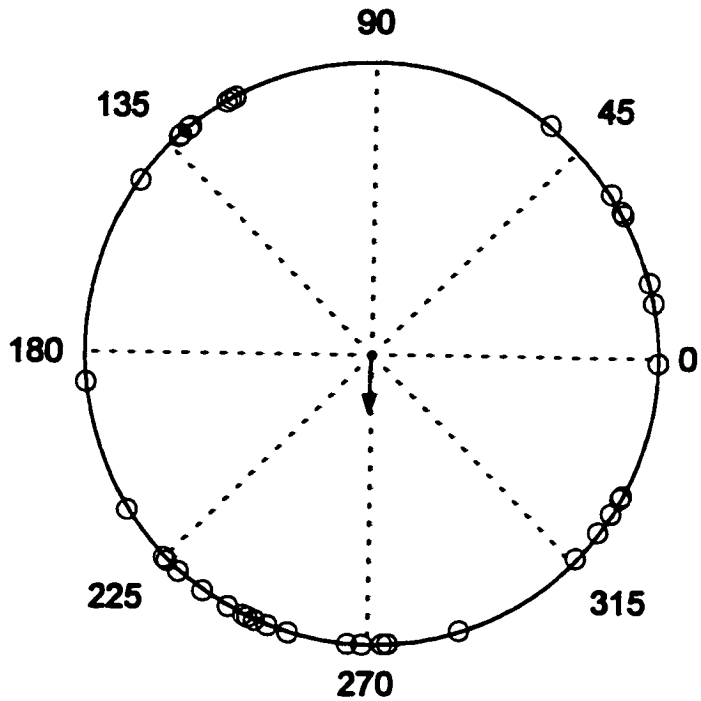

Sample size, *n*	38
Sample mean angle, $\bar{a}$	269°
Length of mean vector, *r*	0.20
Angular deviation, *s*	72.6
Rayleigh's z statistic (nr^2)	1.476
Uniform Distribution? (α= 0.05)	Yes

Fig A2.12. Scatter diagram illustrating track orientations of mussel larvae (*Mytilus edulis*) swimming in a microgravity environment. Data are pooled from all SCAs, Day 7 Night recording session, May 26, 1996. The arrow indicates the sample mean vector *m*, and descriptive statistics are tabulated. Rayleigh's z statistic tests the null hypothesis that larvae exhibit no preferred direction.

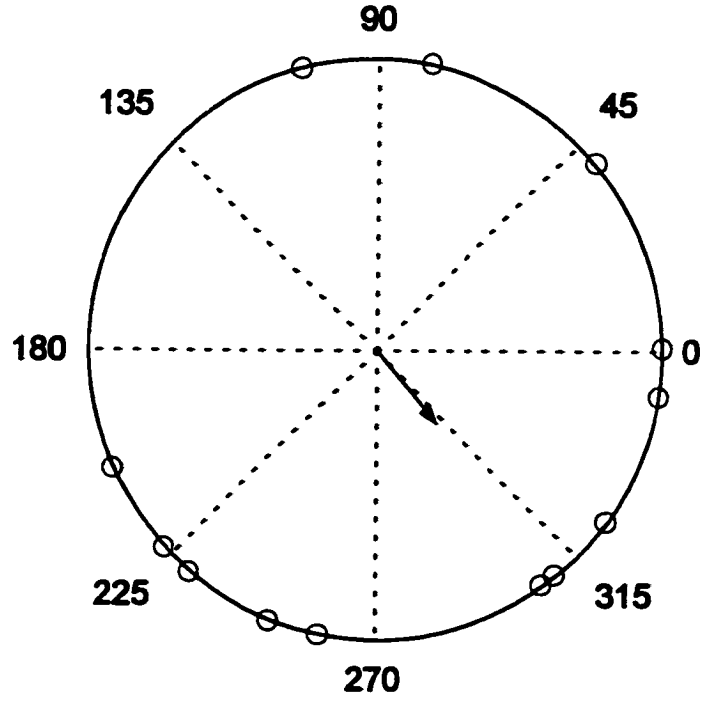

Sample size, n	13
Sample mean angle, $\bar{a}$	311°
Length of mean vector, r	0.33
Angular deviation, s	66.5
Rayleigh's z statistic (nr^2)	1.391
Uniform Distribution? (α= 0.05)	Yes

Fig A2.13. Scatter diagram illustrating track orientations of mussel larvae (*Mytilus edulis*) swimming in a microgravity environment. Data are pooled from all SCAs, Day 7 Day recording session, May 26, 1996. The arrow indicates the sample mean vector m, and descriptive statistics are tabulated. Rayleigh's z statistic tests the null hypothesis that larvae exhibit no preferred direction.

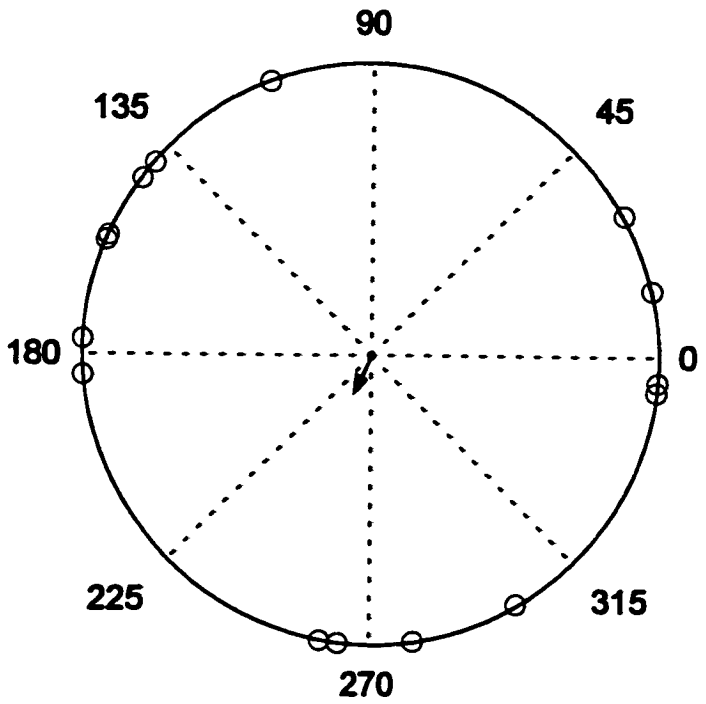

Sample size, *n*	15
Sample mean angle, $\bar{a}$	245
Length of mean vector, *r*	0.14
Angular deviation, *s*	75.0
Rayleigh's z statistic (nr^2)	0.307
Uniform Distribution? (α= 0.05)	Yes

Fig A2.14. Scatter diagram illustrating track orientations of mussel larvae (*Mytilus edulis*) swimming in a microgravity environment. Data are pooled from all SCAs, Day 8 Night recording session, May 27, 1996. The arrow indicates the sample mean vector *m*, and descriptive statistics are tabulated. Rayleigh's z statistic tests the null hypothesis that larvae exhibit no preferred direction.

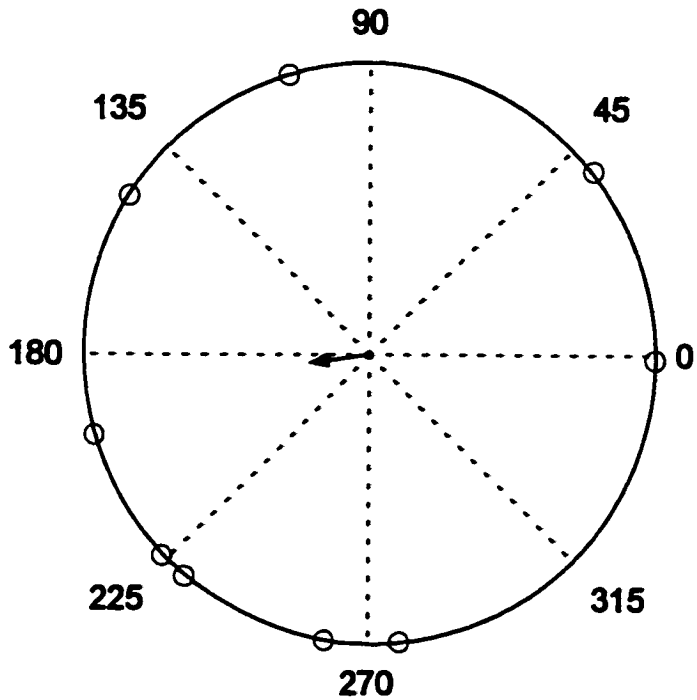

Sample size, n	9
Sample mean angle, $\bar{a}$	187°
Length of mean vector, r	0.21
Angular deviation, s	72.0
Rayleigh's z statistic (nr^2)	0.398
Uniform Distribution? (α= 0.05)	Yes

Fig A2.15. Scatter diagram illustrating track orientations of mussel larvae (*Mytilus edulis*) swimming in a microgravity environment. Data are pooled from all SCAs, Day 8 Day recording session, May 27, 1996. The arrow indicates the sample mean vector m, and descriptive statistics are tabulated. Rayleigh's z statistic tests the null hypothesis that larvae exhibit no preferred direction.

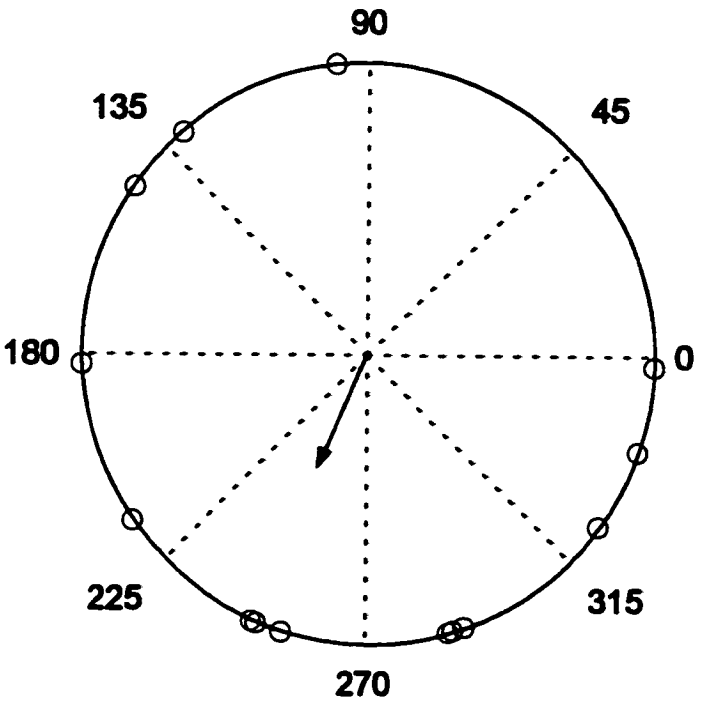

Sample size, *n*	14
Sample mean angle, $\bar{a}$	246°
Length of mean vector, *r*	0.42
Angular deviation, *s*	61.9
Rayleigh's z statistic (nr^2)	2.418
Uniform Distribution? (α= 0.05)	Yes

Fig A2.16. Scatter diagram illustrating track orientations of mussel larvae (*Mytilus edulis*) swimming in a microgravity environment. Data are pooled from all SCAs, Day 9 Night recording session, May 28, 1996. The arrow indicates the sample mean vector *m*, and descriptive statistics are tabulated. Rayleigh's z statistic tests the null hypothesis that larvae exhibit no preferred direction.

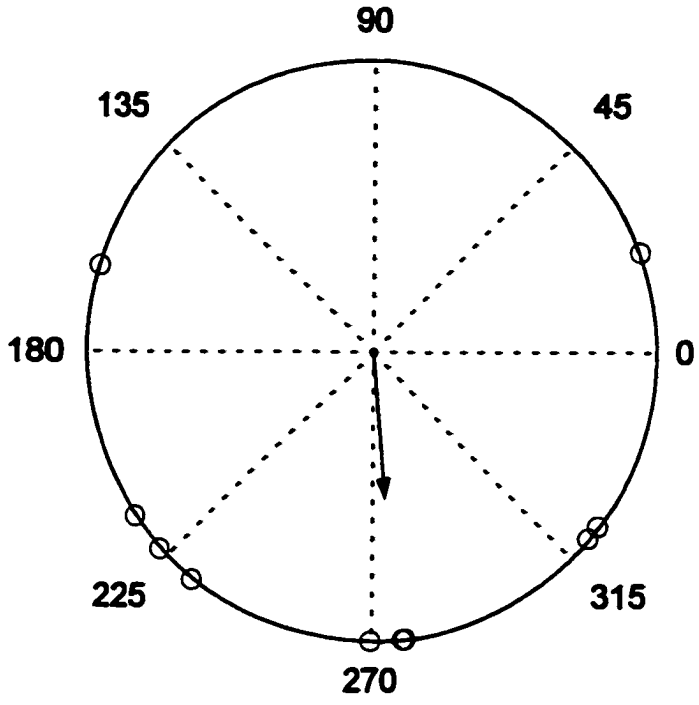

Sample size, n	10
Sample mean angle, $\bar{a}$	275°
Length of mean vector, r	0.50
Angular deviation, s	57.4
Rayleigh's z statistic (nr^2)	2.488
Uniform Distribution? (α= 0.05)	Yes

Fig A2.17. Scatter diagram illustrating track orientations of mussel larvae (*Mytilus edulis*) swimming in a microgravity environment. Data are pooled from all SCAs, Day 9 Day recording session, May 28, 1996. The arrow indicates the sample mean vector m, and descriptive statistics are tabulated. Rayleigh's z statistic tests the null hypothesis that larvae exhibit no preferred direction.

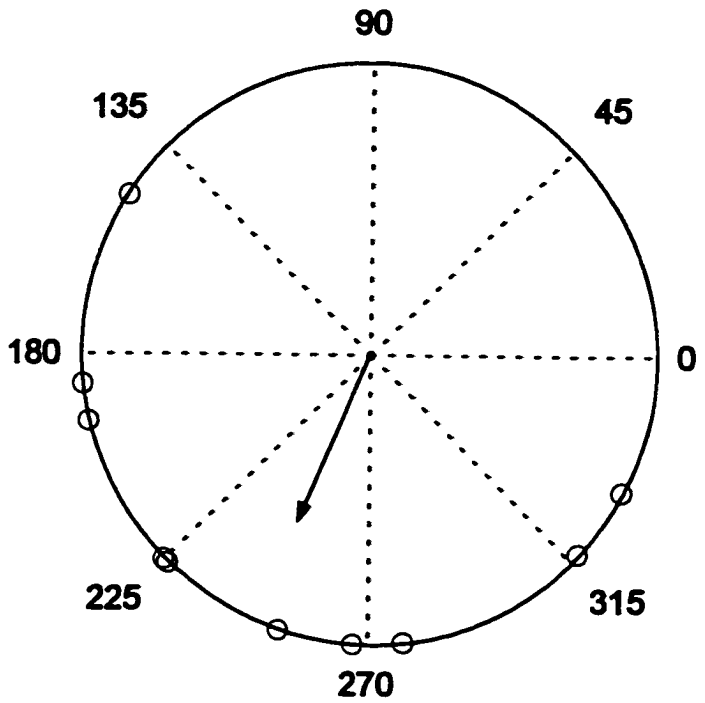

Sample size, *n*	11
Sample mean angle, $\bar{a}$	247°
Length of mean vector, *r*	0.62
Angular deviation, *s*	49.7
Rayleigh's z statistic (nr^2)	4.281
Uniform Distribution? (α= 0.05)	No

Fig A2.18. Scatter diagram illustrating track orientations of mussel larvae (*Mytilus edulis*) swimming in a microgravity environment. Data are pooled from all SCAs, Day 10 Night recording session, May 29, 1996. The arrow indicates the sample mean vector *m*, and descriptive statistics are tabulated. Rayleigh's z statistic tests the null hypothesis that larvae exhibit no preferred direction.

APPENDIX 3

3.1 Detailed In-Flight Procedures

3.2 Detailed Pre-Launch QA'd Procedures

3.3 Non-QA'd Pre-Launch Procedures

3.4 Detailed Post-Launch QA'd Procedures

APPENDIX 3.1
DETAILED IN-FLIGHT PROCEDURES:

FLIGHT DAY #	DATE	TIME OF DAY	EVENT	VIDEO TAPE #	VIDEO SESSION#	VIDEO SESSION TITLE	EVENT file (or SCUs recorded)
1	M. May 20/96	00:28					
1	M. May 20/96	01:28					
1	M. May 20/96	02:28					
1	M. May 20/96	03:28					
1	M. May 20/96	04:28	Night Starts				
1	M. May 20/96	05:28					
1	M. May 20/96	06:28					
1	M. May 20/96	07:28					
1	M. May 20/96	08:28	Day Starts				
1	M. May 20/96	09:28					
1	M. May 20/96	10:28					
1	M. May 20/96	11:28	CAN2 SCUs TRANSFERRED TO MAIN SYSTEM				
1	M. May 20/96	12:28	ECP3 Started				
1	M. May 20/96	13:28					
1	M. May 20/96	14:28					
1	M. May 20/96	15:28					
1	M. May 20/96	16:28					
1	M. May 20/96	17:28					
1	M. May 20/96	18:28					
1	M. May 20/96	19:28					
1	M. May 20/96	20:28	Day Video Session Starts	FS-1	1	Day 1 - DAY	4R1-1, 4L1-1, 3R1-1, 3L1-1 AND 4R0-1, 4L0-1, 3R0-1, 3L0-1
1	M. May 20/96	21:28					
1	M. May 20/96	22:28					
1	M. May 20/96	23:28					
2	T. May 21/96	00:28					
2	T. May 21/96	01:28					
2	T. May 21/96	02:28					
2	T. May 21/96	03:28					
2	T. May 21/96	04:28	Night Starts, & Day-Night Switch Video Session	FS-1		Day 2 - DAY / NIGHT	3L0-S1
2	T. May 21/96	05:28					
2	T. May 21/96	06:28	Night Video Session Starts	FS-1	2	Day 2 - NIGHT	4R1-2, 4L1-2, 3R1-2, 3L1-2 AND 4R0-2, 4L0-2, 3R0-2, 3L0-2
2	T. May 21/96	07:28					
2	T. May 21/96	08:28	Day Starts, & Night-Day Switch Video Session	FS-1		Day 2 - NIGHT / DAY	3L0-S2
2	T. May 21/96	09:28					
2	T. May 21/96	10:28					
2	T. May 21/96	11:28					
2	T. May 21/96	12:28					
2	T. May 21/96	13:28					
2	T. May 21/96	14:28					
2	T. May 21/96	15:28					
2	T. May 21/96	16:28					
2	T. May 21/96	17:28					
2	T. May 21/96	18:28					
2	T. May 21/96	19:28					
2	T. May 21/96	20:28	Day Video Session Starts	FS-2	3	Day 2 - DAY	4R1-3, 4L1-3, 3R1-3, 3L1-3 AND 4R0-3, 4L0-3, 3R0-3, 3L0-3
2	T. May 21/96	21:28					
2	T. May 21/96	22:28					
2	T. May 21/96	23:28					
3	W. May 22/96	00:28					
3	W. May 22/96	01:28					
3	W. May 22/96	02:28					
3	W. May 22/96	03:28					
3	W. May 22/96	04:28	Night Starts, & Day-Night Switch Video Session	FS-2		Day 3 - DAY / NIGHT	3L0-S3
3	W. May 22/96	05:28					
3	W. May 22/96	06:28	Night Video Session Starts	FS-2	4	Day 3 - NIGHT	4R1-4, 4L1-4, 3R1-4, 3L1-4 AND 4R0-4, 4L0-4, 3R0-4, 3L0-4
3	W. May 22/96	07:28					
3	W. May 22/96	08:28	Day Starts, & Night-Day Switch Video Session	FS-2		Day 3 - NIGHT / DAY	3L0-S4
3	W. May 22/96	09:28					
3	W. May 22/96	10:28					
3	W. May 22/96	11:28					
3	W. May 22/96	12:28	Video Fixation Session (Day 3 0g and 1g)	FS-2		Day 3 FIXATION	4R1-FIX, 4R0-FIX
3	W. May 22/96	13:28					

22/06	1422/06	14:28					
22/06	1522/06	15:28					
22/06	1622/06	16:28					
22/06	1722/06	17:28					
22/06	1822/06	18:28					
22/06	1922/06	19:28					
22/06	2022/06	20:28	Day Video Session Starts	FS-3	5	Day 3 - DAY	4L1-5, 3R1-5, 3L1-5 AND 4L0-5, 3R0-5, 3L0-5
22/06	2122/06	21:28					
22/06	2222/06	22:28					
22/06	2322/06	23:28					
3/06	0023/06	00:28					
3/06	0123/06	01:28					
3/06	0223/06	02:28					
3/06	0323/06	03:28					
3/06	0423/06	04:28	Night Starts, & Day-Night Switch Video Session	FS-3		Day 4 - DAY / NIGHT	3L0-S5
3/06	0523/06	05:28					
3/06	0623/06	06:28	Night Video Session Starts	FS-3	6	Day 4 - NIGHT	4L1-6, 3R1-6, 3L1-6 AND 4L0-6, 3R0-6, 3L0-6
3/06	0723/06	07:28					
3/06	0823/06	08:28	Day Starts, & Night-Day Switch Video Session	FS-3		Day 4 - NIGHT / DAY	3L0-S6
3/06	0923/06	09:28					
3/06	1023/06	10:28					
3/06	1123/06	11:28					
3/06	1223/06	12:28					
3/06	1323/06	13:28					
3/06	1423/06	14:28					
3/06	1523/06	15:28					
3/06	1623/06	16:28					
3/06	1723/06	17:28					
3/06	1823/06	18:28					
3/06	1923/06	19:28					
3/06	2023/06	20:28	Day Video Session Starts	FS-3	7	Day 4 - DAY	4L1-7, 3R1-7, 3L1-7 AND 4L0-7, 3R0-7, 3L0-7
3/06	2123/06	21:28					
3/06	2223/06	22:28					
3/06	2323/06	23:28					
4/06	0024/06	00:28					
4/06	0124/06	01:28					
4/06	0224/06	02:28					
4/06	0324/06	03:28					
4/06	0424/06	04:28	Night Starts, & Day-Night Switch Video Session	FS-4		Day 5 - DAY / NIGHT	3L0-S7
4/06	0524/06	05:28					
4/06	0624/06	06:28	Night Video Session Starts	FS-4	8	Day 5 - NIGHT	4L1-8, 3R1-8, 3L1-8 AND 4L0-8, 3R0-8, 3L0-8
4/06	0724/06	07:28					
4/06	0824/06	08:28	Day Starts, & Night-Day Switch Video Session	FS-4		Day 5 - NIGHT / DAY	3L0-S8
4/06	0924/06	09:28					
4/06	1024/06	10:28					
4/06	1124/06	11:28					
4/06	1224/06	12:28	Video Fixation Session (Day 5 0g and 1g)	FS-4		Day 5 FIXATION	4L1-FIX, 4L0-FIX
4/06	1324/06	13:28					
4/06	1424/06	14:28					
4/06	1524/06	15:28					
4/06	1624/06	16:28					
4/06	1724/06	17:28					
4/06	1824/06	18:28					
4/06	1924/06	19:28					
4/06	2024/06	20:28	Day Video Session Starts	FS-4	9	Day 5 - DAY	3R1-9, 3L1-9 AND 3R0-9, 3L0-9
4/06	2124/06	21:28					
4/06	2224/06	22:28					
4/06	2324/06	23:28					
25/06	0025/06	00:28					
25/06	0125/06	01:28					
25/06	0225/06	02:28					
25/06	0325/06	03:28					
25/06	0425/06	04:28	Night Starts, & Day-Night Switch Video Session	FS-4		Day 6 - DAY / NIGHT	3L0-S9
25/06	0525/06	05:28					
25/06	0625/06	06:28	Night Video Session Starts	FS-4	10	Day 6 - NIGHT	3R1-10, 3L1-10 AND 3R0-10, 3L0-10
25/06	0725/06	07:28					
25/06	0825/06	08:28	Day Starts, & Night-Day Switch Video Session	FS-4		Day 6 - NIGHT / DAY	3L0-S10
25/06	0925/06	09:28					
25/06	1025/06	10:28					
25/06	1125/06	11:28					
25/06	1225/06	12:28					

25/06	13y 25/06	13:26					
25/06	14y 25/06	14:26					
25/06	15y 25/06	15:26					
25/06	16y 25/06	16:26					
25/06	17y 25/06	17:26					
25/06	18y 25/06	18:26					
25/06	19y 25/06	19:26					
25/06	20y 25/06	20:26	Day Video Session Starts	FS-4	11	Day 6 - DAY	3R1-11, 3L1-11 AND 3R0-11, 3L0-11
25/06	21y 25/06	21:26					
25/06	22y 25/06	22:26					
25/06	23y 25/06	23:26					
y 26/06	00y 26/06	00:26					
y 26/06	01y 26/06	01:26					
y 26/06	02y 26/06	02:26					
y 26/06	03y 26/06	03:26					
y 26/06	04y 26/06	04:26	Night Starts, & Day-Night Switch Video Session	FS-5		Day 7 - DAY / NIGHT	3L0-S11
y 26/06	05y 26/06	05:26					
y 26/06	06y 26/06	06:26	Night Video Session Starts	FS-5	12	Day 7 - NIGHT	3R1-12, 3L1-12 AND 3R0-12, 3L0-12
y 26/06	07y 26/06	07:26					
y 26/06	08y 26/06	08:26	Day Starts, & Night-Day Switch Video Session	FS-5		Day 7 - NIGHT / DAY	3L0-S12
y 26/06	09y 26/06	09:26					
y 26/06	10y 26/06	10:26					
y 26/06	11y 26/06	11:26					
y 26/06	12y 26/06	12:26	Video Fixation Session (Day 5 0g and 1g)	FS-5		Day 7 FIXATION	3R1-FIX (3R0-FIX not recorded)
y 26/06	13y 26/06	13:26					
y 26/06	14y 26/06	14:26					
y 26/06	15y 26/06	15:26					
y 26/06	16y 26/06	16:26					
y 26/06	17y 26/06	17:26					
y 26/06	18y 26/06	18:26					
y 26/06	19y 26/06	19:26					
y 26/06	20y 26/06	20:26	Day Video Session Starts		13	Day 7 - DAY	3L1-13 AND 3L0-13
y 26/06	21y 26/06	21:26					
y 26/06	22y 26/06	22:26					
y 26/06	23y 26/06	23:26					
27/06	0027/06	00:26					
27/06	0127/06	01:26					
27/06	0227/06	02:26					
27/06	0327/06	03:26					
27/06	0427/06	04:26	Night Starts, & Day-Night Switch Video Session	FS-5		Day 8 - DAY / NIGHT	3L0-S13
27/06	0527/06	05:26					
27/06	0627/06	06:26	Night Video Session Starts	FS-5	14	Day 8 - NIGHT	3L1-14 AND 3L0-14
27/06	0727/06	07:26					
27/06	0827/06	08:26	Day Starts, & Night-Day Switch Video Session	FS-5		Day 8 - NIGHT / DAY	3L0-S14
27/06	0927/06	09:26					
27/06	1027/06	10:26					
27/06	1127/06	11:26					
27/06	1227/06	12:26					
27/06	1327/06	13:26					
27/06	1427/06	14:26					
27/06	1527/06	15:26					
27/06	1627/06	16:26					
27/06	1727/06	17:26					
27/06	1827/06	18:26					
27/06	1927/06	19:26					
27/06	2027/06	20:26	Day Video Session Starts	FS-5	15	Day 8 - DAY	3L1-15 AND 3L0-15
27/06	2127/06	21:26					
27/06	2227/06	22:26					
27/06	2327/06	23:26					
8/06	0028/06	00:26					
8/06	0128/06	01:26					
8/06	0228/06	02:26					
8/06	0328/06	03:26					
8/06	0428/06	04:26	Night Starts, & Day-Night Switch Video Session	FS-5		Day 9 - DAY / NIGHT	3L0-S15
8/06	0528/06	05:26					
8/06	0628/06	06:26	Night Video Session Starts	FS-5	16	Day 9 - NIGHT	3L1-16 AND 3L0-16
8/06	0728/06	07:26					
8/06	0828/06	08:26	Day Starts, & Night-Day Switch Video Session	FS-5		Day 9 - NIGHT / DAY	3L0-S16
8/06	0928/06	09:26					
8/06	1028/06	10:26					
8/06	1128/06	11:26					
8/06	1228/06	12:26					
8/06	1328/06	13:26					
8/06	1428/06	14:26					

9	T. May 28/96	16:28					
9	T. May 28/96	16:28					
9	T. May 28/96	17:28					
9	T. May 28/96	18:28					
9	T. May 28/96	19:28					
9	T. May 28/96	20:28	Day Video Session Starts	FS-6	17	Day 9 - DAY	3L1-17 AND 3L0-17
9	T. May 28/96	21:28					
9	T. May 28/96	22:28					
9	T. May 28/96	23:28					
10	W. May 29/96	00:28					
10	W. May 29/96	01:28					
10	W. May 29/96	02:28					
10	W. May 29/96	03:28					
10	W. May 29/96	04:28	Night Starts, & Day-Night Switch Video Session	FS-6		Day 10 - DAY / NIGHT	3L0-S17
10	W. May 29/96	05:28					
10	W. May 29/96	06:28	Night Video Session Starts	FS-6	18	Day 10 - NIGHT	3L1-18 AND 3L0-18
10	W. May 29/96	07:28	07:08 - ENDEAVOUR LANDED AT KSC				
10	W. May 29/96	08:28	*Day Starts, & Night-Day Switch Video Session*	FS-6		*Day 10 - NIGHT / DAY*	*3L0-S18*

APPENDIX 3.2
DETAILED PRE-LAUNCH QA'd PROCEDURES:

	CANADIAN SPACE AGENCY - AQUATIC RESEARCH FACILITY	
	QUALITY ASSURANCE SHEET - CAN2 SOAKING PROCEDURE	

1. PURPOSE: The purpose of this procedure is to thoroughly wash and soak the SCUs to be used for flight, ground controls and support of scrub turnaround scenarios.

2. REFERENCE DRAWINGS: To be provided by MPB

3. SPECIAL TOOLS/EQUIPMENT:

Bench top vice	#0 Phillips Screwdriver
500 ml Nalgene rinse bottle	#0 Slothead Screwdriver
Kim-wipe tissues	Filtered seawater (FSW)
Aspirator System	Diluted chlorinated water
Pre-labelled Petri dishes	De-ionized water
Torque Drivers	Powder-free gloves
SCU Kit	
Tepid diluted soapy water solution	

4. SAFETY REQUIREMENTS: NONE

5. SPECIAL INSTRUCTIONS: Steps may be performed out of sequence per the direction of the team leader. Any steps performed out of sequence will be annotated with a quality note. There will be separate quality assurance procedure sheets for each SCU. All flight hardware must be handled using powder-free gloves.

   Torque Driver, Slot head6 in-oz, S/Number: _____
   Torque Driver, Phillips 20 in-oz, S/Number: _____

6. Receive a complete SCU kit from MPB representative. Record serial number and SCU category (1G or 0G) from the SCU transport carrier.

   S/N_____
   CAT _____

7. Remove SCU from transport container and carefully secure in a bench top vice (septa up).

8. Beginning with side 'A' of the SCU (refer to DWG 364-D-I092), remove the screw from the specimen filling port (item 8). Place screw in a pre-labelled Petri dish.

9. Referring to same drawing, remove the two screws (item 9) from the Septum Port Flange (item 6). Remove flange (item 6) and septum (item 7). Place all items in a pre-labelled Petri dish.

10. Repeat steps 8-9 for side B.

11. Fill a 500 ml Nalgene rinse bottle with tepid diluted soapy water solution (Alconox detergent or equivalent). Wipe any excess water from the spout with Kim-wipe.

12. Being careful not to wet any other surfaces, fill side A of the SCU with tepid diluted soapy water solution.

13. Repeat step 12 for side B.

14. Wipe any excess water from the top of the SCU with Kim-wipe.

15. Replace septum (item 7), shiny side up, into side A.

16. Replace septum port flange (item 6) and secure with 2 screws (item 9). Torque screws to 20 in-oz.

Side A	Side B
Torque Verification _____	Torque Verification _____
Torque Click/2 _____	Torque Click/2 _____

17. Replace specimen filling port screw (item 8). Torque to 6 in-oz.

Side A	Side B
Torque Verification _____	Torque Verification _____
Torque Click/2 _____	Torque Click/2 _____

18. Repeat steps 14-17 for side B.

19. Wipe top of SCU with a Kim-wipe to remove any excess water.

20. Remove SCU from vice. Invert the SCU three times.

Invert #1 ____
Invert #2 ____
Invert #3 ____

21. Place SCU into its corresponding transport container to soak. Record time.

Time: _____

20. After a minimum of one hour of soaking time, remove SCU from transport container. Record time.

Time: _____

22. Remove SCU from transport container and carefully secure in a bench top vice (septa up).

23. Beginning with side A of the SCU (refer to DWG 364-D-I092), remove the screw from the specimen filling port (item 8). Place screw in a pre-labelled Petri dish.

24. Referring to same drawing, remove the two screws (item 9) from the Septum Port Flange (item 6). Remove flange (item 6) and septum (item 7). Place all items in a pre-labelled Petri dish.

25. Repeat steps 23-24 for side B.

26. Using the aspirator system, carefully aspirate out soapy water from both sides of the SCU.

27. Fill a clean 500 ml Nalgene rinse bottle with diluted chlorinated water. Wipe any excess water from the spout with Kim-wipe.

28. Being careful not to wet any other surfaces, fill both sides of the SCU with the diluted chlorinated water.

29. Wipe any excess water from the top of the SCU with Kim-wipe.

30. Using the aspirator system, carefully aspirate out diluted chlorinated water from both sides of the SCU.

31. Repeat steps 28-30 at least two additional times.
2nd _____
3rd _____

32. Fill a clean 500 ml Nalgene rinse bottle with de-ionized water. Wipe any excess water from the spout with Kim-wipe.

33. Being careful not to wet any other surfaces, fill both sides of the SCU with de-ionized water.

34. Wipe any excess water from the top of the SCU with Kim-wipe.

35. Using the aspirator system, carefully aspirate out de-ionized water from both sides of the SCU.

36. Repeat steps 33-35 at least tree additional times.

2nd _____
3rd _____
4th _____

37. Being careful not to wet any other surfaces, fill both sides of the SCU with de-ionized water.

38. Wipe any excess water from the top of the SCU with Kim-wipe.

39. Replace septum (item 7), shiny side up, into side A.

40. Replace septum port flange (item 6) and secure with 2 screws (item 9). Torque screws to 20 in-oz.

Side A	Side B
Torque Verification _____	Torque Verification _____
Torque Click/2 _____	Torque Click/2 _____

41. Replace specimen filling port screw (item 8). Torque to 6 in-oz.

Side A	Side B
Torque Verification _____	Torque Verification _____
Torque Click/2 _____	Torque Click/2 _____

42. Repeat steps 39-41 for side B.

43. Remove SCU from the vice. Invert the SCU three times.

Invert #1 ____
Invert #2 ____
Invert #3 ____

44. Wipe top of SCU with a Kim-wipe to remove any excess water. Place SCU into its corresponding transport container to soak. Record date and time.

Date: _____
Time: _____

45. After a minimum of 72 hours of soaking time, remove SCU from transport container. Record date and time.

Date: _____
Time: _____

46. Carefully secure in a bench top vice (septa up).

47. Beginning with side A of the SCU (refer to DWG 364-D-I092), remove the screw from the specimen filling port (item 8). Place screw in a pre-labelled Petri dish.

48. Referring to same drawing, remove the two screws (item 9) from the Septum Port Flange (item 6). Remove flange (item 6) and septum (item 7). Place all items in a pre-labelled Petri dish.

49. Repeat steps 47-48 for side B.

50. Using the aspirator system, carefully aspirate out de-ionized water from both sides of the SCU.

51. Fill a clean 500 ml Nalgene rinse bottle with filtered seawater (FSW). Wipe any excess water from the spout with Kim-wipe.

52. Being careful not to wet any other surfaces, fill both sides of the SCU with FSW.

53. Wipe any excess water from the top of the SCU with Kim-wipe.

54. Using the aspirator system carefully aspirate out FSW from both sides of the SCU.

55. Repeat steps 52-54 at least two additional times.

    2nd _____ 3rd _____

56. Wipe any excess water from the top of the SCU with Kim-wipe.

57. Replace septum (item 7), shiny side up, into side A.

58. Replace septum port flange (item 6) and secure with 2 screws (item 9). Torque screws to 20 in-oz.

Side A	Side B
Torque Verification _____	Torque Verification _____
Torque Click/2 _____	Torque Click/2 _____

59. Replace specimen filling port screw (item 8). Torque to 6 in-oz.

Side A	Side B
Torque Verification _____	Torque Verification _____
Torque Click/2 _____	Torque Click/2 _____

60. Repeat steps 57-59 for side B.

61. Remove the SCU from the bench top vice. Replace the clean SCU back in its corresponding transport container.

62. The SCU is now ready for loading of fixative blocks.

63. Close this quality assurance procedure.

	CANADIAN SPACE AGENCY - AQUATIC RESEARCH FACILITY	
	QUALITY ASSURANCE SHEET - CAN2 FIXATIVE LOADING PROCEDURE	

1. PURPOSE: The purpose of this procedure is to fill the SCU fixative blocks with prepared fixative.

2. REFERENCE DRAWINGS: To be provided by MPB

3. SPECIAL TOOLS/EQUIPMENT:

Bench top vice	Waterproof cover(plastic sheet)
5/64"Allen key driver	Chemical Fume Hood
Kim-wipe tissues	Torque Driver
5cc syringe/16 gauge needle	25% Aqueous glutaraldehyde solution
Pre-labelled Petri dishes	Powder-free gloves
Goggles	SCU Kit

4. SAFETY REQUIREMENTS:

Powder-free gloves	Goggles
Certified fume hood	

5. SPECIAL INSTRUCTIONS: Steps may be performed out of sequence per the direction of the team leader. Any steps performed out of sequence will be annotated with a quality note. There will be a separate quality assurance procedure sheet for each specimen container unit. All flight hardware must be handled using powder-free gloves. Verify chemical fume hood is certified.

   Torque Driver, Phillips 20 in-oz, S/N: _____

6. Receive a complete SCU kit from MPB representative. Record serial number and SCU category (1G or 0G) from SCU transport container.

   S/N _____
   CAT _____

7. Remove assembled fixative block 'A' from transport container. Place fixative block in to the fixative block jig .

8. Place loose jig dowel through jig and into fixative block securing fixative block to jig.

9. Tighten thumbwheel on bottom of fixative block jig thereby setting plunger-piston to its proper location.

10. Cover the jaws of the bench top vice with a water-proof cover to prevent incidental spillage of fixative from making contact with the outside of the fixative block.

11. Secure fixative block and jig assembly (thumbwheel down) in a bench top vice.

12. Using #0 phillips screwdriver, remove the two long screws, passing through the mirror base plate and into the fixative block. Place screws in a pre-labelled Petri dish.

13. Remove remaining short screw passing through the mirror base plate. Place screw in a pre-labelled Petri dish.

14. Remove stainless steel base plate. Place in pre-labelled Petri dish.

15. Remove mirror base gasket. Place in a pre-labelled Petri dish.

16. Transport fixative block/jig/vice assembly to chemical fume hood.

NOTE

All of the following steps are to be conducted in a certified chemical fume hood, handler will wear powder-free gloves and goggles

17. Using a 5cc syringe/16 gauge soft tip needle, carefully transfer 25% aqueous solution of glutaraldehyde into fixative block. Slowly fill fixative block until glutaraldehyde just breaks bottom of fixative block filling port (item TBD9). Fill point can be determined by appearance of meniscus forming on top of the fixative.

NOTE

To reduce contamination, the following steps should be performed wearing new gloves

18. Replace mirror base gasket concave side up. Press gasket over dowel pins of fixative block and seat gasket over fixative block filling port.

19. Replace stainless steel base plate, tapered side down. Align slots on plate with fixative block and press through dowel pins.

NOTE

Fit should feel tight

20. Secure base plate to fixative block with two long screws and one short screw. Torque screws to 20 in-oz.

Side A	Side B
Torque Verification_____	Torque Verification _____
Torque Click/2 _____	Torque Click/2 _____

21. Remove assembly from fume hood and remove jig from vice.

22. Carefully unscrew the thumbwheel and remove loose jig dowel pin. Gently pull, top and bottom, the fixative block from the fixative block jig.

23. Place filled fixative block in labelled plastic bag and return to SCU transport container.

24. Repeat steps 7-23 for fixative block 'B'.

25. Close this quality assurance procedure.

CANADIAN SPACE AGENCY - AQUATIC RESEARCH FACILITY
QUALITY ASSURANCE SHEET - CAN2 SPECIMEN LOADING PROCEDURE

1. PURPOSE: The purpose of this procedure is to load the SCU, sides A and B with larvae and algae solution.

2. REFERENCE DRAWINGS: To be provided by MPB

3. SPECIAL TOOLS/EQUIPMENT:

5 C cold room	1 l beakers
Petri dishes	Inverted microscope
Video recorder	Video tape (Hi8)
Nile red	Algae
Filtered seawater (FSW)	30 cc syringes, 18 gauge blunt tip needles
Kim-wipes	Larvae
Bench top vice	Tissue culture plate
#0 Slothead screwdriver	De-ionized water
#0 Phillips Screwdriver	Torque drivers
Pipets	Nalgene rinse bottles
Neoprene bottle insulator	Aspirator system
Pre-labelled Petri dishes	Powder-free gloves
Plastic beakers	Air pump system
Tissue culture plate	SCU Kit
1cc syringe/21 gauge needle	Specimen collection cup

4. SAFETY REQUIREMENTS: None

5. SPECIAL INSTRUCTIONS: Steps may be performed out of sequence per the direction of the team leader. Any steps performed out of sequence will be annotated with a quality note. There will be one quality assurance procedure for each specimen container unit. All flight hardware must be handled using powder-free gloves.

   Torque Driver, Slot head 6 in-oz, S/N: _____, Cal Number: _____
   Torque Driver, Phillips 20 in-oz, S/N: _____, Cal Number: _____

   SCU S/N _____
   CAT: _____

6. Bivalve larvae will be placed in a 1 litre beaker (beaker #1) to allow actively swimming larvae to collect at the top. Most active swimmers will be removed to beaker #2.
7. Between 30 to 100 larvae will be removed from beaker #2 and placed in tissue culture plate well and examined using an inverted microscope. Video imaging of all the larvae will be recorded on video tape for later measurement with image analysis equipment.

8. Repeat steps 6-7 for a total of 13 batches

9. Batch #13 will be removed and stained using Nile Red to observe and measure lipid content.

10. Algae concentration counted with haemocytometer.

NOTE

Algae and algae nutrients will be aerated with aquarium pump throughout remainder of this loading procedure

11. Algae and algae nutrients will be added to one litre of seawater to make a stock concentration between 20,000 and 100,000 cells/ml. Count will be verified with a epifluorescence microscope counting technique.

NOTE

The following steps of this procedure are performed in a 5 C coldroom

12. Receive a complete SCU kit from MPB representative. Record serial number and category (0g or 1g) of the SCU from the SCU transport carrier.

S/N _____
CAT _____

13. Remove SCU from transport container and carefully secure in a bench top vice (septa up).

14. Beginning with side A of the SCU (refer to DWG 364-D-I092), remove the screw from the specimen filling port (item 8). Place screw in a pre-labelled Petri dish.

15. Referring to same drawing, remove the two screws (item 9) from the septum port flange (item 6). Remove flange (item 6) and septum (item 7). Place all items in a pre-labelled Petri dish.

16. Repeat steps 14-15 for side B.

17. Fill a Nalgene rinse bottle with algae/filtered seawater. Wipe any excess water from the spout with a Kim-wipe.

18. Being careful not to wet any other surfaces, fill both sides of the SCU with algae/filtered seawater.

19. Carefully aspirate out algae/filtered seawater from both sides of the SCU.

20. Repeat steps 18-19 for a total of two times.

17. Fill a clean 30cc syringe/18 gauge blunt tip needle with algae/filtered seawater. Wipe any excess water from syringe tip with Kim-wipe.

18. Being careful not to wet any other surfaces, transfer 20-25 mls of algae/filtered seawater from the syringe into side A of the SCU.

19. Remove all air bubbles that may have formed.

NOTE:
A fresh Pasteur Pipet should be used for each batch of larvae

20. Using Pasteur Pipet, transfer larvae from tissue culture plate well through the septum port. Keep tip below water level of the SCU. Record the batch number.

Side A Batch #___ Side B Batch #___

21. Rinse out tissue culture plate well with algae/filtered seawater.

22. Using Pasteur Pipet, remove all specimens from the tissue culture plate well and transfer into the septum port.

23. Repeat steps 21-22 for a total of two times.

24. Repeat steps 21-22 for a total of three times..

25. Place the tissue culture plate under a dissection scope to verify all specimens have been removed from the well. If not, repeat step 24 until all specimens have been removed.

All specimens removed: _____

Number of repetitions of steps 25: _____

26. Remove rubber bulb from the pipet and rinse into the SCU with algae/filtered seawater.

27. Top up the SCU with algae/seawater.

28. Remove any air bubbles that may have formed.

29. Wipe off the top of the SCU with a Kim-wipe.

30. Replace septum (item 7), shiny side up, into side A.

31. Replace septum port flange (item 6) and secure with 2 screws (item 9). Torque screws to 20 in-oz.

Side A	Side B
Torque Verification _____	Torque Verification _____
Torque Click/2 _____	Torque Click/2 _____

32. Replace specimen filling port screw (item 8). Torque to 6 in-oz.

Side A	Side B
Torque Verification _____	Torque Verification _____
Torque Click/2 _____	Torque Click/2 _____

33. Repeat steps 17-32 for side B.

32. Wipe top of SCU with a Kim-wipe to remove any excess water.

33. Using a clean 1cc ml syringe/21 gauge needle, pierce the septum of side A.

34. Extract approximately 0.3 ml of contents, record amount, and empty syringe into a specimen collection cup.

Side A: ___ ml Side B: ___ ml

35. Using a clean 21 gauge needle, repeat steps 33-34 for side B.

36. Dry septa with a Kim-wipe.

37. Remove the SCU from the vice.

38. Place SCU into its corresponding transport container.

39. SCU is now ready for flight/ground control/scrub scenario.

40. Close this quality assurance procedure.

APPENDIX 3.3
NON-QA'd PRE-LAUNCH PROCEDURES:

SCU LOADING DAY LAB OPERATIONS

MATERIALS:
20μm and 60μm Nitex filter
250 ml beaker (Beaker #1) - unstained ISO
250 ml beaker (Beaker#2) - stained, rinsed ISO
2-litre glass beaker (Beaker #3) - ISO/FSW/f/2 solution
100 ml beaker (Beaker #4) - larvae
inverted microscope
dissecting microscopes (2)
Nalgene squeeze bottles (2)
haemocytometer
100ml graduated cylinder
(50ml graduated cylinder)
2-litre graduated cylinder
Petri dishes
tissue culture well plates

1. Clean and rinse all glassware in Materials list.
Pour approximately 50-100 ml from the top of a 4-day old algae culture (*Isochrysis galbana*, clone ISO) over a sterile 20μm Nitex screen, into a clean sterile 250ml beaker (Beaker #1).
2. Stain ISO with 0.025 mg/ml Calcofluor White (CW) (~70-90 minutes)
   - measure amount of ISO in Beaker #1 with sterile graduated cylinder
   - calculate amount of stock CW required; add stock CW to ISO in Beaker #1,
   - stain for 20 minutes
   - pour ISO from Beaker #1 into sterile 50ml centrifuge tubes
   - spin tubes for 15 minutes at 1500rpm. Stop spinning when most cells are on bottom
   - remove supernatant (with sterile syringe), and resuspend cells with FSW
   - spin again for 15 minutes at 1500rpm, remove supernatant, resuspend in FSW
   - pour undamaged ISO cells into a 250ml beaker (Beaker #2)
3. Determine the concentration of the ISO culture in Beaker #2 using a haemocytometer.
4. Make 2 litres of a stock solution of ISO, 5°C filtered seawater (FSW), and Fritz f/2 algae growth nutrients (0.3ml Fritz/litre FSW). The final concentration of ISO should be approximately 25 000 cells/ml. Pour solution into a sterile 2-litre glass beaker (Beaker #3), and keep in 5°C refrigerator until Step #6.
5. Confirm ISO concentration in Beaker #3 using epifluorescence technique. Adjust if necessary, and recount.
6. Partially fill each of two neoprene-insulated 500ml Nalgene squeeze bottles with ISO stock solution from Beaker #3. Cover Beaker #3 with aluminium foil, to keep out dust etc. Place one Nalgene bottle and Beaker #3 in 5°C Cold Room, to allow temperature to equilibrate to loading temperature conditions (~30-60 minutes).

7. Pour off the top of the best larval cultures over a 60µm Nitex screen to collect swimming larvae on the Nitex screen. Rinse larvae into a 100ml beaker (Beaker #4) using ISO solution from the second Nalgene squeeze bottle.
8. Rinse two small sterile Petri dishes with ISO solution, and pour larvae from Beaker #4 into each of these dishes. Keep Beaker #4 in 12°C Percival chamber when not in use.
9. Using dissecting microscopes, two people will simultaneously count out 100 larvae from the Petri dishes into wells of a tissue culture well plate. Plates will be moved to the 5°C Cold Room to allow temperature to equilibrate to loading temperature conditions.
10. All required materials will be moved to the 5°C Cold Room (see Loading Procedures Materials List), where loading operations will commence.
11. Perform SCA Loading Procedures, according to specified protocol.
12. Start Control Experiments in lab.

APPENDIX 3.4
DETAILED POST-LAUNCH PROCEDURES:

CANADIAN SPACE AGENCY - AQUATIC RESEARCH FACILITY
QUALITY ASSURANCE SHEET - CAN2 UNLOADING PROCEDURE

1. PURPOSE: The purpose of this procedure is to unload the larval and algae specimens from the SCU post mission. This includes all flight and ground control SCUs.

2. REFERENCE DRAWINGS: To be provided by MPB

3. SPECIAL TOOLS/EQUIPMENT:

Dissection scope	Post-mission SCU kit
Parafilm	30 & 60 cc syringes
60 m Nitex mesh disc	Millipore Swinnex 13 filter holder
60, 100, 250 ml beakers	Clamp (60 ml beaker)
Ring stand & clamps	16 & 21 gauge blunt tip needles
#0 Phillips screwdriver	#0 slothead screwdriver
Petri dishes	Notebook
Benchtop vice	Nalgene squeeze bottle
Filtered seawater (FSW)	Pre-labeled vials
4 C refrigerator	Ziploc bags (small & large)
Forceps/scalpel/blades	Pasteur Pipet
Certified fume hood	Powder-free gloves
Allen Key Driver	Goggles
Wire cutters	Tissue culture plate multi-well (24 wells x 1.7 x 1.6 cm)

4. SAFETY REQUIREMENTS:
Powder-free gloves, Goggles, Certified fume hood

5. SPECIAL INSTRUCTIONS: Steps may be performed out sequence per the direction of the team leader. Any steps performed out of sequence will be annotated with a quality note. There will be separate quality assurance procedure sheet for each SCU.

6. Receive a complete post-mission SCU kit from MPB representative. Record serial number, SCU category (1G or 0G) and ground/flight unit from the SCU transport carrier.

S/N: _____ Ground: _____
CAT: _____ Flight: _____

NOTE:

All of the following steps are to be conducted in a certified chemical fume hood, handler will wear powder-free gloves and goggles

7. Remove SCU from its container and carefully place on a working surface with the six fasteners of the bottom cover facing up.

8. Remove the six fasteners using a 5/64" allen key driver. Place the fasteners and the lockwashers in a plastic bag.

9. Place the SCU with it's side on the working surface. Move the bottom cover slightly away from the thrid level housing and place it on the table with the electrical custom connector fasteners facing up. Back-off the four fasteners of the electrical connectors uniformly before removing them completely, using a #0 phillips screwdriver. Push the connector out of the bottom cover. Remove the two o-rings from the connector and the bottom cover. Place the fasteners and o-rings in the same plastic bag as the bottom cover fasteners. Put the bottom cover and the plastic bag in the transport container.

10. Remove the 2nd level/SCA from the third level housing box by pulling on the septa feedthru aluminium parts fastened to the bag. Put the third level housing in the tranpsort container.

11. Position the 2nd level/SCA in a benchtop vice so that the mechanical and electrical feedthru face upwards. Grab the bag/SCA at its middle section.

12. Cut the bag all around using a sharp edge razor blade at the opposite end of the heat seal. Then cut a small part (aprox. 0.5") of the top section of the bag (the section that surrounds the SCA on the opposite side of the heat seal along one of its edges to facilitate the SCA removal.

13. Remove the overall assembly from the vice. Slide out the heat seal top section of the Teflon bag from the assembly. Store that section (heat seal section) in a ziplock bag.

14. Remove the Kapton tape on the top of the SCA to free electrical wires, including tape that surrounds the electrical wires.

15. Cut the electrical wires near their solder joint using a small wire cutter. Discard the solder joint and heat shrink tube.

16. Separate the bottom part of the Teflon bag from the SCA by holding the wires between the septa mechanical feedthru and the SCA and then pulling apart. Put the bottom section of theTeflon bag with the electrical sctom connector in the same ziplock plastic bag as the top section Teflon bag. Put the ziplock bag in the transport container.

CHAMBER A

17. Inspect SCU under dissection scope to observe larval specimens before opening Chamber A.

18. Set up screening apparatus by using a 60cc syringe and Millipore Swinnex 13 filter holder, with a 60 m Nitex mesh disc, a 60 ml beaker and clamp in a ring stand.

NOTE
Keep dry, since algae sample must be processed first.

19. Invert SCU four times, to re-suspend algae.

Invert #1 _____ Invert #3 _____
Invert #2 _____ Invert #4 _____

20. Secure SCU in the vice so that the septum and specimen ports are facing up, and is slightly tilted to the right to allow seawater to accumulate in the corner directly beneath the specimen port of Chamber A.

21. Obtain 30cc syringe and attach a 21 gauge needle. Pull plunger of 30cc syringe back until it reads 4-5 cc.

22. Insert needle through septum of Chamber A and remove 2cc of specimen solution. Pour solution into the filter holder of the funnel. (This is to avoid air bubbles within filter holder.)

23. Remove Chamber A's specimen port screw, septum flange, and place in a labeled Petri dish. Remove septum and inspect it under dissection scope to ensure that no larvae are stuck to it. If larvae are found on the septum, rinse larvae, using filtered seawater (FSW) into the screening apparatus. Place septum in the same Petri dish.

24. Replace the 21 gauge needle on the 30 cc syringe with a 16 gauge, 2" blunt tip needle. Pull plunger back until it reads 4-5cc.

25. Using 30 cc syringe, remove as much of the specimen solution as possible. Using a Nalgene squeeze bottle immediately inject 20 ml 0.2 m FSW into Chamber A in order to keep the animals wet. Place 30cc syringe inside filter apparatus, and carefully remove plunger from 30cc syringe. Allow specimen solution to drain over Nitex filter to collect larval specimens on filter, and algae specimens in beaker.

26. Remove 60 ml beaker from screening apparatus, and replace with a 250 ml beaker. Lower filter holder in 250 ml beaker (partially filled with FSW) to ensure that Nitex disc and larvae will remain in seawater during screening procedure.

27. Divide filtrate present in the 60 ml beaker (ie, algae sample) evenly amongst 2 pre-labeled vials, and store in dark refrigerator (4 C) until counting.

28. While SCU is in the vice, carefully rotate fhree times to rinse any larvae off the sides.

    Rotate #1 _____ Rotate #3 _____
    Rotate #2 _____

29. Remove fluid from Chamber A with 30 cc syringe, place 30cc syringe inside filter apparatus, and carefully remove plunger from 30cc syringe. Allow speciment solution to drain over Nitex filter to collect larval specimens on filter. Rinse 30cc syringe and plunger tip with FSW, into filter apparatus.

30. Replace septum, flange, and specimen port screw.

31. Orient SCU in vice so that the Teflon permeable membrane of Chamber A is facing up, and is slightly tilted to allow seawater to accumulate in the corner directly beneath the specimen port.

32. Remove four (4) fasteners and aluminium flange of Chamber A's Teflon permeable membrane and store in the second small Ziploc bag.

34. Remove the Teflon membrane and silicon gasket with forceps. Rinse inside of the Teflon membrane and the silicon gasket with FSW, into Chamber A, to remove any larval specimens. Using dissection scope, inspect Teflon membrane and silicon gasket to determine if any larvae are stuck to these surfaces. If larvae are found, rinse larvae, using FSW into the screening apparatus. Place all parts in the second small Ziploc bag.

35. Rinse all sides of Chamber A with FSW.

36. Carefully pour contents of Chamber A into a clean 100 ml beaker.

37. Repeat steps 35 and 36.

38. Repeat steps 35 and 36.

NOTE

After completion of step 38, Chamber A has been rinsed three times with FSW

39. Carefully set aside the SCU.

40. Carefully pour contents of 100 ml beaker into filter apparatus.

41. Rinse 100 ml beaker with FSW, and carefully pour into filter apparatus.

42. Repeat step 41.

43. Repeat step 41.

NOTE

After completion of step 43, 100 ml beaker has been rinsed three times with FSW

44. Carefully remove Millipore Swinnex filter holder from 60cc syringe, and place upside down in a tissue culture plate well.

45. Attach a 3cm long piece of tygon tubing to the end of a 5cc syringe, filled with 4-5cc FSW. Attach the other end of the tubing to the bottom of the Millipore Swinnex filter holder.

46. Backwash the Millipore Swinnex filter holder into the tissue culture plate well by slowly injecting the FSW from the 5cc syringe through the Nitex filter.

47. Carefully disassemble filter holder, and place all components in a Petri dish. Use a dissection scope to examine all components. If any larvae remain attached to the components, rinse them with FSW into a tissure culture plate well.

48. Using a dissection scope, observe larval specimens collected in the tissue culture plate wells. Count larvae to determine the number of larvae that have been retrieved from Chamber A.

49. Using a clean Pasteur Pipet, remove all larvae from tissue culture plate wells and place into a 5 ml labeled vial. Under a dissection scope, examine the wells; if larvae are present, rinse with FSW. Screw cap tightly and seal with Parafilm. Record number of larvae retrieved from Chamber A on the label of the 5 ml vial, and in notebook.

CHAMBER B

50. Remove SCU from vice and inspect under dissection scope to observe larval specimens before opening Chamber B.

51. Set up screening apparatus by using a 60cc syringe and Millipore Swinnex 13 filter holder, with a 60 m Nitex mesh disc, a 60 ml beaker and clamp in a ring stand.

NOTE
Keep dry, since algae sample must be processed first.

52. Invert SCU four times, to re-suspend algae.

Invert #1 _____ Invert #3 _____
Invert #2 _____ Invert #4 _____

53. Secure SCU in the vice so that the septum and specimen ports are facing up, and is slightly tilted to the right to allow seawater to accumulate in the corner directly beneath the specimen port of Chamber B.

54. Obtain 30cc syringe and attach a 21 gauge needle. Pull plunger of 30cc syringe back until it reads 4-5 cc.

55. Insert needle through septum of Chamber B and remove 2cc of specimen solution. Pour solution into the filter holder of the funnel. (This is to avoid air bubbles within filter holder.)

56. Remove Chamber B's specimen port screw and septum flange, and place in a labeled Petri dish. Remove septum and inspect it under dissection scope to ensure that no larvae are stuck to it. If larvae are found on the septum, rinse larvae, using filtered seawater (FSW) into the screening apparatus. Place septum in the same Petri dish.

57. Replace the 21 gauge needle on the 30 cc syringe with a 16 gauge, 2" blunt tip needle. Pull plunger back until it reads 4-5cc.

58. Using 30 cc syringe, remove as much of the specimen solution as possible. Using a Nalgene squeeze bottle immediately inject 20 ml 0.2 m FSW into Chamber B in order to keep the animals wet. Place 30cc syringe inside filter apparatus, and carefully remove plunger from 30cc syringe. Allow specimen solution to drain over Nitex filter to collect larval specimens on filter, and algae specimens in beaker.

59. Remove 60 ml beaker from screening apparatus, and replace with a 250 ml beaker. Lower filter holder in 250 ml beaker (partially filled with FSW) to ensure that Nitex disc and larvae will remain in seawater during screening procedure.

60. Divide filtrate present in the 60 ml beaker (ie, algae sample) evenly amongst 2 pre-labeled vials, and store in dark refrigerator (4 C) until counting.

61. While SCU is in the vice, carefully rotate three times to rinse any larvae off the sides.

Rotate #1 _____ Rotate #3 _____
Rotate #2 _____

62. Remove fluid from Chamber B with 30 cc syringe, and place 30cc syringe inside filter apparatus, and carefully remove plunger from 30cc syringe. Allow speciment solution to drain over Nitex filter to collect larval specimens on filter. Rinse 30cc syringe and plunger tip with FSW, into filter apparatus.

63. Replace septum, flange, and specimen port screw.

64. Orient SCU in vice so that the Teflon permeable membrane of Chamber B is facing up, and is slightly tilted to allow seawater to accumulate in the corner directly beneath the specimen port.

65. Remove four (4) fasteners and aluminium flange of Chamber B's Teflon permeable membrane and store in the second small Ziploc bag.

66. Remove the Teflon membrane and silicon gasket with forceps. Rinse inside of the Teflon membrane and the silicon gasket with FSW, into Chamber B, to remove any larval specimens. Using dissection scope, inspect Teflon membrane and silicon gasket to determine if any larvae are stuck to these surfaces. If larvae are found, rinse larvae, using FSW into the screening apparatus. Place all parts in the second small Ziploc bag.

67. Rinse all sides of Chamber B with FSW.

68. Carefully pour contents of Chamber B into a clean 100 ml beaker.

69. Repeat steps 67 and 68.

70. Repeat steps 67 and 68.

NOTE

After completion of step 70, Chamber B has been rinsed three times with FSW

71. Carefully set aside the SCU.

72. Carefully pour contents of 100 ml beaker into filter apparatus.

73. Rinse 100 ml beaker with FSW, and carefully pour into filter apparatus.

74. Repeat step 73.

75. Repeat step 73.

NOTE

After completion of step 75, 100ml beaker has been rinsed three times with FSW

76. Carefully remove Millipore Swinnex filter holder from 60cc syringe, and place upside down in a tissue culture plate well.

77. Attach a 3cm long piece of tygon tubing to the end of a 5cc syringe, filled with 4-5cc FSW. Attach the other end of the tubing to the bottom of the Millipore Swinnex filter holder.

78. Backwash the Millipore Swinnex filter holder into the tissue culture plate well by slowly injecting the FSW from the 5cc syringe through the Nitex filter.

79. Carefully disassemble filter holder, and place all components in a Petri dish. Use a dissection scope to examine all components. If any larvae remain attached to the components, rinse them with FSW into a tissure culture plate well.

80. Using a dissection scope, observe larval specimens collected in the tissue culture plate wells. Count larvae to determine the number of larvae that have been retrieved from Chamber B.

81. Using a clean Pasteur Pipet, remove all larvae from tissue culture plate wells and place into a 5 ml labeled vial. Under a dissection scope, examine the wells; if larvae are present, rinse with FSW. Screw cap tightly and seal with Parafilm. Record number of larvae retrieved from Chamber B on the label of the 5 ml vial, and in notebook.

82. Remove SCU from vice and place in a large Ziploc bag. Place all ziplock bags in the transport container.

83. Return SCU transport container to MPB representative.

84. Close out this procedure.

REFERENCES

Alexander, R.M. 1990. Size, speed and buoyancy adaptations in aquatic animals. American Zoologist 30: 189-196.

Azam, F.T., T. Fenchel, J.G. Field, L.A. Meyer-Reil, and T. Thingstad. 1983. The ecological role of water column microbes in the sea. Marine Ecology Progress Series 10: 257-263.

Batschelet, E., 81. Circular statistics in biology. In: Sibson, R. and Cohen, J. E., eds. Mathematics in Biology. London: Academic Press.(371 pp. total).

Bayne, B.L. 1965. Growth and the delay of metamorphosis of the larvae of *Mytilus edulis* (L.). Ophelia 2: 1-47.

Bayne, B.L. 1963. Responses of *Mytilus edulis* larvae to increases in hydrostatic pressure. Nature 198: 406-407.

Bayne, B.L. 1964. The responses of the larvae of *Mytilus edulis* L. to light and to gravity. Oikos 15.

Beaumont, A.R. and M.D. Budd. 1982. Delayed growth of mussel (*Mytilus edulis*) and scallop (*Pecten maximus*) veligers at low temperatures. Marine Biology 71: 97-100.

Blake, J.R. and M.A. Sleigh. 1974. Mechanics of ciliary locomotion. Biol. Rev. Cambridge Philos. Soc. 49: 85-125.

Buskey, E.J. and D.K. Stoecker. 1988. Locomotory patterns of the planktonic ciliate *Favella* sp.: Adaptations for remaining within food patches. Bulletin of Marine Science 43: 783-796.

Cheung, A. T. W. and Winet, H. 1975. Flow velocity profile over a ciliated surface. In: Wu, T. T. Y, Brokaw, C. J., and Brennan, C., eds. Swimming and Flying in Nature. New York: Plenum Press.

Chia, F.-S., J. Buckland-Nicks, and C.M. Young. 1984. Locomotion of marine invertebrate larvae: a review. Canadian Journal of Zoology 62: 1205-1222.

Childress, S., M.A.R. Koehl, and M. Miksis. 1987. Scanning currents in Stokes flow and the efficient feeding of small organisms. J. Fluid Mech. 177: 407-436.

Conover, R.J. 1968. Zooplankton- life in a nutritionally dilute enviroment. American Zoologist 8: 107-118.

Cragg, S.M. 1985. The adductor and retractor muscles of the veliger of *Pecten maximus* (L.) (Bivalvia). J. Molluscan Stud. 51: 276-283.

Cragg, S.M. 1980. Swimming behaviour of the larvae of *Pecten maximus* (L). (Bivalvia). Journal of the Marine Biological Association of the United Kingdom 60: 551-564.

Cragg, S.M. and J.A. Nott. 1977. The ultrastructure of the statocysts in the pediveliger larvae of *Pecten maximus* (L.) (Bivalvia). Journal of Experimental Marine Biology and Ecology 27: 23-36.

Crawford, B.J. and A.C. Martin. 1998. Effect of microgravity on the development of embryos/larvae and the larval esophageal musculature of the purple starfish, *Pisaster ochraceus*. Canadian Journal of Zoology 76: 1641-1650.

Crenshaw, H.C. 1990. Helical orientation - a novel mechanism for the orientation of microorganisms. Lecture Notes in Biomathematics 89: 361-386.

Crenshaw, H.C. 1993. Orientation by helical motion I. Kinematics of the helical motion of organisms with up to six degrees of freedom. Bull. Math. Biol. 55: 197-212.

Crenshaw, H.C. 1996. A new look at locomotion in microorganisms: Rotating and translating. American Zoologist 36: 608-618.

Creutzberg, F., 1975. Orientation in Space: Animals. Invertebrates. In: Kinne, O., ed. Marine Ecology, Vol. II. Physiological Mechanisms. London: John Wiley & Sons. 555-655. 992 pp.

Croll, R.P., D.L. Jackson, and E.E. Voronezhskaya. 1997. Catecholamine-containing cells in larval and postlarval bivalve molluscs. Biological Bulletin 193: 116-124.

Emlet, R.B. 1990. Flow fields around ciliated larvae: effects of natural and artificial tethers. Marine Ecology Progress Series 63: 211-225.

Emlet, R.B. and R.R. Strathmann. 1985. Gravity, drag, and feeding currents of small zooplankton. Science 228: 1016-1017.

Forward, R.B. 1988. Diel vertical migration: zooplankton photobiology and behaviour. Oceanogr. Mar. Biol. Ann. Rev. 26: 361-393.

Fraenkel, G. S. and Gunn, D. L. 1940. The Orientation of Animals. New York, Dover Publishing. 352 pp.

Fraser, A.J. 1989. Triacylglycerol content as a condition index for fish, bivalve, and crustacean larvae. Can. J. Fish. Aquat. Sci. 46: 1868-1873.

Gallager, S.M. 1985. Buoyancy regulation and swimming energetics in larvae of *Bankia gouldi* (Bartsch) (Teredinidae: bivalvia). Abstract of the 77th Annual NSA Meeting, Norfolk, VA. 8.

Gallager, S.M. 1993. Hydrodynamic disturbances produced by small zooplankton: case study for the veliger larva of a bivalve mollusc. Journal of Plankton Research 15: 1277-1296.

Gallager, S. M. 1992. Locomotion and Feeding in Marine Bivalve Larvae. PhD Thesis, Boston University, Boston USA.

Gallager, S.M. 1988. Visual observations of particle manipulation during feeding in larvae of a bivalve mollusc. Bulletin of Marine Science 43: 344-365.

Gallager, S. M., Bricelj, M., and Stoecker, D. K., 89. The effects of brown tide alga on growth, feeding physiology and locomotory behaviour of scallop larvae, *Argopecten irradians*. In: Carpenter, E. J., Bricelj, M., and Cosper, E., eds. Novel Phytoplankton Blooms: Causes and Impacts of Recurrent Brown Tides and Other Unusual Blooms. New York: Springer-Verlag Inc. 799 pp.

Gallager, S.M. and R. Mann. 1986. Growth and survival of larvae of *Mercenaria mercenaria* (L.) and *Crassostrea virginica* (Gmelin) relative to broodstock conditioning and lipid content of eggs. Aquaculture 56: 105-121.

Guillard, R. R. L. 1958. Some factors in the use of nannoplankton cultures as food for larval and juvenile bivalves. Proceedings of the National Shellfisheries Association 48: 134-141.

Guillard, R. R. L. 1975. Culture of phytoplankton for feeding marine invertebrates. In: Smith, W. L. and Chanley, M. H., eds. Culture of Marine Invertebrate Animals. New York, Plenum Press. pp. 29-59.

Häder, D.-P. 1997. Gravitaxis in flagellates. Biological Bulletin 192: 131-133.

Häder, D.-P., A. Rosum, J. Schaefer, and R. Hemmersbach. 1996. Graviperception in the flagellate *Euglena gracilis* during a shuttle space flight . Journal of Biotechnology 47: 261-269.

Häder, D.-P., A. Rosum, J. Schaefer, and R. Hemmersbach. 1995. Gravitaxis in the flagellate *Euglena gracilis* is controlled by an active gravireceptor J. Plant. Physiol. 146: 474-480.

Hansen, B., F.L. Fotel, N.J. Jensen, and L. Wittrup. 1997. Physiological effects of the detergent linear alkylbenzene sulphonate on blue mussel larvae (*Mytilus edulis*) in laboratory and mesocosm experiments . Marine Biology 128: 627-637.

Hemmersbach, R., R. Voormanns, and D.P. Häder. 1996. Graviresponses in *Paramecium biaurelia* under different accelerations: studies on the ground and in space. Journal of Experimental Biology 199: 2199-2205.

Hill, A.E. 1991. Advection-diffusion-mortality solutions for investigating pelagic larvae dispersal. Marine Ecology Progress Series 70: 117-128.

Holland, D. L. 1978. Lipid reserves and energy metabolism in the larvae of benthic marine invertebrates. In: Malins, D. C. and Sargent, J. R., eds. Biochemical and Biophysical Perspectives in Marine Biology. London: Academic Press Inc. p. 85-123.

Hurley, G.V., M.J. Tremblay, and C.Y. Couturier. 1987. Age estimation of sea scallop larvae (*Placopecten magellanicus*) from daily growth lines on shells. J. Northw. Atl. Fish. Sci. 7: 123-129.

Jackson, D. L. 1992. Physiological Ecology of *Placopecten magellanicus*: Food Availability and Larval Growth Response. M.Sc. Thesis, Dalhousie University, Halifax, Nova Scotia, Canada.

Jackson, D.L. 1993. Use of Nile Red as a histochemical technique for monitoring physiological condition of bivalve larvae. Bull. Aquaculture Assoc. Canada 93-4: 32-34.

Jespersen, H. and K. Olsen. 1982. Bioenergetics in veliger larvae of *Mytilus edulis* L. Ophelia 21: 101-113.

Jonsson, P.R., C. André, and M. Lindgarth. 1991. Swimming behaviour of marine bivalve larvae in a flume boundary-layer flow: evidence for near-bottom confinement. Marine Ecology Progress Series 79: 67-76.

Jørgensen, C.B. 1981. Mortality, growth, and grazing impact of a cohort of bivalve larvae, *Mytilus edulis* L. Ophelia 20: 185-192.

Koehl, M. A. R. 1983. Mechanisms of particle capture by copepods at low Reynolds numbers: possible modes of selective feeding . In: Meyers, D. G. and Strickler, J. R. eds. Trophic Interactions Within Aquatic Ecosystems. Boulder, Colorado: Westview Press Inc.

LaBarbera, M. 1984. Feeding currents and particle capture mechanisms in suspension feeding animals. American Zoologist 24: 71-84.

Lebert, M. and D.P. Häder. 1996. How *Euglena* tells up from down. Nature 379: 590.

Levin, L.A. 1990. A review of methods for labeling and tracking marine invertebrate larvae. Ophelia 32: 115-144.

Longhurst, A. R. 1976. Vertical Migration. In: Cushing, D. H. and Walsh, J. J., eds. The Ecology of the Seas. Toronto: W. B. Saunders Co. p. 116-137.

Mallet, A. L. 1989. Culture of the Mussel, *Mytilus edulis*. In: Boghen, A. D., ed. Cold-Water Aquaculture in Atlantic Canada. First ed. Moncton, New Brunswick: Canadian Institute for Research on Regional Development. 410 pp.

Mann, R. 1986. *Arctica islandica* (Linne) larvae: active depth regulators or passive particles. American Malacological Bulletin 3: 51-57.

Marszalek, D.S. 1982. The role of heavy skeletons in vertical movements of non-motile zooplankton. Mar. Behav. Physiol. 8: 295-303.

Marthy, H.J., G. Gasset, R. Tixador, B. Eche, P. Schatt, A. Dessommes, U. Marthy, and R. Bacchieri. 1998. Skeletogenesis of sea urchin larvae under modified gravity conditions. Adv Space Res. 21: 1151-4.

Marthy, H.J., G. Gasset, R. Tixador, P. Schatt, B. Eche, A. Dessommes, T. Giacomini, G. Tap, and D. Gorand. 1996. The sea urchin larva, a suitable model for biomineralisation studies in space (IML-2 ESA Biorack experiment '24-F urchin'). Journal of Biotechnology 47: 167-177.

Mogami, Y., C. Oobayashi, T. Yamaguchi, Y. Ogiso, and S.A. Baba. 1988. Negative geotaxis in sea urchin larvae: a possible role of mechanoreception in the late stages of development. Journal of Experimental Biology 137: 141-156.

Morgan, S. G. 1995. Life and death in the plankton: Larval mortality and adaptation. In: McEdward, L., ed. Ecology of Marine Invertebrate Larvae. Boca Raton, Florida, USA: CRC Press. 279-322. 464 pp.

Paffenhöfer, G.-A. 1983. Calanoid copepod feeding: grazing on small and large particles. In: Meyers, D. G. and Strickler, J. R. Trophic Interactions Within Aquatic Ecosystems. Boulder, Colorado: Westview Press Inc.

Pechenik, J.A., L.S. Eyster, J. Widdows, and B.L. Bayne. 1990. The influence of food concentration and temperature on growth and morphological differentiation of blue mussel *Mytilus edulis* L. larvae. Journal of Experimental Marine Biology and Ecology 136: 47-64.

Pires, A. and R.M. Woollacott. 1983. A direct and active influence of gravity on the behaviour of a marine invertebrate larva. Science 220: 731-733.

Pomeroy, L.R. 1974. The ocean's food web, a changing paradigm. BioScience 24: 499-504.

Power, J.H. 1989. Sink or swim: growth dynamics and zooplankton hydromechanics. American Naturalist 133: 706-721.

Rumrill, S.S. 1990. Natural mortality of marine invertebrate larvae. Ophelia 32: 163-198.

Scheltema, R.S. 1986. Epipelagic meroplankton of tropical seas: its role for the biogeography of sublittoral invertebrate species. UNESCO Technical Papers in Marine Science 49: 242-249.

Silva, M.A. 1987. Larval behaviour of the sea scallop *Placopecten magellanicus* under laboratory conditions: effects of light on swimming behaviour throughout development. Abstract of the 79th Annual NSA Meeting, Halifax, Nova Scotia p.74.

Silva, M.A. and O'Dor. R. K. 1991. Vertical distribution of sea scallop larvae *Placopecten magellanicus* under experimental conditions in a mesocosm. Abstract of the 8th International Pectinid Workshop, Cherbourg, France.

Smayda, T.J. 1970. The suspension and sinking of phytoplankton in the sea. Oceanogr. Mar. Biol. Ann. Rev. 8: 353-414.

Sokal, R. R. and Rohlf, F. J. 1981. Biometry. The Principles and Practice of Statistics in Biological Research. New York, W.H. Freeman and Company. 859 pp.

Souza, K. A., Black, S., and Wassersug, R. 1995. Amphibian development in the virtual absence of gravity. Proc. Natl. Acad. Sci. 92:1975-1978.

Spangenberg, D.B., F. Lattanzio Jr, C. Philput, R. Schwarte, B. Lowe, and J. Philput. 1995. Effects of weightlessness on *Aurelia* budding and ephyra development. ASGSB Bull. 9: 88 (abstract).

Spooner, B.S., J. Metcalf, L. DeBell, A. Paulsen, W. Noren, and J.A. Guikema. 1994. Development of the brine shrimp *Artemia* is accelerated during spaceflight. Journal of Experimental Zoology. 269: 253-62.

Sprung, M. 1984a. Physiological energetics of mussel larvae (*Mytilus edulis*). I. Shell growth and biomass. Marine Ecology Progress Series 17: 282-293.

Sprung, M. 1984b. Physiological energetics of mussel larvae (*Mytilus edulis*). II. Food uptake. Marine Ecology Progress Series 17: 295-305.

Sprung, M. 1984c. Physiological energetics of mussel larvae (Mytilus edulis). III. Respiration. Marine Ecology Progress Series 18: 171-178.

Sprung, M. 1984d. Physiological energetics of mussel larvae (Mytilus edulis). IV. Efficiencies. Marine Ecology Progress Series 18: 179-186.

Strathmann, R.R. and E. Leise. 1979. On feeding mechanisms and clearance rates of molluscan veligers. Biological Bulletin 157: 524-535.

Strickler, J.R. 1982. Calanoid copepods, feeding currents, and the role of gravity. Science 218: 158-160.

Strickler, J.R. 1985. Feeding currents in calanoid copepods: two new hypotheses. Symp. Soc. Exp. Biol. 39: 459-485.

Sulkin, S.D. 1984. Behavioural basis of depth regulation in the larvae of brachyuran crabs. Marine Ecology Progress Series 15: 181-205.

Sulkin, S.D. 1990. Larval orientation mechanisms: the power of controlled experiments. Ophelia 32: 49-62.

Thorson, G. 1950. Reproductive and larval ecology of marine bottom invertebrates. Biological Reviews of the Cambridge Philosophical Society 25: 1-45.

Tremblay, M.J. and M.M. Sinclair. 1990. Diel vertical migration of sea scallop larvae *Placopecten magellanicus* in a shallow embayment. Marine Ecology Progress Series 67: 19-25.

Villanueva, R., C. Nozais, and S. Boletzky. 1996. Swimming behavior and food searching in planktonic *Octopus vulgaris* Cuvier from hatching to settlement. Journal of Experimental Marine Biology and Ecology 208: 169-184.

Vogel, S. 1981. Life in Moving Fluids: the Physical Biology of Flow. Princeton, N. J., Princeton University Press. 352 pp.

Wang, W.X. and J. Widdows. 1991. Physiological responses of mussel larvae *Mytilus edulis* to environmental hypoxia and anoxia. Marine Ecology Progress Series 70: 223-236.

Wang, W.X. and Z.Z. Xu. 1997. Larval swimming and postlarval drifting behavior in the infaunal bivalve *Sinonovacula constricta* . Marine Ecology Progress Series 148: 71-78.

Waterbury, J.B., S.W. Watson, F.W. Valois, and D.G. Franks. 1986. Biological and ecological characterization of the marine unicellular bacterium *Synechococcus*. Can. Bull. Fish. Aquat. Sci. 214: 71-120.

Widdows, J. 1991. Physiological ecology of mussel larvae. Aquaculture 94: 147-163

Widdows, J., P. Donkin, M.D. Brinsley, S.V. Evans, P.N. Salkeld, A. Franklin, R.J. Law, and M.J. Waldock. 1995. Scope for growth and contaminant levels in North Sea mussels *Mytilus edulis*. Marine Ecology Progress Series 127: 131-148.

Young, C. M. 1995. Behaviour and locomotion during the dispersal phase of larval life. In: McEdward, L., ed. Ecology of Marine Invertebrate Larvae. Boca Raton, Florida: CRC Press. 249-277. 464 pp.

Zar, J. H. Biostatistical Analysis. 1984. Englewood Cliffs, New Jersey, Prentice Hall. 718 pp.

Zeuthen, E. 1947. Body size and metabolic rate in the animal kingdom with special regard to the marine micro-fauna. C. r. Lab. Carlsberg, Ser. chim. 26: 17-161.